Final Report

Mira

Group 01

TU Delft

Page left blank intentionally.

Final Report

MIRA

by

Group 01

as part of the

Spring DSE, 2020

Students:	Daniel Ayazyan	4472373
	Luana Capus	4653580
	Nils Faure	4654528
	Pranav Gurumallappa	4541685
	Yannick Heumassej	4667107
	Thomas Litjens	4549821
	Kiva McSorley	4536444
	Lorenza Mottinelli	4546121
	Benno Riha	4685768
	Tim van Voorbergen	4661915
Supervisor:	Jasper Bouwmeester	
Coaches:	Jesse Reusen & Yuqian Tu	

TU Delft

Cover image retrieved from https://hdwallpaperim.com/photography-water-space-netherlands-england/.

Preface

This is the final report in a project which aims to design a mega-constellation to survey the Earth for environmental, safety and security reasons: monitoring gases, humans, vehicles, and potential other aspects such as forest fires. This first phase design comes within the scope of the aerospace faculty bachelor project at TU Delft, more commonly known as the design synthesis exercise or DSE. The authors are, hence, bachelor students and part of DSE group 01.

The name Mira comes from the Spanish meaning of the word, which is: ”look” and from the Italian one, which means ”aim”. In Latin, Mira also means ”wonderful”. Mira is also a red giant in the constellation Cetus, which conveniently happens to have the shape of two boxes connected: with a bit of creativity, one could say Cetus reminds of the TIR and the MS satellite (we invite the reader to find our more about these two satellites in the upcoming pages). As the mission looks at our wonderful planet making use of a constellation, Mira seemed to be the perfect fit for the name.

On behalf of the team would like to thank the tutor, coaches, teaching assistants, external experts and the DSE organising committee for their support, help and motivation throughout this entire synthesis.

Executive Overview

This is the final report of this project, which aims to present a design for a satellite mega-constellation to monitor the Earth's atmospheric gases such as carbon dioxide, using short wave radiation, as well as human activity and potentially fires using thermal radiation.

Project baseline

Mission description
For this mission, the project objectives are clear. They consist of monitoring the gases such as carbon dioxide, methane, and nitrogen dioxide, using short wave, as well as humans, vehicles and fires using the thermal infrared spectrum. This must be done using a satellite mega-constellation. The following mission need, and project objective statement are then formulated. The mission will have to give at least a temporal resolution of 30 minutes for TIR and 60 minutes for gases.

> **Mission Need Statement:** Provide remote sensing through optical instruments with high spatial, radiometric and temporal resolution in order to obtain optical images addressing societal applications related to justice, safety, security, and environmental threats.
> **Project Objective Statement:** Design a Low Earth Orbit satellite constellation equipped with deployable space telescopes to survey locations of interest for societal objectives.

Market analysis
The market is first defined for its geopolitical and economic region: that is NATO and the EU states, as their share in the world's space budget together is 75%. In the EU, the three main potential users are the EU commission, France, and Germany, due to their very high space budgets. The Netherlands' budget, only at 140 Meuros, means that the Dutch authorities need to share this mission. Moreover, the scientific market and the demand are both increasing drastically in the field of optical Earth observing mission, about 9.4% per year for the next ten years.

Furthermore, the analysis of various missions and of SWOT aspects, points out that the mission designed here is unique, as it is a large constellation, with a high temporal resolution, combined with the fact that it analyses both gases and thermal infrared in shortwave, as the spectral ranges are 2.6-3.5 and 8-12 µm respectively.

Technical Risk Analysis
Technical risks refer to events which can take place, and which will have a guaranteed negative impact on the mission. To name a few, short circuiting, collision risks and launch vehicle failure are addressed. Their probability and their potential impact are evaluated and the assessment of possible mitigations to these risks, to lessen their effect on the system are given.

Sustainable Development Strategy
The approach taken towards sustainability is done by elaborating a strategy. Sustainability was taken into account in all subsystems economically, mission or environment wise. Whether it is the lowest number of launches possible, not using non disintegrating materials in the atmosphere, or applying series production, this space mission aims to take sustainability seriously. Possibly, the major factor at play will be the fact that the satellite disintegrates in the atmosphere at its end of life.

RAMS analysis
In the first step, the RAMS analysis is about reliability. Redundancy is present on both a subsystem level and on a system level, with additional satellites being sent in case of some failing. Other kinds of reliability exist as well, such as the reliability in performance of subsystems. This type of reliability is important for off the shelf products, and cannot be determined for parts that need to be developed (ADCS and payload).

Furthermore, availability is achieved mostly by just meeting the user requirements on performance. Of course, here again, redundancy can have a positive impact. Moreover, maintenance in this system is assured by renewing the constellation every 7 years. Mission safety is mostly related to the safekeeping of the satellite's structures and integrity. This is done by thermally controlling the satellite's components and also by choosing a fitting structure for the loads.

System design

Mission analysis
Through a comprehensive mission analysis, the main aspects of the mission are analysed. Firstly, the wavelengths for the multispectral imager were determined to be between 2.65 and 3.52 µm. Additionally, for the thermal imaging, a method to find the SNR is presented. That is the ratio of signal to noise, which finds that between 2-11 people minimum can be found depending on the environment. This calculation also presents the method used to determine how many humans can be detected by the TIR satellite. There will thus be two types of satellites: one for thermal infrared imaging, and the other with MS imaging.

Payload
An individual telescope, is designed for both the TIR and the MS satellite types. The MS telescope is larger than the TIR one, as the first is assumed to be signal limited, and the second diffraction limited. Thus, the volume and the mass of the MS telescope, are between 1.35 and 1.5 times higher than the TIR telescopes. In both cases, a sensor would have to be developed for the imaging, which will be made of $H_gC_dT_e$, driving low operational temperatures, 190K and 81 K respectively.

Constellation Design and Astrodynamic Characteristics
Calculating astrodynamic characteristics is key in the design of the constellation. The constellation will require 816 satellites per generation, including extra satellites for maintenance. They will be placed in 24 planes at an altitude of 350 km. 12 planes are used for both TIR and MS, and another 12 planes are only used for TIR. These numbers are attainable by using both the swath of each type of satellite (100 vs. 200 km) and their respective temporal resolution of 30 and 60 min.

Propulsion and GNC
For propulsion, constant ion thrusting is chosen. For a generation which lasts 7 years, about 35 kg of propellant will be needed. The propulsion design also incorporates launch parameters. For this, the Falcon 9 is chosen for its low price (528-655 Meuros per generation) and performance and Atlas V for its high capacity, for the TIR and MS satellites respectively. For this, 24 launches will be needed per generation. For position and velocity determination, GNSS signal receivers will be used along with Galileo constellation of satellites. Furthermore, software architecture is used to simulate the constellation of satellites to better predict positions of other spacecraft and collision probability.

ADCS
The ADCS subsystem uses reaction wheels (1 Nms) with magnetorquers (42 A m^2). These are custom fit for this mission. Moreover, star trackers are used, with redundancy as they are relatively cheap with regards to the impact they have on the mission if they were to fail.

Communication and Data handling
A phased array antenna consisting of a grid of 14x14 patch elements (1 cm x 1 cm each), equally spaced 0.5 cm apart, was used to transfer data at maximum 2 h after data sampling at an average data rate of 200 Mbit/s for TIR and 2 Gbit/s for MS at a radio-frequency of 10 GHz. To make direct data links possible 22 ground stations, scattered around the globe, are required. The satellites have an on-board data storage capacity of 600 and 5400 GB for TIR and MS respectively, designed for maximum data sampling and the addition of a factor 3 redundancy to account for degradation.

Power
The power subsystem is composed of custom fit batteries, leading to a mass of 2.56 kg. Furthermore, the two solar arrays that are employed will be double sided, deployable, fixed and with areas of 1.35 and 0.93 m^2 and with a total mass of 15.8 kg. Lastly, the PCDU is sized using existing PCDU as reference, and its mass, 3.54 kg and volume 2.4 m^3 are interpolated based on the peak power consumption.

Thermal control
The thermal control subsystem features a deployable baffle that shields the telescope from sunlight. Stray light reaching into the baffle is deviated away by mirrors mounted on the internal baffle surface. The instrument box

of TIR and MS are cooled by a pulse tube cryocooler and the excessive heat generated in the instrument box is transported away with heat pipes and led to a radiator positioned on a bus surface. Louvers are used on the radiator to modulate emissivity for different orbital orientations. The propellant tank is insulated with MLI blankets and cooled by a micro pulse tube and the remaining components in the spacecraft bus remain within their operational temperature range thanks to the relatively warm LEO thermal environment.

Structures and mechanisms
The structure of the satellite mostly consists of aluminium frame and honeycomb panels. The aluminium frame allows for stiffness and load bearing, while the honeycomb panels also support the load, add stiffness and protect against radiation and debris.

Outcome performance, AIT, development and costs
AIT, configuration and layout
AIT, configuration and layout poses an integral challenge requiring innovative solutions, with the deployment of solar arrays, the telescope and its baffle. For each of these aspects, a comprehensive and efficient stowed configuration was envisioned, as well as, a logical deployment sequence and behaviour.

Performance analysis
During the performance analysis of the system, it is found that the TIR and MS satellite are quite similar. Their total masses are 203 kg and 235 kg and their power consumptions are 160 and 133 W, respectively. Their nominal data rate vary because the MS satellite is required to take larger pictures, 1950 for the MS versus 198 MB/s for the TIR satellite.

Moreover, such an analysis on Mira underlines that all user requirements have been met, with the exception of 2: collision avoidance was not thoroughly investigated, and the satellites do not store the data for 3 months. The latter is due to the fact that the data is directly down-linked. Besides these 2 un-met requirements, there are 3 that can not be verified right now as further research needs to be conducted: sustainability with respect to the design methods, the use of toxic materials and sustainability during the life-cycle. These three non-met requirements can be interpreted as recommendation for future related projects.

Operations, logistics and scalability
The constellation is launched in 6 steps after the final model is tested in space. Step 1-4 double the temporal resolution and step 5 and 6 fill in the remaining orbits such that after step 6 the whole constellation is launched. After that, an additional step 7 and 8 can be initiated to further increase the temporal resolution of the TIR satellites. A schedule for launching spans about 7 months, from January 2030 to July 2030. The temporal resolution of the constellation improves step-wise as more and more satellites are launched. The mission is designed modularly: scalability is possible, either by lowering or increasing the number of satellites. This could lead to a respective increase or decrease of temporal resolution, but also a respective lower or higher cost per satellite, but higher or lower cost for the whole constellation. Moreover, if two more steps of launches are added to the already existing 6 ones, the cost would increase exponentially too between steps 6 and 7 and 8, but also provides the ability to double the pre-existing temporal resolutions more.

Project development
Project development analyses at which stage or phase the design is, and what are the future phases. Thus, the reader should keep in mind that this report only presents a pre-phase A level of design. There are at least three phases left before launch and deployment, and two left before production.

Cost analysis
The cost analysis can be divided into two parts: cost breakdown, and cost budget. The cost breakdown divides the costs into: investment, development, manufacturing, operations and maintenance, launch and AIT. The largest cost being in investment: 1.3 B€. Moreover, while making the cost budget, one finds that both the TIR and MS satellites are cheaper than the target budget, with the MS one being more expensive by a factor of 1.35 per satellite. This is mostly because the MS satellite would be produced in smaller numbers. Finally, it can be concluded that there is no return on investment as this mission would solely be government- funded.

Contents

Nomenclature

Abbreviations

AIT	Assembly, Integration and Testing
ADCS	Attitude Determination and Control Subsystem
BLR	Baseline Report
BR	Benno Riha
C&DH	Command and Data Handling
CF	Data Consent Factor
COMMS	Communications
CONST	Constellation
COTS	Commercial off-the-shelf
CR	Data compression Ratio
DA	Daniel Ayazyan
DDST	Delft Deployable Space Telescope
DLF	Direct Link Fraction
DSE	Design Synthesis Exercise
FY	Fiscal Year
GNC	Guidance, Navigation and Control
GNSS	Global Navigation Satellite System
GPS	Global Positioning System
GS	Ground Station
GSCF	Ground Station Coverage Factor
GSD	Ground Sampling Distance
IR	Infrared
ISP	Specific Impulse
KM	Kiva Mc Sorley
LC	Luana Capus
LEO	Low Earth Orbit
LM	Lorenza Mottinelli
LV	Launch vehicle
MA	Mission Analysis
MAI	Manufacturing, Assembly and Integration
MECH	Mechanisms
MIS	Mission
MNS	Mission Need Statement
MR	Midterm Report
MS	Multispectral
MW	Momentum wheel
NF	Nils Faure
NPOP	Non-populated Earth monitoring
PAN	Panchromatic
PAY	Payload

PG	Pranav Gurumallappa
POP	Populated Earth monitoring
POS	Project Objective Statement
POWR	Power
PROP	Propulsion
RAAN	Right Ascension of the Ascending Node
RAMS	Reliability, Availability, Maintainability & Safety
ROI	Return on-investment
RW	Reaction wheel
SNR	Signal-to-Noise Ratio
SR	System Reliability
STK	Systems Tool Kit
STRC	Structures
SUS	Sustainability
THRM	Thermal Control
TIR	Thermal Infrared
TL	Thomas Litjens
TPM	Technical Performance Measure
TV	Tim van Voorbergen
WFD	Work Flow Diagram
WBS	Work Breakdown Structure
WT	Whole Team
YH	Yannick Heumassej

Symbols

a	Semi-major axis	[m]
A_{mon}	Monitored Earth surface area	[m^2]
A_r	Aerodynamic area	[m^2]
$C_\oplus$	Circumference of Earth	[m]
C	Data Storage Capacity	[bits]
d_{swath}	Swath width	[m]
d_g	ground sampling distance	[m]
d_p	pixel pitch	[µm]
DR	Data rate	[B/s]
E	Energy	[J]
E_b	Bit energy	[J]
E_e	Solar irradiance	[W/m^2]
E_{opt}	Optimum elevation angle for the transfer of data to ground stations	[deg]
f	Frequency	[s^{-1}]
F_T	Thrust	[N]
$g_\oplus$	Gravitational constant on Earth	[m/s^2]
H	altitude	[km]
i	Inclination	[deg]
I_{sp}	Specific impulse	[s]

J_2	Gravity field constant	[−]
m	Mass	[kg]
M_p	Propellant mass	[kg]
M_{sc}	Spacecraft mass	[kg]
n	Mean motion	[deg/s]
n_{band}	Number of measured spectral bands	[−]
n_{bit}	Band depth	[bits]
N_gs	Number of ground stations	[−]
$n_{polar,planes}$	Minimum number of polar planes	[−]
$n_{polar,sats}$	Minimum number of polar satellites	[−]
P	Power	[W]
R_E	Radius of Earth	[m]
R_r	Required read-out data rate	[bit/s]
R_s	Required sampling data rate	[bit/s]
S	Solar flux	[W/m^2]
T_r	Receiver Temperature	[K]
t_b	Burn time	[s]
t_{day}	Sidereal day time	[s]
t_{orbit}	Orbital period	[s]
t_{sample}	Temporal resolution	[s]
$t_{transmit}$	Available data transfer time	[s]
V	Orbital velocity	[m/s]
v_g	Ground speed	[m/s]
ΔV_ω	Velocity budget for plane change	[m/s]
$\Delta\omega$	Longitudinal plane change angle	[deg]
$\Delta\Omega_{J2}$	Node precession	[deg/day]
θ	Angle	[deg]
λ	Wavelength	[m]

Constants

c	Speed of light	[2.988×10^8 m/s]
h	Planck's constant	[6.626×10^{-34} J s]
k	Boltzmann constant	[1.381×10^{-23} m^2 kg s^{-2} K^{-1}]

Others

✓	The requirement is met.
×	The requirement is not met.
●	The requirement can not be verified at the moment.

1 Introduction

Since the Montgolfier brothers, human societies have longed to know how the Earth looks from above. It is this simple but key thought which drove some of the most creative inventors, to design and build the majestic U2 or meteorologic balloons. This idea has driven intelligence as well as environmentally related projects and missions. Furthermore, since Sputnik, it became only a matter of time before the humans could monitor the Earth from space. The need for security and defence state organisations to always collect better and faster intelligence on humans and vehicles, as well the need to be faster informed of forest fires or various gaseous emissions regarding climate change and the effects of pollution, are both key drivers in satellite monitoring systems, the TROPOMI mission being such an example. One way of accomplishing such tasks is using a mega-constellation consisting of hundreds of satellites to provide global continuous coverage. For a growing demand in surveillance, this satellite mission configuration is fitting. Recent missions such as SPOT, or Starlink, show the potential applications of Earth monitoring or constellation missions. It is why, in a bachelor project, of ten students for ten weeks, TU Delft has ordered a first phase design of such a constellation. Moreover, the design of such a mission is directly made possible because of the development by TU Delft of a deployable space telescope (DDST) and its stabilising platform, as well as decreasing launch costs. This is the final report.

In the previous report, after extensive trade-offs, one concept for this constellation was chosen. This concept incorporated two kind of satellites: one analysing gases with a multispectral imager, and one monitoring humans, vehicles and potentially forest fires with a thermal infrared imager. Thus, the DDST would be sized for monitoring in the thermal infrared and medium infrared region.

This last report aims to present a final design for this mission. Firstly, through a sustainability strategy, RAMS analysis, requirements overview and conceptual design summary, the report will lay the basis for the final design of the subsystems and other aspects. These will start with the mission analysis and payload design as they are the driving aspects of this constellation. Furthermore, the astrodynamic characteristics as well as all other relevant spacecraft bus subsystems, such as power, thermal control, and propulsion, are designed. Lastly, with a description of the AIT, the performance and of the costs, this report concludes with the project development.

2
Project Objectives

The system's mission is to provide remote sensing for monitoring and surveillance for several societal interests. The main focus is the detection of fires, emissions of greenhouse gases and pollutants, and movement of humans and vehicles. This is clearly defined in the Mission Need Statement (MNS) and Project Objective Statement (POS).

Mission Need Statement: Provide remote sensing through optical instruments with high spatial, radiometric and temporal resolution to obtain optical images addressing societal applications related to safety, security and industrial emissions.

Project Objective Statement: Design a Low Earth Orbit satellite constellation equipped with deployable space telescopes to survey locations of interest for societal objectives.

The challenge consists of designing a mega-constellation with performance in spatial, temporal, spectral and radiometric resolution. The payload needs to be mission-specific. Narrow-band optical imagining will be used to detect emissions while thermal IR will be used to detect vehicles, groups of people and fires. The outcome of the project shall include feasibility study and preliminary design as well as a full specification of the capabilities of the entire system [1].

3
Market Analysis

Market analysis, is valuable as it helps the reader and the engineers to better understand what market the final product will be on. This can be done through defining the market, analysing the demand and supply, and by performing a SWOT analysis and a market viability study.

3.1. Market definition and demand

The market can be defined on two fronts, the geographical and geopolitical market area, and the scientific market area.

3.1.1. Geopolitical/economic market area

The market and regulatory authority on space aimed projects is still largely driven by national governments, specifically with respect to the defence sector. This is primarily due to the high costs, high revenues and often interconnected defence capabilities of space missions. It is logical that it is then dependant on geopolitical spheres.

After a discussion with members of the Dutch ministry of security and justice, it was understood that this mission would be designed to first serve the Dutch authorities and potentially European partners in the EU, as well as, other international allies. Thus, the market is mostly limited to the European Union, specifically the Netherlands, with a potential to partially involve the United States and other NATO countries.

After an initial analysis of the space market, is important to note that the EU countries concentrate 17.25 % of the world space budgets, and the US concentrate 57.82% of them. Currently, the Netherlands spends 143 million dollars, accounting for only 0.2% of the world's budget. Thus, the market would likely have to expand to incorporate at least the EU country members, especially the EU commission, France and Germany which together spend 10.47 % of the world's space budget[a].

3.1.2. Scientific market and demand

Eurocontrol data is used here to get an approximation of the size of the market and its forecast development. This a firm, which has provided space market consulting for a about 20 years[bc], and also provides insights in the optical Earth observing missions. This field of optical imaging is obviously the one for this mission, as the final design satellite will have telescope incorporated in them to monitor the Earth.

The institute comes to the conclusion, that by 2028 the market, that is the spending on Earth observation data would grow by 9.4% each to 2028, that is an increase of 12.1 billion dollars by the end date, having started at 8.1 billion dollars in 2018[de].

All of this growth, is the clear illustration of a constant or rapidly growing demand for Earth observing missions, on both climate issues and military ones.

3.2. Supply

Listed in Table 3.1 are some of the missions, mostly in constellation formats, which fulfill resembling or similar objectives as the one elaborated upon in this report.
Additional information about these missions:

- **Pleides-Neo:** launch mid 2020 [f], 10 years mission lifetime, 550 Meuros investment[g], 0.3 m GSD, from deep blue to panchromatic bandwidths[h]

[a] https://spaceq.ca/euroconsult-releases-its-government-space-programs-report-expenditures-reach-us70-9-in-2018/ [cited 12 June 2020]
[b] https://www.nsr.com/about/ [cited 28 April 2020]
[c] http://www.euroconsult-ec.com/about [cited 28 April 2020]
[d] https://spacewatch.global/2019/11/market-for-earth-observation-data-and-services-forecast-to-grow-by-9-annually-over-next-decade/ [cited 28 April 2020]
[e] https://spacenews.com/forecasts-call-for-rapid-growth-in-earth-observation-market/ [cited 28 April 2020]
[f] https://www.airbus.com/newsroom/press-releases/en/2020/02/pleiades-neo-well-on-track-for-launch-mid2020.html [cited 25 June 2020]
[g] https://satelliteobservation.net/2016/09/15/the-airbus-very-high-resolution-constellation/ [cited 15 June 2020]
[h] https://www.intelligence-airbusds.com/en/8671-pleiades-neo-trusted-intelligence [cited 12 June 2020]

- **Skysat:** latest launch in 31 Oct 2017, 0.72-1 m GSD, 450-900 nm bandwidth, constellation sub-daily temporal resolution[i]
- **Afternoon Constellation:** launched between 2002-2014, wide range of bandwidths[j]
- **Spire:** first launch in 2013, 150M$+ funding[k], covers the globe at least 100 times a day [l]
- **SPOT:** launched in 09/2012 and 06/2014, 10 years mission lifetime, private development costs[m], 26 days temporal resolution, sun synchronous orbit[n]
- **The Vivi-i Constellation:** launches in 2020, 5 launch groups, 12 hours temporal resolution, sun synchronous orbit[o], '3 band true colour, Bayer filter', 1 meter GSD, 5.2 km square image[p]
- **DMC3:** minimum 7 years mission length, launches between 2002 and 2015, oldest operational satellite launched in 2005, 1m to 32m GSD, MS and PAN wavelengths monitored[q]
- **KOMPSAT-3A:** oldest still operational satellite launched in 07/2006, 28 days temporal resolution, 0.55-5.5 m GSD, 450-900 nm bandwidth[r]
- **Planet constellation:** Sun synchronous orbit, first launches in 2013, 3.7-4.9 m, 2-3 years lifetime per satellite [s]

Table 3.1: Comparison with similar Earth Observing missions

Mission	Number of Satellites	Res. [m]		Altitude [km]	Bandwidths	T. Reso.	What is observed
		Pan	MS				
Pleides -Neo	4	0.3		620	Panchro-matic - deepblue	-	Earth images
SkySat	15	0.9	2	500-700	450-900 nm	sub daily	Earth images
Afternoon Constellation	6 different satellites	-		700	very wide	very varying	Vegetation, cloud study greenhouse gasses, water circulation, CO_2
Spire	80	-		400-600	-	14/15 min	Maritime, aviation and weather pattern
SPOT	2 (SPOT6 and SPOT7)	1.5	6	832	NIR	26 days	Earth images
The Vivid-i Constellation	15	0.6		500	3 band true colour	12 hours	Full-color video/still Earth observation
DMC3	3	0.8		651	blue, green, red, NIR	multiple	Earth images
KOMPSAT-3A	1	0.4	1.6	528	450-900 nm	28 days	EO images and IR images
Planet	100-150	3.7/4.9	-	475	420-900 nm	-	EO images

[i] https://earth.esa.int/web/guest/missions/3rd-party-missions/current-missions/skysat [cited 12 June 2020]
[j] https://atrain.nasa.gov/intro.php [cited 12 June 2020]
[k] https://www.newspace.im/constellations/spire [cited 12 June 2020]
[l] https://earth.esa.int/web/sppa/activities/edap/atmospheric-missions/spire [cited 15 June 2020]
[m] https://earth.esa.int/web/eoportal/satellite-missions/s/spot-6-7 [cited 15 June 2020]
[n] https://earth.esa.int/web/guest/missions/3rd-party-missions/current-missions/spot-6-7 [cited 15 June 2020]
[o] webapps.itc.utwente.nl/sensor/getsat.aspx?name=Vivid-i%20Constellatio [cited 15 June 2020]
[p] https://earthi.space/constellations/ [cited 15 June 2020]
[q] https://directory.eoportal.org/web/eoportal/satellite-missions/d/dmc-3 [cited 15 June 2020]
[r] https://directory.eoportal.org/web/eoportal/satellite-missions/k/kompsat-3a [cited 15 June 2020]
[s] https://directory.eoportal.org/web/eoportal/satellite-missions/content/-/article/flock-1-imaging-constellation [cited 26 June 2020]

3.3. SWOT analysis

A SWOT analysis (strength, weaknesses, opportunities and threats) of the mission at hand, is of course useful in a market analysis, as it shows how the potentially developed product fits into the analysed market. It also allows to find any direct competitors.

Strengths: these are, as the name suggests, the aspects which add value to the mission giving interest to a potential client.

- A stabilising platform is being developed at TU Delft for low altitudes (200-500 km)[1].
- Having a constellation of satellites allows for a sub-hour temporal resolution, see Chapter 13, a rarity.
- Monitoring wavelengths infrequently monitored from space, especially thermal infrared.
- Combining both an environmental and defence mission

Weaknesses: These are the aspects which can be improved upon, to become strengths in different design phases, and which, if not remedied, will be considered negatively by the customer.

- The design team is comprised of student engineers, which only have bachelor level knowledge, with some master level inputs.
- The DDST (Delft deployable telescope), is still not fully developed. Thus total costs or sizing are not fully known.
- More research needs to be made on the DDST baffle and stabilising platform.

Opportunities: these are a direct result of strengths, and positive aspects of the market which do or will exist in the future.

- The increase in demand over the next ten years, in optical Earth observation, can, if channelled properly, allow for high investments for this mission.
- Launch costs are lowering, making launching mega-constellations a more achievable possibility [1, [t]].
- Increased competitiveness in this relatively new market of satellite constellation will inevitably drive further technological improvements, in particular with regards to imaging, but also for stabilisation in LEO orbits

Threats: as opportunities present aspects which could become beneficial for the product, threats are contextual items which can affect negatively the outcome of the mission.

- It is complicated to market and sell a defence related product, due to security concerns.
- Due to the increase in demand, competitors are likely to arise.

3.4. Market viability

Having done both a demand and supply analysis, as well as a SWOT analysis, it is possible to assess whether the constellation which is developed in this report is a viable option or not.

It can be said that the Earth observing constellation being developed here, is performance wise unique for two major reasons.

The exceptional high amount of satellites, nearly beats all studied missions, with regards to temporal resolution.

The fact that this constellation system will monitor the thermal infrared spectrum from space, are both traces of its uniqueness.

Moreover, the mission will most likely be relatively expensive compared to other missions, but can be made affordable if defence and environment government budgets are used for it. Requirements are therefore set to a total of a 2 billion initial investment and total of an additional 2 billion spent over 20 years. However, it is believable, that with increasing space budgets, increasing market share of optical Earth imaging, and the right investment strategy, that this mission is financially viable. This will be further investigated, with different temporal resolutions in Chapter 23. Finally, investments can also be driven by the fact that this is a multi-purpose mission.

[t] https://www2.deloitte.com/us/en/pages/public-sector/articles/commercial-space-launch-cost.html [cited 15 June 2020]

4 Technical Risk Analysis

The technical risks that can arise during the operational phase of the mission and their proposed mitigation strategies are discussed in this chapter. A pre- and post-mitigation risk map are also displayed.

4.1. Risk assessment

In Table 4.1, technical risks (TR) regarding environment (E), mission (M), subsystems and systems integration (SI) are grouped and shown. For each risk, the driver, the consequence, the probability (Prob.) and the impact (imp.) are shown. The probability and impact definitions can be seen below. It is worth noting that environmental and other risks (S) have another definition of impact than the subsystem and system integration risks. This was done as the environmental and other risks consider the entire mission while subsystem and system integration risks only refer to one satellite within the constellation.

The following convention has been used when assigning probability points to the risks:

- 1 = Nearly impossible
- 2 = Improbable
- 3 = Probable
- 4 = Frequent

The following convention has been used when assigning impact points to the environmental and mission risks, based on the convention used by Hamann and van Tooren [2]:

- 1 = Negligible: Inconvenience or insignificant impact
- 2 = Marginal: Degradation of secondary mission or small reduction in technical performance
- 3 = Critical: Probability of mission success is decreased or some reduction in technical performance
- 4 = Catastrophic: Mission failure or major impact on performance

The following convention has been used when assigning impact points to the subsystem risks:

- 1 = Negligible: Negligible impact on spacecraft performance: nominal operations can continue without major setbacks
- 2 = Marginal: Small reduction in spacecraft performance
- 3 = Critical: Significant reduction in spacecraft performance, mission objective partially compromised and requirements are not met.
- 4 = Catastrophic: Spacecraft cannot contribute to reaching the mission objective

The risks listed in Table 4.1 have been determined by the group through brainstorming. The first three environmental risks are tied to events that can occur in space and are related to the main items of danger in space: other satellites (which can be in the form of space debris) and radiation (caused by the sun or by other celestial bodies). The fourth environmental risk is caused by hostile environment or by natural disasters on Earth and can have a big impact on the mission as the ground segment is a crucial component of the mission. The mission risks regard some risks that are mission related (launch and nominal operations respectively). The general risk describes a risk that can be encountered in each subsystem. The subsystem risks consists of risks that only occurs in a specific subsystem. Finally, the system integration risks refer to risks occurring during the assimilation of multiple (sub)systems.

Table 4.1: Technical risks

ID	Risk	Driver	Consequence	Prob.	Imp.
TR-E-01	Space debris collision	High density of space debris in LEO	Obliteration of satellite(s), loss of data and money, creation of more debris	2	2
TR-E-02	Solar radiation flares	Enhanced solar activity	Altering of the on-board computers state resulting in unwanted control sequences	2	2

Table 4.1: continued from previous page

ID	Risk	Driver	Consequence	Prob.	Imp.
TR-E-03	Cosmic radiation flares	Unpredictable changes in radiation activity from celestial bodies	Altering of the on-board computers state and outputting of unwanted control sequences	2	2
TR-E-04	Damage to ground equipment	Unforeseen events, e.g. earthquakes, hurricanes, terrorist attacks, etc.	Ground station is unable to send commands and to receive data	2	2
TR-M-01	Failure of the launch vehicle	Due to structural failures or propulsion failures e.g.	Satellites can not be launched causing launch delays and increased mission costs	1	3
TR-M-02	In-orbit constellation collision	Calculations mistakes about position of other satellites, propulsion system malfunction	Destruction of multiple satellites: loss of money and data	2	3
TR-GEN-01	Miscommunication at ground station or on-board satellite	Mistake in command code or on-board computer misdirects the command	Subsystems may disrupt or kill the mission by causing damage to the satellite	1	3
TR-PROP-01	Propulsion system overheating	Thermal control miscalculations	Reduced lifespan	3	2
TR-PROP-02	Lower available power for propulsion system	Solar array misalignment, poor power management	Reduced thrust capabilities	3	2
TR-PROP-03	Propellant leakage	Tank not sealed properly	Not enough propellant to perform manoeuvres	1	4
TR-PROP-04	Spacecraft contamination	Due to thruster erosion and non-propellant flux	Inefficient satellite thrust and damage to other components	2	3
TR-PROP-05	Ion charge plasma from thruster creates noise	High electrical energy and plasma generated in close proximity to instruments	Inaccurate data collected by on-board payload and other instruments	3	2
TR-GNC-01	Position and navigation signal is blocked	Interference, spoofing attack, signal blockage or constellation failure	Movement of spacecraft cannot be controlled	2	3
TR-PAY-01	Stops functioning for unknown reasons	Possibly due to temperature differences or radiation	Satellite can not function properly so no images can be made	2	3
TR-PAY-02	Sensor reaches non working temperatures	Failed thermal control	Sensor stops working meaning photons can not be converted into images	2	3
TR-POWR-01	Internal short circuiting	High current densities and local temperatures inside the batteries	No power available for the different (sub)systems	1	3

Table 4.1: continued from previous page

ID	Risk	Driver	Consequence	Prob.	Imp.
TR-POWR-02	External short circuiting	Incorrect battery usage and incorrect power connections between systems	May cause fire/rupture	1	2
TR-POWR-03	Extra solar array degradation	Due to atmosphere/debris	Less power can be generated	1	2
TR-POWR-04	Battery charge-discharge failures	Too many discharge cycles	Not enough or no power can be supplied to the other subsystems	1	2
TR-THRM-01	Overheating or freezing of an instrument	Temperature sensor failure, active thermal control failure	Potential component failure or reduced component performance	2	3
TR-THRM-02	Louver blade failure	Mechanism failure	Reduced heat radiation from damaged louver	3	2
TR-THRM-03	Micro meteorites puncturing the coatings	Exposure of surfaces to outer space	Reduce coating effectiveness	3	2
TR-THRM-04	TIR temperature sensor failure	Sensor overheating, poor sensor placement	Potential overheating due to erroneous temperature readings, mission objective compromised	2	3
TR-THRM-05	Differential expansion of a deployable structure	Exposure to harsh thermal environment, interaction with thermal blankets during deployment	Failure of deployment	2	3
TR-C&DH-01	Data storage device malfunction	Overheating	No/less data stored, storage requirements not met	2	2
TR-COMMS-01	Interference from other communication frequencies	Satellites close to each other and within the same bandwidth	Distorted signal	2	1
TR-COMMS-02	Unable to communicate with spacecraft	Misalignment with ground station antenna	No communication possible, commands and data cannot be exchanged	2	3
TR-STRC-01	Failure to deploy the telescope	Assembly errors, deployment mechanism failure	No images can be taken by the satellite, the mission objectives can not be achieved	2	3
TR-STRC-02	Failure during separation from launcher	Separation command not received	Satellites can not be released from launcher: increasing costs and delays progress	2	3
TR-STRC-03	Failure to get rid of the payload fairing	Explosion failed	Orbit not reached	2	3

Table 4.1: continued from previous page

ID	Risk	Driver	Consequence	Prob.	Imp.
TR-STRC-04	Failure in solar panel deployment	Assembly error, mechanism failure	No power can be generated	2	2
TR-STRC-05	Misalignment of solar panels to the sun	Error in calculations, mechanism failure	Very little to no power can be generated	2	3
TR-ADCS-01	Failure of a magnetorquer	Malfunction of component, harsh environment	Momentum dumping cannot be performed	2	2
TR-ADCS-02	Failure of the magnetometer	Malfunction of component, harsh environment	Magnetic field cannot be determined	2	1
TR-ADCS-03	Failure of multiple reaction wheels	Reaction wheel cannot handle momentum storage, overused	Loss of attitude control	3	2
TR-ADCS-04	Failure of a gyro	Malfunction of component, harsh environment	Spacecraft needs to go into safe mode	1	2
TR-ADCS-05	Failure of both star trackers	Malfunction of component, harsh environment	Spacecraft unable to determine its attitude	1	4
TR-ADCS-06	Loss of attitude stability during a limited time	Satellite is hit by space debris	Payload produces unusable imagery	1	2
TR-SI-01	Compromises between subsystems	Interaction of subsystems necessary, miscommunications	Leads to bad performance on individual aspects	2	3
TR-SI-02	Different assumptions used in subsystem designs	Miscommunications between subsystems	Error in design, affects performance	3	2
TR-SI-03	Final product can not be verified/validated	Design does not meet requirements	Redesign necessary, malfunction or bad performance	2	4

Table 4.2 presents a risk map for the risks stated above, with the probabilities on the left side and the impact on top row of the table. To generate this table the risk assessment matrix from Hamann and van Tooren [2] is used. A combination of occurrence probability and impact, defined in Table 4.1 gives rise to the associated risk.

Table 4.2: Risk map pre-mitigation

	Negligible (1)	Marginal (2)	Critical (3)	Catastrophic (4)
Nearly impossible (1)		[POWR-02], [POWR-03], [POWR-04], [ADCS-04], [ADCS-06]	[M-01], [POWR-01], [GEN-01]	[ADCS-05], [PROP-03]
Improbable (2)	[COMMS-01], [ADCS-02]	[E-04], [E-01], [E-02], [E-03], [C&DH-01], [STRC-04], [ADCS-01]	[M-02], [PROP-04], [GNC-01], [PAY-01], [PAY-02], [THRM-01], [THRM-04], [THRM-05], [COMMS-02], [STRC-01], [STRC-02], [STRC-03], [STRC-05], [SI-01]	[SI-03]
Probable (3)		[THRM-03], [ADCS-03], [SI-02], [PROP-01], [PROP-02], [PROP-05] [THRM-02]		
Frequent (4)				

Low risk | Moderate risk | Significant risk | High risk

4.2. Risk management

To reduce or prevent the risks given by Table 4.2, mitigation is used. In Table 4.3, each risk is associated to a mitigation plan. Furthermore, the mitigated (”mit.”) probability and impact are given, by which are meant the probability and impact if the mitigated plan is executed.
The risk mitigation plans shown in Table 4.3 were also found during a brainstorming session. Looking at Table 4.3, the mitigation plans can also be grouped. For instance, the space environmental risks can be battled by using a shield on the satellites. This shield will absorb most of the heat and radiation emitted from various sources like the Sun. As for **TR-E-04**, making sure that the ground station can handle storms and earthquakes consequently decreases the impact on the mission. The mission risks can be mitigated by adding larger margins to the design and budgets. This will decrease the impact of the risk. Looking at the subsystem risks, the general approach to mitigation is to either use flight proven and high quality components and parts or perform multiple tests. The system integration risks can mainly be mitigated by ensuring a comprehensive and efficient communication between group members.

Table 4.3: Mitigation plan

ID	Risk	Mitigation Plan	Mit. Prob.	Mit. Imp.
TR-E-01	Space debris hitting satellites	Identify potential incoming debris and maneuver the satellites	1	2
TR-E-02	Solar radiation flares	Use metal shield or material to protect the satellite from harmful rays	2	1
TR-E-03	Cosmic radiation flares	Use a shield or metallic materials to protect from radiation rays	2	1
TR-E-04	Damage to ground equipment	Reinforce the foundation of the equipment, e.g. improve antenna structure	1	2

Table 4.3: continued from previous page

ID	Risk	Mitigation Plan	Mit. Prob.	Mit. Imp.
TR-M-01	Failure of the launch vehicle	Ensure LV is thoroughly checked and quality control occurs regularly. Add Fail safe systems	1	2
TR-M-02	In-orbit constellation collision	Use sensors on satellites providing information on the positions of the other satellites, so if necessary adjust position to prevent collision (see Chapter 14)	1	2
TR-GEN-01	Miscommunication at ground station or on-board satellite	Use good procedures and implement error checking code	1	2
TR-PROP-01	Propulsion system overheating	Controlling burn time and propellant temperature	2	2
TR-PROP-02	Lower available power for propulsion system	Ensure proper power supply to propulsion system	2	2
TR-PROP-03	Propellant leakage	Design fail safe propellant tank, include early leak detection system to modify mission characteristics as soon as leak starts	1	2
TR-PROP-04	Spacecraft contamination	Protective casing over thruster	2	1
TR-PROP-05	Ion charge plasma from thruster creates noise	Science instruments are shielded and do not face thruster plumes	2	2
TR-GNC-01	Position and navigation signal is blocked	Use software that can predict position	1	3
TR-PAY-01	Stops functioning for unknown reasons	Develop a deep and detailed SWOT, qualitative analysis and scenario building	1	3
TR-PAY-02	Sensor reaches non working temperatures	Increase testing for thermal control and make improvements	1	2
TR-POWR-01	Internal short circuiting	Use detection and isolation circuitry to keep the battery temp. <40 °C	1	2
TR-POWR-02	External short circuiting	Use multicell batteries	1	1
TR-POWR-03	Extra solar array degradation	Include extra margins for solar panel degradation and use fail safe system	1	1
TR-POWR-04	Battery charge-discharge failure	Use multicell batteries	1	1
TR-THRM-01	Overheating or freezing of an instrument	Apply thermal margins when testing	1	2
TR-THRM-02	Louver blade failure	A single point failure is associated with one blade, so make them independently actuated	3	1

Table 4.3: continued from previous page

ID	Risk	Mitigation Plan	Mit. Prob.	Mit. Imp.
TR-THRM-03	Micro meteorites puncturing the coatings	Apply multi-layer/collision resistant coatings	3	1
TR-THRM-04	TIR temperature sensor failure	Use multiple sensors to add redundancy in case of failure	2	1
TR-THRM-05	Differential expansion of a deployable structure	Test deployable mechanisms while simulating harsh thermal environment	1	3
TR-C&DH-01	Malfunctioning of data storage devices	Have redundant storage capacity	2	1
TR-COMMS-01	Interference from other communication frequencies	Make use of little used radio frequencies or optical communication	1	1
TR-COMMS-02	Unable to communicate with spacecraft	Use inter satellite crosslinks to communicate	1	3
TR-STRC-01	Failure to deploy the telescope	Test the deployment of the telescope and improve the structural integrity where necessary	1	2
TR-STRC-02	Failure during separation from the launcher	Thoroughly check launcher and satellite interface, separation mechanism should be tested and inspected	1	3
TR-STRC-03	Failure to get rid of the payload fairing	Thoroughly check separation mechanism should be tested and inspected	1	3
TR-STRC-04	Failure in solar panel deployment	Spring mechanism is relatively safe; reliable thermal knife should be used and tested	2	1
TR-STRC-05	Misalignment of solar panels to the sun	A possibility of using non-rotating solar arrays could be considered; thicker cable protection could be used to prevent wear out of cables	2	1
TR-ADCS-01	Failure of a magnetorquer	Impact is reduced by using inherently redundant torquers	2	1
TR-ADCS-02	Failure of the magnetometer	Use a magnetic model for magnetorquing as a backup for magnetometers	1	1
TR-ADCS-03	Failure of multiple reaction wheels	Use of high quality, high reliability components, with extensive testing	1	2
TR-ADCS-04	Failure of a gyro	Use flight proven gyros	1	1
TR-ADCS-05	Failure of both star trackers	Use flight-proven highly reliable hardware and redundant sensors	1	3
TR-ADCS-06	Loss of attitude stability during a limited time	Use collision avoidance systems (see Chapter 14)	1	1
TR-SI-01	Compromises between subsystems	Perform internal trade-offs and communicate decisions	2	1

Table 4.3: continued from previous page

ID	Risk	Mitigation Plan	Mit. Prob.	Mit. Imp.
TR-SI-02	Different assumptions used in subsystem designs	Improve communication and check for consistency	1	2
TR-SI-03	Final product can not be verified/validated	Check requirements and perform intermediate verification/validation on subsystems	1	3

Most of the risks mitigated in Table 4.3, were turned into risk requirements. For example, requirements related to collisions risks can be found in Chapter 14, requirements on use of multicell batteries in Chapter 17 and risk requirement on thermal control in Chapter 18 to name a few. In Table 4.4, the mitigated risks are shown in an improved risk map.

Table 4.4: Risk map post-mitigation

	Negligible (1)	Marginal (2)	Critical (3)	Catastrophic (4)
Nearly impossible (1)	[ADCS-02], [COMMS-01], [POWR-02], [POWR-03], [POWR-04], [ADCS-04], [ADCS-06]	[E-01], [E-04], [M-01], [M-02], [GEN-01], [ADCS-03], [SI-02], [PROP-03], [STRC-01], [PAY-02], [POWR-01], [THRM-01]	[SI-03], [ADCS-05], [STRC-03], [GNC-01], [STRC-02], [PAY-01], [THRM-05], [COMMS-02]	
Improbable (2)	[E-02], [E-03], [PROP-04], [SI-01], [THRM-04], [C&DH-01], [STRC-04], [STRC-05], [ADCS-01]	[PROP-01], [PROP-02],[PROP-05]		
Probable (3)	[THRM-02], [THRM-03]			
Frequent (4)				

Low risk | Moderate risk | Significant risk | High risk

As it can be seen in Table 4.4, most of the risks are now in the 'low risk' zone, by decreasing their impact, probability or both. On the other hand, there are still some risks left in the moderate risk zone. They may be lowered even further by performing tests and analysis and investigating in state-of-the-art technology, but that has to be within the budget and time resources of the team.

5
Sustainable Development Strategy

In an effort to ensure sustainability, it is considered throughout the design and various aspects of sustainability are identified and described. These aspects subsequently form a guide to analyse design choices in terms of sustainability. The aspects themselves are described in Section 5.1 while the mission impact to sustainability is addressed in Section 5.2. This chapter is based on the sustainable development strategy presented in the Baseline Report [3] and Midterm Report [4]. Additionally, requirements relating to the sustainability of the project have been described in Chapter 7.

5.1. Aspects of sustainability

In this chapter, six aspects of sustainability are addressed. First they are explained to be used as a guide for the subsystem level design, then each is given a brief overview on how it was treated throughout the design is given, this is usually expanded on further in the relevant subsystem and mission design chapters.

1. **Sustainable production and distribution** relates to the reduction of: hazardous byproducts, the generation of excess waste, costly or time-consuming methods, and other similarly unsustainable practices. It also relates to designing a product with minimal assembly time and risks. Reducing the need for transportation of the product to assembly and launch sites is a recommendation for further research.
2. **Sustainability of resources** includes materials considerations based on environmental impact and availability. This is majorly treated in Chapter 14, the propulsion subsystem, the choice of Krypton is considered an unsustainable one due the energy intensive nature of harvesting, however attempts will be made to reduce this, and chemical propulsion would have been infeasible due to mission length.
3. **Mission sustainability** mainly implies the environmental impact of the launch and potential contributions to space debris. The launch has been considered however there are limitations to what can be achieved with regards to sustainability of the launch, a recommendation for the future would be to look into more sustainable fuel replacements for launchers, as the number of launchers is set by the number of orbitals required and can not be improved on for sustainability. Space debris contribution will be reduced through collision avoidance and de-orbiting at end of life, this is treated in Chapter 14. Additionally, for risks with high probability and critical or catastrophic impacts mitigation strategies are given to reduce the probability of a satellite prematurely becoming dysfunctional, more information can be found in Chapter 4.
4. **End-of-life sustainability** space debris contribution is decreased by requiring obsolete satellites are de-orbited. Additionally, it needs to be ensured that the satellite will completely disintegrate during reentry without the release of toxic gas. This can not yet be assured but would need to be further investigated.
5. **Economic sustainability** is analysed and continuously updated by considering the requirements set on the cost of development and operation of the system. Cost estimations and market analysis give information regarding the economical sustainability of the mission. Furthermore, the costs associated with the development and manufacturing of the satellites are reduced through series production.
6. **Social sustainability** the social sustainability of the project includes issues such as: Light pollution, interference with radio waves and privacy issues. The latter two are addressed in, Chapter 16, the communication and data handling systems by ensuring the international regulations regarding privacy are met. The issue with light pollution is discussed in the section on constellation design, however mitigations to this, including coating options, are not treated due to the thermal coating requirements.

5.2. Mission contribution to sustainability

Finally, in the discussion on sustainability it is interesting to look at how the constellation can contribute to reducing environmentally impacting practices on Earth. Environmental emissions will be monitored on a local scale, allowing the opportunity to see when these levels reach high concentration. This could promote sustainable practices on land and expose emission violations. Monitoring for problems such as fires provides valuable information to allow for early mitigation of future occurrences of the same problem. Some practices that have become illegal due to sustainability concerns can also be monitored and possibly prevented, such as, dumping massive amounts of greenhouse gases.

6

Reliability, Availability, Maintainability and Safety Analysis

In order to ensure that the operation of the system goes as planned and the performance of the system does not deteriorate with time, reliability, availability, maintainability and safety of the whole system should be analysed.

6.1. Redundancy philosophy and reliability

Reliability of some of the subsystems and components could be improved by adding a redundancy. However, for many of the components, redundancy adds complexity to the system and significantly increases the total mass and cost. Therefore more reliable components, high quality production techniques and more extensive testing should be used as additional types of reliability.

After 7 years (1 generation) it is estimated that the failure rate of one satellite is approximately 6 % [5]. On one hand, MIRA satellites have complicated payload (deployable telescope), which should increase failure rate, but on the other hand constellation has many satellites that are the same, so the failure rate should decrease. By taking those factors into account it was estimated that the failure rate is 3 % which means that 24 satellites in one generation are expected to fail which is approximately 1 satellite per orbital plane.

6.1.1. Subsystem level redundancy

Some of the subsystems include redundant components in their design to improve reliability. This is mostly useful for components that are identified as specifically risk-full and have a major wear-out risk. For example, the ADCS subsystem includes redundant sensors. The thermal subsystem also includes redundant temperature sensors. The GNC subsystem has a redundant GNSS signal receiver. Those redundant components do not significantly increase the total mass and cost but significantly improve the reliability of the system as those components have relatively high probability of failure [5] and in case they fail, the performance of satellite seriously decreases.

For other subsystems it is not viable to include redundancy, because of the increase in size, mass and price of the overall satellite. For instance, the payload or the structure can not include factors of redundancy. The payload for the simple reason that the satellite can not double its telescope as that would essentially increase the size of the satellite roughly by a factor, and the price increase would be needlessly high, and for the structure, by definition there can not be two structures. Therefore, for such subsystems other types of reliability should be considered.

6.1.2. Constellation level redundancy

It is decided that there will be 1 redundant TIR satellite for each TIR orbital plane and 2 redundant (1 MS and 1 TIR) satellites for TIR+MS orbital planes. So, in total 36 redundant satellites per generation. In case failure of multiple satellites in one orbital plane will occur, Vega rocket with 1-2 new satellites will be launched to replace faulty satellites. There can be 4 launches of Vega rocket per generation with 2 new satellites in each rocket, so 4-8 extra satellites could be launched.

6.1.3. Other types of reliability

Reliability can also be seen through the prism of performance per subsystem. Naturally, off the shelf products for subsystems are more reliable due to flight proven technology and their reliability records, so that reliability does not have to be assessed. Therefore reliable off the shelf components are used as much as possible. A problem with off the shelf components is that often they are not optimal in terms of mass, size, performance for the mission design so a custom component has to be designed. It is identified that it could be possible to achieve decent reliability of custom developed components for the constellation due to in-depth testing and due to a reliability record after the first generation of satellites.

High quality production techniques including inspection and testing for component production and for the overall subsystem should be used to increase the reliability. These techniques should be implemented beforehand into production cycle to have high component tolerances. Once the techniques are implemented before

the start of production, they would significantly benefit production in terms of component quality and reliability. In addition to that, proper testing of the spacecraft on the ground and in-orbit testing of a few test satellites could reveal reliability issues of some of the components.

It is identified that ADCS and payload subsystems have to be developed and are complicated due to the presence of many mechanically moving parts. Reliability of those subsystems is difficult to quantify. Therefore, during the development of those subsystems it should be aimed for extremely high reliability, especially with regards to payload, as it is a key subsystem with respect to the mission.

6.2. Availability

The availability of the constellation depends on several aspects. The first one is the time it takes to fix or replace satellite with a failure or damage. It was estimated that at most 7 satellites per generation could fail in order to satisfy the availability requirement. The second aspect is about how long and how often do some satellites can not perform their operational tasks due to insufficient amount of power at some of the orbit locations. It is expected that there would always be sufficient power for payload operation due to sufficient battery. By dealing with the above mentioned aspects, it is ensured that the requirement MIRA-USR-SR-4 is satisfied.

If the reliability of the whole constellation is assured, that is if there is always the minimum number of satellites for full operation, the availability of the mission performance is as follows. The **TIR** satellite will be able to make a whole Earth coverage every 30 minutes, that is including populated and non-populated area. The **MS** satellite will be able to make earth coverage every 60 minutes during daylight. At night the MS telescope will not be able to work.

6.3. Maintenance

Maintaining individual satellites while they are in operation is unfeasible. Therefore, maintenance will primarily consist of having slightly more than necessary satellites in orbit. In this case, if a satellite fails it will be de-orbited and its place can be filled by an extra satellite in that orbit. If this is not possible, then maintenance for this constellation consists of de-orbiting failed satellites and launching new satellites using Vega rocket. Cost of redundant satellites and 4 Vega launches is included in the total cost in Section 21.1. There is also a possibility of launching a satellite as a secondary payload on board of a rocket for some other mission. This option needs further investigation, but is preferred over the use of a Vega rocket due to cost reasons. Transition from one generation to the next one by de-orbiting all the old satellites and launching new ones is expected to be the major part of maintenance.

6.4. Safety

There can be two aspects related to safety: human related safety and technical or system safety. Human safety is virtually non-existent during the satellite's operational lifetime. However, there are some aspects which have to be taken into account related to pre-operational life and post-operational lifetime. Firstly, during the production of satellites, only registered, already working and certified factories and testing facilities should be used. Also, the use of toxic materials is minimised during production. Krypton is used as a propellant and there are two most common ways to obtain krypton. One way to obtain it is from air using distillation-liquefaction process, whereas the other way is to recover it from spent fuel rods of nuclear power plant[a]. The first way of obtaining krypton will be used. In addition to that, risk of explosion of the propellant tank is minimised by keeping the tank at the temperature controlled environment. The tank should be filled only for the testing and for the launch to reduce the probability of explosion. Moreover, at the launch, already proven launchers should be used to minimise the risk of failures during the launch that would provoke any human related physical harm. Lastly, the satellites, when de-orbited, should fully disintegrate into the atmosphere to avoid any parts landing on the Earth and causing any casualties. Minimum amount of titanium and steel components are used in the structure of the satellite as tough components from titanium and steel could survive the re-entry into the atmosphere and hit the Earth[b].

Furthermore, system safety relates more to the well being of the subsystems and ensuring their integrity. Harsh environment and interference with other systems could cause threats to some of the subsystems. This is considered during the structure's design, thermal system design and integration to ensure that there are appropriate operational conditions for each of the subsystem.

[a] https://www.chemicalbook.com/ProductChemicalPropertiesCB3305472_EN.htm [cited 16 June 2020]
[b] https://www.youtube.com/watch?v=wkJ3vEUiC9g [cited 16 June 2020]

7 Requirements Overview

This chapter provides the vital requirements that form the base for the design. First, the nomenclature is explained, followed by the user requirements. From these, the key and driving requirements for a successful mission are highlighted. Then, the overall system requirements of the spacecraft are mentioned. The detailed sub-system level requirements are located in their corresponding chapters.

7.1. Requirements nomenclature

The parent/user requirements are labelled with **MIRA-USR-XXX-YY**, where ”USR” stands for user, ”XXX” denotes one of the following: mission (MIS), safety and reliability (SR), sustainability (SUS), cost (COST), or miscellaneous (MISC), and ”YY” denotes the number. These requirements lead to child (or lower level) requirements.

The lower level requirements consist of the various subsystems. The requirements are classified into types such as performance (PERF), functional (FUNC), and operational (OPS) requirements. They are labelled in the following way: **MIRA-AAA-BBB-YY** ; *MIRA - Subsystem - Classification type - Requirement*.

7.2. User requirements

The requirements presented in Table 7.1 were provided by the user and were derived from the Project Guide Booklet (PGB) [1]. In the Midterm Report (MR)[4], MIRA-USR-MIS-1, stating that the system shall monitor an area of 100x100 km between +/-70° latitude every 5 minutes, was removed in accordance with the customer. Moreover, MIRA-USR-MIS-1, stating that the system shall monitor the populated land Earth every 30 minutes, was changed into MIRA-USR-MIS-12 and MIRA-USR-MIS-13.

Table 7.1: User requirements

Requirement ID	Requirement	Origin
MIRA-USR-MIS-2	The system shall have an on-board retention of 3 months.	PGB
MIRA-USR-MIS-3	The system shall monitor the whole Earth every 12 hours.	PGB
MIRA-USR-MIS-4	The system shall downlink the monitored data within 2 hours.	PGB
MIRA-USR-MIS-6	The system shall downlink the footage of an event of interest (as defined in Chapter 11) in real time.	PGB
MIRA-USR-MIS-7	The system shall monitor the thermal infrared band (8 µ – 12 µ) with a ground sampling distance of 5 m.	PGB
MIRA-USR-MIS-8	The system shall monitor CO_2, CH_4, NO_2 emissions using narrow-band optical imaging with a ground sampling distance of 10 m.	PGB
MIRA-USR-MIS-9	The operational lifetime of satellites within the network shall be 5 years.	PGB
MIRA-USR-MIS-10	The overall mission duration of the network shall be 20 years.	PGB
MIRA-USR-MIS-11	The satellites shall be launched into a Low Earth Orbit below 500 km.	PGB
MIRA-USR-MIS-12	The system shall provide a minimum of 60 minutes temporal resolution when monitoring emissions.	MR
MIRA-USR-MIS-13	The system shall provide a minimum of 30 minutes temporal resolution when monitoring in the thermal infrared region.	MR
MIRA-USR-SR-1	The remote control access of the satellites shall be encrypted.	PGB
MIRA-USR-SR-2	The down-linked data shall be encrypted.	PGB
MIRA-USR-SR-3	The satellites in the constellation shall not collide with any other spacecraft during their de-orbit.	PGB
MIRA-USR-SR-4	The constellation shall have an availability of 99 % of the orbital period.	PGB

Table 7.1: continued from previous page

Requirement ID	Requirement	Origin
MIRA-USR-SR-5	The constellation shall be built-up in steps, as defined in Chapter 22.	PGB
MIRA-USR-SUS-1	The satellites in the constellation shall not collide any other spacecraft during nominal operations.	PGB
MIRA-USR-SUS-2	The satellite design shall include collision avoidance features.	PGB
MIRA-USR-SUS-3	Satellites shall be de-orbited within 5 years after their nominal operational lifetime.	PGB
MIRA-USR-SUS-4	The environmental impact of the launch shall be minimised for the derived launch mass.	PGB
MIRA-USR-SUS-5	The environmental impact of the launch shall be minimised for the orbital distribution.	PGB
MIRA-USR-COST-1	The initial investment for an in-orbit qualification (demonstrating all aspects of the full spacecraft bus and including launch cost) shall be less than 200 M€.	PGB
MIRA-USR-COST-2	The total investment cost shall be a maximum of 2000 M€ for the operation of the entire system (including ground segment and launch cost).	PGB
MIRA-USR-COST-3	The operational cost shall be less than 100 M€ per year, including replenishment of dysfunctional and retired satellites (satellite plus launch cost).	PGB
MIRA-USR-MISC-1	All satellites with the same payload (thermal infrared/multispectral) shall use the same generic bus platform.	PGB
MIRA-USR-MISC-2	The Delft Deployable Space Telescope (DDST) shall be used as a baseline for the payload.	PGB
MIRA-USR-MISC-3	The satellites shall be launched using existing and proven launch vehicles.	PGB

7.2.1. Identification of Key and Driving requirements

Driving requirements: The driving requirements, listed in Table 7.2 have remained similar to those in the baseline report. They are divided into four design driving aspects and all driving requirements are mission requirements.

Table 7.2: Driving requirements

Design driving factor	Explanation	Driving requirement ID's
Temporal resolution	Determines number of satellites needed (per payload type).	MIRA-USR-MIS - (1, 2, 3, 4, 5, 6, 12, 13)
Spatial resolution	Determines altitude of the satellites, hence required propellant to keep the satellites in orbit.	MIRA-USR-MIS - (7, 8, 11)
Number of measured bandwidths	Affects number of payload needed (thus satellites) to measure all desired aspects.	MIRA-USR-MIS - (8, 2)
Lifetime	Determines type of attitude, orbit and amount of fuel required.	MIRA-USR-MIS - (9,10)

Key requirements: New requirements of MIRA-USR-MIS-12 and MIRA-USR-MIS-13 are key due to the temporal resolutions characteristics of the mission. The following requirements have been categorised as "key requirements":

- *MIRA-USR-MIS-2, MIRA-USR-MIS-3, MIRA-USR-MIS-4, MIRA-USR-MIS-6, MIRA-USR-MIS-7, MIRA-USR-MIS-8, MIRA-USR-MIS-10, MIRA-USR-MIS-12, MIRA-USR-MIS-13.* All of these requirements are

key, as they are closely related to the mission objective which is the area of interest for the customers of the surveillance system.
- *MIRA-USR-SR-1 and MIRA-USR-SR-2.* These requirements both affect the secure transmission of data. They are therefore key to the customers as the data collected will be used for governmental applications and law enforcement purposes, which makes the data sensitive and unfit for third party usage.

In conclusion, the identified driving requirements will be of utmost importance in the upcoming design phase. Finally, the key requirements will be monitored continuously and the approach taken towards their satisfaction will be presented to the customers during product reviews.

7.3. Overall system requirements

Table 7.3 shows requirements that are relevant for the whole system. The origin column explains from which previous requirement it comes from, and they are linked to different analysis (RAMS, risk, sustainability) in the analysis ref. column. In the compliance matrix that follows in the subsystem chapters a column is added to denote the state of the requirement (met, not met, not verifiable).

Table 7.3: Non-subsystem specific requirements that stem from analysis

ID	Requirement	Origin	Analysis ref.
	Sustainability requirements		
MIRA-SUS-FUNC-1	The spacecraft shall be capable of de-orbiting at mission end.	BLR, MIRA-SUS-SUS-FUNC-3.1	MIRA-USR-SUS-3
MIRA-SUS-FUNC-2	The spacecraft in the constellation shall not produce more space debris.	BLR, MIRA-SUS-SUS-FUNC-3.2	MIRA-USR-SUS-3
MIRA-SUS-FUNC-3	The launch impact of the spacecraft shall be limited by maximising the number of spacecraft per launch.	BLR, MIRA-MISC-SUS-FUNC-3.5	MIRA-USR-MISC-3
MIRA-SUS-FUNC-4	The spacecraft systems shall include redundancy in cohesion with the risk mitigation plan defined in Chapter 4.	BLR, MIRA-MIS-SUS-FUNC-9.9	MIRA-USR-MIS-9
MIRA-SUS-PERF-1	Emissions produced during design and testing shall be minimised.	BLR,MIRA-MIS-SUS-10.1	MIRA-USR-MIS-10
MIRA-SUS-PERF-2	Emissions produced during the life-cycle of the spacecraft shall be minimised.	BLR, MIRA-MIS-SUS-10.2	MIRA-USR-MIS-10
	Scheduling requirements		
MIRA-SHED-PERF-1	The launch of the spacecraft shall nominally occur by the year 2030.	BLR, MIRA-MIS-SHED-10.3	MIRA-USR-MIS-10
	Manufacturing requirements		
MIRA-MANU-PERF-1	The use of toxic materials shall be minimized during production.		RAMS
MIRA-MANU-PERF-2	Krypton shall be obtained from air using distillation-liquefaction process.		RAMS
MIRA-MANU-SUS-1	The constellation shall use series production for the built-up.		Sustainability

Table 7.4 shows the system requirements derived from the performance analysis chapter in the Midterm Report.

Table 7.4: System requirements

Requirement ID	Requirement	Origin
MIRA-SYS-TIR-PERF-1	The total mass of each thermal infrared satellite shall be at most 339 kg.	MR, target value in TIR mass budget
MIRA-SYS-TIR-PERF-2	The total power requirement of each thermal infrared satellite shall be at most 300 W.	MR, target value in TIR power budget
MIRA-SYS-TIR-COST-1	The total cost of each thermal infrared satellite shall be at most 12.5 M€ (FY2020).	MIRA-USR-COST-2 divided by # satellites
MIRA-SYS-MS-PERF-1	The total mass of each multispectral satellite shall be a maximum of 370 kg.	MR, target value in MS mass budget
MIRA-SYS-MS-PERF-2	The total power requirement of each multispectral satellite shall be at most 300 W.	MR, target value in MS power budget
MIRA-SYS-MS-COST-1	The total cost of each multispectral satellite shall be at most 12.5 M€ (FY2020).	MIRA-USR-COST-2 divided by # satellites
MIRA-SYS-FUNC-1	The satellite shall be able to manoeuvre to avoid space debris.	Risk TR-E-01
MIRA-SYS-FUNC-2	The satellite shall have protection from solar and cosmic radiation flares.	Risk TR-E-02
MIRA-SYS-FUNC-3	The satellites shall be equipped with sensors to track positioning of other satellites in same orbit.	Risk TR-M-02
MIRA-SYS-FUNC-4	The satellite shall be equipped with a deployable baffle to ensure the DDST functions properly.	
MIRA-SYS-PERF-1	The number of redundant components in the spacecraft shall be minimum.	RAMS

8

Conceptual Design Summary

During the design phase of this project, five initial concepts have been considered. In this chapter, an overview of these concepts is presented. Furthermore, the mid-term trade process is described and the results are summarised. This chapter shows previously obtained results up till the Mid-Term phase of this project [4].

8.1. Initial concepts

In Figure 8.1, the visual configuration of the five concepts is presented and explained. Concept 1, 2 and 3 consist of one type of satellite platform and they differ in the amount of telescopes per platform. Concept 4 and 5 consist of different satellite platforms, each containing one telescope.

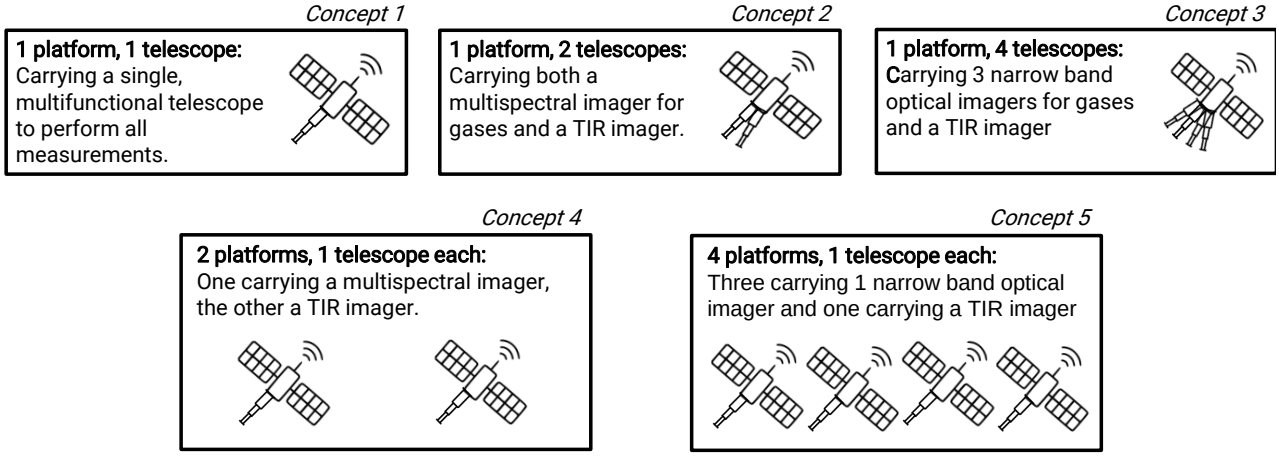

Figure 8.1: Visualisation and description of the five possible concepts

The individual satellites of Concept 4 and 5 are less complex than those of Concept 1, 2 and 3, but will have a higher amount of total satellites, which increases complexity and total cost of the constellation. In general, a multispectral imager adds utility to the system, as more gases can be measured without requiring additional instruments. However, it increases costs and complexity.

8.2. Trade summary

A requirement analysis was performed, after which Concept 1, 3 and 5 were excluded from entering the trade-off. During the trade-off analysis, Concept 2 and 4 were compared on reliability, sustainability and cost. Their weight have been determined using a pairwise weighting method [a], which gives weights to the criteria based on weighing each possible pair of criteria w.r.t. eachother. Reliability was given a 61 % priority, sustainability 17 % and cost 22 %.

Mission Analysis

To monitor the emissions of CO_2, NO_2 and CH_4 in the atmosphere, narrow band optical imagers are used. This relies on the fact that gases absorb light in different wavelengths. For this, both monochromatic narrow band optical imagers or multispectral imagers can be used. Monochromatic imagers use only one narrow spectral band whereas, MS imagers can measure a wider bandwidth. This wider band can be broken up into multiple smaller spectral bands that can be analysed as individual monochromatic bands. For the given mission requirements, the MS imager is chosen as it can monitor different kinds of gasses with only one instrument. A spectral range of 2.65-3.52 µm is identified as a suitable option, which will be split up into multiple smaller bands to be analysed for the gases of interest. For thermal imaging, Planck's law is used to translate an object's temperature to radiation in a certain wavelength range which can be measured by the satellite. This has to be integrated along the desired wavelength, which was specified to be 8-12 µm. This radiation diminishes throughout the atmosphere and with distance. By categorising radiation levels, potential sources can be identified.

[a] https://mechanicalc.com/reference/trade-study

Payload Design

Five payload designs were described where Concepts 1-3 consist of a single satellite platform, Concept 4 of two satellite platforms and Concept 5 of four satellite platforms. The payload design for Concept 1 consists of one telescope for two sets of instruments, one for MS imaging and one for thermal infrared imaging. For Concept 2, the two instruments, TIR and MS, now have their own telescope, where they can monitor different spectral ranges. However, this concept therefore becomes more complex. The two payloads have to co-exist in the same satellite whilst having different properties. In Concept 3, there are four payloads, one for TIR and one for each gas, each with a separate instrument box. For Concept 4, instead of a single satellite platform two platforms are introduced, where one has a telescope for MS imaging system and the other a telescope for TIR imaging system. Concept 5 uses four satellite platforms which are all equipped with their own telescope.

An analysis of the five payload designs was made to check whether they fulfilled the requirements with respect to utility. Including an MS imager contributed to make the design concept continue or not in the design process. This was mostly due to the fact that narrow band imagers require more telescopes since they can not differentiate between different gases. Thus, only the payload designs of Concept 2 and 4 were fit to continue to the trade-off process.

Constellation Design, Characteristics and Launch Configuration

There are no major differences in the general astrodynamic characteristics like orbital altitude and type of orbit for concept 2 and 4. The orbital altitude was set at 300 km and polar orbits were decided upon. The number of satellites for both Concept 2 and 4 were calculated for the temporal resolution requirements leading to 605 and 757, respectively. The number of orbital planes was also calculated for a temporal resolution of 30 minutes.

The main aerodynamic characteristics are the total drag on the satellite and the aerodynamic torque. The total drag at 300 km was found to be equal to 2.88×10^{-3} N and the aerodynamic torque was determined to be zero, as it was assumed that the centre of aerodynamic pressure and the centre of gravity coincide.

The launch options provided by the DOT were briefly described. A table showcasing the cost, payload mass and payload fairing dimensions of multiple launchers compares the launch possibilities and showed that the Falcon 9 rocket looks promising. Furthermore, it was assumed that satellites can be inserted into multiple orbits using one launcher meaning 6 launches would be needed for Concept 2 and 4 launches for Concept 4.

Technical Characteristics Summary for all Concepts

The technical summary details the budgeting of each concept with regards to power, mass, costs and ΔV, based on estimations and product features. For Concept 2, the total: mass is 303 kg, power is 569 W, cost per satellite is 25 M€ and ΔV is 1428 m/s. For Concept 4 MS and TIR satellites, respectively, total mass is 221 and 259 kg, power 482 W for both, cost per satellite around 18 M€ and, ΔV 2401 and 2167 m/s. The nominal data rate for Concept 2 satellites is 119 MB/s, while in Concept 4 the TIR satellites need 68 MB/s whereas the MS need 203 MB/s.

Final trade-off

In the trade summary, Concept 4 is selected as the final design to expand on. This is because it is more reliable, mainly because it only has one telescope, whereas the telescopes in Concept 2 can affect each other's performances. Two telescopes in one platform lead to an increase in the number of moving parts, and there is no researched investigation on it, presumably due to the fact that the field of deployable telescopes is relatively new. The cost is also slightly higher for Concept 2 due to the higher launch costs, caused by higher masses and volume. The summarised trade-off for Concept 2 and 4 is shown in Table 8.1. The main differences of the scoring of the trade criteria can be summarised as follows:

- Payload: The complexity of the spacecraft increases with additional payload, which leads to increased costs for construction. Considering the relatively new field of deployable space telescopes, launching payloads on different spacecraft, such as the case of Concept 4, ensures that failure of one does not affect the other, thereby decreasing financial consequences while keeping a high severity of failure.
- Propulsion subsystem: Concept 4 has a lower severity of failure due to the reduction in lifetime of only one payload operations.
- Communication subsystem: The higher number of satellites required to be communicated with in Concept 4 makes it less favourable in terms of additional ground segment infrastructure and operational costs.
- Power subsystem: The lower power required per satellite for Concept 4 makes it more favourable due to

the reduction in number of components.

- Thermal subsystem: For Concept 4, only the satellites with the TIR payload would be required to have on-board the cryogenic cooling system. This reduces the severity of failure of Concept 4, as they only affect one of the two satellite types.
- Structures and mechanisms: Considering the deployability of the space telescope, the division of payloads onto different satellites reduces the complexity of each satellite. Deployable space telescopes have close to no flight history and hence have relatively low TRL. Concept 2 would have not one, but two telescopes on board, which increases the complexity of the mechanisms and leads to high costs. Concept 4 also has the advantage that the severity of failure due to loss of one payload does not affect the other payload.
- AIT: Higher complexity of satellite architecture for Concept 2 leads to increased costs of AIT. Furthermore, Concept 2 does not allow the mirrors to wrap around the spacecraft body, which is a big downside for integration.
- ADCS: The ADCS design for both concepts will be similar. Therefore, ADCS does not influence the outcome of the trade-off.

Table 8.1: Final trade-off

Criteria / Options	Reliability	Cost	Sustainability
Concept 2	Telescopes affect each others performance, increased number of moving parts, very low TRL for double deployable telescope integration (significant thermal, structural challenges) *Score = 3.2* (blue)	Higher launch cost higher payload cost *Score = 1* (red)	Lower production (kg material) related emissions *Score = 3* (blue)
Concept 4	Lower complexity, significant amount of proposed missions and advanced designs of deployable telescope satellites *Score = 3.9* (green)	Lower launch cost, lower payload cost per constellation, lower series production cost *Score = 2* (yellow)	Lower launch related emissions *Score = 3* (blue)

green 4 blue 3 yellow 2 red 1

9 Verification and Validation

Verification and validation are important to bring confidence to the design and are hence necessary on a model and product level. The procedures to verify and validate the model, which consists of the tools used for the design are presented in Section 9.1. In Section 9.2, the procedures to verify and validate the final product are explained.

9.1. Model verification and validation

Figure 9.1 shows the procedure to conduct verification and validation on a model level. The darker blocks illustrate main actions, while the lighter ones show how to achieve that. The model is first verified and then validated. If errors and inconsistencies are found they need to be fixed and the process starts again.

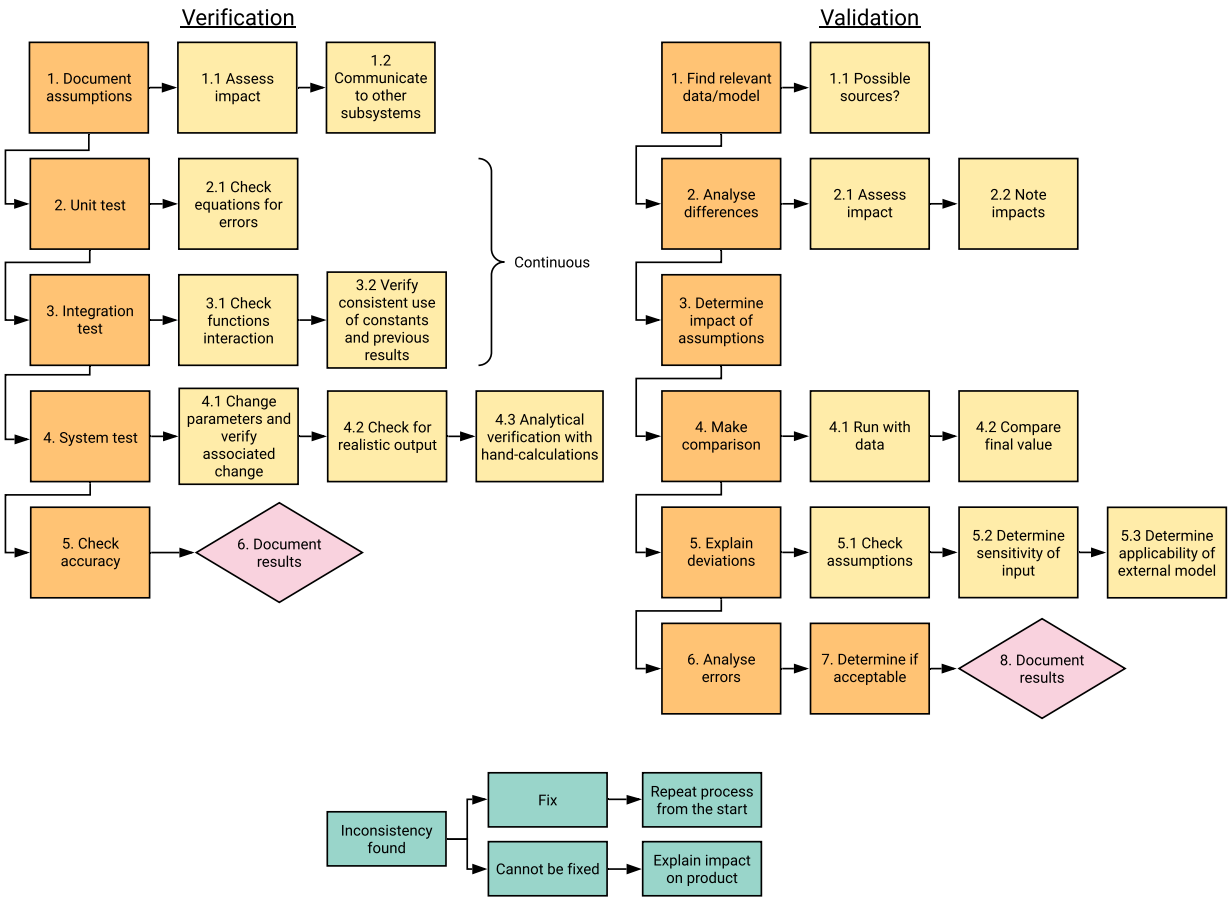

Figure 9.1: Model verification and validation procedures

The first step of verification is related to the assumptions. They need to be documented and their influences assessed. It is important to communicate individual subsystem assumptions to the other engineers so that there is a common basis for the model. The second and third step is to perform unit and integration tests, these should be done continuously while the model is being made. Unit testing aims at checking individual equations while integration testing aims at checking combined equations to see how they react together. Communication is key for a good interaction in the system so 3.2 also verifies that the right intermediate results from other subsystems are being used. The next step is system testing which is done when the writing of the model is complete. Several checks can be performed: changing input parameters to see how these influence the result, checking the outputs for physical sense, and checking the results analytically by doing hand-calculations. At the end of the system test the results can be checked for accuracy, this determines if the difference between

the tests and the results is acceptable. Finally, all these findings need to be documented, they will be presented in the individual subsystems chapters.

After the model is verified to correctly describe the model, validation can start. The first step is to research and find relevant proven models and/or data from similar products. Without this, validation cannot take place. It is unexpected to find exact representations so the second step is to analyse the differences and their possible impacts to validation. Next, it is necessary to determine the impact of the assumptions as these alter the model. After these preliminary steps, the actual validation process can start by making comparisons. If an external model is found it will be run with this systems input or the other way around if external data is found. Otherwise, if validation is done through similar products the final values can be compared. As assumptions and differences are expected the deviations between the model and validation method need to be explained, this can be done by explaining the different assumptions or checking the sensitivity of the results to the inputs. The last steps go together, the errors are identified; they can be random or systematic, and the results are evaluated to see if they are acceptable. As with verification the results need to be documented.

The final flow presented in Figure 9.1 shows what process to follow when an error/inconsistency is found. The mistake needs to be fixed and the process repeated, however if it cannot be fixed this needs to be clearly documented and the impact explained. This verification and validation procedure is used as a baseline in each subsystem chapter but will be adapted to their individual possible tests.

9.2. Product verification and validation

Product verification ensures that the final product was realised correctly, within the requirements and specifications while validation checks that the final product can be used as intended in the environment. The subsystems need to be checked to meet the subsystems requirements and the product needs to be validated to meet the system requirements. These procedures go hand-in-hand with the requirement compliance matrix described in Chapter 24. There are four main methods to perform verification and validation:

1. *Analysis.* This is used when a prototype is not available and so mathematical models and other analytical techniques are used to verify/validate. Verification can also be conducted by similarity of a heritage product.
2. *Demonstration.* This shows compliance to specific requirements and confirms performance capabilities of the system; can be done by actual operation of the end product.
3. *Inspection.* This is a visual examination that is mostly used to verify/validate physical features.
4. *Test.* This is needed to obtain data to verify/validate performance under controlled conditions aiming to simulate the environment. It is the most costly method, several types of testing are listed in [6].

Product verification is necessary on different levels, the requirements can be verified for the whole system when possible but also independently. The procedure is to identify the best method for a certain requirement and realising it. The completeness of the verification process is ensured by performing verification of integrated subsystems while simulating environmental conditions. If the verification procedure finds that the product fails to meet certain requirements then a discrepancy report with planned corrective actions needs to be drawn. The output should be a verified product accompanied by a verification report and an updated requirement compliance. Other procedures that follow from verification are qualification and acceptance. Qualification verification consists of checking that functional and performance requirements are met in the environmental conditions expected, while acceptance verification checks that the hard/software are in compliance with the requirements and ready for launch.

When the product is verified it can enter the validation process where other inputs are the stakeholders expectation and enabling products, such as the tools and special facilities needed. The outcome should be a validated product that complies to the stakeholder expectations and functions well with the interfacing products. The analysis of the validation should present the deficiencies, re-planning and corrective reports as well as the validation report. If the product does not pass validation a redesign is necessary or possible compromises need to be discussed with the user.

Moreover, product verification and validation is conducted with the development of the prototypes. The MS and TIR designs will have a prototype that will be checked and only if it is acceptable then the final model will be built. The final models will be launched for in-orbit qualification for final verification and validation. After implementing the necessary adjustments the constellation can be produced and launched.

10 Functional Analysis

This chapter gives an overview of the functional flow diagram and the functional breakdown structure, two essential tools used to get a better idea what the system should be capable of and to draw requirements from. The highest level of both diagrams is shown along with a description for both diagrams.

10.1. Functional Flow Diagram

The Functional Flow Diagram (FFD) is presented in Figure 10.1 and represents the multi-tier, time-sequenced functional flow of the mission. The FFD indicates the functions that a system has to perform throughout its lifetime, starting from the mission design phase. At the top level, the main mission phases are defined, which are then broken down into two lower levels. It also shows how possible anomalies are to be handled. The full Functional Flow Diagram can be found in Figure 10.3, 10.4, 10.5, 10.6 and 10.7.

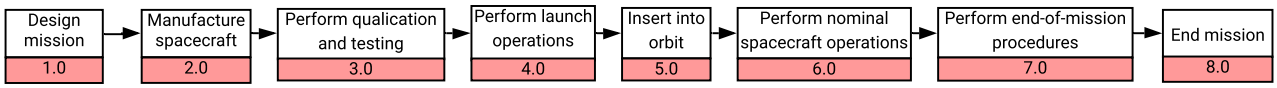

Figure 10.1: Top level of the functional flow diagram

10.2. Functional Breakdown Structure

The Functional Breakdown Structure (FBS) is presented in Figure 10.2 and presents the functions a system has to perform in a hierarchical fashion. It is an AND tree, which means that every block is the sum of the blocks below it. The functional breakdown structure goes one level deeper than the functional flow diagram. Rather than grouping functions by the mission phases seen in the top level of the FFD, the blocks are grouped and structured by subsystem. This way, a logical grouping of similar functions is achieved, shown by the yellow blocks. Note that this means not all of the mission phases from the top level of the FFD are included in the FBS, as it would not make sense to assign these to just one subsystem. Some of the top level blocks of the FFD are still present in the FBS in the form of the red blocks with identifiers. The red blocks that do not have identifiers are there to provide further clarity within functional groupings. Lower level functions that could not be assigned to just a single subsystem and rather work on a system basis, were grouped under 'central computer operations'. The full Functional Breakdown Structure can be found in Figure 10.8 and 10.9.

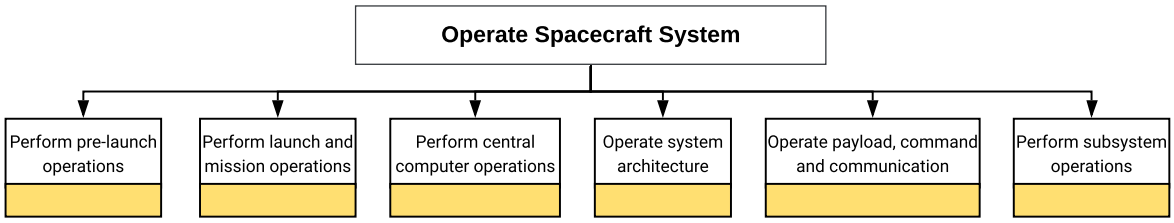

Figure 10.2: Top level of the functional breakdown structure

Top Level I

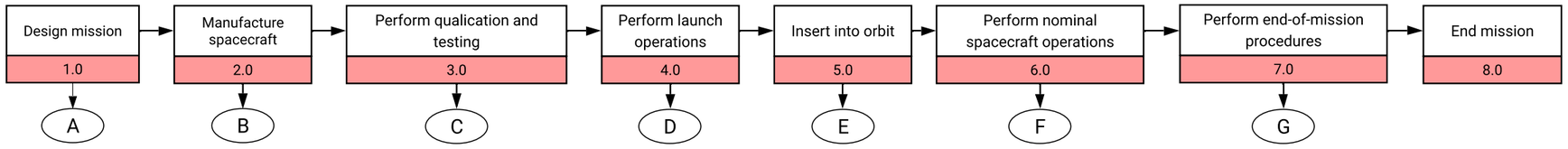

Second Level II

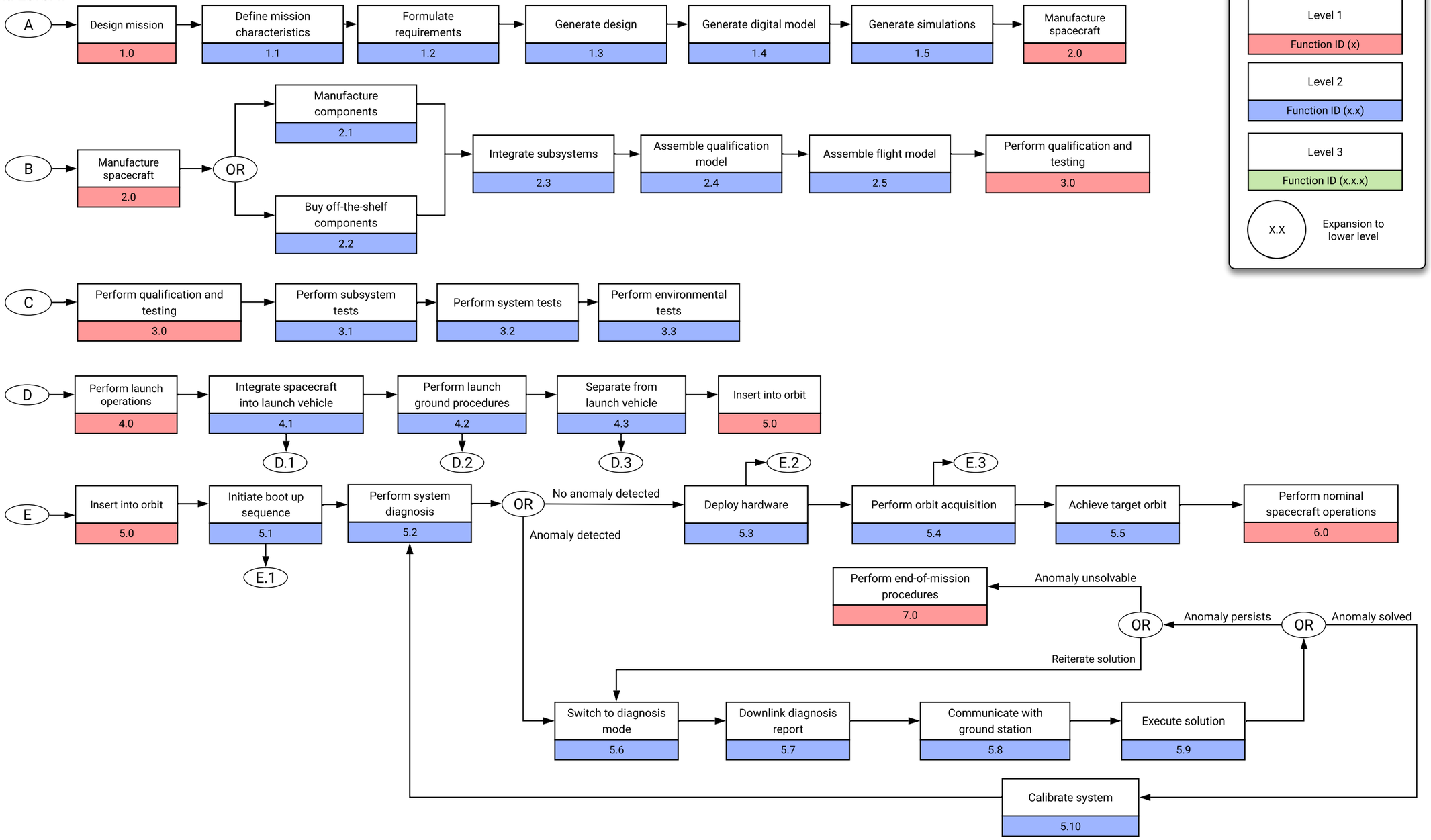

Figure 10.3: The functional flow diagram

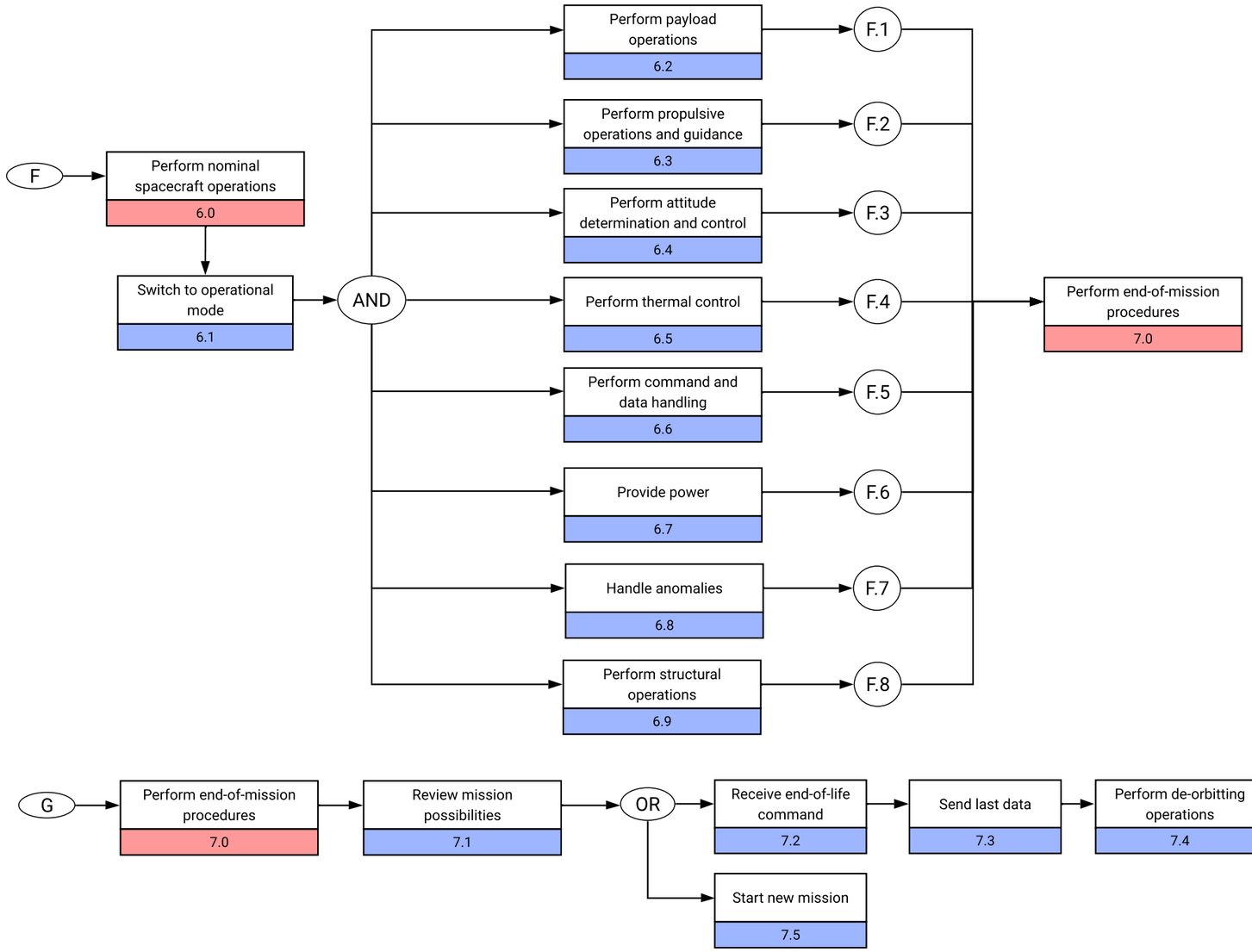

Third level III

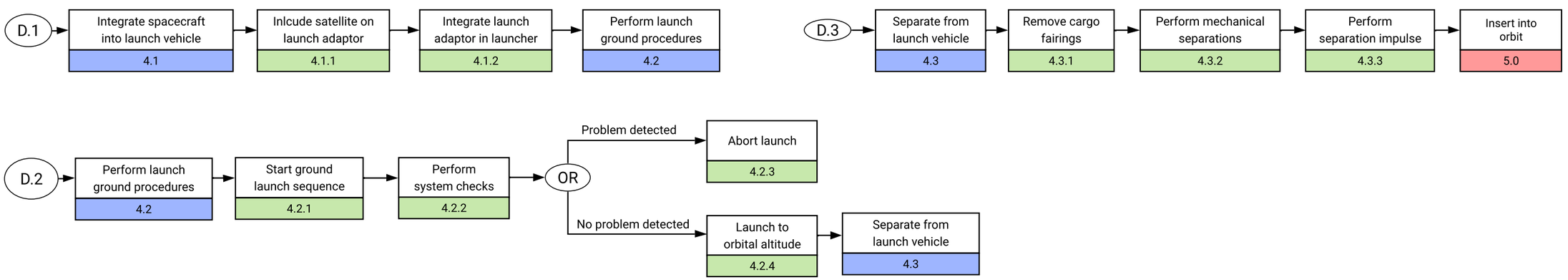

Figure 10.4: The functional flow diagram (continued)

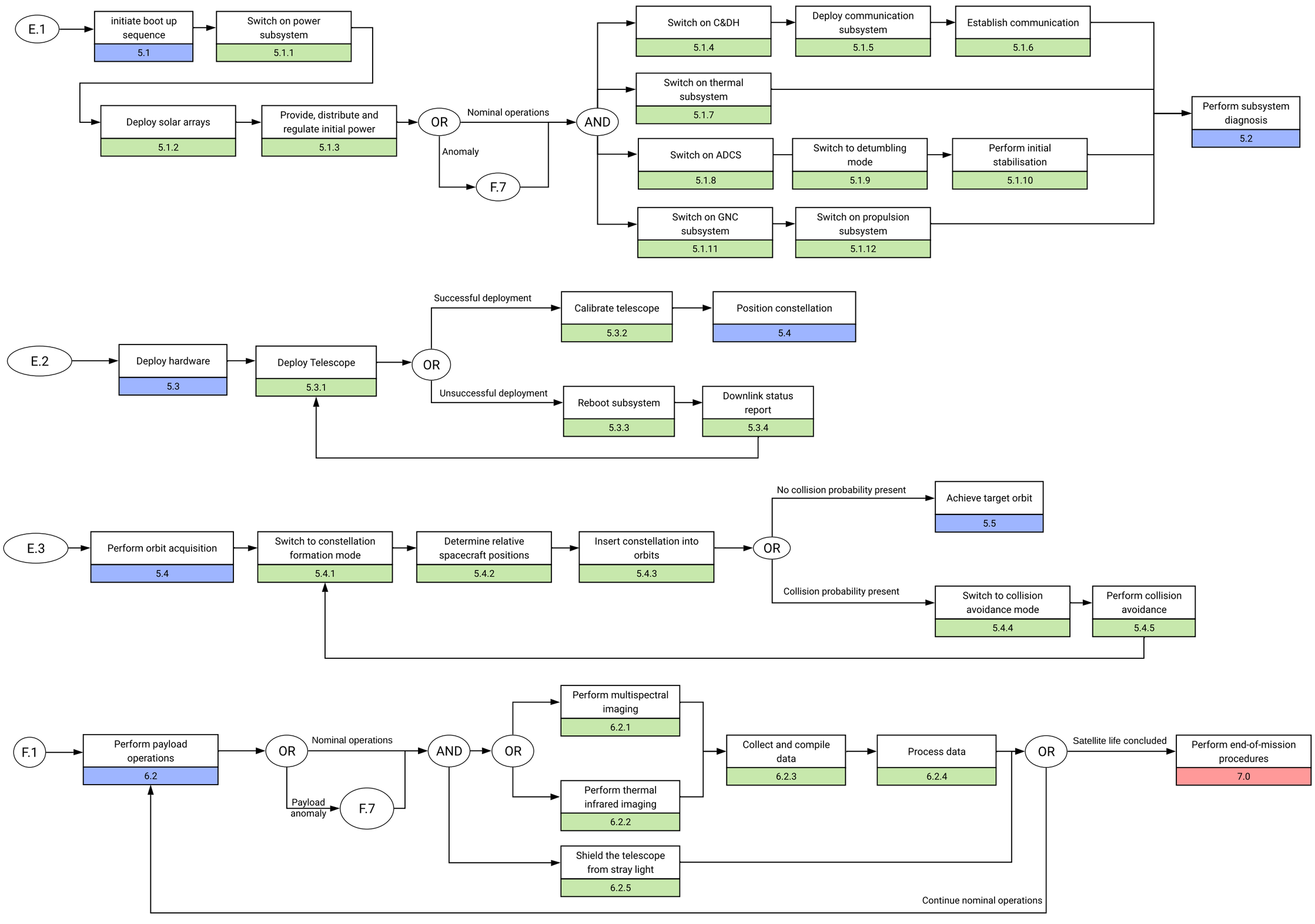

Figure 10.5: The functional flow diagram (continued)

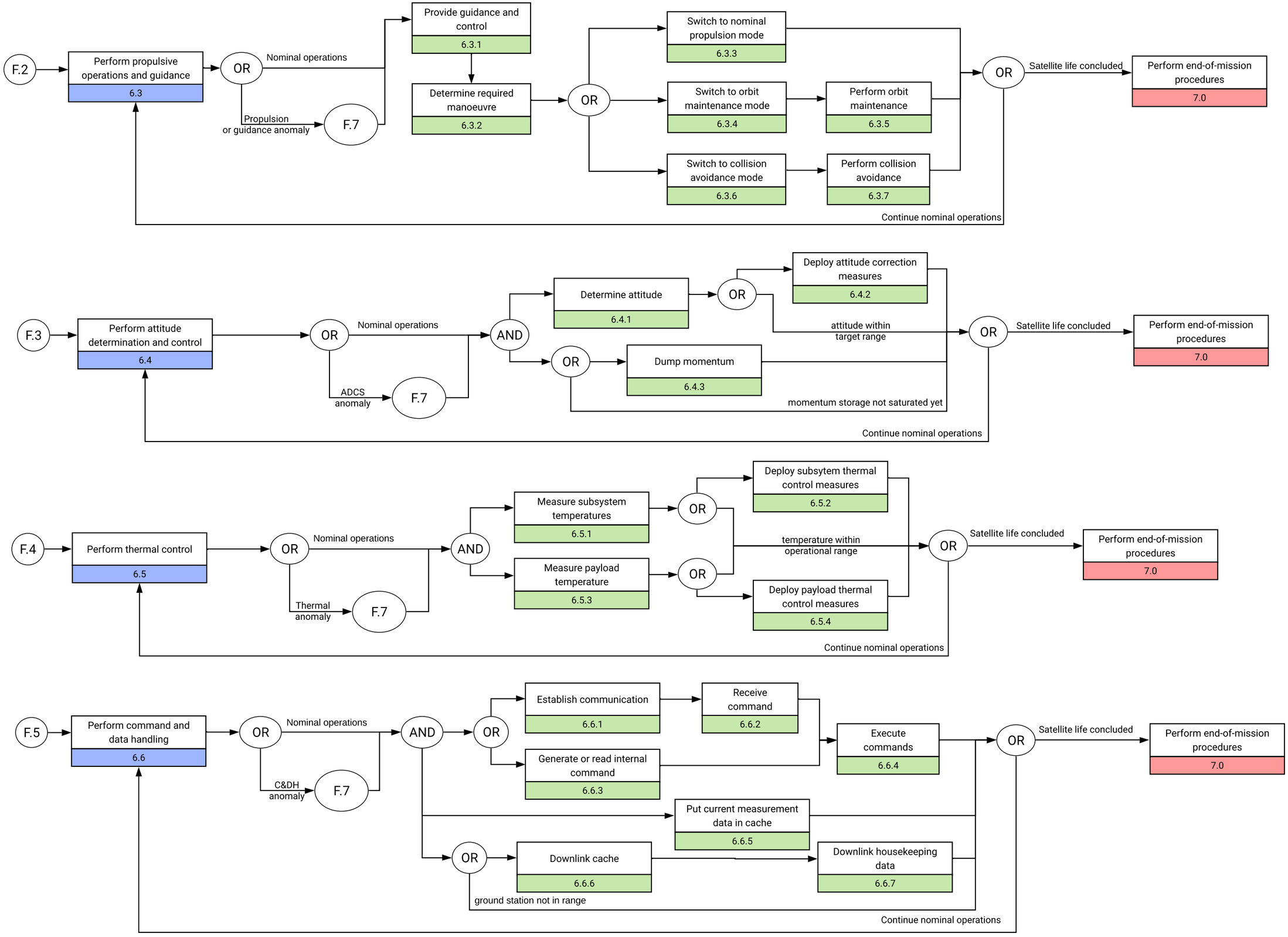

Figure 10.6: The functional flow diagram (continued)

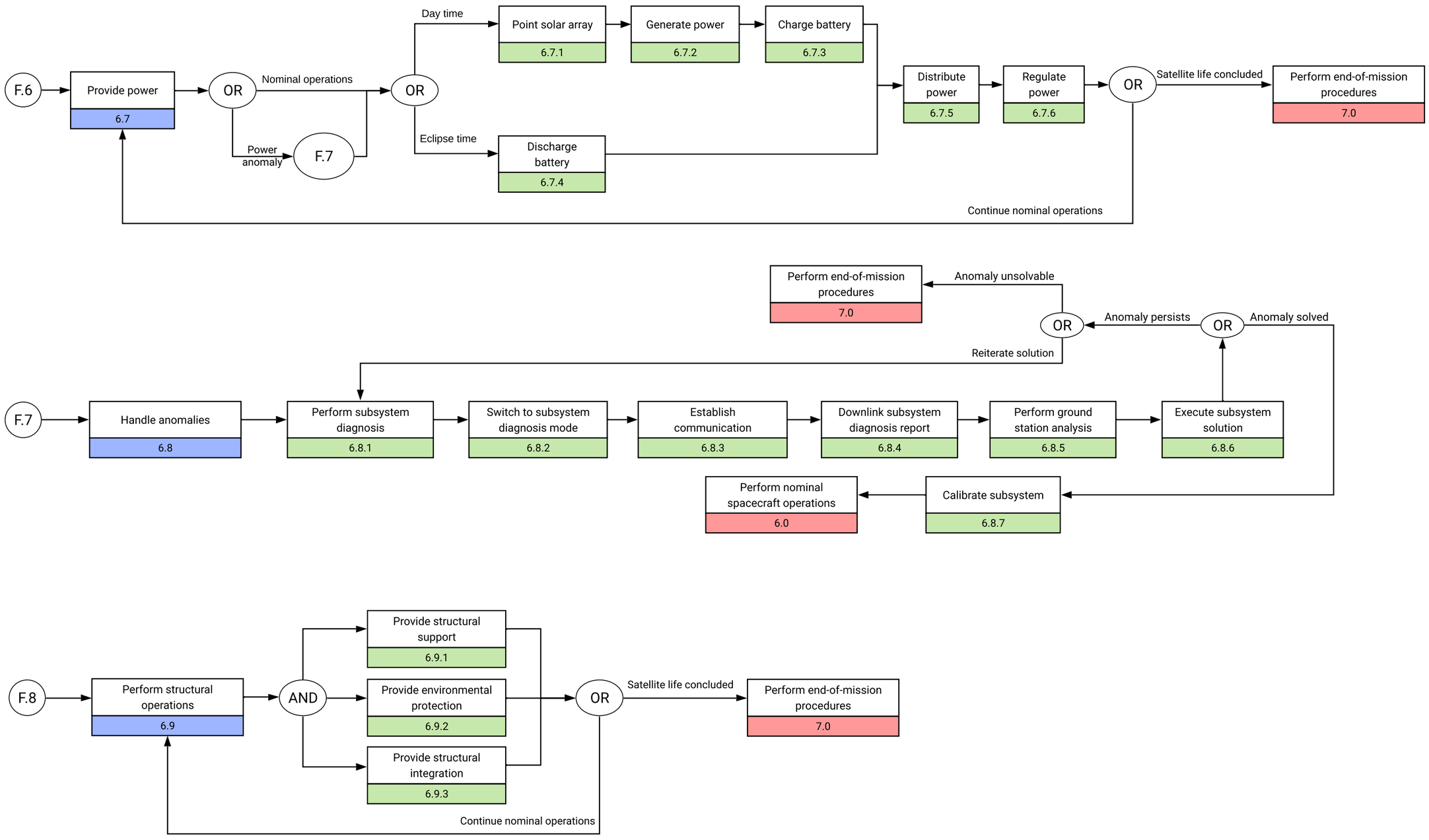

Figure 10.7: The functional flow diagram (continued)

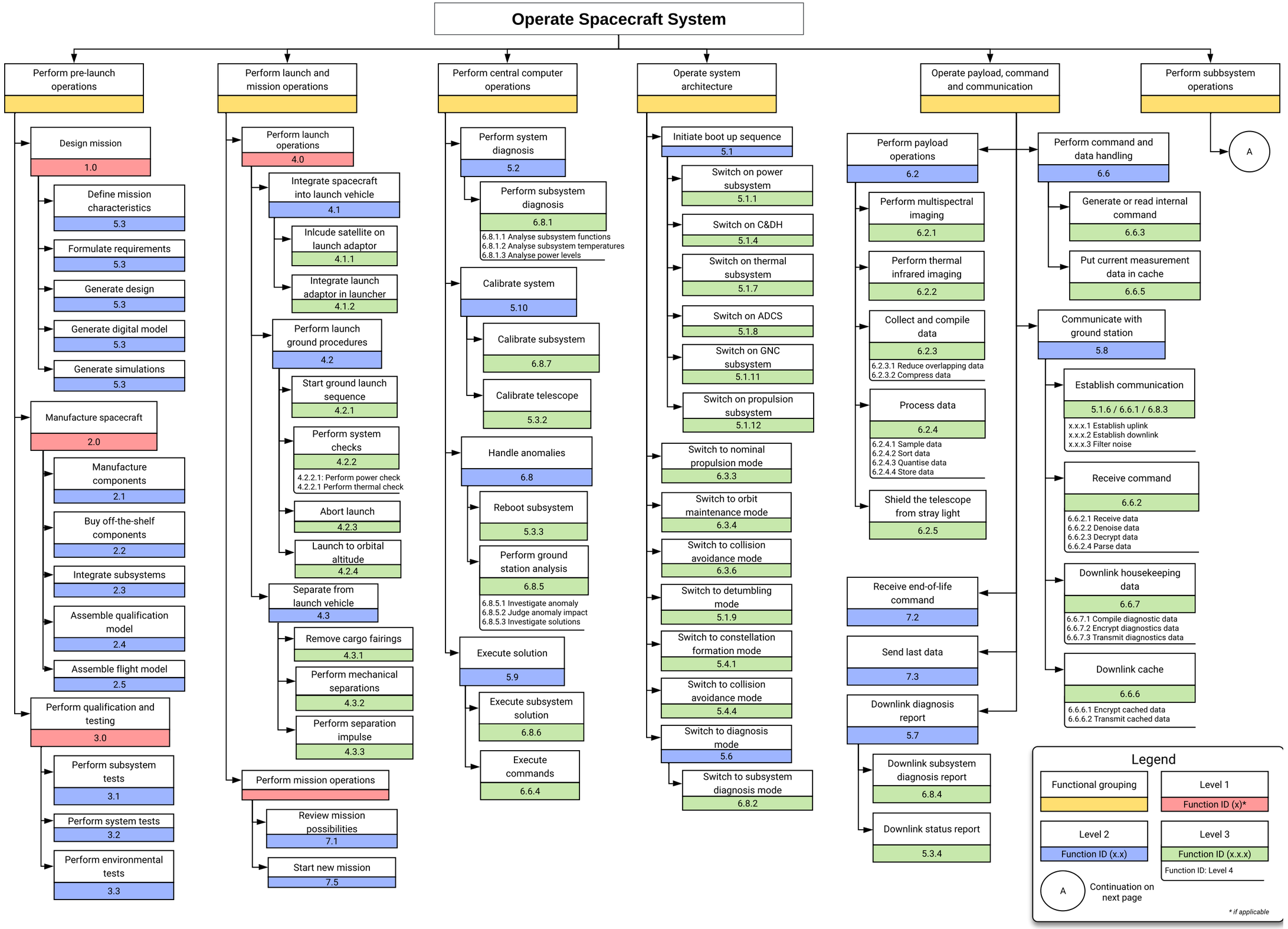

Figure 10.8: The functional breakdown structure

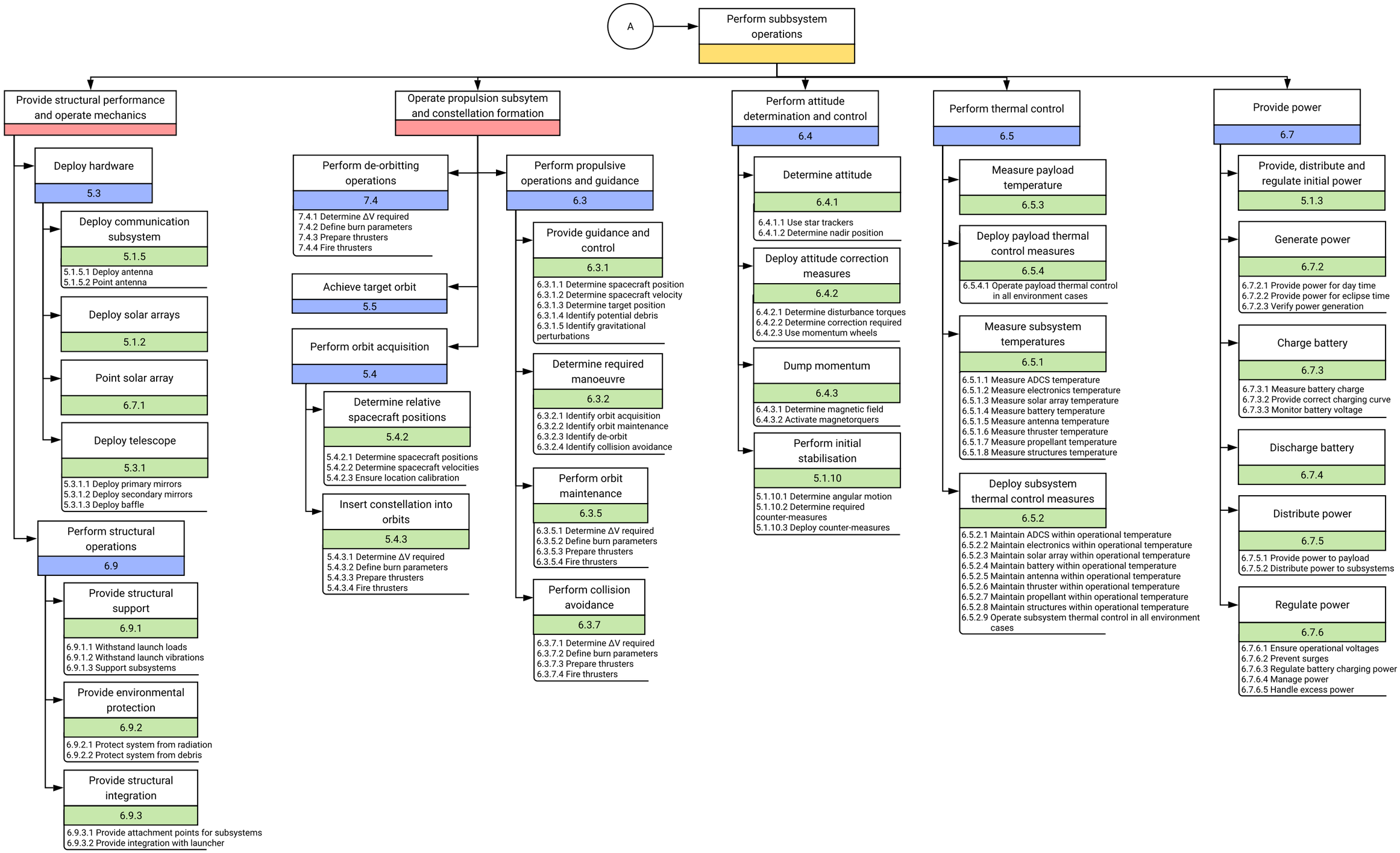

Figure 10.9: The functional breakdown structure (continued)

11 Mission Analysis

In this chapter, a complete mission analysis will be performed. The required performance of the system will be investigated, translating user requirements to the technical domain. First of all, potential applications and limitations of the system are identified. Second, this chapter discusses the monitoring of gases with the principle of narrow band optical imaging. Here, the design considerations and principles will be detailed, as well as the spectral window for the multispectral instrument. Finally, the thermal imaging will be discussed, detailing the governing principles for identifying entities and the considerations that should be taken into account.

11.1. Applications and limitations

The functionality of the Mira mission can be split up into two parts. On one hand, the system will monitor emissions in the short-to-medium wave infrared spectrum while on the other hand, it will identify and track entities in the far infrared spectrum. These two functions have different philosophies and will be analysed independently.

When measuring emissions, the goal is to monitor the emission levels on the scale of individual factories, roads and farms. The position of these landmarks is often known and they are a relatively constant source of emissions. Especially in this day and age, ever changing environmental regulations require close monitoring of growing infrastructure and factories. The high spatial temporal resolution could allow the pinpointing of potential violators on the level of individual buildings. Besides regulation, other applications of the system include the potential identification of illegal activities such as mining operations. Even environmental needs such as the monitoring of volcanic activity and forest fires, with their high levels of carbon-dioxide, could be addressed by the system.

Consultation with external experts led to the conclusion that the monitoring of gases has a rather strong heritage in the field of remote sensing. Different techniques and processing principles are used for different gases. For example, methane levels are often characterised by the unit ppb (parts per billion)[a], taken for the entire atmospheric column. For nitrogen-dioxide however, the unit is often[b] $\mu mol/m^2$. The TROPOMI mission, as described by Veefkind et al. [7], has been a benchmark for this mission throughout the design process. It monitors two of the three current gases of interest, which makes this a very relevant mission. The aforementioned experts were a valuable source of information, as they worked on the TROPOMI instrument directly. TROPOMI, however, is a very complex instrument with a scientific performance that will not be beaten by the constellation currently being designed in this DSE, which focuses more on a higher temporal and spatial resolution with limited radiometric performance. The aim is not to use it for science but for local societal and governmental needs.

When monitoring the far infrared spectrum, the goal is to identify entities on the ground, characterising them by the amount of thermal radiation they produce. The range of wavelengths was given to be 8-12 µm, which corresponds with the emission peak of human bodies. By combining high spatial and temporal resolution, entities on the ground can not only be identified but also tracked in 30 minute intervals. Unlike the monitoring of gases, thermal infrared imaging is more reactive with its purpose leaning towards identification and tracking rather than regulation. The identification and monitoring of groups of humans and their movements can be applied to a wide range of societal and environmental needs, including justice and security. Applications include border control, refugee movements and the potential identification of drug laboratories should they emit enough heat. More specifically environmental applications include the identification and monitoring of forest fires, in which the temporal resolution is key in notifying first responders on the ground when every minute counts. The applications however do not strictly apply to land-based operations. For example, illegal fishing vessels could be identified, especially in the arctic regions where surveillance is generally performed less. However, it is also important to address the military applications of a constellation like this. Movement of troops and vehicles, both allied or enemy is critical intelligence that could be detected by the system. Again, high temporal resolution is key here.

[a] http://www.tropomi.eu/data-products/methane [cited June 15 2020]
[b] http://www.tropomi.eu/data-products/nitrogen-dioxide [cited June 15 2020]

Applications and temporal resolution

Currently, the requirements regarding the temporal resolution for the monitoring of gases and the thermal infrared imaging were set at 60 minutes and 30 minutes respectively. Even though these resolutions are quite high compared to traditional Earth observation missions, it is important to touch upon any potential shortcomings of the system. Gases tend to stay present in the air for quite a while, well beyond the current 60 minute temporal resolution. Performance regarding the monitoring of gases is therefore not impacted very greatly if one were to increase the temporal resolution. The thermal imaging applications however, are more impacted by this metric. While the 30 minute temporal resolution remains, the option for near real-time monitoring, with 5 minute resolution, no longer being present limits the responsiveness of the system. For things such as forest fires, close monitoring in early stages can be important in containing the fire. The same goes for the movement of people, especially in military applications. This system is more designed as a warning mechanism, which would need complementary systems to assist it in identification of targets.

An overview of the overall applications and their benefits or shortcomings for discrete steps of temporal resolution can be found in Table 11.1 and Table 11.2 for the monitoring of emissions and thermal imaging respectively. It can be seen once again that for emissions, there is not much benefit to increasing the temporal resolution beyond 60 minutes. For thermal imaging however the higher the temporal resolution gets, the more reliable tracking becomes.

Table 11.1: Applications regarding the monitoring of emissions, for varying temporal resolutions.

Temporal resolution	Agriculture & Industry	Traffic
Real time	Limited additional use	Limited additional use
5 minutes	Limited additional use	Peak hour congestion monitoring
30 minutes	Small scale monitoring possibilities	Potential for congestion prediction
60 minutes	Localised monitoring of factories, farms and roads	General congestion and road activity monitoring
12 hours	Monitoring industrial areas, deforestation, long term mapping	Post-fact analysis, high level mapping

Table 11.2: Applications regarding thermal imaging, for varying temporal resolutions.

Temporal resolution	Humans	Vehicles	Forest fires
Real time	Active tracking everywhere	Active tracking everywhere	Rapid identification, spreading can be prevented
5 minutes	Active tracking in suburban areas	Active tracking in scarcely populated areas	Active support to first responders, close monitoring
30 minutes	Active tracking in unpopulated areas. Tracking groups, crowd surveillance	Limited tracking possibilities	Mainly reactive, spread prediction, support ground personnel
60 minutes	Post-fact analysis, no active tracking	Tracking capabilities mostly lost	Major updates only, loss of responsiveness
12 hours	Limited use	Vehicle identification and tracking capabilities lost	High level mapping only, no support for ground personnel

11.2. Monitoring emissions

For emissions, the three main gases of interest are carbon-dioxide (CO_2), nitrogen-dioxide (NO_2) and methane (CH_4). The principle of narrow band optical imaging is used in order to determine the quantity of gases in the atmosphere. This method is based on the fact that every gas absorbs light in different wavelengths, also called spectral bands. Light travels from the sun, through the atmosphere, reflecting on the ground and travelling back through the atmosphere only to be collected by the spacecraft. Every gas in the atmosphere interacts with sunlight in a different way. Depending on how much of a gas is present in the atmosphere, more or less of the original light is absorbed. This varies across wavelengths. By measuring the absorption at wavelengths corresponding to the gases of interest, these quantity of gases in the atmosphere can be determined.

Table 11.3 shows the main and minor spectral bands that have been identified for the gases of interest, using the HITRAN spectral database[c]. Note that both main and minor bands can be used for the instrument, though main bands give a stronger absorption peak. These bands are also visualised in Figure 11.1.

Table 11.3: Main and minor absorption bands of CO_2, NO_2 & CH_4 in the infrared spectrum

Gas	Main bands [µm]	Minor bands [µm]
Carbon-dioxide (CO_2)	2.65-2.8, 4.2-4.35	1.95-2.1, 1.4-1.45, 1.51-1.55, 1.59-1.63
Nitrogen-dioxide (NO_2)	3.4-3.52, 6.1-6.35	0.350-0.475
Methane (CH_4)	2.25-2.4, 3.2-3.45, 7.3-8.1	1.63-1.8

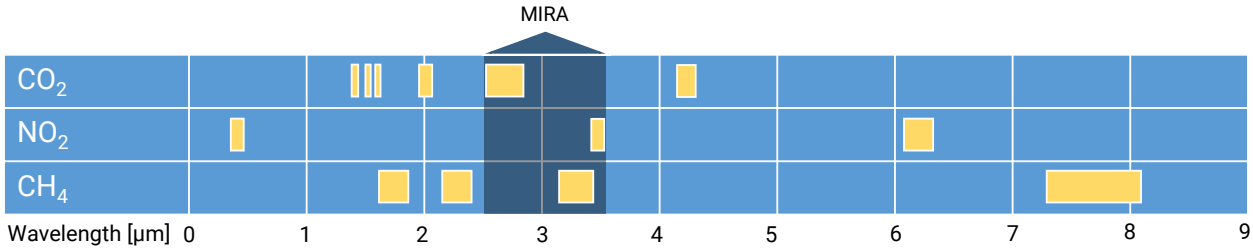

Figure 11.1: Spectral window for the Mira mission

In earlier design stages, the choice between monochromatic and multispectral imagers was detailed. It was concluded here, that multispectral imagers, though inherently more complex, are better suited for this mission. Monochromatic imagers rely on the possibility of having exclusive bands to measure individual gases. Multispectral imagers do not have this constraint. This means that when using monochromatic imagers, a dedicated telescope would be required for each gas of interest, which even when not considering exclusivity, making this a very expensive option. Moreover, no exclusive spectral bands for the gases of interest could be identified, thus, the ability to monitor multiple gases without the need for additional telescopes was a decisive factor in choosing a multispectral imager. The spectral range for it was chosen to be 2.65-3.52 µm, as it includes main absorption bands for each of the gases of interest. This is also demonstrated in Figure 11.1, which shows this spectral window for the Mira mission. The minimal spectral resolution required was determined to be the dimension of the overlap, which is 0.05 micrometers. Furthermore, a multispectral instrument allows for the possibility to monitor other gases, beyond the three originally considered, at little to no added cost, given that these gases have absorption bands in the 2.65-3.52 µm range..

Consultation with an external expert, who has worked on the TROPOMI mission, has revealed that the measuring of atmospheric gases is a complex field which involves different measuring procedures for a combination of different atmospheric gases. Most of these use complex models as well, which are not available for this DSE. Therefore, the design for the narrow band optical imaging system is kept at a higher level.

In order to asses radiometric performance, a relative approach is taken. Instead of assuming the system to be diffraction limited, the dimensions are scaled with the TROPOMI instrument such that the same SNR is achieved. Due to TROPOMI's scientific nature, its respectful SNR is deemed to be sufficient for the applications of the current mission design.

[c]https://hitran.org/ [cited 13 May 2020]

11.3. Thermal imaging

At any temperature above absolute zero (0 K), all objects continuously emit thermal radiation. This radiation can be measured by the spacecraft in orbit in order to identify the source on the ground. Equation 11.1 shows Planck's law, which is used as a starting point in order to relate a subject's temperature to the radiation it produces.

$$E_\lambda = \frac{2 \cdot \pi \cdot h \cdot c^2}{\lambda^5} \cdot \frac{1}{e^{h \cdot c / k \cdot T_{eq} \cdot \lambda} - 1} \tag{11.1}$$

E_λ is also called the spectral radiant exitance (W m^{-2} μm^{-1}), h is Planck's constant, c is the speed of light, k is Boltzmann's constant, λ is the wavelength and T_{eq} is the equivalent blackbody temperature of the subject. That is, the temperature of a blackbody that emits the same radiant flux density. The absolute temperature of an object can be converted to the equivalent blackbody temperature using Equation 11.2.

$$T_{eq} = \epsilon^{\frac{1}{4}} \cdot T_{abs} \tag{11.2}$$

Where T_{abs} is the absolute temperature of the subject, also called the kinetic temperature. In reality, objects are not ideal black bodies, which is why the equivalent blackbody temperature is used. The emissivity ε is a material property that relates the fraction of an object's heat that is radiated to its environment. The upwelling spectral radiance is then calculated using Equation 11.3, as described by Wertz and Larson [8]:

$$L_\lambda = \frac{E_\lambda}{4 \cdot \pi} \cdot \tau(\lambda) \tag{11.3}$$

Where τ(λ) is the transmission factor that has to be taken into account since the atmosphere will absorb a fraction of the outgoing radiation. Note that this is still only for a specific wavelength. In order to determine the total outgoing radiance in the 8-12 μm spectral range, the upwelling spectral radiance has to be integrated along these wavelengths, as shown in Equation 11.4. Multiplying the outcome with the ground sample area A as shown in Equation 11.5, which was required to be 25 m^2, yields the total radiated power from a ground pixel at nadir [8].

$$L_{int} = \int_{8\mu m}^{12\mu m} L_\lambda d\lambda \tag{11.4}$$

$$L_{total} = L_{int} \cdot A \tag{11.5}$$

Note that this is the radiated power distribution on ground level. Radiation scales with the inverse square of the distance. Therefore, the radiation power at the entrance of the optics of the spacecraft in-orbit can then be calculated as follows [8].

$$P_{in} = \frac{L_{total}}{h^2} \cdot D_A \tag{11.6}$$

Where h is the orbital altitude and D_A the primary mirror area. It is assumed here that the distance between the satellite and the ground, is the distance between the satellite and the source. This is because the elevation of subjects above the ground is negligible compared to the satellite altitude. Even for aircraft, the average cruise is at a maximum elevation of approximately 11 km[d]. This is an order of magnitude smaller than the orbital altitude of 350 km, with a signal actually 6 % stronger than if the source was on the ground. As such, the elevation of subjects is neglected in Equation 11.6. Another reason is that the height of subjects is unknown before imaging.

The original objective of thermal imaging was to identify and track groups of humans and vehicles. However, throughout the technical design phases it became evident that it is inherent complicated to derive concrete technical requirements for the monitoring of vehicles. The main reason for this is the fact that it is not known beforehand what is actually present on the ground. Vehicles have a wide range of operational temperatures, besides the fact that parts that produce heat, such as the engines, are to an extent usually internally insulated. Furthermore, the emissivity of objects plays a large role in the thermal signature they produce. Different colours and materials have widely varying emissivities which results in a widely varying signal level, which makes trying to characterise them difficult. However, this does not mean that vehicles cannot be identified at all. Rather, an indirect approach can be taken by making use of the high temporal resolution of the system. By seeing how fast an object moves between images, the nature of the object can potentially be identified. Note however that this is still not a fully accurate method which serves only as a first estimation. For larger, stationary objects such as buildings, the emissivity could be corrected for in post-processing.

[d] https://time.com/5309905/how-high-do-planes-fly/

When performing thermal infrared imaging, an important characteristic in terms of the radiometric performance of the instrument is the noise equivalent temperature difference. This is the minimal temperature the instrument is able to resolve for a given background temperature. This is determined by an iterative process, finding the temperature difference which results in a signal to noise ratio equal to 1. This will be calculated in Chapter 12, after the thermal infrared instrument is sized. It is important to note that this metric assesses the performance on a per-pixel basis. That is, it is the difference in temperature between pixels the system is able to discern. However, humans are much smaller than the 25 m^2 (5 x 5 m) ground sample for thermal imaging.

Therefore, it is interesting to also look at how many humans the system can actually detect against different backgrounds. This can be determined by placing a single human in an environment the size of one ground sample and comparing the signal with the signal from just a ground sample of that same environment. This time, L_{total} in Equation 11.5 can be written in a relative sense, comparing the two situations:

$$L_{total} = [(L_{int})_{human} \cdot A_{human} + (L_{int})_{environment} \cdot A_{environment}] - (L_{int})_{environment} \cdot A_{GSD} \tag{11.7}$$

One human body is assumed to occupy a projected area of 0.15 m^2 when viewed from the top, which leaves 24.85 m^2 for the environment. If the relative signal, that is the signal of the human in the environment minus the signal from empty environment (as shown in Equation 11.7), yields a signal-to-noise ratio greater than one, the system is able to resolve the difference. If not, then the procedure is repeated with two humans and so on. To ensure sufficient confidence in the differentiation, a minimal SNR of 10 is set as a requirement for the system to actually resolve a difference. This analysis will be performed in Chapter 12, after the TIR telescope is sized.

12 Payload Design

The Delft deployable telescope will be an inherent part of this mission's success. A version to monitor in the visible light spectrum is currently being developed at TU Delft. Thanks to this research, it is possible to use a deployable telescope which will allow to save volume for the total satellite during launch. This telescope, follows a three-mirror anastigmat design of the 'annular field Korsch' type. It was initially investigated in [9].

12.1. Requirements and assumptions

Here are the payload requirements, Table 12.1. Moreover, requirement 3 is fulfilled as vehicles in movement operate at higher temperatures than humans, thus giving off a higher signal. See Chapter 11 for further explanation for requirement 1 and 3, MIRA-PAY-PERF-1 and MIRA-PAY-PERF-3 respectively.

Table 12.1: Payload design requirements

ID	Requirement	Origin	Analysis ref.	
MIRA-PAY-PERF-1	The spacecraft shall be capable of tracking people with an minimum accuracy of 5 m.	BLR, MIRA-MIS-PAY-PERF-1.6		✓
MIRA-PAY-PERF-2	The spacecraft shall be capable of tracking the number of people in a group with a minimum accuracy of 10 people.	BLR, MIRA-MIS-PAY-PERF-1.7		✓
MIRA-PAY-PERF-3	The spacecraft shall be capable of tracking vehicles of a minimum size of 5 m × 5 m.	BLR, MIRA-MIS-PAY-PERF-1.8		✓
MIRA-PAY-PERF-4	The spacecraft shall be capable of tracking gases with an minimum SNR of 100.	BLR, MIRA-MIS-PAY-PERF-1.9		✓
MIRA-PAY-SUS-1	The payload shall only use flight proven materials.			✓

12.1.1. Assumptions

1. The TIR telescope is assumed to be diffraction limited
2. The light incidence is assumed equal to the reflected angle relative to the plane of the mirrors
3. The signal to noise ratio is assumed to scale linearly with ground sample area. This is used whens scaling the TROPOMI aperture to the MS telescope.
4. The telescope is assumed to be able to be resized from the reference DDST using the aperture of the primary mirror, the focal length and the length of the secondary mirror
5. Assuming the body temperature of human being 310 K (37 °C)
6. The standard sea level, snow, human and desert emissivities are assumed to be: 0.96, 0.85, 0.98, 0.85[a]

12.2. Design aspects

For both the multispectral satellite and the TIR one, designs are developed with respect to different aspects such as dimensions, components used, temperature ranges, power required and the radiometric budget.

12.2.1. Dimensions

For dimensions, there are several aspects to be considered: various lengths, volume and mass. The method for calculating them is the same for the TIR and MS, apart for aperture. Firstly, the focal length, (12.1) [9], depends on the altitude H and the ground sampling distance d_g. Additionally, it depends on the pixel pitch d_p.

$$f = \frac{H}{1 + (\frac{d_g}{d_p})} \tag{12.1}$$

[a] https://www.jpl.nasa.gov/spaceimages/details.php?id=PIA18833 [cited 7 June 2020]

Moreover, from [10] and [11], the aperture and various widths such as the secondary mirrors or the slit are known. These can be re-sized by keeping the ratio between the aperture and that specific dimension the same between the reference telescope and the TIR or MS ones. Furthermore, from those same sources, it is known that the primary mirror is parabolic concave, and the secondary deduced convex parabolic. A parabolic shape limits spherical aberrations [12]. More can be read about this in the Appendix A.

TIR aperture For the thermal infrared, we can assume a diffraction limited system. This is because the signal is quite strong, as explained later in the radiometric budget. Thus, for the aperture, (12.2) is used [9]. λ being the limiting wavelength which is the highest measured wavelength.

$$A = \frac{1.22 \cdot H \cdot \lambda}{d_g} \tag{12.2}$$

MS aperture: It is safe to assume that the MS telescope is signal limited, as the gas signals are weak due to their scattering in the atmosphere. However, making a radiometric budget for gas emissions is immensely complicated. Thus, what is done is to scale the aperture with respect to the TROPOMI model.

In essence, the same SNR is assumed for the respective gases. It is known that the signal to noise ratio is directly influenced by the ratio of the ground sampling distance and the altitude. Thus, wishing to keep the signal to noise ratio the same: 100-120 for short wave infrared, and keeping in mind that the altitude of TROPOMI is 824 km, the ground sampling distance 7 km and the aperture 4 mm [13], the new aperture for the MS telescope can be found, as shown in Table 12.3.

Mass and volume The mass and volume of the telescope are estimated in more detail than in previous reports. Using both the actual and reference areas [10, 11], and weights of 80 % and 20 % of the total mass/volume for the primary and secondary mirror, a ratio of the reference mass and volume is found.

Instrument housing There are more optical aspects to be sized: the tertiary mirror, the deformable mirror, the fold-able mirror and the sensor [11], with the first three re-directing light to the fourth. Given the level of maturity of this design, only the sensor will be investigated. However, it can be said that the size of the tertiary mirror scales proportionally with its distance to the slit and it will be be concave spherical or parabolic. Lastly, a 'piston cap' is used to find the possible misalignment of the secondary and primary mirror [10]. The length of the instrument box, is approximated to be the length of one primary mirror, as they fold on the side of it [9].

12.2.2. Components

Sensors In terms of sensors, off-the shelf ones are available. However, ones which fulfill high requirements of the number of pixels, high quantum efficiencies, and which are available for the desired spectral bands are hard to find on public sensor lists. Thus, it can be concluded that one would need to be developed, or one would need to be investigated, which would have these characteristics.

1. A high quantum efficiency, preferably higher than 70 %
2. 20,000 pixels across
3. A pixel pitch of at least 25 µm
4. Monitoring wavelengths: 2.65 - 3.52 µm for the MS sensor, 8-12 µm for the TIR one
5. A sensor able to make TDI. This is necessary for as satellites move at high speed.

Given the maturity of this design, choosing between CCD and CMOS sensor at this stage is not very relevant and needs deep investigation. However, as this is needed for power budgets, the choice for CCD sensor over CMOS is made, similar to the original DDST thesis [9]. This is because the CCD has far less read out noise. CCD typically use 2-5 W [14]. This power consumption would decrease in eclipse for the MS satellite, as it functions less during night time.

However, is it possible to develop either sensor, as the requirements are within the realm of reason. Both sensors can have TDI. The only difference between the sensors in the TIR and the MS telescope is the sensor operating wavelength. For wavelengths between 2.5 and 3.5 µm it is preferable to use $H_{g0.3}C_{d0.7}T_e$, for its high quantum efficiency: around 80 % [15]. For the TIR imaging detector, it is also preferable to choose $H_gC_dT_e$ for a quantum efficiency of around 70 %[b].

[b] https://ntrs.nasa.gov/archive/nasa/casi.ntrs.nasa.gov/20100030592.pdf [cited 12 June 2020]

Lastly, a 20,000 pixel width sensor is sensible. This can be achieved by for instance lining sensors next to each other, which is usually done for CCD sensors. The total area of the sensors is then about 0.25m^2

Other Another aspect of choosing components is the material choice for the mirrors. For this [9] Silicon Carbide is a viable option. It is light, 5 kg/m^2, and provides high strength and high conductivity. Additionally, a silicon coating can be used for the mirror: it is easy to smooth and can undergo high temperature variations. Lastly, Silicon Carbide is flight proven and with certain manufacturing techniques, it is realistic to produce these mirrors in a matter of weeks instead of months [9]. This is later relevant for the sustainable part of this mission.

Furthermore, a silver enhanced coating is chosen, as already determined by a thesis [9], with a transmittance factor of 0.96 [c]. This is relevant as it determines the transmittance factor of the mirror, used in SNR. A high transmittance factor is needed for optical signal to noise ratio, and for thermal cooling.

Lastly, the structure of the telescope can be an 'inflatable aluminium frame' [10].

12.2.3. Temperature ranges

Multispectral This satellite's telescope is considered to have sensors made of $H_gC_dT_e$, and monitors wavelengths approximately between 2.5 and 3.5 µm. There exists little sensors with this specific spectral range and material. However, there exists one, developed by Sofradir, which monitors a spectral range between 2.5 and 4.2 µm, and is made of $H_gC_dT_e$. This sensor material has an operating temperature of about 190 K [15]. This is used as a reference. A buffer of 10 K can be used here, as used in the WISE mission for similar wavelengths[d]. Lastly, as mentioned in the mid-term report, the sensitivity of the CCD sensor is about 0.1 °C [16].

Thermal infrared From a NASA published document[e], it is possible to take as reference 81 K. This is from the same sensor which was used for the material choice.

TIR mirros For the TIR, the temperature of the mirrors do affect the final outcome of SNR. These temperatures ranges can be computed, assuming that the emissivity equals the absorption, which all equal 0.04 for the primary mirror illuminated area, as the transmittance is at 0.96[f], to be between 201.17 K and 224.86 K. The emissivity of the back mirror is assumed to be 0.96[g]. See Chapter 18 for more details on this type of calculation. These are the limit temperatures inside the baffle.

12.2.4. Radiometric budget

MS For the MS satellite, the SNR is taken from TROPOMI (100-120) [13], as the aperture was scaled relatively to that.

TIR For this telescope, calculating the SNR is a long and tedious process, but yields a SNR situated approximately between 1072 to 2068. The method from Chapter 11 is used. Major aspects can be noted from this.

- The Quantum efficiency was taken from the sensor material, which is about 70 %.
- The CCD sensor was estimated to have a read-out noise of 20 [14].
- Upwelling integrated radiance: calculated by integrating (trapezoidal rule) the upwelling radiance and transmission factors over the monitored wavelengths.
- Transmittance: assumed 0.88 (0.96 for three mirrors), from using a silver enhanced coating [9]
- Mirror IR noise: all the IR emittance from the top of the primary mirrors get into the sensor (worst case)

Moreover, the dynamic range and noise equivalent temperature difference could be calculated here to be around 202 and 0.035K, the latter using the method described in Chapter 11.

12.2.5. Summary

The summary of the payload final design for both the MS and TIR satellite is presented: Table 12.2, Table 12.3. Moreover, pictures of the reference DDST (Figure 12.1) are shown to add some visual understanding of the dimensions.

[c] https://www.weocorp.com/optical-coating/ [cited 18 June 2020]
[d] http://wise2.ipac.caltech.edu/docs/release/prelim/expsup/sec3_2.html#optics [cited 3 June 2020]
[e] https://ntrs.nasa.gov/archive/nasa/casi.ntrs.nasa.gov/20100030592.pdf [cited 12 June 2020]
[f] https://www.weocorp.com/optical-coating/ [cited 18 June 2020]
[g] https://www.engineeringtoolbox.com/emissivity-coefficients-d_447.html [cited 18 June 2020]

Table 12.2: Summary of the payload design TIR

Aspect	Reference	Value/ Item
Aperture	1500 mm	1024 mm
Focal length	11,000 mm	1750 mm
Distance primary-secondary	- mm	786.7 mm
Secondary mirror length	320 mm	219 mm
Primary mirror width	450 mm	307 mm
Secondary mirror width	96 mm	66 mm
Slit width	250 mm	171 mm
Cross central width	636 mm	434 mm
Stowed away volume	650 dm^3	303 dm^3
Mass	130 kg	60.620 kg
Sensor material	-	$H_gC_dT_e$
Sensor operational temperature range	-	80.5-81.5 K
Sensor Area	-	0.25 m^2
Mirror max calculated temp.	-	224.86 K
Mirror min calculated temp.	-	201.17 K
Sensor power usage nominal operations	-	5 W
Min/Max SNR	-	1077-2068
Dynamic range	-	202
Noise equivalent temperature difference	-	0.035 K

Table 12.3: Summary of the payload design MS

Aspect	Reference	Value/ Item
Aperture	1500 mm	1189 mm
Focal length	11,000 mm	875 mm
Distance primary-secondary	- mm	787 mm
Secondary mirror length	320 mm	254 mm
Primary mirror width	450 mm	357 mm
Secondary mirror width	96 mm	76 mm
Slit width	250 mm	198 mm
Cross central width	636 mm	504 mm
Stowed away volume	650 dm^3	409 dm^3
Mass	130 kg	81.72 kg
Sensor material	-	$H_{g0.3}C_{d0.7}T_e$
Sensor operational temperature range	-	190 K
Sensor power usage nominal operations	-	5 W
Signal to noise ratio	-	100-120

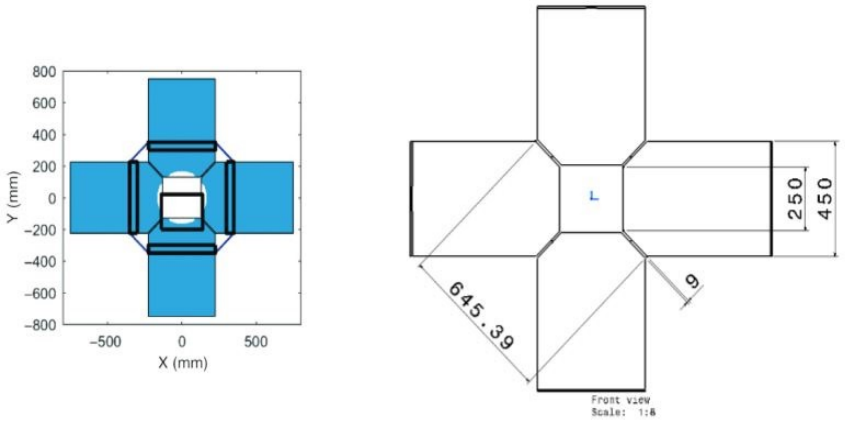

Figure 12.1: Dimensions discussed in this chapter for the reference telescope. Figures from Dolkens et al. [10, p. 366] and Krikken [11, p. 17], respectively

12.3. Verification and validation

Verification can be first done by inspecting assumptions. The most relevant one is the one regarding the fact that the MS telescope is signal, and not diffraction, limited. This is verified, by finding that the diffraction limited MS would have a smaller aperture than the signal limited: 0.1281 against 1.189 m. A smaller aperture means a smaller SNR. As put by the SNR calculation method Chapter 11, the SNR scales with the square of the aperture. If the aperture is of a factor 0.1281/1.189 smaller, then the SNR is decreased by 0.011. The SNR range is then 1.161 to 1.393. This proves that the scaling with TROPOMI is verified.

Lastly, the model to calculate the signal to noise ratio can be verified, as well as its equations, by increasing one input, for instance doubling the ground sample distance, and expecting the SNR to double. If the GSD is doubled from 5 to 10 m, with random, other but similar between both cases inputs, the SNR does increase by a factor of two: 4048 to 8096.

The largest aspect to validate is the SNR calculations for the TIR telescope. There the final SNR was calculated to be maximum 2068. However, an example used in SMAD [17], involving fire detection optics, calculated one of 2707. This difference is mostly due to different values used, such as: quantum efficiency, aperture or even altitude. If the values from the example are entered in the model, while accounting for a mistake in the book, the difference is of 3% which is deemed acceptable and thus validates the model used.

12.4. Compliance

Compliance refers to how well the requirements were met. Thus, analysis of the system was made, according to the method detailed in Chapter 11 what is the minimal number of humans (1 human: 0.15m^2), in Table 12.4.

Table 12.4: Precision in human detection for the TIR telescope

Environment	Temp.	Min. people - SNR	
		(mirror @201.17 K)	(mirror @224.86 K)
Desert	38 °C	6 - 10.63	11 - 10.15
Snow	0 °C	2 - 14.02	3 - 10.95
Standard sea level	15 °C	3 - 11.93	5 - 10.35

Furthermore, the maximum temperature was found to be 256.5 K for the primary mirror, which was in the case where the telescope could only detect a minimum of people similar to the desert at the lowest operating temperature, that is a minimum of 6 individuals.

It can be also said, that the TIR in combination with the MS, are able to find the thermal footprint and the gas density of events such as forest fires or volcanic eruptions. This is because the carbon dioxide, methane and temperature footprint are detectable by the system. With temperatures in multiples of hundreds of degree °C, the signal would definitely be high enough to be detectable.

12.5. Sensitivity analysis

Due to a low level of maturity, the volume and mass estimation needs more investigation. Thus, a sensitivity analysis can be performed to investigate the rigidity and contingencies of this method. The method assumed that the secondary to primary components have a ratio of 0.2/0.8 for contribution to mass and volume. Other ratios are investigated to test the rigidity of the method. The absolute difference here is the difference in percentage between the actual and the recalculated value of mass and volume.

Table 12.5: Sensitivity analysis for mass and volume

Mirror area ratio (secondary/primary)	Absolute difference [%]	
	TIR	MS
0.1/0.9	0.00624	0.00028
0.2/0.8 (original)	0	0
0.3/0.7	0.00790	0.00036
0.4/0.6	0.01824	0.00082

From the table above, Table 12.5 can estimate the method rigid. However, this does not allow to formulate contingencies. These are formulated with the help of the weight estimation method from a previous thesis [9].

Table 12.6: Sensitivity analysis for mass and volume

Mirror area ratio (secondary/primary[/rest])	MS		TIR	
	Mass [kg]	Volume [dm^3]	Mass [kg]	Volume [dm^3]
0.2/0.8	81.76	408.8	60.52	302.6
0.25/0.31/0.44	89.16	445.8	61.52	241.7

The percentage difference between the mass of one method against the other gives the contingencies of 9.05% and 1.65% for mass and volume of MS and TIR respectfully, shown in Table 12.6.

12.6. Risk mitigation

In Chapter 4, three risks were developed for the payload: TR-PAY-01, TR-PAY-02 and TR-PAY-03. Respectively, these were related to worse quality images, the telescope stopping to function for unknown reasons and the sensor not working due to its temperature being outside of its operational limits. The first risk was remedied by picking a CCD detector with time integration, as this is extremely proven technology. Moreover, the risk of unknown failure was not investigated here, as this is still an early design phase. Lastly, the third risk is partially answered here by providing clear temperature ranges and sensitivities. This will be further addressed when the overall satellite's thermal design will be made, and if a testable prototype is actually ever built.

12.7. Sustainability

Sustainability is in this chapter addressed for 3 criteria out of the 6 ones presented in Chapter 5.

- **Sustainable production and distribution:** The telescopes will be produced more than a 300 times each, thus allowing for series production and optimizing the use of various materials and allow less waste. Moreover, both the sensor material and mirror material are flight proven already, which decreases production time and resources, in comparison with a new material which would have to be developed. Moreover, for the mirrors, Silicon Carbide, allows for mirror production in weeks rather months [9]. Only using flight proven materials, allow this design to meet the payload sustainable requirement.
- **Economic sustainability:** Although, the telescopes still have to be developed, the series production of them will allow to reduce their individual costs drastically.
- **End-of-life sustainability:** Not a lot was made for this criterion. However, it can be said that the telescope does not have a lot of parts constituting it, which is favourable for minimising space debris.

Moreover, it is also worth noting that the telescope is key in completing the mission, and make the mission itself contribute to sustainability by providing data on gases in the atmosphere.

13

Constellation Design and Astrodynamic Characteristics

The constellation design is of paramount importance, as the decisions taken here affect most of the other subsystems if not all. In this chapter, first the requirements and compliance, as well as the assumptions will be shown in Section 13.1. Then, the constellation design and astrodynamic characteristics are shown and explained in Section 13.2. Then in Section 13.3, verification and validation is performed on the calculations and simulations.

13.1. Requirements and Assumptions

The requirements that are specific to this design aspect, followed by the assumptions made throughout the design phase are presented hereafter.

13.1.1. Requirements on Constellation Design

The main requirements that were identified as constellation design requirements are shown in Table 13.1.

Table 13.1: Constellation Design requirements and compliance

ID	Origin	Analysis ref.	
MIRA-USR-MIS-3	Customer	—-	✓
MIRA-USR-MIS-11	Customer	—-	✓
MIRA-USR-MIS-12	MR	FBS 6.2.1	✓
MIRA-USR-MIS-13	MR	FBS 6.2.2	✓

13.1.2. Assumptions

During the calculations and simulations the following assumptions were made:

- **A-CONST-01** *The Earth is assumed to be a perfect sphere.*
- **A-CONST-02** *No gravity perturbations were taken into account, except for the two-body perturbation in the simulation (STK).*
- **A-CONST-03** *Pure polar orbits are assumed, which implies zero precession.*
- **A-CONST-04** *The eccentricity is assumed to stay constant and equal to zero.*
- **A-CONST-05** *The altitude is assumed to stay constant.*

13.2. Constellation Design & Astrodynamic Characteristics

In this part, the constellation design parameters and the astrodynamic characteristics will be described and explained.

13.2.1. Orbital Altitude

The user requirements demand that the constellation operates at an altitude lower than 500 km (LEO). So, for an observational mission like this one, the lower the altitude, the better the quality of the images. It was therefore examined if low altitudes can be achieved for this mission. In Figure 13.1, the aerodynamic torque, ΔV for orbit maintenance and the ground sampling distance for the TIR and MS satellites are shown.

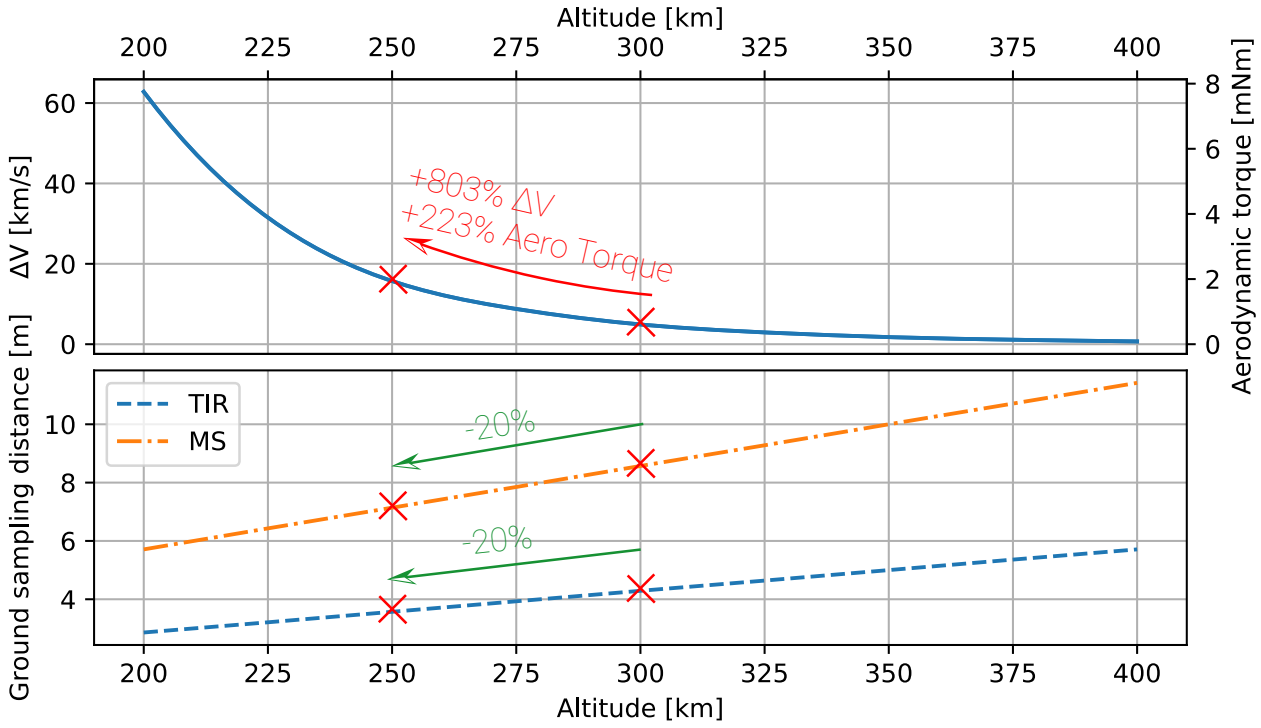

Figure 13.1: Graphs of aerodynamic torque, ΔV for orbit maintenance, ground sampling distance for TIR and MS satellites against altitude

Given the results seen in Figure 13.1, the team decided that altitudes below 300 km would not benefit the mission, as the negative influences of the aerodynamic torque and the ΔV far outweigh the gain in ground sampling distance. Therefore, altitudes above 300 km were examined.
Due to the addition of the baffle, which caused a significant increase in drag, causing a snowball effect, the altitude had to be chosen in such a way that the propulsion system could provide enough thrust to counteract the increased drag. Therefore, the altitude had to be increased. It was found that raising the altitude to 350 km was enough to solve these issues and maintain sufficiently high imaging quality. However, there are more LEO missions, which have to be taken into account as well. For example, Starlink orbits at a minimum altitude of 335 km[a]. This is however far enough from the MIRA constellation. So the altitude was chosen to be 350 km, which means requirement MIRA-USR-MIS-13 is met.

13.2.2. Orbit Type

Circular polar orbits are conceived as being the best choice in terms of orbit type. The main reason for that being that for polar orbits the constellation optimisation is much simpler [18]. However, having pure polar orbits increases the collision risk, as all satellites pass through the poles. Another option to prevent this is to tilt the orbits a little bit, but this complicates the built-up of the constellation significantly. Therefore, this option will not be investigated further and is considered to be outside of this project's scope. Extra attention will thus be paid to ensure no collision occurs near the poles by simulation and investigating the risk of collision.

13.2.3. Number of Satellites and Orbital Planes

To calculate the minimum number of satellites in polar orbits, Equation 13.1 can be used [18].

$$n_{polar,sat} = \frac{C_{\oplus}}{d_{swath}} \frac{1}{2} \frac{t_{orbit}}{t_{sample}} \tag{13.1}$$

From Equation 13.1, it can be seen that the number of TIR and MS satellites will be different, because there is a difference in the swath and temporal resolution for the two different satellites. The satellite carrying the TIR imager has a temporal resolution of 30 minutes and the MS satellite 60 minutes. So the number of satellites for both configurations varies, and has to be summed up to find the total number of satellites.

As mentioned before, and stated in Chapter 2, the requirements regarding the temporal resolution have changed. The Earth has to be monitored entirely by the multispectral imager every 60 minutes (raised from

[a] https://spacenews.com/spacex-asks-fcc-to-make-exception-for-leo-constellations-in-connect-america-fund-decisions/ [cited May 13 2020]

previously 5 minutes), which means a minimum of 152 satellites are needed. For the TIR imager, the temporal resolution is 30 minutes (raised from previously 5 minutes, too), meaning the minimum required number of TIR satellites is 605. This amounts to a total minimum of 757 satellites.

The minimum number of polar orbital planes can be calculated using Equation 13.2 [18], where t_{day} is the time of a sidereal day (86,164 s) and t_{sample} is the sampling time.

$$n_{polar,planes} = \frac{1}{2}\frac{t_{day}}{t_{sample}} \tag{13.2}$$

This results in 24 orbital planes for the TIR satellites and 12 orbital planes for the MS satellites. It was found out that the MS satellites can be placed in the same orbital plane as the TIR satellites. This resulted in a total of 24 planes of which 12 consists of only TIR satellites and 12 consists of both TIR and MS satellites.

The number of satellites in each orbit can then be found by dividing the number of satellites by the number of orbital planes. Doing so, one finds that the TIR satellites need 25.5 satellites per orbit while the MS satellites require 12.75. Since there is no possibility of having 0.5 or 0.75 satellite in an orbit, these numbers were rounded up. Multiplying again with the number of planes gives 624 TIR satellites, and 156 MS satellites, providing a total of 780 instead of the previously found 757. However, due to cost restrictions, maintenance primarily consists of having slightly more satellites in each orbit than necessary, to prevent the costly launches. In Chapter 6 it was already explained that 36 extra satellite will be launched. One satellite more in every TIR orbit and one TIR and one MS satellite more in every TIR and MS orbit. This results in a total of 816 satellites per generation.

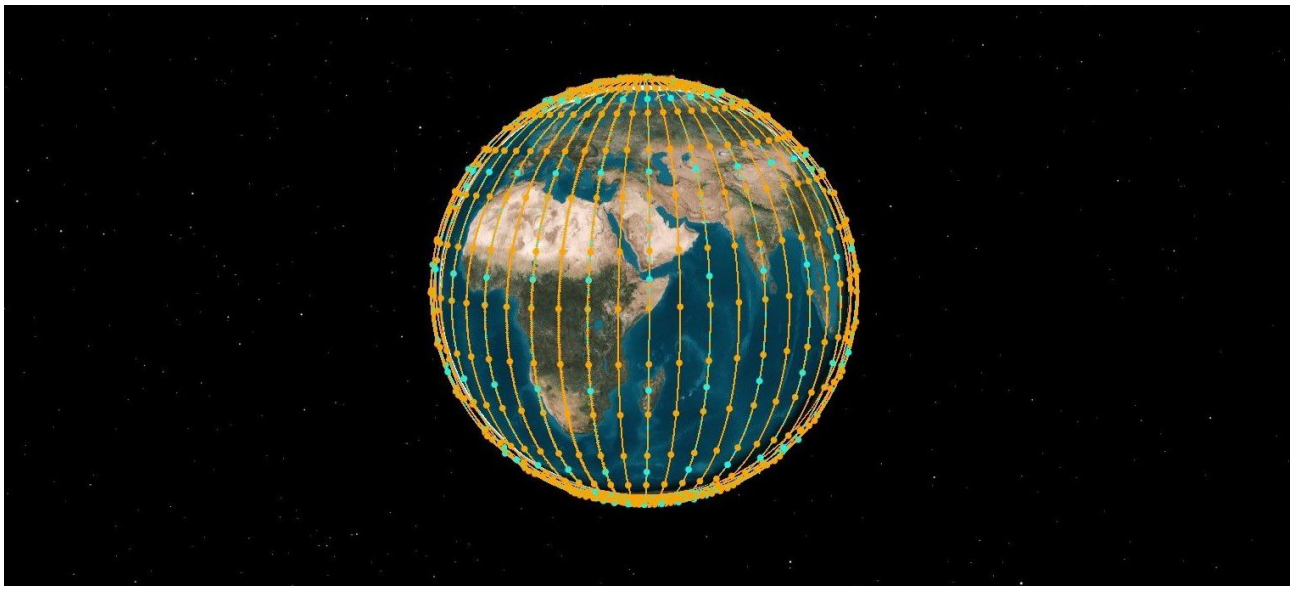

Figure 13.2: Visual representation of the constellation

To visualise the constellation and to show whether the requirements are met, the Systems Tool Kit (STK) [19] software was used. The constellation is composed of 24 orbital planes with 26 TIR satellites in each, and one MS satellite in alternating orbits between every second and third TIR satellite. This layout comes down to 13 MS satellites in every alternating orbit. In Figure 13.2, a part of the whole constellation can be seen, where the orange dots represent the TIR satellites and the light blue dots represent the MS satellites.

To verify if the requirements are met, a 2D ground map of Earth of both the TIR and MS satellites, was made and can be seen in Figure 13.3 and Figure 13.4. The image on the left side is at the starting time and is used as a reference for the image on the right side, which represents the ground map after the stop time, which spans a time interval equal to the corresponding temporal resolution of the TIR and MS satellites. Note that the direction of the satellites is either up or down, so it has to be checked if the squares, which represent the ground covered, do not leave gaps in the horizontal direction. In the vertical direction, it can be noticed that there are large gaps, however, this is due to the time step of the program. This was set equal to 60 seconds, because of computational power. Decreasing the time step crashed the program multiple times, so the time step stayed equal to 60 seconds. So, every 60 seconds an area with swath either 100 km or 200 km is stamped on the map. This thus leaves horizontal gaps. The main thing that has to be investigated is whether there are

any gaps between two neighbouring area stamps. This is the case in Figure 13.3, however, it can also be seen that there are satellites close to those gaps. Running the simulation just less than a few minutes longer then shows that these areas are covered nonetheless. For Figure 13.4, there are also tiny gaps, but these were also filled just less than half a minute after the required temporal resolution. So, in deliberation with the client, $\leq$ 10% deviation from the temporal resolution is still considered acceptable.

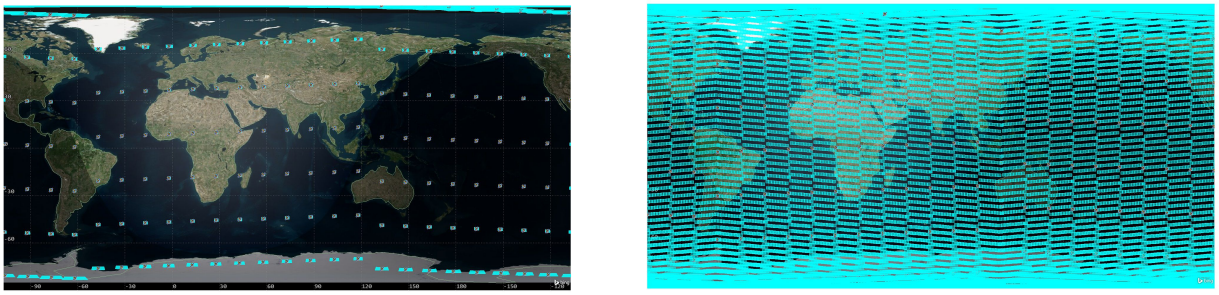

Figure 13.3: 2D ground map of MS satellites with t=0 min on the left and t=60 min on the right

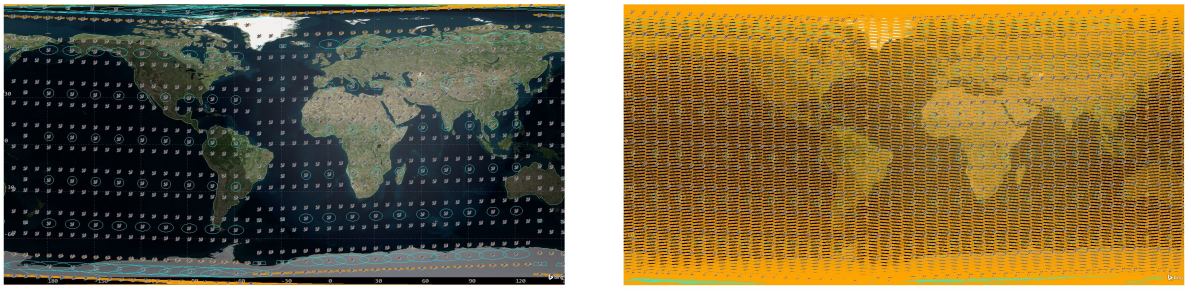

Figure 13.4: 2D ground map of TIR satellites with t=0 min on the left and t=30 min on the right

As can be seen from Figure 13.3 and Figure 13.4, the whole map is colored. It can be noticed that the ground map behind it is still visible. This was done on purpose as otherwise the figure would show one color with nothing visible on it. It can be seen that only a very small part is not monitored after 60 minutes for MS and 30 minutes for TIR, however the simulation ran after these times and it was observed that these gaps were filled in very quickly, after less than 2 minutes for MS and after less than a minute for TIR. Because these gaps were filled in so quickly, these small deviations in the temporal resolution are accepted by the customer after consultation. Therefore, the requirements on the temporal resolutions of the TIR and MS satellites are met, which automatically means that requirement MIRA-USR-MIS-3 is met as well.

13.2.4. Repeating Sunlight Period

For the power and thermal control subsystems, the amount of time spent in sunlight is of high importance. It is the driving factor for solar panel sizing and passive thermal control, for example. It is therefore necessary to get an insight into how much sunlight hits the satellites in different positions in the constellation.

In STK, a small model was made to graph the beta angle, which is the angle between the orbital plane and the sun vector. The simulation was run against time, for a time span of 7 years. In Figure 13.5 the graphs can be seen. The blue graph belongs to the satellite with a RAAN of 0°, the black one to the satellite with a RAAN of 45° and the light green graph belongs to the satellite with a RAAN of 90°. They were all simulated with at an altitude of 350 km with an inclination of 90° and a true anomaly of 0°. It can be noticed that the orbital planes find themselves in the same orientation with respect to the Sun at the same point in space every year: the maximum and minimum beta angles thus remain the same over the satellites' lifetime. This is consequence of the fact that perfectly polar orbits were assumed and there is therefore no precession of the orbit. This can also be seen by filling in i = 90° in Equation 13.3 [8].

$$\Delta\Omega_{J_2} = -1.5 \cdot n^2 \cdot J_2 \cdot \left(\frac{R_E}{a}\right)^2 \cdot \cos i \tag{13.3}$$

Further analysis on sunlight duration and beta angles can be found in Chapter 17 and Chapter 18. There, the data sets consist of single years to reduce computation time and to prevent repetitive graphs.

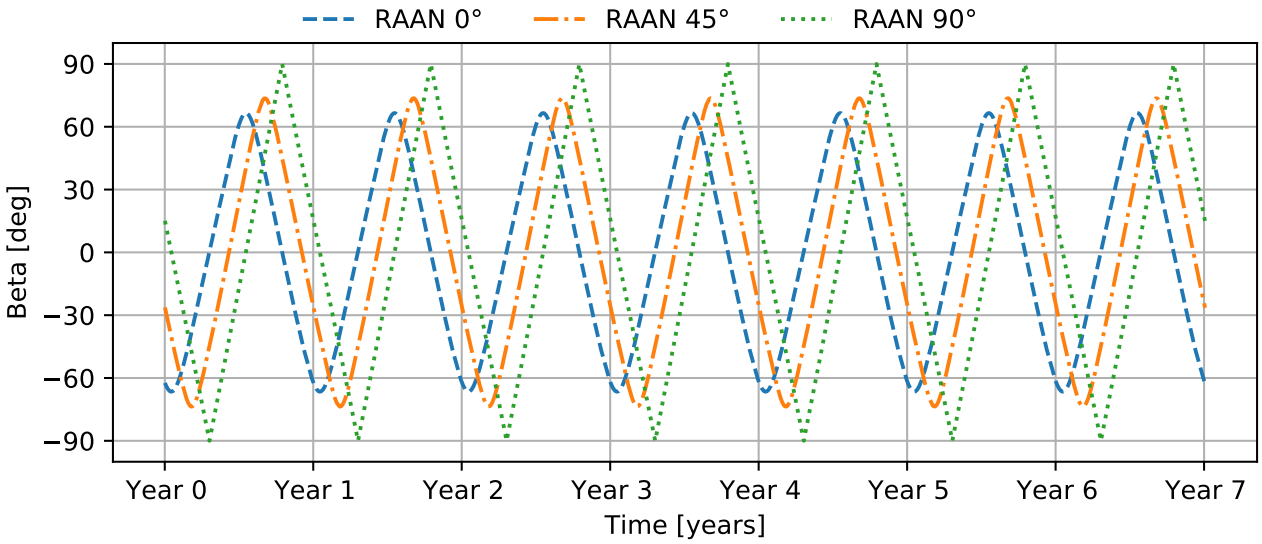

Figure 13.5: Beta angle for satellites with RAAN 0°, 45° and 90° vs satellite lifetime (7 years)

13.2.5. Inputs and outputs of this chapter

Table 13.2 shows the input and output parameters encountered in this chapter.

Table 13.2: Input and output parameters for Constellation Design

Input Parameter	TIR	MS	Unit
Circumference Earth	40075		km
Orbital period	91.54		min
Sidereal day	86164		s
Swath	100	200	km
Temporal resolution	30	60	min

Output Parameter	TIR	MS	Unit
Altitude	350		km
Number of satellites	648	168	-
Number of planes	24	12	-

13.3. Verification and validation

Verification of the equations used consists of using hand calculations to check if the right answers are obtained and double checking by other group members whether equations were used correctly. Also STK was used to verify answers as STK is an already verified and validated tool. For example, doubling the orbital altitude from 300 km to 600 km should increase the orbital period by 1.068. This is indeed the case, the period goes from 90.51 minutes to 96.69 minutes. This was also checked in STK and it showed indeed the same results.

Validation consists of using STK to check the answers obtained throughout this chapter. The most important results come from Figure 13.3 and Figure 13.4. As was already explained earlier, the difference in temporal resolution is only 3.33%, which was deemed acceptable. Therefore, these results can be validated with STK.

13.4. Sustainability analysis

For constellation design, the following sustainability criteria are addressed:

- **Social sustainability:** Light pollution coming from satellites in LEO is a well-known problem amongst the astronomical community. Satellites from the Iridium mission for example, create multiple so-called satellite flares each day, varying in magnitude. The MIRA constellation is much bigger and therefore also poses a threat. Even though the TIR and MS satellite bus is relatively small, their coatings are highly reflective and will therefore also produce flares. Therefore, it is recommended to investigate further into less reflective coatings for both the bus and the solar panels.

14
Propulsion and GNC

The propulsion subsystem is vital for ensuring the longevity of the mission. Overcoming drag and the capability of orbital manoeuvres is essential. The first part of the chapter provides a detailed analysis of the functions, requirements and characteristics of the propulsion subsystem, followed by the guidance, navigation and control (GNC) subsystem. The GNC is required for position and co-ordination characteristics, as explained in Section 14.7.

14.1. Functional analysis

The driving functions of the propulsion subsystem are listed below:

- **Plane change manoeuvres** With 24 orbital planes and an angle of 7.5 deg between each plane, an investigation into the feasibility of this is conducted in Subsection 14.4.2. Plane manoeuvres for spacecraft adjustments to counteract mission perturbations [20] and provide a level of mission flexibility.
- **Orbit phasing** If one or more spacecrafts in an particular orbit are decommissioned, the temporal resolution for that orbit becomes non-uniform. Although the absolute temporal resolution will be lowered, the effect can be minimised by evenly re-distributing the spacecrafts within the same orbit. The absolute temporal resolution will be lowered, but will be even for the whole orbit.
- **Drag compensation** Due to the low orbital altitude of 350 km, the drag experienced by the spacecraft can significantly decrease the lifetime of the mission. Hence a propulsion subsystem is required to counteract this drag force and extend the lifetime of the satellites and thus also of the mission.
- **Collision Avoidance** Low earth orbit consists of a multitude of spacecrafts and debris. The ΔV requirements are investigated in Subsection 14.7.3.
- **De-orbiting** Also as a result of the low altitude, the drag of the spacecraft is sufficient for de-orbiting procedures.

14.2. Requirements and assumptions

The subsystem requirements as shown in Table 19.1 characterises the functions and performance that spacecraft shall be capable of to ensure a successful mission. The assumptions highlight the main considerations that can influence and change the subsystem sizing and design.

14.2.1. Subsystem requirements

Table 14.1: Propulsion requirements

ID	Requirement	Origin	Analysis ref.	
MIRA-PROP-FUNC-1	The propulsion unit shall be capable of providing a minimum velocity change of 250 m/s for orbit plane manoeuvres.	BLR, MIRA-MIS-PROP-FUNC-11.1		✓
MIRA-PROP-FUNC-2	The propulsion unit shall be capable of providing the minimum velocity change for spacecraft drag compensation.	BLR, MIRA-MIS-PROP-FUNC-9.4		✓
MIRA-PROP-FUNC-4	The propulsion unit shall be designed to be compatible with any operational spacecraft attitude.	BLR, MIRA-MIS-PROP-FUNC-11.2		✓
MIRA-PROP-FUNC-5	The propulsion thruster shall be placed in a protective casing to limit electromagnetic interference with other subsystems.		Risk, TR-PROP-04	✓

Table 14.1: continued from previous page

ID	Requirement	Origin	Analysis ref.	
MIRA-PROP-PERF-1	The propulsion subsystem shall have a maximum weight of 62 kg.	BLR, MIRA-COST-PROP-PERF-2.7		✓
MIRA-PROP-PERF-2	The propulsion subsystem shall use a maximum power of 200 W.	BLR, MIRA-COST-PROP-PERF-2.8		✓
MIRA-PROP-PERF-3	The propulsion subsystem shall be able to provide the delta V required for a maximum phase change angle of 8.58 deg per 24 hours.			✓
MIRA-PROP-PERF-4	The propulsion subsystem shall be capable of detecting propellant tank leakage.		Risk TR-PROP-03	✓
MIRA-PROP-SUS-1	The total mass of the propellant used shall be minimised.		Sustainability	✓

14.2.2. Assumptions

For sizing and designing the propulsion subsystem, the assumptions considered are listed below:

- **A-PROP-01** *The reduction in temporal resolution during spacecraft phasing after launcher separation will not effect mission success.* After separation from the launcher, the spacecrafts have to undergo a phasing manoeuvre to position them across various points in the orbit. The minimum needed phase change for a satellite to go to any point in the orbit is 180°. During this phasing manoeuvre, there is a reduction in temporal resolution as the spacecrafts have to thrust for a specific duration to position themselves. It is assumed that this period of reduced temporal resolution will not effect the mission success.
- **A-PROP-02** *The spacecraft shall be capable of continuous low thrust operations.* Extended thrusting durations can have adverse effects on the spacecraft subsystems such as temperature build up of thruster components or transverse torques due to thrust misalignment. These factors are assumed to be within the design envelope of the spacecraft subsystems.

14.2.3. Risk Mitigation

- **TR-PROP-01** The risk shall be mitigated by ensuring that all thrusting durations are temperature monitored, along with subsystem orientation with respect to sunlight in orbit.
- **TR-PROP-02** The risk shall be mitigated using a circuit breaker switch in the electronics control unit.
- **TR-PROP-03** The risk shall be mitigated using pressure sensors that are monitoring propellant storage pressure and temperature. In the event of a leakage, the rate of leak will be estimated using pressure values and due to the criticality level of the risk, the spacecraft will be decommissioned. Critical levels include cases of propellant leaking leading to un-controllable satellite, explosion risk and incapability of payload operations.
- **TR-PROP-04** All sensitive instruments will be encased in protective casing.
- **TR-PROP-05** The thruster noise will be simulated and the science instruments will be calibrated to overcome this. Furthermore, there will be protective casing between the subsystems.

14.3. Subsystem characteristics

This section highlights the various performance and sizing characteristics of the electric propulsion subsystem, to meet the requirements. First, the propellant parameters are mentioned, followed by the thruster sizing and the propulsion subsystem operations.

14.3.1. Propellant determination and sizing

The propellant storage and its parameters are further being explained, with the results highlighted in Table 14.2.
Propellant: Krypton is cheaper and more readily available than xenon, although some degradation in perfor-

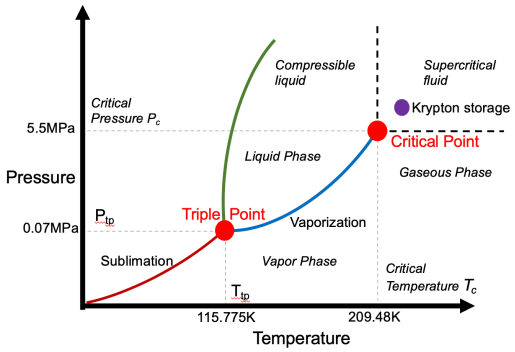

Figure 14.1: Propellant storage analysis

mance is expected. The average cost of Xenon is 2460 €/kg while Krypton costs an order of magnitude lesser, at 185 €/kg [21]. The lower atomic mass of krypton leads to an increased power requirement for a given thrust, but initial drag estimates for the MIRA spacecraft should low orders of magnitude of drag. Furthermore, the overall performance of Krypton and Xenon are similar, as studied in Fazio et al. [21]. Hence krypton was chosen as the propellant of choice.

Storage: To optimise the volume needed, it is stored as a high-pressure supercritical fluid, as shown in Figure 14.1. To maintain a single-phase state throughout the entire mission, it is necessary to maintain a minimum propellant temperature of 209.48 K and minimum pressure of 5.5 MPa. In this state, Krypton is at a temperature above its critical point, where liquid and gas phases exist in combination [21]. Below this minimum temperature, krypton could go into a liquid state and that may result in sloshing or injection of liquid into the feed system resulting in krypton-flow spikes.

Furthermore, the propellant tank contains temperature and pressure sensors for monitoring. Equation 14.5 and Equation 14.6 are used to size the required tank thickness and to account for over pressurization, the tank is sized upto a maximum pressure of 8.25 MPA [22].

Table 14.2: Propellant tank parameters

Parameters	Value	Unit	Parameters	Value	Unit
Tank material	Ti-6Al-4v	-	Propellant utilisation efficiency	0.95	-
Material density	4.43	g/cm^3	Propellant density	2.56	g/cm^3
Material yield stress	880	MPA	Propellant temperature	-64	°C
Tank thickness	0.15	cm	Propellant pressure	5.5	MPa
Tank safety factor	1.5	-	Tank design pressure	8.25	MPa
Atomic mass of propellant	83.9	amu	Minimum flow rate	170	µg/s

14.3.2. Performance characteristics

Equations used: Using the input parameters shown in Table 14.4 and Equation 14.1 to Equation 14.2 represent some of the equations used to size the propulsion subsystem performance, where M is the atomic mass of the propellant (in kg), η_m is the propellant utilisation efficiency, and q in Equation 14.2, for a singly charged propellant, is e (the electron charge) [23]. The factor γ refers to the thrust correction coefficient. Based on a 10° half angle of beam divergence and a 10° doubles - to - singles ratio, γ is assumed to be equal to 0.958 [23]. The electrical efficiency of the thruster is shown by η_e, which is the output beam power of the thruster divided by the total input power. The total input power contains beam power and additional power required to overcome discharge losses. For the thruster of MIRA, it is assumed that a 5 V and 2 A discharge is needed to produce a 0.2 A thruster beam. The discharge loss is then given by $\frac{2.5\times1}{0.2}$, resulting in 12.5 eV/ion, denoted by V_o [23] [24]. The power loss due to discharge can then be obtained by I_b and V_o.

Drag: A drag coefficient of 2.8 is chosen to account for the drag from baffle and the solar panels [8].

Thruster operation: For the same total applied power and required ΔV, the differences in performance of

the ion propulsion subsystem are presented in Table 14.3. The drag was determined to be in the order of millinewtons, as shown in Table 14.5 and hence optimising for thrust was not the driving parameter. The operational mode of lower propellant mass, with Equation 14.6, is determined to be more favourable due to a lower spacecraft mass, along with satisfying the sustainability requirement of MIRA-PROP-SUS-1. The lower total spacecraft mass is also favourable due to the lower cost propellant required and lower launch costs. Therefore, the thruster is to be designed to operate with high beam voltages and low beam currents. The advantages of this operational mode are further highlighted with Figure 14.2.

Hence, the MIRA spacecraft shall constantly thrust for its operational lifetime (nominal thrust), to overcome the drag force experienced [25]. During manoeuvring or adjustments, the spacecrafts input power will increase to enable higher thrust forces.

Table 14.3: Thruster Operation

Operational Mode	Advantage	Disadvantage
High Voltage - Low Current	High ISP, Low propellant mass	Low thrust
High Current - Low Voltage	High thrust	Low ISP, High propellant mass

Thruster efficiency: is given by η_T which relates to the beam characteristics, electrical efficiency η_e and propellant utilisation efficiency, as shown in Equation 14.3 and Equation 14.4. The applied voltages and currents refer to the total power obtained from the power subsystem. The difference between the applied power and ion thruster beam power is accounted for by the applied electrical and thruster efficiencies. Electrical efficiency is the efficiency of converting applied input power to the ion beam power, whereas the thruster efficiency is total efficiency of subsystem [23].

$$F_T = \sqrt{\frac{2M}{q}} \cdot \gamma \cdot I_b \cdot \sqrt{V_b} \tag{14.1}$$

$$I_{sp} = \frac{\gamma \cdot \eta_m}{g} \cdot \sqrt{\frac{2 \cdot q \cdot V_b}{M}} \tag{14.2}$$

$$\eta_e = \frac{P_b}{P_t} = \frac{I_b \cdot V_b}{I_b \cdot V_b + I_b \cdot V_o} \tag{14.3}$$

$$\eta_T = \gamma^2 \cdot \eta_e \cdot \eta_m \tag{14.4}$$

$$\sigma_t = \frac{r_i^2 \cdot P}{2 r_i t + t^2} \tag{14.5}$$

$$M_p = M_{sc} \cdot \left(e^{\frac{\Delta V}{g \oplus I_{sp}}} - 1 \right) \tag{14.6}$$

Table 14.4: List of input values for subsystem sizing

Input Parameters	Value	Unit	Input Parameters	Value	Unit
Orbit altitude	350	km	Plane change angle (max.)	0.0698	rad
Operational lifetime	7	years	Phase change angle (max.)	3.14	rad
End of life orbit	150	km	Phase change rate (max.)	0.15	rad/day
Eccentricity of orbit	0	rad	Discharge loss	12.5	eV/ion
Inclination of orbit	1.57	rad	Thrust diameter	5	cm
Atmos. density (avg.)	6.66×10^{-12}	kg/m^3	Thrust correction factor (γ)	0.958	-
Prop. contingency	10%	-	Electric charge (q)	1.602×10^{-19}	C

Using Equation 14.1 and Equation 14.2; Figure 14.2 display how the ISP and thrust are influenced by the ion beam voltage and currents. In all the cases, the maximum ion beam power is constant. The figures display how higher ion beam voltage leads to higher ISP and hence a lower propellant mass (see Table 14.3). When the beam current is kept constant, with increasing voltage, the thrust has a smaller gradient when compared to that of increasing input beam current. With a constant beam voltage and increasing beam current, the gradient of thrust increase is greater as shown. It is hence more advantageous to operate at a higher beam voltage (leading to higher ISP and lower propellant mass, as shown in Table 14.3) and modulate the thrust levels by modulating the ion beam current.

Table 14.5: List of output values for subsystem (est. = Estimated)

Output Parameters	TIR	MS	Unit
Drag coefficient	2.8	2.8	-
Frontal area	3.15	3.65	m^2
S/c dry mass	181.11	207.82	kg
Input vol.	100	100	V
Input cur. (nominal)	0.5	0.5	A
Input cur. (max.)	0.7	0.71	A
Ion beam vol. (est. V_b)	85	85	V
Ion beam cur. (est. I_b)	0.2	0.23	A
Electrical eff. (η_e)	87.1%	87.1%	-
Thruster eff. (η_T)	76%	76%	-
Specific Impulse	1355.7	1355.7	s
Orbital velocity	7.7	7.7	km/s

Output Parameters	TIR	MS	Unit
Drag force (avg.)	1.75	2	mN
Phasing time (max.)	18	19	days
Phasing thrust (max.)	6.6	6.8	mN
Thrust (nominal)	1.8	2	mN
Thrust (max.)	6.75	6.85	mN
Plane change ΔV	251.8	251.8	m/s
Orbit phasing ΔV	54.33	51.47	m/s
Drag ΔV	2121	2147.7	m/s
Total ΔV	2427.1	2445	m/s
Propellant mass	30.2	34.8	kgs
Propellant volume	12504.5	14445.2	cm^3
Tank diameter	28.8	30.2	cm
Dry tank mass	1.75	1.9	kgs
De-orbit time	117	116	days

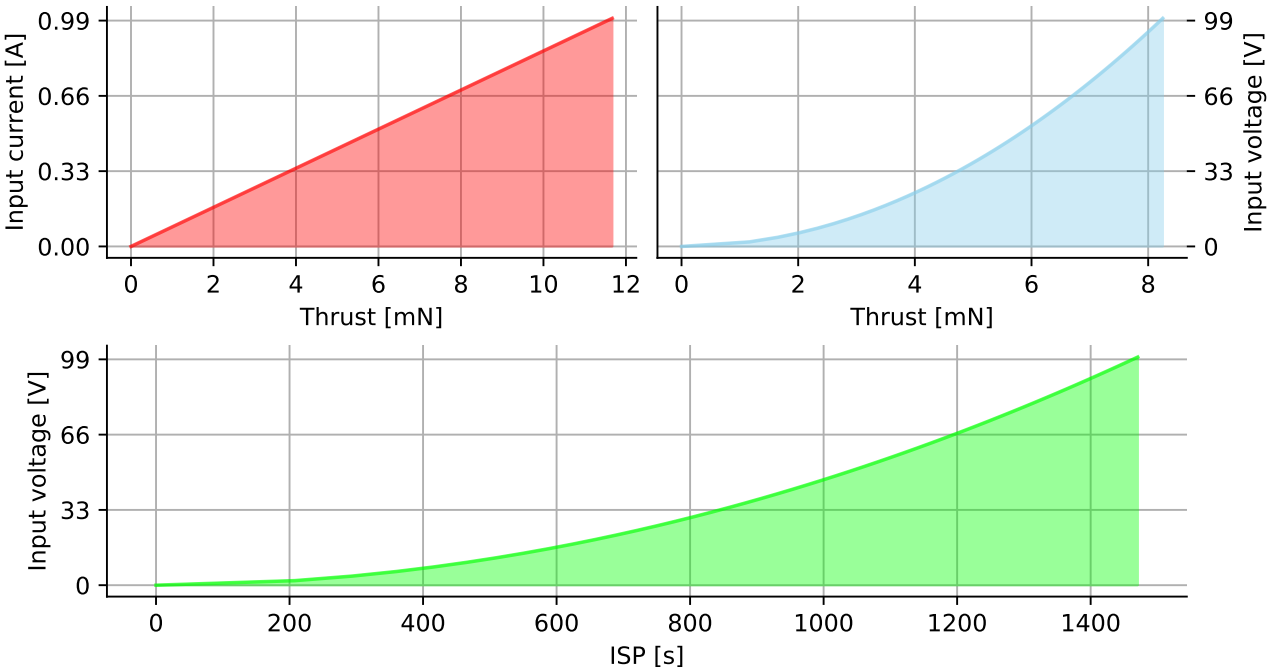

Figure 14.2: Relations between thrust, ISP, ion beam current, and ion beam voltage, for same total input power

14.3.3. Subsystem Components

Table 14.6: Propulsion components

Component	Mass [kg]	Volume [cm^3]
Ion thruster unit	3	18
Power processing unit	4	15
Digital control unit	1	5
Propellant feed system	4	7

The propulsion subsystem contains four main components, namely: The krypton propellant feed system, the power processing unit, the digital control interface unit, and the ion thruster assembly [26] [27]. These are shown in Table 14.6. All components are specified to MIL-STD-461 and communications between the components occur through the RS-485 lines. The thruster and components will be encapsulated in a protective casing to ensure no other subsystems are effected by electromagnetic interference during thrusting operations.

Krypton feed system (KFS): The propellant feed system being powered by power processing unit (PPU) which converts power from the solar arrays to the voltage and current required by the thruster, all being controlled by the digital control interface unit (DCIU). The DCIU will execute high-level commands and will provide subsystem telemetry to the on-board computer. To account for variations in input power, the subsystem is designed to operate in a power range of 40 W to 100 W. The discrete power levels that lead to variations in thrust within this range, are considered as ”throttle levels” [27]. Valves will be present to allow for over-pressuring release of the propellant in case of safety risks.

Ion thruster assembly: The thruster will be 50 mm in diameter and shall be capable of gimbaling [28] up to a maximum of 5°. The difference between applied power and ion beam power is due to the additional power requirements of the components mentioned in Subsection 14.3.3. It is assumed that during thrusting, ion temperature is maintained with the heaters and only having additional power requirements at lower throttle levels.

Power Processing Unit (PPU): The PPU is designed to take input of 40 V to 200 V directly. It is packed in a separate enclosure from the DCIU and is design to be bolted onto the spacecraft bus in an area where the excess heat output can be thermally radiated to space. During nominal operations, the PPU provides four steady state outputs: beam voltage, accelerator-grid voltage, discharge current and neutraliser-keeper current. During thruster startup, the PPU provides the heater power and also contains internal protection against input over- and under-voltage conditions. Each power supply line is also short-circuit protected.

The Digital Control and Interface Unit (DCIU): The DCIU is the data acquisition control and communications unit. The main functions are: acquisition, storage, processing of the signals from the sensors and telemetry from PPU; control of the valves, control of the power supplies in the PPU, and communications with the spacecraft data-and-control system. The DCIU executes stored sequences that control thruster operating modes in response to the commands generated. The DCIU is designed to operate from −15°C to 50°C with survival limits of −25°C to 55°C [27].

Thermal during operations: Cooling parameters of the propellant tank have been analyzed in Subsection 18.7.6. The PPU can dissipate heat and the top plate is used as the PPU thermal radiator. The nominal operations range for the PPU is between −5° and 50 degree, with maximum survival-temperature limits of −25° and 50°. During thrusting, the internal dissipation of the PPU maintains the PPU temperature, with the heaters being required only for operation at lower throttle levels. To minimise the power needed to heat the PPU at lower throttle levels, the PPU temperature is kept near the lower limit allowed for nominal operations. For the power required by the subsystem, higher throttle levels will require the 50 W for thrusting, whereas during lower throttle levels, the 50 W is distributed between the thruster and PPU maintenance with minimum operational power for the component [27].

14.4. Launch Parameters

The constellation is required to be launched into orbit for a successful mission. In this section, various launcher are investigated in terms of mass, capacity (volume) and launch cost, to obtain the optimal launch considerations.

14.4.1. Requirements on Launch Parameters

The requirements to do with the launch parameters can be seen in Table 14.7.

Table 14.7: Launch Parameter requirements

ID	Origin	Analysis ref.
MIRA-USR-SUS-4	Customer	
MIRA-USR-SUS-5	Customer	
MIRA-USR-MISC-3	Customer	
MIRA-SUS-FUNC-3.5	BLR, MIRA-MISC-SUS-FUNC-3.5	MIRA-USR-MISC-3

14.4.2. Launch Vehicle and Number of Launches

Since the constellation consists of many satellites and many planes, it has to be thoroughly investigated how to optimise the number of launches, with the final choice driven by the launch cost. The parameters considered are volume, mass and number of satellites. A number of options were considered:

1. Use a large launch vehicle that can carry multiple satellites. After launcher separation, the satellites will thrust to their assigned orbital plane.
2. Use smaller launch vehicle that can only fill one orbit or lesser, with satellites.
3. Use a large launch vehicle with a smaller amount of satellites and more propellant mass to have the rocket change orbital planes.
4. Use one launch vehicle per orbital plane.

Option 1: the capability for satellites changing orbital planes was investigated. The difference between planes is equal to 7.5 degrees and using Equation 14.8, the ΔV for a plane change manoeuvre can be calculated using Equation 14.7. [29]. [18]

$$\Delta V_\omega = 2 \cdot V \cdot \sin\left(\frac{\Delta\omega}{2}\right) \tag{14.7}$$

$$t_b = \frac{M_p I_{sp} g_\oplus}{F_T} \tag{14.8}$$

Table 14.8: Satellite parameters for plane change of 7.5°

Plane change (deg)	Delta V (m/s)	Propellant Mass (kg)	Burn time (days)
7.5	1007	18.5	776

The team concluded that due to the burn time being nearly 30% of mission duration per satellite generation, the Option 1 of satellite plane changes can not be considered as a feasible option.

Option 2: A list of existing and active launch vehicles is made and can be seen in Table 14.9. A support cylinder is assumed within the launcher, to hold the satellites until orbital deployment. Sizing equations of this cylinder and the associated structures can be found in Section 19.4. A supporting structure is used inside the payload fairing to which the satellites can be mounted. It is then investigated whether capacity or mass would be the limiting factor in the amount of satellites that can be launched. This was first done for volume and detailed explanations are provided in Chapter 19. For the smaller launchers like Electron and Pegasus, a N/A is shown for most entries. This is because these launchers are too small to carry satellites. For Vega, a different supporting structure will be used, namely a Vespa payload adapter[a]. This was done, because this launcher is too small to use a supporting cylinder structure.

The supporting structure will be a hollow cylinder, larger the outer radius, the more satellites can attach to it. The maximum radius is given in Table 14.9 and α is the angle between the outer side of one satellite to the middle of the cylinder. By using this parameter, it can be determined how much satellites can attach to the cylinder on one layer. The number of layers is then calculated using the height one satellite and the usable height of the payload fairing. Finally, the maximum number of satellites that can fit inside the launcher is given. More detailed information is provided in Section 19.4.

[a] http://www.esa.int/Enabling_Support/Space_Transportation/Deploying_multiple_satellites_with_Sylda_and_Vespa [cited 28 June 2020]

For relating launch mass capability and number of satellites, the launcher payload mass minus the cylinder mass is divided by the averaged mass of the satellites, which is 275 kg. The cylinder mass was obtained by setting up a relation between the mass of cylinder necessary per satellite, using previous similar mission. It was found that around 50 kg of supporting structure is required per satellite. Then the cylinder mass for each launcher was then calculated based on the maximum capacity of the launcher.

The minimum number of satellites that can be launched is based on either capacity or mass and will be used to calculated the number of launches needed with that particular launch vehicle. As can be seen, Electron, Pegasus and Vega are small launch vehicles and consequently, these launchers can not bring a significant amount of satellites into orbit or any at all. The costs of using only those types of launch vehicles would increase drastically and in addition the sustainability deteriorates. So, option 2 was discarded. However, if necessary, Vega will be used for maintenance, in essence, launching one or two satellites when orbiting satellites fail, because Vega is the cheapest launch vehicle capable of launching a couple of satellites.

Option 3: The larger launch vehicles were investigated. It was noticed that no launch vehicles exist, that can bring 65 satellites into orbit. This lack of suitable launchers means that at least 24 launches are required, and thus Option 3 is eliminated. The number of satellites is limited by either launcher capacity and payload mass.

Option 4 (chosen option): As can be seen in Table 14.9, there are many launch vehicles that can be used. To pick the best option(s), the number of satellites has to be considered. For instance, if a launcher can bring more than 26, but less than 39 satellites into orbit, it can be used to fill orbits with only TIR satellites. If a launcher can launch 39 satellites or more, it can be used to fill orbits with both TIR and MS satellites. Looking in Table 14.9, and considering cost as the main criterion, Falcon 9 FT would be the best option to launch TIR satellites and Atlas V would be the best option to launch both TIR and MS satellites.

14.4.3. Launch site

To launch in polar orbits, the options for launch sites are limited. Because the launcher of choice is the Falcon 9, an American launcher, the best option is to launch in the US as well. From the Falcon user guide [30], the only launch site that is able to launch the Falcon 9 at a 90 degree inclination is the Vandenberg Air Force Base located in California.

14.5. Verification and Validation

Looking at Table 14.5, hand calculations were done to verify the results. Linearity checks were conducted by increasing input mass and power, to check the trends observed and confirm proportionality, thereby verifying the tool. For validation, input parameters from previously flown missions and commercial off-the-shelf components were considered [21]. Validated test platforms will simulate real life mission scenarios for flight qualification and validation of the electric propulsion subsystem [31].

14.6. Sustainability

For the ground based sustainability aspect, as the subsystem is electric propulsion based, combustion emissions are not released during all testing procedures. Furthermore, the electricity required can be obtained through renewable energy methods. Krypton manufacturing will be done through the process of distillation-liquefaction, which is more sustainable than other methods, as also explained in Section 6.4. Furthermore, as highlighted in Table 14.3, minimum propellant mass is chosen as a more driving criteria than thrust, this reduces the total amount of propellant required to be manufactured.

For space based sustainability, as krypton is an inert gas, propellant leaking in space will not effect the ozone layer. Furthermore, the spacecraft can be de-orbited without thruster operations and the remaining propellant mass will remain non-reactive during atmospheric re-entry and disintegration of the satellite during de-orbiting.

Table 14.9: List of potential launch vehicles

	Falcon 9 FT [30]	**Antares**[b]	**Electron**[cd]	**Atlas V**[ef]	**Delta IV**[gh]	**Pegasus**[i]	**Ariane 5**[jk]	**Vega**[lm]
Payload fairing height [m]	7.73	9.87	1.91	14.64	9.53	2.13	13.49	3.18
Payload fairing diameter [m]	4.6	3.74	1.08	4.57	4.57	1.12	4.57	2.43
Maximum radius of cylinder [m]	1.04	0.60	N/A	1.03	1.03	N/A	1.03	N/A
α [rad]	1.03	1.56	N/A	1.04	1.04	N/A	1.04	N/A
No. of satellites in one layer [-]	6	4	N/A	6	6	N/A	6	N/A
No. of layers [-]	5	7	0	10	7	0	9	0
Vespa payload adapter	N/A	N/A	N/A	N/A	N/A	N/A	N/A	2
No. of satellites based on capacity [-]	30	28	0	60	42	0	54	2
Max payload mass allowed [kg]	16800	8000	185	15760	11600	443	14000	2000
Support cylinder mass [kg]	1500	1200	N/A	2700	1800	N/A	2400	N/A
Vespa payload adapter mass[n] [kg]	N/A	N/A	N/A	N/A	N/A	N/A	N/A	390
Mass leftover for satellites [kg]	15300	6800	185	13060	9800	443	11600	1610
No. of satellites based on mass [-]	69	31	0	59	44	2	52	7
No. of launches per generation [-]	>24	>24	0	>12	>12	0	>12	408
Cost launcher [M€]	44 (Reused)	70.4-74.8	5.28	96.8	114.4-132	35.2	145.2-193.6	32.56
Launch cost per generation [M€]	1056 (Reused)	>1690	N/A	>1161	>2746	N/A	>1740	13284

[b] http://spaceflight101.com/spacerockets/antares-200-series/ [cited May 12 2020]
[c] https://www.rocketlabusa.com/electron/ [cited May 12 2020]
[d] https://www.rocketlabusa.com/assets/Uploads/Rocket-Lab-Payload-Users-Guide-6.4-2020.pdf [cited May 12 2020]
[e] https://en.wikipedia.org/wiki/Atlas_V [cited May 12 2020]
[f] https://www.ulalaunch.com/rockets/atlas-v [cited June 18 2020]
[g] https://en.wikipedia.org/wiki/Delta_IV [cited May 12 2020]
[h] https://www.ulalaunch.com/rockets/delta-iv [cited June 18 2020]
[i] https://web.archive.org/web/20160113130631/https://www.orbitalatk.com/flight-systems/space-launch-vehicles/pegasus/docs/Pegasus_UsersGuide.pdf [cited May 12 2020]
[j] https://en.wikipedia.org/wiki/Ariane_5 [cited May 12 2020]
[k] https://www.arianespace.com/wp-content/uploads/2011/07/Ariane5_Users-Manual_October2016.pdf [cited June 18 2020]
[l] https://en.wikipedia.org/wiki/Vega_(rocket) [cited May 12 2020]
[m] https://www.arianespace.com/wp-content/uploads/2015/09/Vega-Users-Manual_Issue-04_April-2014.pdf [cited June 18 2020]
[n] https://www.arianespace.com/wp-content/uploads/2018/07/Vega-C-user-manual-Issue-0-Revision-0_20180705.pdf [cited 28 June 2020]

14.7. Guidance, Navigation and Control

The driving functions of the GNC subsystem are listed below:

- **Location and Velocity tracking** The spacecrafts function of determining it absolute position with respect to the ground and the relative position with respect to the other spacecrafts in the constellation. Along with this, the spacecraft should be capable of determining its velocity
- **Collision avoidance** The spacecrafts function of predicting the probability of collision with space debris or other spacecrafts in the constellation. Along with spacecrafts on-board computer, the subsystem shall be able to determine the required manoeuvre to be undertaken by the ADCS and propulsion subsystem to avoid collisions and debris formation.

Table 14.10: GNC design requirements

ID	Requirement	Origin	Analysis ref.	
MIRA-GNC-FUNC-1	The GNC system shall be capable of preventing collisions that result from orbit drifting.	BLR, MIRA-MIS-GNC-FUNC-5.3		✓
MIRA-GNC-FUNC-2	The GNC system shall be capable of determining the absolute position of the ground station for data uplink.	BLR, MIRA-MIS-GNC-FUNC-4.2		✓
MIRA-GNC-FUNC-3	The GNC system shall be capable of determining the absolute position of the ground station for data downlink.	BLR, MIRA-MIS-GNC-FUNC-4.3		✓
MIRA-GNC-FUNC-4	The GNC system shall be able to determine the required manoeuvres for orbit maintenance.	BLR, MIRA-MIS-GNC-FUNC-9.1		✓
MIRA-GNC-FUNC-5	The GNC system shall be able to determine the required manoeuvres for de-orbit.	BLR, MIRA-SR-GNC-FUNC-3.1		✓
MIRA-GNC-FUNC-6	The GNC system shall be able to withstand Earth gravity perturbations.	BLR, MIRA-MIS-GNC-FUNC-9.2		✓
MIRA-GNC-FUNC-7	The GNC system shall be able to manoeuvre to avoid predetermined debris.	BLR, MIRA-MIS-GNC-FUNC-9.3		✓
MIRA-GNC-FUNC-8	The GNC system shall ensure location calibration with respect to other spacecrafts to a minimum accuracy of 1 km.	BLR, MIRA-MIS-GNC-FUNC-5.4		✓
MIRA-GNC-FUNC-9	The GNC system shall be capable of determining the absolute position of the spacecraft to a minimum accuracy of 10 m at all times for the duration of the mission.	BLR, MIRA-MIS-GNC-FUNC-5.2		✓
MIRA-GNC-FUNC-10	The satellites shall use a sensor that will provide information on the positions of the other satellites.		Risk TR-GNC-01	✓
MIRA-GNC-PERF-1	The GNC subsystem shall have a maximum weight of 5 kg.	BLR, MIRA-COST-GNC-PERF-2.5		✓
MIRA-GNC-PERF-2	The GNC subsystem shall use a maximum power of 10 W.	BLR, MIRA-COST-GNC-PERF-2.6		✓

14.7.1. Assumptions

- **A-GNC-01** *The satellites will be capable of receiving GNSS signals for at least 99% of the orbit.* The GNSS constellation has been built up enough to provide the MIRA satellites receivers, position and location data for at least 99% of each orbit.

14.7.2. Subsystem Components

A commercially available GNSS signal receiver is utilised for the spacecraft location and velocity tracking Table 14.11. This hardware is combined with software architectures of coordination and control approaches. The spacecraft will contain software architecture that will be using position and velocity measurements to simulate the orbit and predict collisions [32].

Table 14.11: GNSS receiver [33]

Commercial Component	Signals	Position accuracy	Velocity accuracy	Power	Mass
Navileo	Galileo E1b, E5a	<5 m	4 mm/s	8 W	1.3 kg

Table 14.12: Spacecraft coordination approaches [34]

	Advantages	Disadvantages
	Coordination approach	
Swarming	Simple heuristic control laws for arranging arbitrarily large numbers of vehicles into regular arrangements based on local formation. They can be easily scaled to large number of vehicles without incurring large communication or computation burden.	Does not optimise fuel use and yet to be flight proven. Additional architecture required for precise collision avoidance.

Position and velocity tracking with GNSS receivers in real-time allow for a quicker and increased accuracy in spacecraft location tracking. Besides that, a level of autonomy incorporated into spacecraft operations which benefits from precise knowledge of its position [35]. Furthermore, on a software level, various methods for coordination and control approaches were studied [36]. Ground station databases will be used to track and monitor other spacecrafts in the constellation to predict possible collisions and apply appropriate measures.

14.7.3. Collision Avoidance

Collision avoidance in space is an important aspect. All satellites should be able to avoid collision with space debris, other satellites from the constellation and other satellites in general.

Using ESA's MASTER and DRAMA software [37], which has already been verified and validated by the developers of the software, the collision risk for space debris can be calculated and graphed. As input parameters, the most simple satellite was chosen having an altitude of 350 km, an inclination of 90 degrees, RAAN of 0 degrees and True Anomaly of 0 degrees. In Figure 14.3, the probability of collision is shown against the size of the space debris.

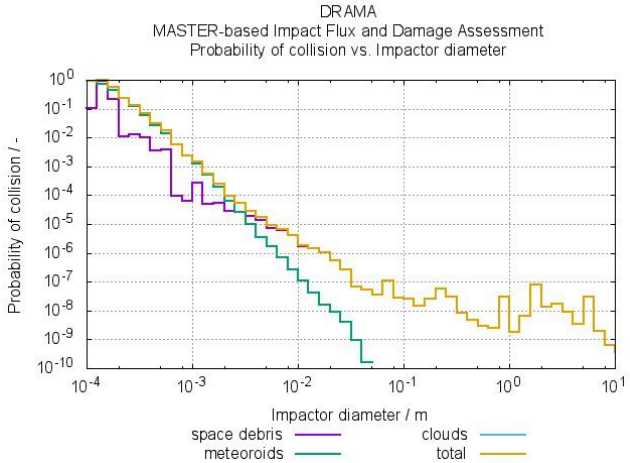

Figure 14.3: Collision probability against diameter of debris

Debris collision risk: As can be seen in Figure 14.3, smaller debris leads to higher collision probability. The

highest value only occurs for the smallest of space debris and then quickly and significantly lowers the larger the debris becomes. Due to overall low probability, that the team considered there is no need for a dedicated ΔV for collision avoidance regarding space debris. For the larger pieces of space debris, if a collision was to occur, the thruster can be gimbaled [28] to avoid any incoming space debris. For collision risk with small space debris that have high probability, this has a size so small that it can not be detected, so it can not be counteracted.

Collision risk with other satellites in constellation: The in-orbit collision with other satellites from the constellation is low for the general mission duration, but high during certain specific events. For instance, the risk is higher during passage over the poles, where the probability of collision increases significantly due to the fact that all satellites pass through the same point. With the use of STK, a model was made of the entire constellation and the poles were monitored during one revolution. It was noticed that the satellites do come close to one another, collisions were not predicted. Furthermore, the satellites are equipped with an on-board computer calculating whether a collision will occur with another satellites or not. If so, the thruster will gimbal [28] up or down to avoid a potential collision.

Collision risk after launcher separation: The probability of collision also increases right after release from the launch vehicle. The released satellites are then close to each other and still have to perform orbit phasing. Since the satellites are equipped with an electrical propulsion system, this can take an extended duration of time, in the magnitude of days, based on which position the spacecraft has to phase to. Hence, the satellites will be able to adjust to their correct respective positions during multiple revolutions. During these revolutions, the distances between the satellites are different from what has been calculated and simulated. They will also change each revolution. To account for these volatile distances, the earlier mentioned on-board computers will be used to track satellites, and the thruster will be gimbaled to avoid collisions.

Collision risk with satellites outside the constellation: Looking at the collision risk with other satellites outside of the constellation, it has to be investigated whether there are satellites orbiting around 350 km and lower, which pose a potential risk of collision during de-orbitting. As of now, there are still satellites, active or inactive, at an altitude of 350 km and lower, with some of them in elliptic orbits. However, since the launch will not happen until 2030, all of these satellites will by then be de-orbited and deactivated. So, planned missions around 350 km and lower have to be investigated to determine whether the constellation is at risk of collision. It was found that, besides Starlink, the planned missions that were registered are all aiming at orbiting at higher altitudes than 350 km, so the constellation does not encounter the risk of collision with other satellites[o]. The only risk would be a collision with one of the Starlink satellites during de-orbit. When de-orbit is planned, however, the risk of collision will to be thoroughly investigated.

[o]https://www.wmo-sat.info/oscar/satellites [cited June 10 2020]

15 Attitude Determination and Control

To get clear measurements out of the telescope, and enable the attribution of these measurements to a position on Earth, stable and precise attitude pointing and knowledge is required. This is what this chapter is all about.

The chapter starts with a section about the assumptions taken while designing the subsystem (Section 15.3). It goes on with the derivation of the key functional requirements (Section 15.2), followed by a description of the operational modes the spacecraft will encounter in Section 15.4. Once those things are set, in Section 15.5, the selection and sizing of the pointing actuators is handled. The actuator part is rounded off with the selection, sizing and simulation of momentum dumping devices (Section 15.6).

Finally, some other aspects of the ADCS design are briefly discussed, like potential sources for pointing error and pointing stability hazards (Section 15.7) and the selection of attitude determination sensors (Section 15.8). Finally, possible control algorithms are briefly discussed in Section 15.9, followed by a verification and validation of the methods used throughout this subsystem's design (Section 15.10).

15.1. Functional analysis

The ADCS subsystem has to fulfil the following functions, taken from the Functional Breakdown Structure.

- **6.4.1:** Determine attitude
- **6.4.2:** Deploy attitude correction measures
- **6.4.3:** Dump momentum
- **5.1.10:** Perform initial stabilisation

15.2. Subsystem requirements

Table 15.1 shows the requirements for the ADCS design. Two nominal operations requirements are driving the pointing actuator design, which are:

MIRA-ADCS-FUNC-1: *The ADCS shall provide a pointing accuracy of 0.1° for the duration of the mission.*
The value of 0.1° is used, as it is presumed reachable while an overlap of 0.66 % is deemed acceptable.

MIRA-ADCS-FUNC-2: *The ADCS shall provide a pointing stability of 478″/s for the duration of the mission.*
The stability criterion – which is a quantification of the allowable movement during integration – is obtained by using the allowable deviation of $0.1 \cdot \text{GSD}$, per Yoshida et al. [38]. Using basic geometry and applying the small-angle assumption ($\arctan\theta = \theta$), Equation 15.1 is reached, which can then be applied to the mission.

$$\dot{\theta} = \frac{\Delta\theta_{allowable}}{t_{int}} = \arctan\left(\frac{0.1 \cdot \text{GSD}}{h}\right) \cdot \left(\frac{0.9 \cdot \text{GSD}}{v_{ground}}\right)^{-1} \approx \frac{1}{9}\frac{v_{ground}}{h} = \frac{1}{9}\frac{r_{earth} \cdot \sqrt{\mu/a^3}}{h} \tag{15.1}$$

Table 15.1: ADCS design requirements

ID	Requirement	Origin	Analysis ref.	
MIRA-ADCS-FUNC-1	The ADCS shall provide a payload pointing accuracy of 0.1° for the duration of the mission.	BLR, MIRA-MIS-ADCS-FUNC-7	sec. 15.8	✓
MIRA-ADCS-FUNC-2	The ADCS shall provide a pointing stability of 478 ”/s for the duration of the mission.	BLR, MIRA-MIS-ADCS-FUNC-7.2	sec. 15.2, sec. 15.7	●
MIRA-ADCS-FUNC-3	The ADCS shall maintain the spacecraft attitude such that communication with ground stations is maintained.	BLR, MIRA-MIS-ADCS-FUNC-4.1		✓
MIRA-ADCS-PERF-1	The spacecraft shall determine its attitude up to an accuracy of 0.001°.	BLR, MIRA-MIS-ADCS-PERF-5.1	sec. 15.8	✓

Table 15.1: continued from previous page

ID	Requirement	Origin	Analysis ref.	
MIRA-ADCS-PERF-2	The ADCS shall be able to detumble the spacecraft within 3 orbits.	BLR, MIRA-MISC-ADCS-PERF-3.1	subsec. 15.6.3	✓
MIRA-ADCS-PERF-3	The ADCS shall have a maximum weight of 30 kg.	BLR, MIRA-COST-ADCS-PERF-2.1		✓
MIRA-ADCS-PERF-4	The ADCS shall use a maximum power of 100 W.	BLR, MIRA-COST-ADCS-PERF-2.2		✓

15.3. List of assumptions

A-ADCS-1 The magnetorquers are assumed to act instantly.

A-ADCS-2 The spacecraft moment of inertia matrix is assumed to be diagonal, i.e, potential cross-coupling effects between axes are neglected.

A-ADCS-3 The magnetorquers and reaction wheels share a power budget, i.e. when the magnetorquers torque, the reaction wheels consume less by the amount the magnetorquers need. This can be said because the power requirement of reaction wheels mainly depends on sustaining the rotation, which is not needed while torquing.

A-ADCS-4 The spacecraft assembly is assumed to be a rigid body.

A-ADCS-5 The solar array facing the direction of travel is assumed to not be relevant aerodynamically.

A-ADCS-6 The centre of mass is assumed to be in the body, where some flexibility (including adding trim weights if needed) is assumed to be present for both designs.

A-ADCS-7 Given the dimensions of the spacecraft, the disturbances are assumed to be applied to all the axes in the following relations (after application of a design margin of 2): 25 %, 45 %, and 30 % to x, y, and z, respectively.

A-ADCS-8 Year to year changes of the magnetic field are assumed to be negligible.

15.4. Operational modes

During the spacecraft mission, the ADCS will encounter the following modes:

De-tumbling. The spacecraft dumps the angular motion originating from launcher separation or debris impact. To do so, attitude determination is also needed.

Orbital insertion. The payload is not yet active, but the thrusters need to be kept pointing into opposite direction of travel.

Nominal operations. The spacecraft needs to fulfil its performance (pointing) requirements.

Special manoeuvres. The ADCS needs to accommodate special manoeuvres by pointing the way needed. This could, e.g., be for collision avoidance.

De-orbitting. The ADCS needs to point the thrusters the correct way, such that a de-orbitting is achieved within specifications.

15.5. Pointing actuator trade-off

In the following, the feasibility of the different actuators for this specific use-case is analysed (Subsection 15.5.1). The disturbance environment is quantified in Subsection 15.5.2, followed by a sizing of the actuators in Subsection 15.5.3. The section then ends with the actuator selection, which takes place in Subsection 15.5.4.

15.5.1. Feasibility analysis

Reaction wheels. Reaction wheels have successfully been used at a similar altitude for even higher pointing accuracies. One example of that, is the ASTERIA mission, which managed to – in a SmallSat form-factor, on

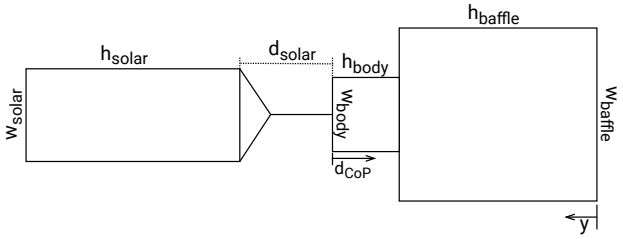

Dimension		TIR	MS	Dimension		TIR	MS
body	w	600	600		w	900	900
	h	410	410	solar	h	1500	1500
baffle	w	1200	1400		d	730	770
	h	1450	1600	**CoP**	**d**	**8**	**185**

Figure 15.1: Centre of pressure estimation, dimensions in mm

an ISS orbit (400 km) – maintain a pointing stability of about 420 µ"/s (0.5″ RMS over a period of 20 min) [39].
Momentum wheels. Momentum wheels provide gyroscopic stiffness, which, in case enough angular momentum is contained, gives the platform high pointing stability. An example of a demonstrator in this regard, albeit only theoretical though for even lower altitudes, would be the SHAPE platform [40, 41].
Control moment gyros. Control moment gyros are generally used for slewing manoeuvres, not for fine control. While research for the latter is yet to be done [42], using them in combination with reaction wheels has been investigated [43]. As slewing capabilities are not required, CMGs will not be investigated further.

15.5.2. Environment analysis

In order to size the actuators, one must first quantify the environment in which the stabilisation needs to happen. When doing so, one can clearly see that the aerodynamic pressure and, potentially, the baffle-induced thruster misalignment are driving the whole analysis. The magnitude of these disturbances highly depends on their effective location w.r.t. the centre of mass. After carefully consideration with the power and AIT department (for more details see Chapter 20), the following points were determined:

- The solar array with the greater area is placed on top and assumption A-ADCS-5 holds.
- Assumption A-ADCS-6 with a deviation of 15 % of the body height (80 mm) is taken into account.
- The thruster is placed such that its line of action goes through the centre of mass (± 5 mm).
- The centre of pressure is determined geometrically, as seen in Figure 15.1.

All the disturbances taken into account can be found in Table 15.2, where one can clearly see the driving impact of the aerodynamic disturbance. The resulting disturbance torques have been classified into secular and cyclic. Torques due to pointing of structures (i.e. solar arrays and antennas) are not expected and the torques originating from deployment of those structures are neglected.

Table 15.2: The considered disturbance torques, the deviation (moment arm/angular deviation) and the resulting torques for the respective satellites

		Equation	Deviation [mm]/[deg]	TIR [µNm]	MS [µNm]	Comments
Secular	Aerodynamic	$T_d = C_d \frac{1}{2} \rho V^2 A_r d$	80	318.62	366.90	[17]
	Thruster misalign.	$T_T = d \cdot 4.83\,\text{mN}$	5	24.15	24.15	see chap. 14
	Solar rad. pressure	$T_s = \frac{E_e}{c} A_s (1+q) d$	80	3.29	3.02	[17]
Cyclic	Magnetic dipole	$T_m = M \cdot B$	-	61.25	61.25	[29]
	Gravity gradient	$T_g = 3 \frac{\mu}{a^3} \lvert I_{zz} - \mathbf{I_C} \rvert \cdot \theta$	1°	1.39	1.39	[29]
	Total			=408.70	=456.71	

Table 15.3 shows the spacecraft dependent parameters while the orbital ones are taken from Chapter 13. The atmospheric density and drag coefficient are the worst-case values found in Wertz et al. [17] ($\rho = 1.85 \times 10^{-11}$ kg/m^3, $C_d = 2.2$). The World Magnetic Model[a] was used to determine the polar strength ($B = 50\,\mu\text{T}$), which is the highest encountered during one orbit. The mass moments of inertia were estimated by arbitrarily placing the objects as point masses within the spacecraft. This estimation is deemed acceptable, as the value is negligible compared to the aerodynamic torques. The magnetic dipole is based on typical values found in Wertz et al. [17], in addition to the magnetic residual of the magnetorquers, which is estimated to be 0.25 A m^2 each.

[a] https://www.ngdc.noaa.gov/geomag/WMM/DoDWMM.shtml [cited 9 June 2020]

Table 15.3: Input parameter used to quantify disturbances

Parameter	TIR	MS	
Sun-lit area (A_s)	6.0	5.5	m^2
Aerodynamic area (A_r)	3.38	3.88	m^2
Average reflectance (q)	0.5	0.5	−
Magnetic Dipole (M)	1.75	1.75	A m^2

Parameter	TIR	MS	
I_{xx}	61.0	61.0	kg m^2
I_{yy}	35.0	35.0	kg m^2
I_{zz}	54.0	54.0	kg m^2

15.5.3. Momentum and reaction wheel sizing

To find the required momentum storage capacity, the relations given by Wertz et al. [17] are used (Equation 15.2 and Equation 15.3), which represent the momentum accumulating (a time integral with a design margin of 2) for the reaction wheels and the momentum required for gyroscopic stability for the momentum wheels.

$$L_{RW} = T_{tot} \cdot P \cdot 2 \tag{15.2}$$

$$L_{MW} = T_{tot}/\delta \cdot P/4 \tag{15.3}$$

From the momentum requirements determined one can then size the wheels, through the relations found in Equation 15.4, assuming a thickness to radius ratio of $1/5$, a wheel density ρ of 7850 kg/m^3 [44], and a rotational frequency of 6000 RPM.

$$L = f \cdot 2 \cdot \pi \cdot I \quad \cup \quad I = \frac{1}{2} \cdot m \cdot r^2 = \frac{1}{2} \cdot \rho \cdot r^5 \cdot \pi \cdot \left(\frac{t}{r}\right)_{ratio} \quad \Rightarrow \quad r = \sqrt[5]{\frac{L}{\rho \pi^2 f \left(\frac{t}{r}\right)_{ratio}}} \tag{15.4}$$

For sizing and mass calculations, a casing with a wall thickness of 2 mm, a clearance of 3 mm and a box density of 2800 kg/m^3 (aluminium) is assumed. In addition to that, assumption A-ADCS-7 applies. This yields the values shown in Table 15.4.

Table 15.4: Results from the sizing using power approximations based on statistical values given by Cherukuri [45]

		Momentum [Nms]	Width [mm]	Length [mm]	Height [mm]	Power [W]
RW TIR	x	1.58	137	137	23	8
	y	2.85	153	153	24	11
	z	1.90	142	142	23	9
RW MS	x	1.77	140	140	23	9
	y	3.19	156	156	25	11
	z	2.13	145	145	23	9
MW TIR	-	321.02	377	377	47	96
MW MS	-	358.72	385	385	48	101

15.5.4. Trade-off

The trade-off will be based solely on volume, mass, and power of the full wheel assembly. Other criteria like reliability and resulting vibration levels were considered, but as those cannot be quantified in a meaningful way, they were excluded. Choosing weights turned out to be completely irrelevant, as the reaction wheels win in every category. Through the choice of reaction wheels, MIRA-ADCS-FUNC-1 can be met for certain [17].

The scale used for comparison of the options is the proportional share of the sum of values for the respective criterion. The results are presented in Table 15.5, which are a summation of the options presented in Subsection 15.5.3.

Table 15.5: Actuator trade-off (TIR and MS yield identical results, up to two digits): lower is better

	TIR			MS		
	Volume [dm^3]	Mass [kg]	Power [W]	Volume [dm^3]	Mass [kg]	Power [W]
RW	1.46	5.31	28.21	1.54	5.65	29.60
MW	6.65	32.27	95.60	7.06	34.45	100.89

15.6. Momentum dumping

The momentum that is accumulated throughout every orbit needs to be dumped before the reaction wheels saturate. First, the actuators are selected in Subsection 15.6.1. Next, dumping actuators are sized in Subsection 15.6.2, and rounded off by a simulation (Subsection 15.6.3) to find and confirm the final sizing of the actuators.

15.6.1. Actuator selection

Two prominent options are available to dump the momentum accumulating in the reaction wheels. Those are thrusters and magnetorquers. The latter are very well suited for LEO, as the Earth's magnetic field still has considerable strength there. As ion thrusters are used for propulsion, those can not easily be used for momentum dumping and, to circumvent the need of additional thrusters, propellants, and to increase the reliability, magnetorquers are chosen.

15.6.2. Initial sizing

The initial sizing of the magnetorquers is done assuming a momentum dumping time of 30 min/orbit and magnetorquers (with dipole M) perfectly aligned with Earth's magnetic field (B = 35 µT avg[a]) (see Equation 15.5).

$$T = \frac{h}{t} \quad \cup \quad M = \frac{T}{B} \quad \Rightarrow \quad M = \frac{h}{t \cdot B} \tag{15.5}$$

The values for TIR and MS are sized for the greatest momentum axis: 32.02 A m^2 and 35.78 A m^2, respectively.

15.6.3. Simulation of torquing

In order to accurately size and determine the actuating behaviour of the magnetorquers, Earth's magnetic field is analysed. For that, the current World Magnetic Model[a] is used with a time input of t = 2020.5 years.

Based on this model, the momentum build up and torquing throughout an orbit is simulated. Observing this over one day allows to determine whether sufficient torquing for momentum dumping is taking place, as then the entirety of the magnetic field is encountered. A simulation run in such a way clearly shows the momentum boundaries (seen for one orbit in Figure 15.2) is done to determine the actual momentum envelope encountered (which is, for x, y, and z, [-0.81, 0.06] Nms, [-0.12, 0.45] Nms, [-0.01, 0.84] Nms). The simulation works in the following way:

- Assumption A-ADCS-1, A-ADCS-2, A-ADCS-3 and A-ADCS-7 apply.
- At every time-step, the momentum building up is assumed to be the product of the time-step and the disturbance torque.
- The torque output of the actuators (which is $T = \vec{M} \times \vec{B}$, where $\vec{M}$ is the torquers' magnetic dipole and $\vec{B}$ Earth's magnetic field) is varied in such a way, that at every time-step the L^2 norm of the resulting momentum vector is minimised.
- The magnetorquers are active as soon as the field potential ($\vec{1} \times \vec{B}$) is above its 33th percentile for the current orbit (This limitation does not apply during detumbling).

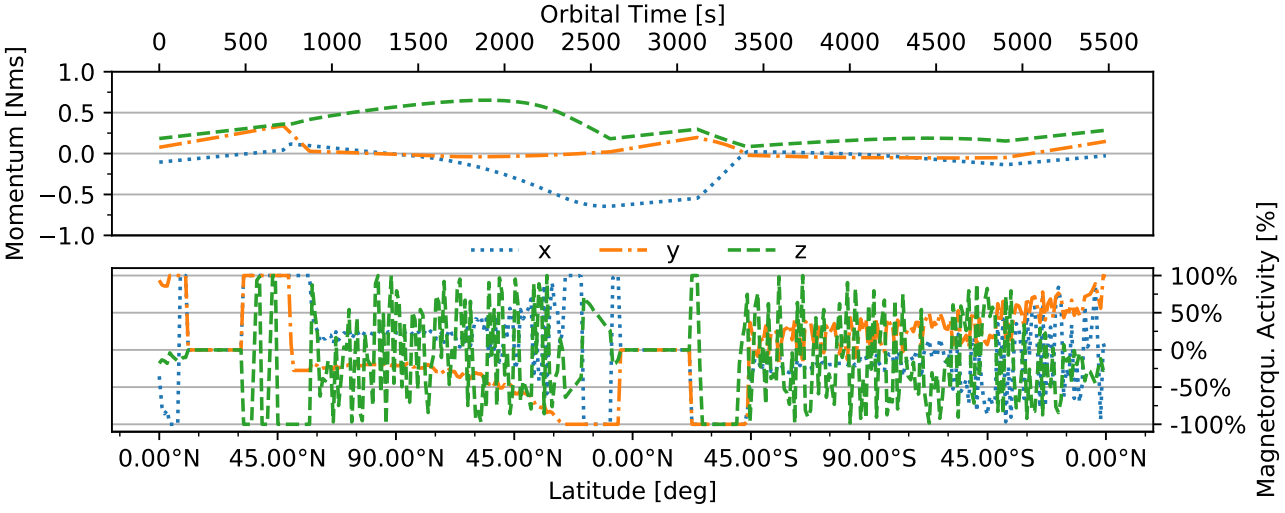

Figure 15.2: Example of the torquing and momentum storage simulation (the orbit after one full simulated day, RAAN = 80°E)

This essentially simulates a P controller, but it is done to show the feasibility of the design, not of the controller (Section 15.9). The simulation shows that, reaction wheels with a momentum storage capacity of 1 Nms (specifically the BCT RW1[b], one on each axis) in combination with magnetorquers with 42 A m^2 each (here, Andrews Space TQ-40 in dual-wind configuration[c]) are sufficient to absorb and shed the momentum for the full spacecraft lifetime (both values based on simulation results and commercial availability). The momentum wheels are the same size for all axis for reasons of simplicity and to take advantage of series production. They are smaller than what has been estimated before, as they do not have to hold the momentum capacity of a full orbit.

The detumbling, determined by running the same simulation with the initial momentum suggested by Jonsson [46] ($[5.7 \;\; 5.7 \;\; 5.7]$ deg/s), happens within 3 orbits. MIRA-ADCS-PERF-2 is thus met.

Having selected the actual reaction wheels the slew rate for a slew of 30° is determined, although the design is not sized for it, determine. This is done using basic Newtonian physics in Equation 15.6, assuming a constant torque of 0.1 Nm and no power constraints.

$$T = I \cdot \ddot{\theta} \qquad \cup \qquad \theta = \frac{1}{2}\ddot{\theta}t^2 \qquad \Rightarrow \qquad t = \sqrt{\frac{2 \cdot \frac{\theta}{2} \cdot I}{T}} \cdot 2 \tag{15.6}$$

The resulting rates are $[0.84 \;\; 1.11 \;\; 0.89]$ deg/s, respectively. In other words: The spacecraft can slew about every axis in about 30 seconds. The power required to do this might be significant in magnitude.

15.7. Potential pointing error sources

The main contribution towards reduced stability are the vibrations originating from internal components, like reaction control wheels, gyroscopes, fuel movement, cooling devices movement, thermal distortions and other mechanism [38, 47]. While Early et al. [47] found payload pointing mechanisms to be the biggest hazard, Yoshida et al. [38] showed that small disturbances can lead to pointing stability issues. Especially high frequency vibrations can be a concern, as they come with many resonance modes and cannot be simulated by finite element methods, but have to be measured on the finished product. In addition to the aforementioned elements, pointing error can originate from additional sources, like star tracker, gyroscope, and quantisation errors but also command and white noise, and aberration [48].

When the reaction wheels reverse their speed, short-time disturbances in the pointing accuracy are induced. When looking at Pong [39] (disturbance of 200″ over a period of 5s) and Carrara and Kuga [49] (disturbance of 288″), those disturbances seem to be acceptable for MIRA, both in terms of magnitude and rate. Were the resulting disturbances to be outside the acceptable range, Bayard [50] suggests reducing their effects by high-bandwidth control loops local to every wheel.

All these effects still have to be analysed in further design stages, together with their transmission paths. Only then meeting the pointing requirements – especially the one concerning pointing stability – can be ensured. For this reason, MIRA-ADCS-FUNC-2 is the only requirement for which the compliance can not yet be determined.

15.8. Sensor selection

Given MIRA-ADCS-PERF-1, star trackers are the only option. A market study suggested, that the KU Leuven Star Tracker[d] represents the best option, as it has 2″/10″ accuracy (cross- and around boresight respectively). To increase the performance as per Hasha [48], (three) gyros (Honeywell GG1320AN Digital Laser Gyro[e]) are added. These gyros are also necessary for initial detumbling and any subsequent detumbling, should the attitude be lost at a later stage of the satellites life. In addition to that, five passive sun sensors (Bradford Mini-FSS[f]) are added (one on each side, except for the instrument side). These are, again, to add redundancy in case of attitude loss and for attitude determination during detumbling. Finally, the sensor suite is rounded off with magnetometers (SpaceQuest MAG-3[g], two for redundancy), which can be, if needed, used to determine the attitude based on a magnetic model. They are, however, mainly meant to measure the magnetic field such that the magnetorquers can be used. The GNSS receiver already on-board can be used as a back-up attitude

[b] https://www.bluecanyontech.com/static/datasheet/BCT_DataSheet_Components_ReactionWheels.pdf [cited June 19 2020]
[c] https://spaceflight.com/wp-content/uploads/2015/05/201501-Torque-Rods-Datasheet.pdf [cited June 19 2020]
[d] http://www.cubesatpointing.com/DownloadFiles/Datasheets/KULSTDatasheet.pdf [cited 15 June 2020]
[e] https://aerospace.honeywell.com/content/dam/aero/en-us/documents/learn/products/sensors/brochures/GG1320ANDigitalLaserGyro-bro.pdf [cited 15 June 2020]
[f] https://www.bradford-space.com/assets/pdf/be_datasheet_mini_fss_2017jan.pdf [cited 15 June 2020]
[g] https://satcatalog.com/datasheet/SpaceQuest%20-%20MAG-3.pdf [cited 15 June 2020]

sensor (by adding redundant antennas) up to some level of precision (up to 0.1°), or as additional input for better overall results [51].

15.9. Control algorithm

The different control modes require different ADCS systems. A preliminary simulation of the detumbling performance has taken place in Subsection 15.6.3. For later design stages, the widely adopted B-dot controller [52–55] is an option worth investigating. For the general control algorithm, PD control can be adequate although PID control might be needed. Wheel friction torque variation that call for the integral controller can, e.g., be compensated by individually monitoring each wheel [50]. To process the incoming sensor signals, reducing the error by means of a Kalman filter is advisable [56].

15.10. Verification and validation

In Subsection 15.5.1 it was established, that reaction wheels are indeed a feasible solution for this endeavour. The sizing functions are validated using statistical data, taken from Cherukuri [45] (see Figure 15.3).

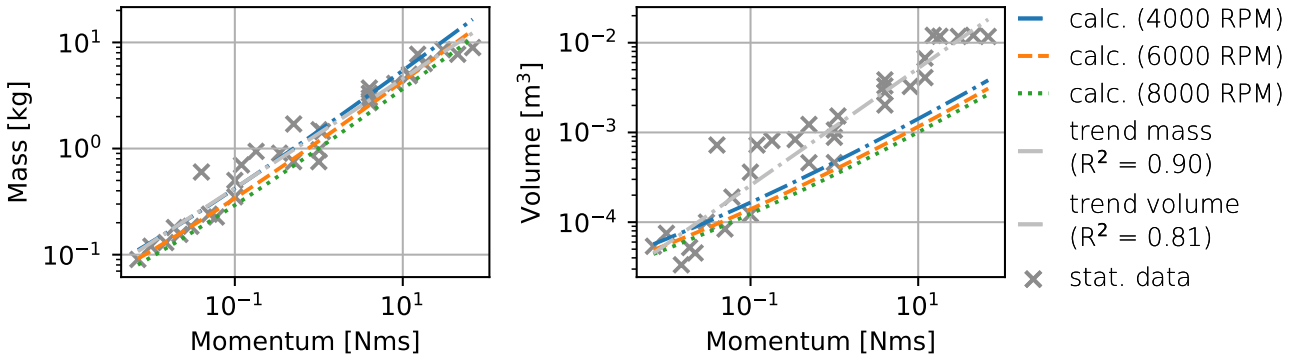

Figure 15.3: Comparison of the volume and mass estimators with real-life values (data taken from [45])

While the volume values calculated in Subsection 15.5.3 underestimated the statistical values by 60-80 %, the mass is overestimated by 6-19 %, both for the 1 and 10 Nms, respectively. Both are deemed acceptable, as those functions are only used during initial sizing of the design, where the values still fluctuate a lot. Neither power nor volume result in significant changes to other subsystem, while power is quite insensitive to variations of the required momentum. The trade-off is not sensitive to these fluctuations, either. After the iterative part of the design, real-life hardware was used to gain real volume, mass and power values. Throughout the design process, statistical values were used in conjunction with the calculated ones to ensure the design stays realistic.

The magnetorquing simulation has been verified in multiple ways:

- The base equations are the ones found here, which have been calculated using Python, Excel and by hand, to make sure no mistakes find their way in.
- The momentum build-up without any magnetorquing happening is the one that is expected by calculations.
- The magnetic field results were cross-referenced with the online implementation available from the National Oceanic and Atmospheric Administration[h].
- The orbital coordinates taken were checked by projection on a map.
- Parts of the values (e.g. field potential) have been plotted next to the actual data throughout the design process to ensure logical cohesion.

15.11. Sustainability analysis

By using a consistent configuration, the manufacturing process for the components used can be optimised to its fullest. The adoption of magnetorquers instead of thrusters for momentum dumping also prevents the handling and production of additional hazardous propellants. All components are flight-proven, or are expected to be so once production begins (the KU Leuven star tracker has already been licensed for production to at least one company[i]). This forestalls the use of excessive redundancy, and thus minimises the overall energy and material use of this subsystem. All the components used are expected to burn up during the de-orbitting procedure.

[h] https://www.ngdc.noaa.gov/geomag/WMM/calculators.shtml [cited 13 June 2020]
[i] https://www.cubesatshop.com/wp-content/uploads/2020/06/arcsec-Star-Tracker-Datasheet.pdf [cited June 19 2020]

16 Communications and Data Handling

In this chapter, the design of the communication system is presented. Firstly, the functional analysis for this subsystem is given, showing the relevant functions from the Functional Breakdown Structure. Then, the the subsystem requirements are presented. After this general overview, the design process is explained. The required data rates and storage capacity are computed and an overview of advantages and disadvantages of optical and radio-frequency communication is given.

16.1. Functional analysis

The communications and data handling subsystem should be able to perform the following functions, as described in the functional breakdown structure in Figure 10.8.

- **5.1.6** Establish communication
- **5.3.4** Downlink status report
- **6.6.2** Receive command
- **6.6.6** Downlink cache
- **6.6.7** Downlink housekeeping data
- **6.8.4** Downlink subsystem diagnosis report

16.2. Subsystem requirements

In this section, the requirements for both C&DH and communication system are listed in Table 16.1

Table 16.1: Communications and data handling design requirements

ID	Requirement	Origin	Analysis ref.	
	Command and data handling requirements			
MIRA-C&DH-FUNC-1	The DHS shall be capable of managing the data storage required for the spacecraft subsystems throughout the mission.	BLR, MIRA-MIS-C&DH-FUNC-2.2		✓
MIRA-C&DH-FUNC-2	The DHS shall be capable of managing the data storage required for the payload throughout the duration of the mission.	BLR, MIRA-MIS-C&DH-FUNC-2.3		✓
MIRA-C&DH-FUNC-3	The DHS shall be able to command the payload instruments on-board the spacecraft.	BLR, MIRA-MIS-C&DH-FUNC-1.5		✓
MIRA-C&DH-FUNC-4	The DHS shall be capable of retrieving data from the on-board storage system.	BLR, MIRA-MIS-C&DH-FUNC-2.4		✓
MIRA-C&DH-PERF-1	The C&DH subsystem shall have a maximum weight of 25 kg.	BLR, MIRA-COST-C&DH-PERF-2.12		✓
MIRA-C&DH-PERF-2	The C&DH subsystem shall use a maximum power of 45 W.	BLR, MIRA-COST-C&DH-PERF-2.13		✓
	Communication subsystem requirements			
MIRA-COMMS-FUNC-1	The communication system shall be able to downlink real-time information an area of interest of 100x100 km.	BLR, MIRA-MIS-COMMS-FUNC-6.1		✓
MIRA-COMMS-FUNC-2	The satellite shall only accept authorised commands.	BLR, MIRA-SR-COMMS-FUNC-2.1	FBS 6.6.2	✓
MIRA-COMMS-FUNC-3	The spacecraft shall encrypt the downlinked data.	BLR, MIRA-SR-COMMS-FUNC-2.2	FBS 6.6.7.2	✓

Table 16.1: continued from previous page

ID	Requirement	Origin	Analysis ref.	
MIRA-COMMS-FUNC-4	The telecommunication system shall be capable of simultaneously transmitting telemetry and payload data.	BLR, MIRA-SR-COMMS-FUNC-2.5		✓
MIRA-COMMS-PERF-1	The communication system shall be capable of downlinking 12 hours of information within 2 hours.	BLR, MIRA-MIS-COMMS-PERF-3.1		✓
MIRA-COMMS-PERF-2	The communication subsystem shall have a maximum weight of 23.5 kg.	BLR, MIRA-COST-COMMS-PERF-2.14		✓
MIRA-COMMS-PERF-3	The communication subsystem shall use a maximum power of 65 W.	BLR, MIRA-COST-COMMS-PERF-2.15		✓

16.3. Required data rates

The sample data rate of a satellite and the total required sample data rate for full Earth coverage is given by Equation 16.1 and Equation 16.2 respectively. [18]

$$R_{s,sat} = \frac{d_{swath} \cdot v_g}{GSD^2} \cdot n_{band} \cdot n_{bit} \cdot \frac{1}{CR} \cdot \frac{1}{CF} \quad (16.1) \qquad R_{s,tot} = \frac{A_{mon}}{t_{sample} \cdot GSD^2} \cdot n_{band} \cdot n_{bit} \cdot \frac{1}{CR} \cdot \frac{1}{CF} \quad (16.2)$$

In Table 16.2, the sample data rates per satellite and required average sample data rate per satellite are computed. A division is made between TIR and MS satellites, and between populated (POP) and non-populated (NPOP) Earth. For h_{orbit} = 350 km, v_g = 7300.1 m/s and a compression ratio of 2.5 for populated and 3.5 for non-populated Earth monitoring is assumed [18].

It is assumed that most data will be downlinked between the optimum elevation angles for data link optimisation, which can be computed from Equation 16.3 [18]. A ground station coverage factor (GSCF) is introduced for the downlink of the populated Earth monitoring data. For populated Earth monitoring, the required downlink data rate is given by Equation 16.4.

$$E_{opt} = 45.0° - 0.00000446 \cdot h_{orbit} \quad (16.3) \qquad R_{d,avg} = \frac{R_{s,avg}}{GSCF} \quad (16.4)$$

In some cases, it might be useful to downlink data near real-time. In these cases, the required downlink data rate equals the output datarate for 1 satellite ($R_{DL} = R_{s,sat}$). It is assumed that the minimum elevation angle for direct links is 2°. A grid of ground stations has to be designed to account for both direct downlink data rates at minimum elevation and average downlink data rates at optimum elevation.

16.4. Required data storage capacity

Data shall be downlinked within 2 hours after collection. This means that the required data capacity is equal to the amount of data generated in these 2 hours. This is represented in Equation 16.5, where $t_{storage}$ is the maximum storage time of data.

$$C_{req} = R_s \cdot t_{storage} \quad (16.5)$$

With t_s = 7200 s the maximum and average required storage capacity is computed in Table 16.2. Addition of the storage capacities for the TIR and MS satellites gives the capacities presented in Table 16.3. The storage device is designed with maximum required capacity and taking a redundancy factor of 3 into account to account for degradation and the unlikely event of not being able to set up a data link within 2 hours. With the designed storage capacity, data can be stored on-board for 60 and 54.4 hours on average for the TIR and MS satellite respectively (2.5/2.26 days).

Table 16.2: Required data rates and storage capacity

		TIR_{POP}	TIR_{NPOP}	MS_{POP}	MS_{NPOP}
Fraction of global area		26%	74%	26%	74%
Area [m^2]	A_{mon}	1.33×10^{14}	3.77×10^{14}	1.33×10^{14}	3.77×10^{14}
Bands [-]	n_{band}	1	1	18	18
Radiometric resolution [bits]	n_{bit}	10	10	10	10
Spatial resolution [m]	GSD	5	5	10	10
Temporal resolution [s]	t_{sample}	1800	43200	3600	43200
Ground velocity [m/s]	v_g	7300.1	7300.1	7300.1	7300.1
Swath width [m]	d_{swath}	100×10^3	100×10^3	200×10^3	200×10^3
Compression ratio [-]	CR	2.5	3.5	2.5	3.5
Data Consent Factor [-]	CF	0.9	0.9	0.9	0.9
Sampled datarate per satellite [bit/s]	$R_{s,sat}$	1.30×10^8	9.27×10^7	1.17×10^9	8.34×10^8
Total sampled datarate	$R_{s,tot}$	1.31×10^{10}	9.99×10^8	2.95×10^{10}	4.99×10^9
Total number of satellites [-]	n_{sat}	624	624	156	156
Avg. datarate per satellite [bit/s]	$R_{s,avg}$	2.10×10^7	1.60×10^6	1.89×10^8	3.20×10^7
Storage time [s]	$t_{storage}$	7200	7200	7200	7200
Max. required storage capacity [bits]	C_{max}	9.34×10^{11}	6.67×10^{11}	8.41×10^{12}	6.01×10^{12}
Avg. required storage capacity [bits]	C_{avg}	1.51×10^{11}	1.15×10^{10}	1.36×10^{12}	2.30×10^{11}

Table 16.3: Storage capacities in GB

	TIR	MS
Maximum required storage capacity [GB]	200	1802
Average required storage capacity [GB]	20	199
Designed storage capacity [GB]	600	5408
Average available data storage time [h]	60.0	54.4

16.5. Choice of communication system

For the communication system, two different types of communication have been taken into account: radio-frequency communication (RF) and optical communication. For RF, a phased array of antennas is considered to be the best option. Phased arrays consist of multiple radiating elements. By adding a phase difference between the signals sent by the different elements, signals can be pointed in a certain direction. This increases the transmitter gain that can be obtained (and therefore allowing for a smaller antenna or lowering the transmitted power) and avoids the need of more complex mechanisms for pointing e.g. a parabolic antenna dish.

Optical communication For optical communication, the signal can be easily directed by pointing the laser in the right direction. Furthermore, high data rates (up to 1 Tbit per second) can be obtained. However, optical communication is a less common technology used for satellite communication and induces therefore higher cost. As an example, investment costs for a optical ground station (in the range from 1 to 4 M€) is significantly higher than the investment cost for a radio-frequency ground station (around 70,000 € [a]. Also, with a baffle included in the design, little space is left to fit a laser terminal, where a phased array can be easily placed on either the solar panels or at the bottom of the telescope mirror.

Phased Arrays The gain obtained by a phased array is determined by the amount of elements. As a rule of thumb, after taking required distance between elements for a certain signal wavelength and antenna efficiency into account, the gain obtained by a phased array is equal to the amount of elements. To be able to steer signals by phase difference, the elements in the phased array should be spaced at a distance $s = \lambda/2$. The chosen

[a] https://www.isispace.nl/product/full-ground-station-kit-s-band/ [cited June 27 2020]

frequency is 10.0 GHz , which implies $\lambda = 0.03m$. Therefore, the elements should be spaced with their centres 1.50 cm apart. For the choice of elements, multiple options exist. In Dang [57] these options are analysed. Patch antenna's are considered to be the best option for this mission, due to their very low mass and size, low cost and high flexibility.

The minimum width and length of the individual patches can be calculated using Equation 16.6, Equation 16.7, Equation 16.8 and Equation 16.10 [58].

$$W = \frac{c}{2f\sqrt{\frac{(\epsilon_r+1)}{2}}} \quad (16.6) \qquad L = L_{eff} - 2 \cdot \Delta L \quad (16.7) \qquad L_{eff} = \frac{c}{2f\sqrt{\epsilon_{eff}}} \quad (16.8)$$

$$\epsilon_{eff} = \frac{\epsilon_r + 1}{2} + \frac{\epsilon_r - 1}{2}\left[1 + 12\frac{h}{W}\right]^{-\frac{1}{2}} \quad (16.9) \qquad \Delta L = 0.412h\frac{(\epsilon_{eff} + 0.3)(\frac{W}{h} + 0.264)}{(\epsilon_{eff} - 0.258)(\frac{W}{h} + 0.8)} \quad (16.10)$$

In these equations, the dielectric constant, ϵ_r, and the dielectric height, h, are properties of the plate on which the patches are placed. They are assumed to be 4.0 and 1 mm respectively. These assumptions lead to a minimum required patch width of 0.95 cm and minimum required patch length of 0.71 cm. For simplicity of production, square patches of 1.0 by 1.0 cm are assumed. The phased array will be placed at the back of the secondary mirror (21.9 x 21.9 cm). A matrix of 14 by 14 elements fits. Therefore, the phased array will consist of a 14 by 14 matrix of 1 by 1 cm patch elements, with a 0.5 cm space between them, as can be seen on the sketch in Figure 16.1. For each patch a phase shifter and attenuator is needed.

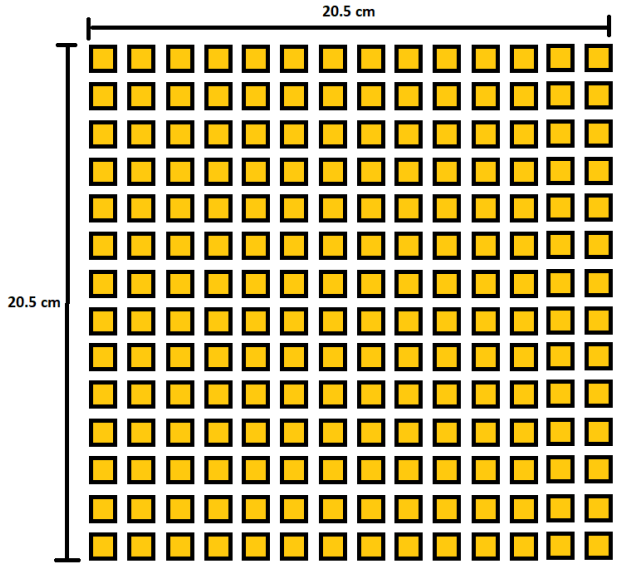

Figure 16.1: Phased array configuration

16.6. Power consumption

To compute the required power to handle and downlink data, a link analysis is performed. During the link analysis, all gain and loss factors are analysed. In general, the required transmitter power is given by Equation 16.11. The most common and simplest modulation and coding schemes are assumed (Binary Phase Shift Keying for modulation and Reed Solomon Viterbi for coding) [18]. With an assumed required Bit Error Rate of 10^{-5}, a signal to noise ratio of 4.0 is required [18]. The transmitter gain is equal to the number of patch elements (196) and the receiver gain is 54283, obtained using Equation 16.13, assuming a receiver antenna diameter of 3 m and receiver antenna efficiency of 0.55 [29]. A transmitter and receiver system loss of 0.7 have been assumed, as well as a minimum link margin of 0.5 and a transmitter power efficiency of 60%. The path loss can be calculated with Equation 16.12, in which S is the slant range (the distance between satellite and ground station at the start of data transmission, dependent on the elevation angle at which data transmission starts) that can be calculated using Equation 16.14 [b] and λ the wavelength of the RF signal (0.03 m for f = 10.0 GHz).

[b] https://www.fxsolver.com/browse/formulas/Slant+Range [cited June 15 2020]

Furthermore, an atmospheric loss, L_a, is estimated, to account for signal loss due to the atmosphere. For E = 2°, L_a is around 0.845 and for E = 43.4° around 0.990 [18].

$$P_t = \frac{E_b/N_0 \cdot k \cdot T_r \cdot R_d}{G_t \cdot G_r \cdot L_t \cdot L_r \cdot L_p \cdot L_a \cdot M \cdot \eta_t} \tag{16.11}$$

$$L_p = \frac{\lambda^2}{(4\pi S)^2} \tag{16.12}$$

$$G_r = \eta_r \left(\frac{\pi D_r}{\lambda}\right)^2 \tag{16.13}$$

$$S = \sqrt{(R_{earth} \cdot \cos(90^o - E))^2 + (R_{earth} + h_{orbit})^2 - R_{earth}^2} - R_{earth} \cdot \cos(90^o - E) \tag{16.14}$$

In Table 16.4, the results of the link budget are presented. For the optimal link, 22 ground stations have been assumed, which is the minimum amount to make direct links at $E = 2°$ possible, as will be explained in the next section.

Table 16.4: Link Budget for direct and optimal link

		Direct Link (E = 2°)	Optimal Link (E = 43.439°)
Transmitter System Loss [-]	L_t	0.7	0.7
Transmitter Antenna Gain [-]	G_t	196.0	196.0
Path Loss [-]	L_p	1.532×10^{-18}	2.705×10^{-17}
Atmospheric Loss [-]	L_a	0.845	0.990
Receiver Antenna Gain [-]	G_r	54,283	54,283
Receiver System Loss [-]	L_r	0.7	0.7
Minimum Link Margin [-]	M	0.5	0.5
Receiver Temperature [K]	T_r	298	298
Boltzmann constant [J/K]	k	1.38×10^{-23}	1.38×10^{-23}
Required TIR Datarate [bit/s]	$R_{d,TIR}$	1.30×10^{8}	1.59×10^{9}
Required MS Datarate [bit/s]	$R_{d,MS}$	1.17×10^{9}	1.56×10^{10}
Required Signal to Noise Ratio [-]	E_b/N_0	4.0	4.0
Transmitter Power Efficiency [-]	η_t	0.6	0.6
Required TIR Transmitter Power [W]	$P_{t,TIR}$	1.05	0.63
Required MS Transmitter Power [W]	$P_{t,MS}$	9.49	6.12

The mass and volume of the transceiver can be estimated using Equation 16.15 and Equation 16.16, assuming a specific power, P_{sp} of 2.9 W/kg and transceiver density, ρ_{trans}, of 0.75 kg/dm^3 [29].

$$M_{trans} = \frac{P}{P_{sp}} \tag{16.15}$$

$$V_{trans} = \frac{M_{trans}}{\rho_{trans}} \tag{16.16}$$

Filling in the values for the obtained power, the mass and volume are estimated to be 0.22 kg and 0.29 dm^3 respectively for the TIR satellite and 2.11 kg and 2.81 dm^3 for the MS satellite.

16.7. Ground station configuration

To obtain the required ground station configuration, two possibilities are analysed. They are visually presented in Figure 16.2. On the left side of the figure, the situation for direct links is sketched and on the right part of the figure the situation for optimal links. The small yellow dots represent ground station locations and the yellow line in-between represents the distance between two ground stations, for which their ground cover area is presented by the bigger red and blue circles. The radius of these circles is the slant range (absolute distance between ground station and satellite, calculated with Equation 16.14) multiplied with the cosine of the elevation angle.

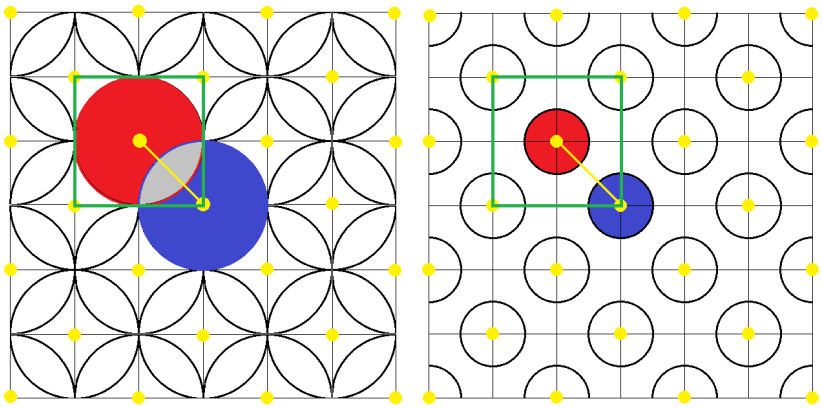

Figure 16.2: Ground station configurations

From geometry, it is obtained that the (maximum) distance between two ground stations to provide direct links for all populated Earth is given by Equation 16.17. To account for a non-optimal distribution of ground station, it is assumed that the actual average distance between ground stations will be 90% of the maximum distance. The number of required ground stations is then calculated with Equation 16.19.

For optimal links, when GCSF < 0.25π (approximately 0.785), an arbitrary square area, visualised by the green square, is covered by 2 ground stations. The distance between two ground stations can be expressed by setting the area of the green square equal to 2 x GSCF x area of the red circle. This gives the expression in Equation 16.18. Rearranging terms leads to the expression in Equation 16.20 for $D_{gs,max}$.

$$D_{gs,max} = \sqrt{2} \cdot S \cdot cos(E_{min}) \quad (16.17) \qquad \left(2 \cdot \frac{D_{gs,max}}{\sqrt{2}}\right)^2 = 2 \cdot GSCF \cdot \pi \cdot \left(S \cdot cos(E_{opt})\right)^2 \quad (16.18)$$

$$N_{gs,min} = \frac{A_{mon}}{(0.9 D_{gs,max})^2} \quad (16.19) \qquad D_{gs,max} = \sqrt{\frac{\pi}{GSCF}} \cdot S \cdot cos(E_{opt}) \quad (16.20)$$

In Table 16.5, the results are presented. The minimum amount of ground stations required for direct linking of the complete populated Earth area is given as well as a relationship between GSCF and the required amount of ground stations for optimal linking.

Table 16.5: Minimum amount of ground stations for two situations

		Direct Link	Optimal Link
Elevation Angle [deg]	E	2.000	43.439
Slant Range [km]	S	1929	459
Area [km^2]	A_{mon}	132.6×10^6	132.6×10^6
Maximum distance between ground stations [km]	$D_{gs,max}$	2727	$637.1/\sqrt{GSCF}$
Average distance between ground stations [km]	D_{gs}	2455	$573.4/\sqrt{GSCF}$
Minimum amount of ground stations [-]	$N_{gs,min}$	22	$403.4 \cdot GSCF$

The obtained relationship between GSCF and N_{gs} can be combined with the previous obtained relationship between P_t and GSCF, to obtain the minimum required average power, as show in Equation 16.21 and Equation 16.22.

$$P_{E=E_{opt},TIR} = \frac{141.76}{N_{gs}} \quad (16.21) \qquad P_{E=E_{opt},MS} = \frac{230.89}{N_{gs}} \quad (16.22)$$

16.8. Real-Time Monitoring

The thermal infrared satellites have to be able to downlink data of a 100 x 100 km area in real time. In Equation 16.23, the relationship between the fraction of Earth that can be monitored real time (DLF), direct link power, optimal link power and average required power is given.

$$P_{avg} = DLF \cdot P_{E=E_{min}} + (1 - DLF) \cdot P_{E=E_{opt}} \quad (16.23)$$

Furthermore, when keeping the relationship between GSCF, sample and downlink rate, as shown in Equation 16.4, the power required for optimal links is given in Equation 16.24

$$P_{E=E_{opt}} = \frac{0.034125}{GSCF} \tag{16.24}$$

For the 100 x 100 km area, DLF is negligibly small (DLF = 1.9×10^{-5}), so $P_{avg} = P_{E=E_{opt}}$. By increasing the amount of ground stations, the area for which direct linking is possible can be increased, assuming that the average power should remain at 0.63 W. Furthermore, Equation 16.21 and Equation 16.23 lead to a relationship between DLF and the number of ground stations, as presented in Equation 16.25.

$$DLF = \frac{0.63 - 13.76/N_{gs}}{P_{max} - 13.76/N_{gs}} \tag{16.25}$$

In Equation 16.25, P_{max} depends on the elevation angle at which data links start. As stated before, the absolute minimum is 2°. However, by increasing the number of ground stations, the minimum required elevation angle can be increased, which reduces the maximum required power, and therefore increasing DLF.

For each elevation angle between 0 and 45°, the required amount of ground stations is computed using Equation 16.14, Equation 16.17 and Equation 16.19. For the same elevation angles, the required power is computed using Equation 16.11, for which L_a is assumed to be 0.9 on average for all elevation angles, and L_p is obtained from Equation 16.12. From this the DLF could be calculated, which results in Figure 16.3, showing the required amount of ground stations for a given DLF.

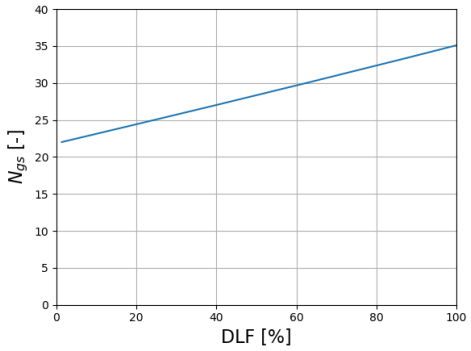

Figure 16.3: Required amount of ground stations for a certain DLF

It is worth recalling that an RF ground station can be set up for around 70,000 € and that for DLF = 100% the complete populated part of Earth's surface (26% of the total Earth's surface), which equals 132.6 km^2, can be monitored in real time.

Inter-satellite links In some cases, it is not preferred to directly downlink data to the area that is being observed. For these cases an interesting solution is the use of inter-satellite links. Data can be sent to a relay network in higher orbits, such as Iridium [c]. This could be an interesting topic for research during a continuation of this project.

16.9. Verification and validation

For the calculation of the required sample data rates and the minimum amount of ground stations for direct links, the same approach as described in Bouwmeester et al. [18] is used. A tool was created in Excel to compute the required results. For verification it was first checked if the tool produced the same outputs with the same inputs as in Bouwmeester et al. [18]. For validation, the outcomes for mass and power have been compared to similar communication and data handling systems.

16.10. Sustainability analysis

Regarding the communication and data handling, social sustainability is relevant, as explained in Chapter 5. Interference with radio waves in the same frequency range should be dealt with and international regulation regarding privacy shall always be taken into account when monitoring. Furthermore, to account for risks, some redundant data storage capacity has been added, as explained in Section 16.4.

[c]www.iridium.com [cited June 28 2020]

17 Electrical Power System

This chapter deals with the sizing and design option choices related to the electrical power system. It begins by outlining the functional analysis, giving a overview of the requirements and list of assumptions made. This is followed by an explanation of the calculations used for the sizing. Finally, the verification and validation of methods, as well as, the sustainability choices are discussed.

17.1. Functional analysis

The electronic power subsystem should be designed to perform the functions specified in Figure 10.9:

- **5.1.3:** Provide, distribute and regulate initial power
- **6.7.2:** Generate power
- **6.7.3:** Charge battery
- **6.7.4:** Discharge battery
- **6.7.4:** Distribute power
- **6.7.4:** Regulate power

17.2. Subsystem requirements

The requirements for the electrical power system are outlined in Table 17.1.

Table 17.1: Power design requirements

ID	Requirement	Origin	Analysis ref.	
MIRA-POWR-FUNC-1	The power subsystem shall provide power required for nominal daytime operation.	BLR, MIRA-MIS-POWR-FUNC-1.1	FBS 6.7.2.1	✓
MIRA-POWR-FUNC-2	The power subsystem shall provide power required for nominal eclipse operation.	BLR, MIRA-MIS-POWR-FUNC-1.2	FBS 6.7.2.2	✓
MIRA-POWR-FUNC-3	The power subsystem shall be capable of storing a minimum power of 87.51 Wh.	BLR, MIRA-MIS-POWR-FUNC-1.3		✓
MIRA-POWR-FUNC-4	The satellite shall use multicell batteries.		Risk TR-POWR-04&05	✓
MIRA-POWR-PERF-1	The power subsystem shall have a minimum efficiency of 0.8.	BLR, MIRA-MIS-POWR-FUNC-1.4		✓
MIRA-POWR-PERF-2	The power subsystem shall have a maximum mass of 42.64 kg.	MR, target value in mass budget		✓
MIRA-POWR-SUS-1	The power subsystem shall not use nuclear power for the power generation.		Sustainability	✓

17.3. List of assumptions

The following assumptions were used in the design and sizing of the power subsystem.

- **A-PWR-01** Earth's orbit around the sun is circular.
- **A-PWR-02** Solar flux is constant throughout the mission.
- **A-PWR-03** Satellites are in perfect polar orbit and thus have no precession.
- **A-PWR-04** The Earth's shadow is cylindrical.
- **A-PWR-05** The sunlight on the arrays is unidirectional.

17.4. Calculations

The parameters and power requirements given in Table 17.2 and Table 17.3 respectively, are used for the sizing calculations for the batteries and the solar arrays.

Table 17.2: List of parameters and values for power system sizing [8]

	Symbol	Value	Unit		Symbol	Value	Unit
Solar flux	S	1371	W/m^2	Depth of discharge	DOD	0.4	-
Density array	ρ_{Ar}	40	kg/m^2	BOL efficiency	E_{BOL}	0.32	-
Orbit period	t_{orbit}	5431	s	Inherent degradation	I_d	0.77	-
Satellite lifetime	t_{op}	220752000	s	Array degradation	-	0.0275	/year
Specific energy	E_{spec}	500400	Ws/kg	EPS efficiency	η_{Eps}	0.8	-

17.4.1. Solar array sizing

For solar array sizing choices on development and integration need to be carried out. For this analysis only technology that has been flight or experimentally proven is considered. From a literature investigation a beginning of life (BOL) efficiency is given in Table 17.2. This efficiency is reduced further by inherent degradation upon installation and every subsequent year by the array degradation. To ensure the power generated is sufficient to the end of the mission the solar arrays are sized on the efficiency expected at end-of-life (EOL).

The power required by the satellite is divided into two sections. Daylight and eclipse power required. These power requirements are defined as the largest expected power requirement for each subsystem averaged over the time daylight and eclipse time, and are given in Table 17.3. This means for example, although the ADCS unit will have a varying power requirement with a peak requirement over the value stated, this is averaged over time as this peak is not constant. If at any instance the power required is above the power generated by the solar array, in daylight, it is estimated that the power system will run on both the solar array and the battery.

The requirements are given for both MS and TIR. However, due to the similarity, the power system is only sized according to the larger power requirement and for this reason, the target value, contingencies, and actual value are only given for the TIR satellite. The contingencies are altered based on the level of maturity of the subsystem design and are based on indications from the tutor (e.g. for payload) or on the AIAA recommendations [59]. The actual value derivations can be found in the respective subsystem chapters and the target values was adapted from the Midterm Report budgets. The current and specification values are the actual and target values with the contingency applied. The contingency for thermal is found due to the cooling fluctuations depending on the heat fluxes on the primary mirror which in turn lead to a variation of heat dissipation within the instrument box. The higher contingency for the propulsion subsystem indicates it is a crucial driver of the power requirement.

Table 17.3: Power budget (value in [W])

Actual value	*MS*		*TIR*		Tar. value	Contingency	Cur. value	Spec. value
	P_d	P_e	P_d	P_e				
PAY	5.0	0.0	5.0	5.0	10.0	0.15	5.8	11.5
PCDU	10.0	10.0	10.0	10.0	15.0	0.15	11.5	17.3
ADCS	33.9	33.9	33.9	33.9	70.0	0.15	39.0	80.5
THRM	1.03	1.03	27	27	30.0	0.20	32.4	36.0
C&DH	13.0	13.0	13.0	13.0	20.0	0.15	15.0	23.0
PROP & GNC	60.0	60.0	60.0	60.0	70.0	0.20	72.0	84.0
COMMS	6.1	6.1	0.6	0.6	10.0	0.15	0.7	11.5
STRC	0.0	0.0	0.0	0.0	5.0	0.10	0.0	5.5
Total	**129.0**	**124.0**	**149.5**	**149.5**	**230.0**		**176.3**	**269.3**

The solar arrays are sized such that they can produce sufficient power throughout the daylight time of the orbit to meet these power requirements and to charge the battery sufficiently to power the satellite in the eclipse associated with the given daylight time. The power derived per m^2, given by Equation 17.1, from the solar arrays is affected by the angle of incidence, the efficiency of the solar array, and the solar flux of the sun.

$$P_A = S \cdot E_{EOL} \cdot \cos\theta \tag{17.1}$$

The angle of incidence of the solar array varies by different parameters depending on the chosen array integration and orbit type. For the solar array sizing the first decision to be made is the orientation of the solar array with respect to the satellite. The simplest configuration would be a single fixed array. However, due to the fact that the satellite is assumed to be in perfect polar orbit, there is no way to orient the array such that it would not experience times of the year when it is essentially at a right angle to the sun meaning no power generation. As this would last days, the battery would need to become very large to power the satellite for such long times, hence this option is considered to be unfeasible. The next option would be to have arrays in two separate orientations. Looking at figure Figure 17.1, if the direction of motion of satellite is given by the y axis then the solar arrays would be in the x,y and x,z planes, referred to as A1 and A2, respectively.

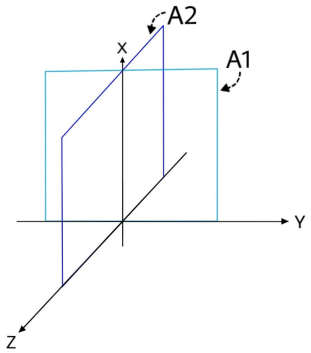

Figure 17.1: Planes of Array 1 and 2 with y axis representing direction of motion

When considering the solar array sizing it is necessary to calculate the angle of incidence for each array, θ_{A1} and θ_{A2}. For Array 1, θ_{A1} is affected by the Earth's tilt angle, ϵ, and the stage in the orbit of the Earth around the sun. θ_{A2} varies with both the stage in the orbit of the Earth around the sun and with the stage in the orbit for the Satellite around the Earth. Due to the nature of designing a constellation and the fact that the orbits are considered to be perfectly polar with no precession, the satellites will experience different sunlight conditions throughout the year depending on their right ascension of the ascending node (RAAN). For a given RAAN, the sunlight conditions will repeat periodically. However, between the differing RAAN orbits the conditions will differ, due to the tilt angle of the Earth. Figure 17.2 shows the orbits for three RAAN values corresponding to 0, 45 and 90° throughout the orbit of the Earth around the Sun. The offset between the x-mark and the north location represents the tilt of the Earth. This shows that the RAAN 90 orbit is unaffected by this tilt angle, whereas, the RAAN 0 orbit is fully affected. The angle associated with this for each RAAN, ϵ_{eff}, is given in Equation 17.2.

$$\epsilon_{eff} = \epsilon \cdot \cos(RAAN) \tag{17.2}$$

Looking again at Figure 17.2, it can be observed that each orbit corresponding to a different RAAN experiences a maximum daylight time per orbit at a different time throughout the orbit of the Earth around the Sun. This maximum repeats after half the orbit around the Sun. They also experience a minimum daylight time a quarter orbit after the maximum. The angle with respect to the Sun experienced by each satellite is given as θ_{sun}. For this a zero degree angle corresponds to the time when the daylight time is at maximum. In Figure 17.2, $\theta_{sun} = 0$ is true for RAAN 90 in location (1.), for RAAN 45 in location (2.) and for RAAN 0 in location (3.). For the solar array sizing only a θ_{sun} angle between 0 and 90° is considered. This is because both solar arrays are double sided so the power generated is expected to be mirrored about 90°.

As mentioned, Array 2 is affected by the rotation of the satellite around the Earth due to the nadir pointing requirement. This means for a fixed solar array oriented 90° against the direction of travel the angle will be constantly changing. To estimate the power generated by this solar array an average angle over the sunlight section of the orbit is estimated. This is done using Equation 17.3, first for the section of the sunlight orbit between 0 to 90 deg and then for the average angle between the eclipse angle and 90 deg, labelled *Average1* and *Average2*, respectively. The eclipse angle is found using Equation 17.4. The angles are then multiplied by their fraction of the daylight orbit and doubled, due to symmetry about centre which leads to θ_{Orbit}, Equation 17.5.

$$\theta_{Average} = \frac{1}{b-a} \cdot \int_a^b \cos(x)dx \tag{17.3}$$

$$\theta_{Eclipse} = \frac{T_{Eclipse} \cdot \pi}{T_{Orbit}} \tag{17.4}$$

$$\theta_{Orbit} = \theta_{Average1} \cdot \frac{\pi}{\pi + 2 \cdot \theta_{Eclipse}} + \theta_{Average2} \cdot \frac{\theta_{Eclipse} \cdot 2}{\pi + 2 \cdot \theta_{Eclipse}} \tag{17.5}$$

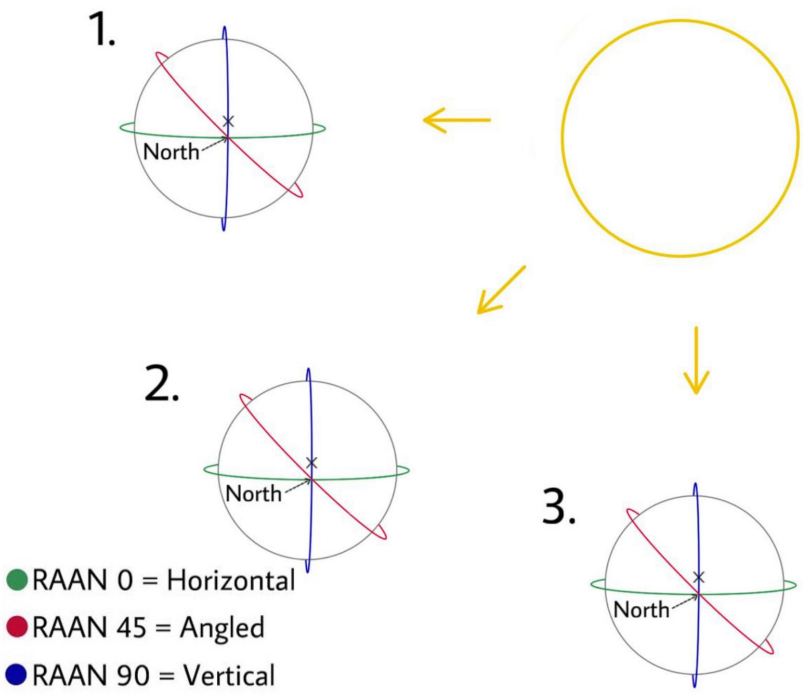

Figure 17.2: Three example orbits at different times of the year

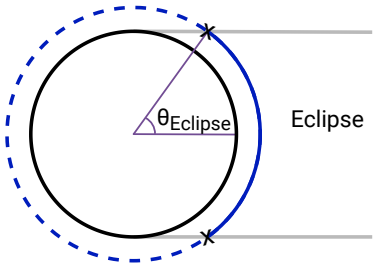

Figure 17.3: The eclipse angle

As can be seen from the image, the orbit corresponding to RAAN 90 is unaffected by the earth tilt angle ϵ, however the other two orbits are both affected by this angle. The Angle of Incidence for the two arrays is given by θ_{A1} and θ_{A2}. In Table 17.4, the angle of incidence for the three different RAAN orbits are calculated against the θ_{sun} angle throughout the orbit of the Earth with the Sun. The θ_{sun} is given in 10° increments. θ_{A1} is calculated using Equation 17.6 and θ_{A1} is calculated using Equation 17.7.

Using the information above, the angle of incidence experienced by both *A1* and *A2* can be calculated for a given θ_{Orbit} using Equation 17.6 and 17.7, respectively. These can then be used in Equation 17.1 to calculate the power produced per m^2 for each solar array. This can then be calculated along the orbit of the Earth around the sun by incrementally increasing θ_{sun}.

$$\theta_{A1} = \cos(\epsilon_{eff}) \cdot \cos(\theta_{sun}) \tag{17.6}$$

$$\theta_{A2} = \cos(\theta_{Orbit}) \cdot \cos(90 - \theta_{sun}) \tag{17.7}$$

The time for daylight and eclipse, T_{Day} and $T_{Eclipse}$ respectively, is found using the STK model. The P_{A1} and P_{A2} are the power generated per meter squared by each solar array. P_{Rec} is the required power for the given daylight times, shown in Equation 17.9. For each RAAN, there is a period of time where only one solar array is receiving solar radiation. This orbit corresponds to the maximum solar array size needed per RAAN. For $A1$ the maximum area required, A_{A1} is at $\theta_{sun} = 0$ for RAAN 0 and for $A2$, A_{A2} it is at $\theta_{sun} = 90$ for RAAN 90. The solar arrays are then sized using these requirements, and P_{Gen} can be calculated using Equation 17.10. Using these areas, the power generated, P_{Gen}, per orbit throughout the year can be plotted with the P_{Rec}. The reason for using three RAAN is that the RAAN 0 and RAAN 90 were expected to be the extreme cases for solar array size requirements. However, RAAN 45 was used to check this was true and that it would also still meet the requirements. Figure 17.4 shows power required against the power generated along the different θ_{sun} angles. From these it can be seen that the key positions are when $\theta_{sun} = 0$ for RAAN 0 and $\theta_{sun} = 90$ for RAAN 90. All other θ_{sun} values are therefore generating extra power. It is expected that the solar arrays and the PCDU unit are able to manage and dissipate this over generation of power. Additionally, the values of power generated and power required are given in Table 17.4, where the blue highlighted values correspond to the key sizing values. This leads to a final required array area of $A_{A1} = 0.93$ m^2 and $A_{A2} = 1.35$ m^2, using Equation 17.8.

$$A = \frac{P_{Rec}}{P_{Gen}} \tag{17.8}$$

$$P_{Rec} = \frac{P_{Day} \cdot T_{Day} + P_{Eclipse} \cdot T_{Eclipse}}{T_{Day} \cdot \eta_{Eps}} \tag{17.9}$$

$$P_{Gen} = A_{A1} \cdot P_{A1} + A_{A2} \cdot P_{A2} \tag{17.10}$$

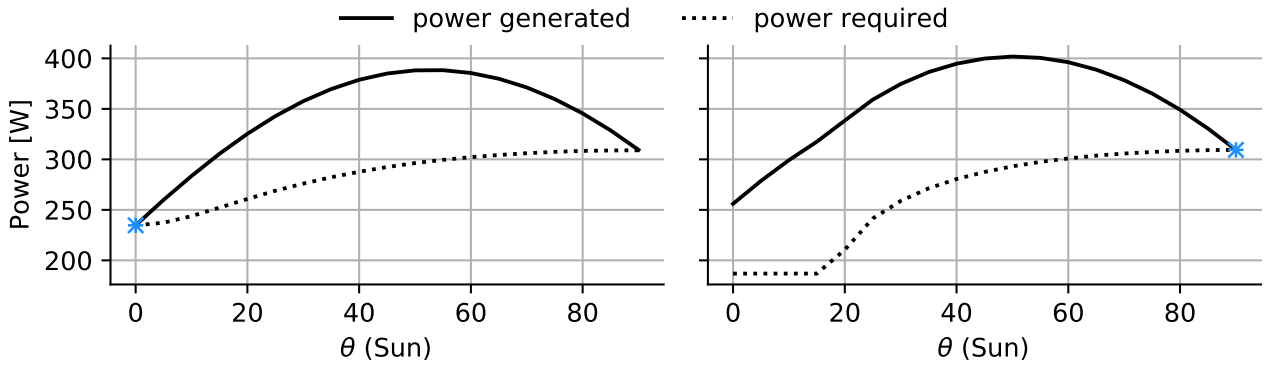

Figure 17.4: Powered required and generated vs θ_{sun} for RAAN 0 and 90, respectively.

Table 17.4: Table to show the power for the different RAAN orbits

RAAN	θ_{sun}	θ_{A1}	θ_{A2}	T_{Day}	$T_{Eclipse}$	P_{A1}	P_{A2}	P_{Rec}	P_{Gen}
0	0	23.5	90.0	4373	1119	254.9	0.0	226.8	226.8
	45	49.6	54.2	3511	1981	180.2	162.6	282.5	371.90
	90	90.0	34.2	3322	2170	0.0	229.7	298.5	298.90
90	0	0.0	90.0	5492	0	277.9	0.0	180.6	247.30
	45	45.0	54.2	3570	1922	196.5	162.5	277.8	386.30
	90	90.0	34.2	3318	2174	0.0	229.7	298.9	298.9
45	0	16.6	90.0	5492	0	266.3	0.0	180.6	237.00
	45	47.3	54.2	3556	1936	188.3	162.5	278.9	379.00
	90	90.0	34.2	3320	2172	0.0	229.7	298.7	298.90

Now, these calculations can be repeated for rotating solar arrays. Using solar arrays that are capable of rotating around one axis it would be possible to use only one solar array. However, due to the way the solar arrays have been sized even a rotating solar array would not be capable of being sized smaller than the $A_{A2} = 1.35$ m^2. This is because the size is based on the required area for when this solar array is perpendicular to the sun at RAAN 90 and $\theta_{sun} = 90$. Therefore, the area saved is not considered to be worth the added complexity, loss of reliability and, extra developmental and testing costs associated with rotating solar arrays hence a detailed analysis is not carried out. Additionally, the analysis could be repeated for A2 in the yz plane in Figure 17.1. It was found in this case the angle of incidence of the solar array would be affected by both ϵ_{eff}, as well as, θ_{sun} resulting in a larger A2 area. Therefore, the array sizings are given only for the xy and xz planes.

Up to this point, the arrays have been discussed only in plane position. The way the arrays can then be placed in the optimum way on the spacecraft under the condition that they remain in the specified planes. So the final positioning of the solar arrays can be adjusted as required. These positioning are shown in Chapter 20. One unaccounted for scenario is a solar eclipse, however, this is considered to be within the 99% availability, MIRA-USR-SR-4.

17.4.2. Battery sizing

The number of cycles experienced by the battery is given by Equation 17.11. Equation 17.12 gives estimations for the battery mass, m_{bat}, where P_e is the power required during eclipse, $\eta_{bat_{EOL}}$ is the battery's end-of-life efficiency and η_{Eps} is the efficiency of the power regulator, acquisition and distribution system. It is estimated using various sources [17, 60, 61].

$$N_{cycles} = \frac{t_{op}}{t_{orbit}} \tag{17.11}$$

$$m_{bat} = \frac{P_e \cdot t_e}{E_{spec} \cdot DOD \cdot \eta_{bat_{EOL}} \cdot \eta_{Eps}} \tag{17.12}$$

The battery is custom fit for this specific mission. The reference battery used is the YUASA LSE51 battery. It is chosen due to its high specific energy and density when compared to other batteries. Additionally, it has a high depth of discharge, DoD, at: 40% [a]. The battery developed by YUASA has an energy density and specific

[a] http://www.gsyuasa-lp.com/SpecSheets/GS_Yuasa_LSE_GEN_III_Power_&_Energy.pdf [cited 13 June 2020]

energy lower than the Heritage 2nd Generation batteries: 289 Wh/kg and 139Wh/L respectively, compared to 168 Wh/kg and 348 Wh/L. However, as said previously, it is the DoD of the YUASA battery (40%) which makes it a more attractive choice as a reference for the battery sizing, as it allows for a higher power handling.

17.4.3. PCDU sizing

Just as a battery, a PCDU unit can also be custom fit for the mission. As there is a lack of available PCDU online which fit the power needed of this mission, it was decided to size it using interpolation. In sum, the method is to find multiple PCDU's which are either above or below in terms of peak power handling than the satellite mission considered, and then find the volume with respect to the peak power.

For this, a linear trend is used to perform the interpolation. The linear trend has the largest correlation between volume/mass and peak power, thus the largest R^2 over other functions. Choosing an interpolation is a preferred method as the PCDU does not have a significant effect on the satellite mass or volume. The mass and volume of the PCDU are then: 3.54 kg and 2.4dm^3 with a contingency on mass of 31.4%. This is calculated by taking the difference between the exponential and linear interpolation at the peak power. Its efficiency is at least 93%, using the Galileo mission as a reference [b]. Furthermore, the power consumption of the PCDU is assumed from the Galileo mission's PCDU, this had a maximum power use of 28.3 W, therefore this is scaled down and a maximum of 10 W is assumed with contingency of 50 %. Lastly, given the maturity of the design, it is safe to assume that similar to the Galileo mission the reliability is at least 98.3%. This reliability is relatively low for a series production, however, a recommendation for the next phase of the design would be to do extra testing and research to improve this level.

17.4.4. Summary of calculations

The electrical power subsystem calculations can be summarised in Table 17.5. A note, the area stated is for one side of the solar array, therefore, technically the area for the double sided arrays is doubled. Additionally, the masses related to the solar array assume the double sided arrays have a similar mass to single sided arrays, however, further research would be required to find the factor that may need to be applied to this.

Table 17.5: Summary of power system sizing outputs

Subsystem	Mass [kg]	Area [m2]	Subsystem	Mass [kg]	Volume [dm^3]
Array 1	6.4	0.93	Battery	2.56	1.3
Array 2	9.4	1.35	PCDU	3.54	2.4

17.5. Verification and validation

Verification of the model was carried out using hand calculations to verify the excel model used. Additionally, some of the parameters were varied to check the effect on the final sizing. For example, doubling the power requirement for both daylight and eclipse operations leads to a doubling in area required for the array, which is to be expected. Validation is carried out by comparing solar arrays also in use in LEO orbit. For example, the GOCE satellite uses a solar array size roughly equal to five m^2, generating a power of 1.3 kW. Using the sizing method for an expected mission of five years, a sun synchronous orbit and 18:00 MLTAN, to find the daylight and eclipse times associated gives a solar array size of 7.4 m^2, only a single solar array is needed due to the sun synchronous orbit. This is a factor of 1.48 larger, which in this case is considered acceptable seeing as the exact placement of the array is unknown and the parameter assumptions made above [c]. Repeating for the battery gives a mass of 28.8 kg, a factor of 1.41 larger then the real 20.4 kg [62].

17.6. Sustainability analysis

The main factors that effect the electrical power system with respect to sustainability are the production, resources and economic sustainability. The other aspects outlined in Chapter 5 are considered less affecting. For all three aspects, keeping the solar array, battery and PCDU sizing minimal will be beneficial as less resources are wasted. The option of using nuclear power or primary batteries was considered unfeasible due to economic sustainability as well as wasteful of resources and with respect to nuclear, dangerous for production.

[b] https://www.terma.com/media/177707/power_conditioning_and_distribution_unit.pdf [cited June 15 2020]
[c] https://earth.esa.int/web/eoportal/satellite-missions/g/goce [cited 18 March 2020]

18
Thermal Control

The goal of the thermal control subsystem is to ensure that all the spacecraft components are kept within operating temperature ranges, as explained in Section 18.1 and Section 18.2. Assumptions considered are explained in Section 18.3. The thermal environment is analysed in Section 18.4, the equations for steady state thermal analysis are described in Section 18.5 and the spacecraft surface nomenclature is introduced in Section 18.6. The thermal design has been executed for 4 segments independently, for both TIR and MS satellites: the spacecraft bus (Subsection 18.7.1), the baffle (Subsection 18.7.2 and Subsection 18.7.3), the instrument box (Subsection 18.7.4 and Subsection 18.7.5) and the propellant tank (Subsection 18.7.6). The placement of components is then defined in Section 18.8, while verification and validation are to be found in Section 18.9 and sustainability considerations in Section 18.10.

18.1. Functional analysis

The Thermal Control subsystem is designed with the goal to perform the functions specified in Figure 10.9:

- **6.5.1:** Measure subsystem temperatures (further specified in Figure 10.9)
- **6.5.2:** Deploy subsystem thermal control measures (further specified in Figure 10.9)
- **6.5.3:** Measure payload temperature
- **6.5.4:** Deploy payload thermal control measures

These functions outline the importance of thermal control. The thermal infrared telescope's thermal control will be analysed in more detail compared to the other subsystems, due to its low operating temperature.

18.2. Subsystem requirements

The requirements listed in Table 19.1 will drive the design decisions in this chapters. All requirements have been complied with: their fulfilment will become evident when the design steps are explained in the following sections in the chapter.

Table 18.1: Thermal Control requirements

ID	Requirement	Origin	Analysis ref.	
MIRA-THRM-FUNC-1	The thermal control system shall be able to maintain the thermal infrared payload temperature within -223°C and -173 °C.	BLR, MIRA-MIS-THRM-FUNC-7.2	FBS 6.5.4	✓
MIRA-THRM-FUNC-2	The thermal control system shall be able to remain operational in all environments throughout the entire mission duration.	BLR, MIRA-MIS-THRM-FUNC-7.4	FBS 6.5.2.9	✓
MIRA-THRM-FUNC-3	The spacecraft shall provide information about the thermal infrared payload temperature to the telemetry subsystem.	BLR, MIRA-MIS-THRM-FUNC-7.5	FBS 6.5.3	✓
MIRA-THRM-FUNC-4	The thermal control system shall be able to maintain the multispectral payload temperature within -223°C and 20°C.		FBS 6.5.4	✓
MIRA-THRM-FUNC-5	The thermal control system shall be able to maintain the reaction wheels temperature within -15°C and 60°C.		FBS 6.5.2.1	✓
MIRA-THRM-FUNC-6	The thermal control system shall be able to maintain the magnetic torquers temperature within -25°C and 70°C.		FBS 6.5.2.1	✓

Table 18.1 continued from previous page

MIRA-THRM-FUNC-7	The thermal control system shall be able to maintain the magnetic torquers temperature within -25°C and 70°C.		FBS 6.5.2.1	✓
MIRA-THRM-FUNC-8	The thermal control system shall be able to maintain the star tracker temperature within -10°C and 40°C.		FBS 6.5.2.1	✓
MIRA-THRM-FUNC-9	The thermal control system shall be able to maintain the magnetometer temperature within -55°C and 85°C.		FBS 6.5.2.1	✓
MIRA-THRM-FUNC-10	The thermal control system shall be able to maintain the sun sensors temperature within -50°C and 80°C.		FBS 6.5.2.1	✓
MIRA-THRM-FUNC-11	The thermal control system shall be able to maintain the gyroscope temperature within -54°C and 85°C		FBS 6.5.2.2	✓
MIRA-THRM-FUNC-12	The thermal control system shall be able to maintain the solar panels temperature within -150°C and 110°C.		FBS 6.5.2.3	✓
MIRA-THRM-FUNC-13	The thermal control system shall be able to maintain the battery temperature within 0°C and 40°C.		FBS 6.5.2.4	✓
MIRA-THRM-FUNC-14	The thermal control system shall be able to maintain the antenna temperature within -100°C and 100°C.		FBS 6.5.2.5	✓
MIRA-THRM-FUNC-15	The thermal control system shall be able to maintain the thruster temperature within -30°C and 250°C.		FBS 6.5.2.6	✓
MIRA-THRM-FUNC-16	The thermal control system shall be able to maintain the propellant tank temperature within -157.3°C and -152°C.		FBS 6.5.2.7	✓
MIRA-THRM-FUNC-17	The thermal control system shall be able to maintain the inactive structure temperature within -100°C and 100°C.		FBS 6.5.2.8	✓
MIRA-THRM-FUNC-18	The surface area of the satellite shall be covered with multi-layer/collision resistant coatings for surface protection.		Risk TR-THRM-03	✓
MIRA-THRM-PERF-1	The thermal subsystem shall have a maximum mass of 15 kg.	BLR, MIRA-COST-THRM-PERF-2.3		✓
MIRA-THRM-PERF-2	The thermal subsystem shall use a maximum power of 100 W.	BLR, MIRA-COST-THRM-PERF-2.4		✓
MIRA-THRM-PERF-3	The thermal control subsystem shall have 1 operational and 1 backup sensor for every temperature measurement.		Risk TR-THRM-04	✓

18.3. List of assumptions

The following assumptions apply to all the calculations explained in the next sections:
A-THRM-01: To comply with MIRA-USR-MISC-1, satellites of the same type (TIR/ MS) will have the same thermal coatings, able to withstand the worst (hot and cold) thermal environments met by the constellation.
A-THRM-02: The change in surface emissivity and absorbtivity due to the presence of externally mounted

spacecraft components is negligible.
A-THRM-03: Each external surface is modelled as a flat plate with an insulated back, leading to area ratio of 1 (absorbing area/ radiating area).
A-THRM-04: Earths shadow is cylindrical.
A-THRM-05: Averaged values for Solar constant, albedo factor and Earth black body temperature are taken (meaning that changes in: solar intensity, due to Earth's orbit, Earth's surface reflectivity, and black body temperature are neglected).
A-THRM-06: Heat dissipation within the spacecraft $\dot{Q}_{in}$ is limited to battery heat dissipation, cryocooler power dissipation and propellant tank excessive heat.
A-THRM-07: Solar eclipse, caused by the Moon passing between the Sun and Satellite is ignored (it causes eclipse time to suddenly increase for one orbit only).
A-THRM-08: The satellite background temperature (space temperature) is 0 K.
A-THRM-09: The instrument housing is thermally isolated from the bus.
A-THRM-10: Filtering of Albedo and other noisy wavelengths occurs in the instrument box.
A-THRM-11: Heat pipes don't dissipate any heat in the bus.

18.4. Thermal environment analysis

For the analysis of each of the 4 segments (bus, instrument box, baffle and tank), the worst case hot and cold heat flux scenarios that the segment encounters were designed for; the thermal design solutions found ensures that under these extreme scenarios, the temperature of the segment considered remains in the operational range, and consequently when the satellite is anywhere in between the hottest and coldest case scenario, the operational temperature range is automatically satisfied.

The coldest and hottest orbits that the orbital planes in the constellation will encounter have been identified analysing daylight duration and beta angle data from STK for RAAN 0,45 and 90 orbital planes (see Figure 18.1 and Figure 18.2 respectively). The beta angle is defined as the angle between the orbital plane and the Sun light.

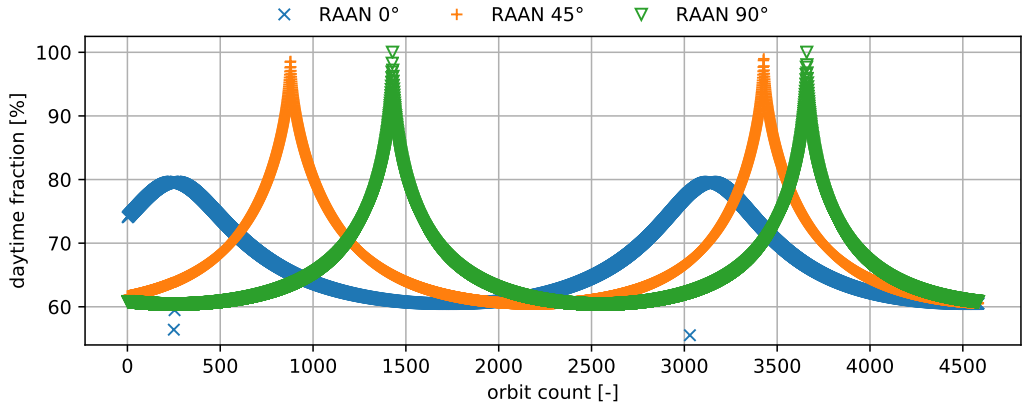

Figure 18.1: RAAN 0, 45, 90 °orbit - daylight orbit fraction vs time (1 year cycle)

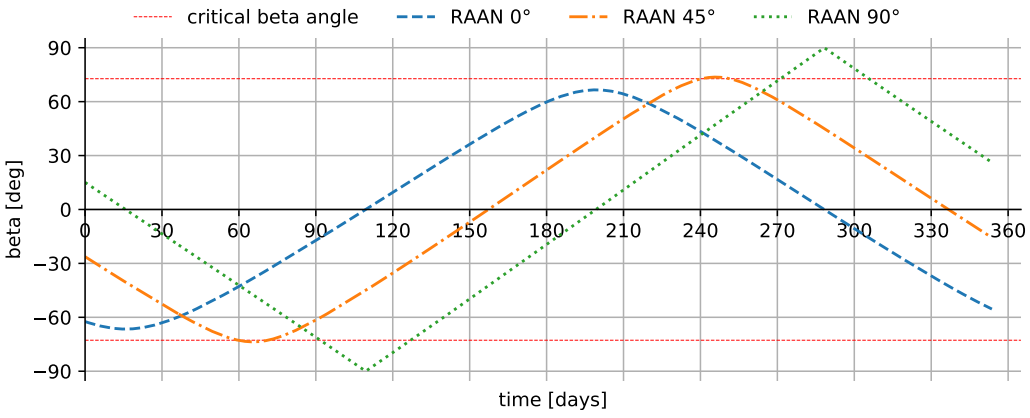

Figure 18.2: RAAN 0, 45, 90 °orbit - beta angle vs time (1 year cycle)

In Table 18.2, the outcomes of the beta angle and daylight times analysis are summarise and exact values taken from the datasets are reported:

Table 18.2: Summary of beta angles and daylight times encountered by the entire constellation

	Cold orbit		**Hot orbit**	
	β_{min}	$t_{d_{min}}$	β_{max}	$t_{d_{max}}$
0 $\leq$ RAAN < 45	0°	0.6	$\pm$ 73.66°	0.8
45 < RAAN $\leq$ 90	0°	0.6	$\pm$ 90°	1

The **coldest case orbit** is then experienced by all the orbital planes in the constellation and therefore all satellites when beta is 0 and the eclipse time is the longest (40 % of the orbit). The coldest case is first going to be computed for the steady state eclipse condition followed by a non stationary analysis that takes into account the spacecraft's heat capacity.

The **hottest case orbit** is experienced by all orbital planes with a RAAN $\geq$ 45 experience beta angles above the critical beta angle (corresponding to the eclipse angle in Figure 17.3 and to the red line in Figure 18.2, under the assumption **A-THRM-04**): these angles are associated with the presence of dawn dusk orbits. The hottest case is therefore going to be considered as a steady state fully sunlit condition, as that occurs in dusk-dawn. These cases will apply to both MS and TIR thermal analysis as both type of satellites are present in the type of orbital planes described above.

18.5. Method used for thermal analysis

To calculate the heat fluxes relevant to the 4 segments (as listed in Section 18.4), Equation 18.2 and Equation 18.3 were used. Equation 18.1 will be used to define the equilibrium temperature of the bus and of heat dissipating components (filter in the instrument box, radiators...). $\dot{Q}_{in}$, is the power dissipated by the components defined in **A-THRM-06** (this heat component only needs to be considered for the bus segment thermal control - the baffle and instrument box are isolated from the dissipating components) and $\dot{Q}_{env}$ is given by Equation 18.2 and Equation 18.3 [17].

$$\dot{Q}_{env} + \dot{Q}_{in} = \dot{Q}_{out} \tag{18.1}$$

$$\dot{Q}_{env} = \dot{Q}_{Sun} + \dot{Q}_{Albedo} + \dot{Q}_{IR} \tag{18.2}$$

$$\dot{Q}_{env} = S\sum_{1}^{n} \alpha_{avg_n} A_{abs_n} cos(\theta_n) + SFa\sum_{1}^{n} \alpha_{avg_n} A_{abs_n} + \sigma T_{Earth}^4 F \sum_{1}^{n} \epsilon_{avg_n} A_{abs_n} \tag{18.3}$$

Where F, the view factor from the satellite to Earth, is defined by Equation 18.4, which applies to a small flat surface facing a sphere. The average values of S, a and T_{Earth} are given in Table 18.3 [17] and the total IR dissipation capability of the spacecraft $\dot{Q}_{out}$ can also be computed using Equation 18.5 [17].

$$F = \frac{1}{\left(\frac{R_E + h_{orbit}}{R_E}\right)^2} \tag{18.4}$$

$$\dot{Q}_{out} = \sigma T^4 \sum_{1}^{n} \epsilon_n A_n \tag{18.5}$$

The equilibrium temperature of the spacecraft surfaces analysed can then be obtained by solving equation Equation 18.6 for the worst cold and hot cases:

$$T = \left(\frac{\dot{Q}_{in} + \sum_1^n \dot{Q}_{env_n}}{\sigma \sum_1^n \epsilon_n A_n}\right)^{\frac{1}{4}} \tag{18.6}$$

The parameters that are constant throughout the design are listed in Table 18.3 [17].

Table 18.3: Thermal environment input table

Parameter	Symbol	Value	Unit	Parameter	Symbol	Value	Unit
Solar constant	S	1371	W/m^2	Albedo factor - beta 0	a	0.27	
Orbital altitude	h_{orbit}	350	km	Albedo factor - beta 90	a	0.54	
Earth radius	R_E	6371	km	Stefan- Boltzman constant	σ	5.67E-08	-
View factor (flat plate to Earth)	F	0.899	-	Earth black body temperature	T_{Earth}	255	K

18.6. Spacecraft geometry

The absorbing and radiating surfaces on the bus are 5: surface 1: ”antiram”, surface 3: ”antisun”, surface 4: ”zenith” and surface 5: ”sun”. Surface 1,3,5,6 are 0.195 m^2 while surface 4 is 0.355 m^2, as described in Chapter 20. These are visualised for RAAN 90 in Figure 18.3.

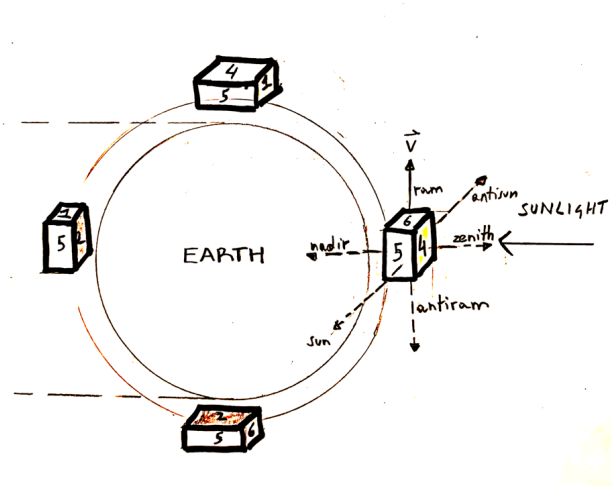

Figure 18.3: RAAN 90, bus surfaces orientation

18.7. Thermal Control Analysis

In the following subsections, the thermal control of the 4 segments is discussed (bus, instrument box, baffle and tank).

18.7.1. TIR and MS bus thermal control

Spacecraft temperature requirements

The operational temperature ranges are summarised in Section 18.2. The range for which the following heat balance is geared towards corresponds to the battery’s operational temperature range (it is the smallest range: ensuring that this is achieved within the bus will ensure that also all the rest of the components will work).

Heat balance of TIR ans MS satellites

Following the method described in Section 18.5, with the eclipse and hot case (beta= 0 and beta= 90) described in Section 18.4, the inputs in Table 18.3, Section 18.6 and in Table 18.4 are considered to solve Equation 18.6. The power dissipation for TIR and MS is computed as follows in Equation 18.7.

$$\dot{Q}_{in} = (1 - \eta_{bat_{EOL}})P_e + \dot{Q}_{pulse.tube} \tag{18.7}$$

Where the battery efficiency and eclipse power requirement are specified in Chapter 17, the heat dispersed by the pulse tube is specified in Table 18.8 and in Subsection 18.7.5 for the MS satellite.

Table 18.4: Overview of power dissipation within the bus

Parameter	Symbol	Value	Unit
Power dissipated bus - beta 0 TIR	$\dot{Q}_{in}$	40.36	W
Power dissipated bus - beta 90 TIR	$\dot{Q}_{in}$	48.19	W
Power dissipated bus - beta 0 MS	$\dot{Q}_{in}$	29.02	W
Power dissipated bus - beta 90 MS	$\dot{Q}_{in}$	29.03	W

The maximum and minimum temperatures experienced by all TIR and MS satellites in the constellation are shown respectively in in Table 18.5 and Table 18.6. The different values of absorbtivity and emissivity of surface 3 are due to the presence of the radiator coupled to the instrument box, its sizing is summarised in Table 18.9 for TIR and in Subsection 18.7.5 for MS.

Table 18.5: TIR heat balance

Surface orientation	A_{abs} **(**m^2**)**	α	**beta –>**	**0**	**90**	**0**	**90**	**0**	**90**	**0**	**90**	Q_{out}/T^4	**0**	**90**
			ϵ	Q_{Sun} **(W)**		Q_{Albedo} **(W)**		$Q_{EarthIR}$**(W)**		$Qenv$ **(W)**			**T ° C**	
Anti Ram	0.195	0.59	0.82	0	0	0	25.26	11.37	11.37	11.37	36.62	9.07E-09		
Antisun	0.195	0.32	0.94	0	0	0	0	13.07	13.07	13.07	13.07	1.04E-08		
Zenith	0.355	0.59	0.82	0	0	0	0	0	0	0	0	1.65E-08		
Sun	0.195	0.59	0.82	0	157.73	0	76.54	11.37	11.37	11.37	245.64	9.07E-09		
Ram	0.195	0.59	0.82	0	0	0	25.26	11.37	11.37	11.37	36.62	9.07E-09		
Tot				0	157.73	0	127.05	47.17	47.17	47.17	331.96	5.41E-08	**-67.28**	**17.34**

Table 18.6: MS heat balance

Surface orientation	A_{abs} **(**m^2**)**	α	**beta –>**	**0**	**90**	**0**	**90**	**0**	**90**	**0**	**90**	Q_{out}/T^4	**0**	**90**
			ϵ	Q_{Sun} **(W)**		Q_{Albedo} **(W)**		$Q_{EarthIR}$**(W)**		$Qenv$ **(W)**			**T ° C**	
Anti Ram	0.195	0.59	0.82	0	0	0	25.26	11.37	11.37	11.37	36.62	9.07E-09		
Antisun	0.195	0.4	0.9	0	0	0	0	11.37	11.37	11.37	11.37	9.99E-09		
Zenith	0.355	0.59	0.82	0	0	0	0	0	0	0	0	1.65E-08		
Sun	0.195	0.59	0.82	0	157.73	0	76.54	12.52	12.52	12.52	245.64	9.07E-09		
Ram	0.195	0.59	0.82	0	0	0	25.26	11.37	11.37	11.37	36.62	9.07E-09		
Tot				0	157.73	0	127.05	46.63	46.63	46.63	331.41	5.37E-08	**-78.41**	**14.09**

To reduce series production costs, the same coating has been applied to both TIR and MS satellites: anodised 7075-T7351 [16], with its absorptivity and emissivity as indicated in the tables. This leads to a hot case temperature of 17 °C for TIR and 15 °C for MS, both below the maximum allowed temperature of 40 °C for the battery, meaning that there is no need to radiate any excess heat. The cold case temperature is −67 °C for TIR and −78 °C for MS. The battery would get too cold, but the steady state cold case never occurs, as opposed to the steady state hot one.

Non stationary thermal analysis - cold case

To better quantify the worst cold case, a non stationary analysis has been performed for both TIR and MS, for the orbit of beta=0 (longest eclipse). Equation 18.8 was solved numerically as described by Equation 18.9.

$$\frac{1}{m \cdot c} \cdot \frac{dT}{dt} = Q_{env} + Q_{in} - Q_{out} \tag{18.8}$$

Where Q_{env} is expanded in Equation 18.3, Q_{in} in Equation 18.7 and Q_{out} in Equation 18.5. The numerical solution then becomes:

$$\frac{dT_{i+1}}{dt} = \frac{1}{m\dot{c}} \cdot (Q_{env}(t_i) + Q_{in}(t_i) - Q_{out}(T_i)) \tag{18.9}$$

The Earth IR heat flux has been assumed to be constant throughout the orbit and the same as the one in Table 18.6 and Table 18.5. The Albedo flux has been assumed to be 0 during eclipse, and constant (see Equation 18.3) during daylight (44.65 W for TIR, 50.51 W for MS). The heat flux coming from the Sun has

been assumed to be 0 during eclipse and for daylight, geometrical relations were derived to find the incidence angle on every surface for every second in the orbit. The power dissipation for TIR ans MS have been taken from Table 18.4. The mass m of the TIR/ MS spacecraft has been taken from Chapter 24. To define the heat capacity, the mission Libertad 2 was taken as reference [63]: this cube sat of 4 kg is approximated as a block of 1 kg of aluminium with a heat capacity of 1000 J/K, the same ratio of spacecraft to aluminium mass has been considered for MIRA (25%). The resulting plot for TIR can be seen in Figure 18.4 where other options of aluminium mass to spacecraft mass ratios are shown.

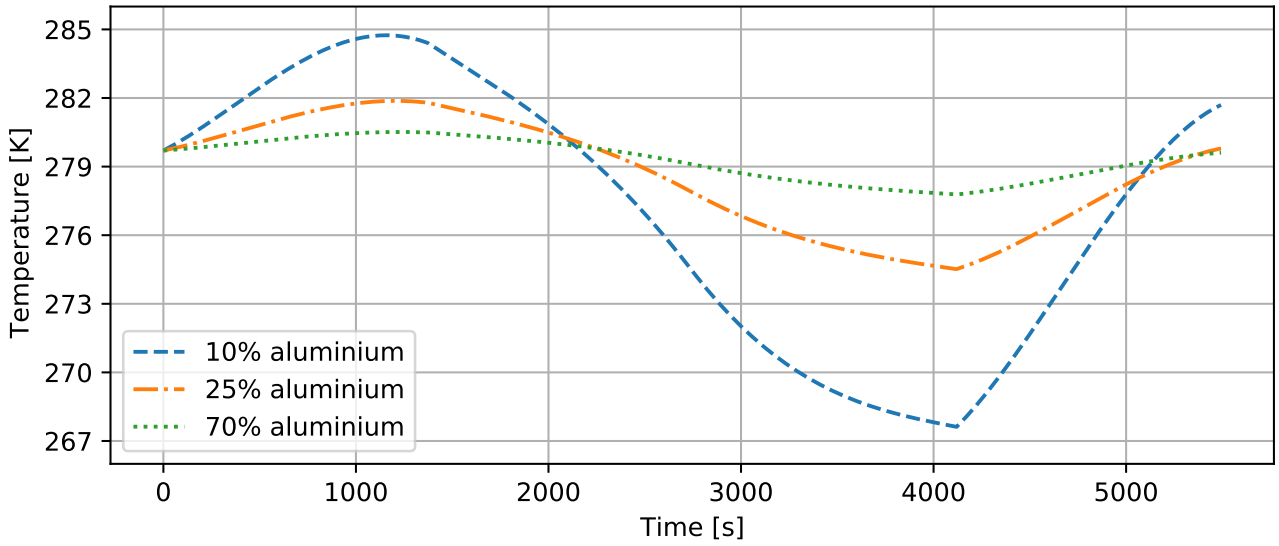

Figure 18.4: Temperature vs time (1 orbit cycle) for different TIR heat capacities

The plot converged when inputting an initial temperature of T = 279.7 K for the TIR and 283 K for MS. With these values, the temperature after one orbit returns to its initial value. The main takeaway from this analysis is that, for an aluminium to spacecraft mass of 25%, the minimum (cold case) temperature experienced by TIR is 274.5 K (2.3 °C). The same plot was computed for MS reaching a minimum temperature of 279.2 K (7 °C). Both values are above the required battery minimum operating temperature of 0 °C and therefore a heater would not be needed, however a more tailored calculation of heat capacity might lead to a different conclusion.

18.7.2. TIR primary mirror thermal control

As explained in Section 12.4, the maximum allowed temperature for the primary mirrors is 256.5 K. Such a low temperature can be achieved thanks to the presence of the baffle, which shields the telescope components from direct sunlight. A steady state thermal analysis of the baffle has been performed, to be able to compare the temperature inside the baffle to the primary mirrors operational temperature and see if active baffle cooling is needed. The equation to be solved is Equation 18.6 (more details in Subsection 18.7.1). The inputs and outputs for the first iteration are reported in the left side of Table 18.7. The baffle inner absorptivity and emissivity has been taken from Arink [64]'s analysis, while the absorbing area A_{abs} has been approximated by subtracting to the baffle's projected circular area the cross- shaped projected area of the mirrors (as the heat flux is stray light, it would be too conservative to consider the entire inner area as absorbing). The heat fluxes considered are for the cold case: Earths IR, while for the hot case: stray light from the sun (at an incident angle of 75: leading to a low solar flux - see Equation 18.3), Earth Albedo (considering the view factor F - Equation 18.3) and Earth IR. As seen, with no cooling solution for the baffle, the temperature inside would become too high for the primary mirrors to operate. In iteration 2 (right side of Table 18.7), the inner baffle temperature is lowered by ∼191 K with the use of reflective surfaces "mirrorlets" covering 95 % of the baffle's inside (as designed by Linlor [65]): this is a passive solution for baffle cooling of IR telescopes. To prevent reflected light to interfere with the secondary mirror, this solution, visualised in Figure 18.5, carefully considers the angling of the mirrors (see Figure 18.6). It is worth noting that for MIRA, the mirrorlets would need to be foldable and deployable (this could be achieved by using flexible, foldable surfaces to mount the mirrorlets; they could then be spring loaded, connected to a tensioned cable and deployed similarly to the arrays).

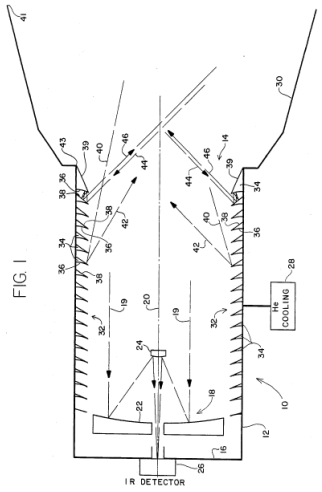

Figure 18.5: Baffle with mirrorlets mounted along its perimeter [65, p. 2]

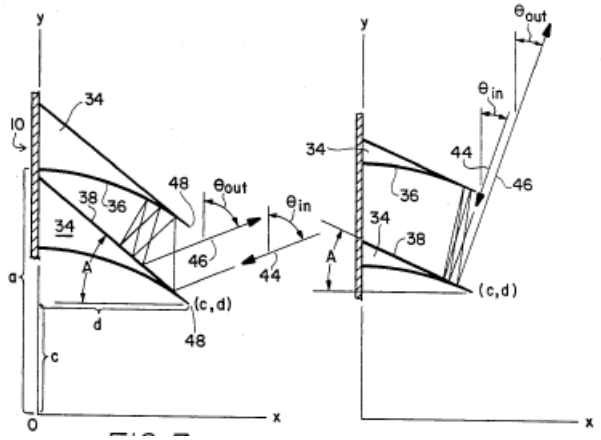

Figure 18.6: Mirrorlet geometry close-up [65, p. 3]

Table 18.7: TIR baffle heat balance input-output table: outputs in bold (iteration 1, left; iteration 2, right)

Parameter	Symbol	Value	Unit
Absorbing area	A_{abs}	0.578	m^2
Angle of incidence	θ	75	°
Baffle inner absorbtivity	α	0.93	-
Baffle inner emissivity	ϵ	0.84	-
		beta=0 **beta=90**	
Sun heat absorbed	Q_{Sun}	0 190.74	W
Albedo heat absorbed	Q_{Albedo}	0 357.59	W
Earth IR absorbed	Q_{IR}	97.27 97.27	W
T Baffle not cooled	**T**	**243.81** **391.33**	**K**

Parameter	Symbol	Value	Unit
Absorbing area	A_{abs}	0.578	m^2
Angle of incidence	θ	75	°
Area fraction covered by mirrors	$\%A$	95%	-
Mirrorlet absorbtivity	α	0.04	-
Mirrorlet emissivity	ϵ	0.04	-
Baffle resultant absorbtivity	α	0.0845	-
Baffle resultant emissivity	ϵ	0.08	-
		beta=0 **beta=90**	
Sun heat absorbed	Q_{Sun}	0 17.33	W
Albedo heat absorbed	Q_{Albedo}	0 32.49	W
Earth IR absorbed	Q_{IR}	0.84 0.84	W
T Baffle cooled passively	**T**	**71.92** **200.32**	**K**

The temperature inside the baffle with the mirrorlets applied indeed does satisfy the primary mirror temperature requirement.

18.7.3. MS primary mirror thermal control

The same calculations apply for the MS satellite, as the orbit is the same (same fluxes, different absorbing area - this difference is not relevant when A_{abs} = A_{rad} and therefore the same fluxes bring to the same temperatures). The maximum allowed temperature for the primary mirrors of the MS satellite is 323 K [64]. The mirrorlets suffice as cooling method also in the MS case.

18.7.4. TIR instrument box thermal control

The thermal control design of the TIR instrument box, bottom part in Figure 20.2, is carried out in this section. The reference temperature requirement is **MIRA-THRM-FUNC-1** in Section 18.2. To ensure that the TIR detector works at its operating temperature and to come up with an appropriate solution for cooling, first the excess heat at the detector needs to be quantified. This is done using Equation 18.10:

$$\dot{Q}_{detector} = \int_{8\mu m}^{12\mu m} L_\lambda \cdot \tau d\lambda \cdot F \cdot A_{tot_{prim-mirror}} \cdot \epsilon_{prim} \cdot \epsilon_{sec} \cdot \epsilon_{ter} \tag{18.10}$$

The first part of the equation has been introduced in Section 11.3 and has been integrated on Python. With the primary mirror characteristics defined in Chapter 12, assuming all mirrors are made of the same material, leads to a value of 0.828 W of heat at the detector.

Passive cryogenic cooling

Passive cryogenic cooling has been analysed and dismissed for the following reasons:

- There is no surface of the spacecraft that is cold enough to radiate at ~80K and big enough to radiate the detector's heat: a Sun and Earth shield would be needed and the radiator would need to be deployed
- The Sun shield and the deployed radiator would lead to a significant increase in drag
- The complexity of the system would then become significant and therefore defeat the advantage of passive cooling

Active cryogenic cooling

Active cryogenic cooling has been chosen as the solution for instrument box cooling. At 80 K, the specific power ratio ($P_{in}/Q_{instr.box}$) of cryocoolers is ~ 20, as seen in Figure 18.7 (red cross).

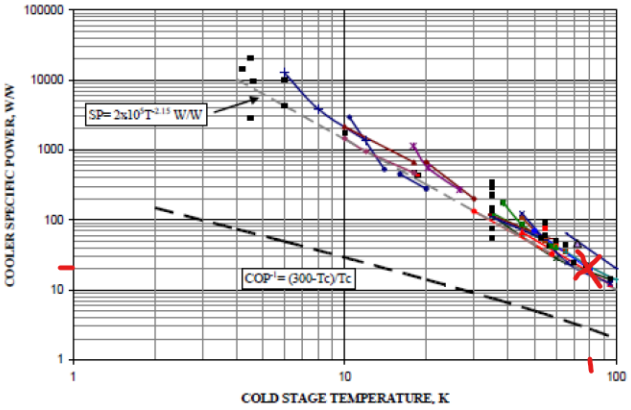

Figure 18.7: Specific power of cryocoolers [66]

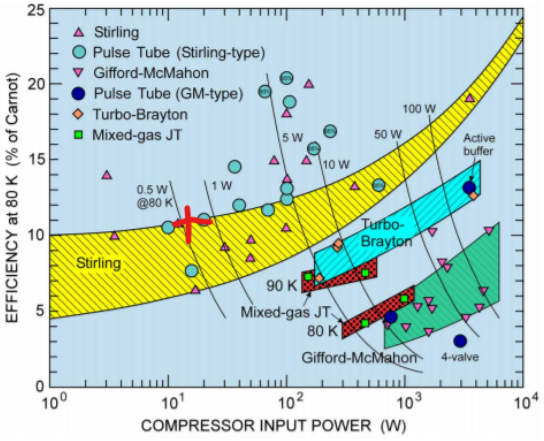

Figure 18.8: Recent, high efficiency refrigerators [67], pg.12

The power input needed to run a cryocooler can be obtained by Equation 18.11:

$$P_{in} = P_{spec} \cdot \dot{Q}_{instr.box} \tag{18.11}$$

As the cryocooler's cold finger would be inserted into the entire instrument box, the heat lift also includes the heat dissipated by the filtering of noise (see Equation 18.12). The wavelengths that are not observed (Albedo, UV and some IR) hit the primary, secondary, tertiary mirror, then a filter that sends the signal to the detector and dissipates the noise as heat in the box. This is quantified in Equation 18.13 and Equation 18.14:

$$\dot{Q}_{instr.box} = \dot{Q}_{detector} + \dot{Q}_{radfilter} \tag{18.12}$$

Where:

$$\dot{Q}_{radfilter} = A_{filter}\epsilon_{filter}\sigma(T_{filter}^4 - T_{instr.box}^4) \tag{18.13}$$

Where:

$$T_{filter} = \left(\frac{\dot{Q}_{in_{filter}}}{\sigma\epsilon_{filter}A_{filter}}\right)^{\frac{1}{4}} \tag{18.14}$$

The input power for the cryocooler can therefore be obtained based on the equations above, with the inputs specified in Table 18.8. It depends on beta angle as the heat dissipated in the instrument box depends on the amount of noise generated which depends on the changing thermal environment.

Table 18.8: Input and output table for instrument box heat and pulse tube power: outputs in bold

Parameter	Symbol	Value		Unit
Filter area	A_{filter}	0.066		m^2
Filter emissivity	ϵ_{filter}	0.80		-
Filter absorbtivity	α_{filter}	0.20		-
Instrument box temperature	$T_{instr.box}$	80.5		K
Heat at detector	$\dot{Q}_{detector}$	0.828		W
Efficiency as percentage of Carnot	COP	0.11		-
		beta =0	**beta =90**	
Environmental fluxes on primary mirror	$Q_{env_{primary}}$	0.18	21.55	W
Heat in filter	$Q_{in_{filter}}$	0.034	4.13	W
Filter temperature	T_{filter}	58.26	192.58	K
Heat radiated by filter	$Q_{rad_{filter}}$	-	0.475	W
Instrument box heat	$Q_{instr.box}$	**0.828**	**1.3**	**W**
Power input in cryocooler	P_{in}	**17.25**	**26.05**	**W**
Power dissipated cryocooler	$Q_{pulse.tube}$	**15.36**	**23.19**	**W**

As seen in Figure 18.8, for an 80 K temperature requirement, with an average input power of 21.654 W, pulse tubes are the indicated cryocoolers. Pulse tubes are Stirling cycle refrigerators characterised by lower vibration levels and longer lifetime than the standard Stirling coolers [68]. Figure 18.8 indicates a COP of ~ 0.11, leading to a power dissipation by the cooler assembly in the bus of 15.46 W at beta=0 and 14.74 at beta=90. The pulse tube system mass would be 0.834 kg (0.032 kg/W extrapolated from [68]).

The heat taken away from the filter "$Q_{rad_{filter}}$" would need to be radiated away from the instrument box. For this purpose, a dedicated radiator needs to be sized (note that in the cold case scenario, the filter is at a lower temperature than the instrument box and therefore does not generate heat to be radiated away). Considering the thermal resistance of the heat pipes ($T_{rad_{instr.box}} = T_{filter} - \Delta T_{heatpipe}$) and the environmental heat load on the radiator, an iterative process is started: the radiator area in fact depends on the environmental heat [W] ($\dot{Q}_{env}$ in Table 18.5 for the Antisun surface where the radiator will be mounted) which in turn depends on the optical properties of the exposed surface (average ϵ and α), which change when a radiator is placed on a surface). The heat pipes will be circulating nitrogen[a] and will have an approximate thermal resistance of 0.85 K/W [69] (ΔT is then obtained by multiplying with $Q_{rad_{filter}}$). Convergence was found for the radiator area in Table 18.9:

Table 18.9: Input and output table for instrument box radiator area

Parameter	Symbol	Value		Unit
Heat pipe thermal resistance	t_{pipe}	0.85		K/W
Area fraction of radiator over surface	$A_{\%_{rad}}$	0.945		-
		beta=0	**beta=90**	
ΔT heat pipe	$\Delta T_{heatpipe}$	-	0.4	K
Radiator absolute T	$T_{rad_{instr.box}}$	58.26	192.18	K
Radiator emissivity (louver open)	$\epsilon_{louver.open}$	0.95	-	-
Radiator area	$A_{rad_{instr.box}}$	-	**0.184**	**m^2**

The final radiator area will be the bigger one required for beta = 0: when beta is 0 °, no radiator would be needed. To avoid cooling below temperature requirements, a louver should be added to the radiator. The louver will gradually close when beta increases from 0 to 90, allowing emissivity to decrease. At beta = 0 the louvers should be closed. Considering a mass estimation of 3.3 kg/m^2[b], the radiator would weigh 0.608 kg and

[a] https://www.boydcorp.com/thermal/two-phase-cooling/cryogenic-heat-pipes.html
[b] https://www.valispace.com/wp-content/uploads/2018/12/TCS-sizing-tutorial.pdf

considering a mass estimate of 3.2 kg/m^2 for the louver [16], the louver would weigh 0.59 kg.

18.7.5. MS instrument box thermal control

The same sizing process as described in Subsection 18.7.4 has been applied to the MS satellite, for which active cryogenic cooling will also be used, with a lower power requirement. The inputs that are not specifically reported below, can be assumed to be common to the TIR satellite (filter area, emissivity...). The smaller heat at the detector is mostly due to the fact that the atmosphere does not let as much light through in the MS spectrum; the spectrum range is much smaller too. In the cold case scenario, the filter is at a lower temperature than the instrument box and therefore does not generate heat to be radiated away. The results are summarised in Table 18.10:

Table 18.10: Inputs and outputs (bold) of the MS active thermal control and radiator sizing

Parameter	**Symbol**	**Value**		**Unit**
Instrument box temperature	$T_{instr.box}$	190		K
Heat at detector	$Q_{detector}$	0.003		W
		beta=0	**beta=90**	
Environmental heat fluxes on primary mirror	$Q_{env_{primary}}$	0.24	29.10	W
Heat in filter	$Q_{in_{filter}}$	0.05	5.59	W
Filter temperature	T_{filter}	62.8	207.6	K
Heat radiated by filter	$Q_{rad_{filter}}$	-	3e-04	W
Instrument box heat	$Q_{instr.box}$	0.003	0.006	W
Power input in cryocooler	P_{in}	0.027	0.03	W
Power dissipated cryocooler	$Q_{pulse.tube}$	0.02	0.03	W
Area fraction of radiator over surface	$A_{\%_{rad}}$	0.642		-
ΔT heat pipe	$\Delta T_{heatpipe}$	-	2.4e-04	K
Radiator absolute T	$T_{rad_{instr.box}}$	-	207.6	K
Radiator area	$A_{rad_{instr.box}}$	-	**0.125**	m^2
Radiator mass	m_{rad}	**0.413**		**kg**
Louver mass	m_{louver}	**0.4**		**kg**

18.7.6. TIR & MS propellant tank thermal control

The storage temperature and pressures of the propellant are shown in Figure 14.1. The propellant tank heat dissipation is quantified by Equation 18.15[c].

$$Q_{radiated_{MLI}} = \frac{A_{tank}\sigma\left(T_{bus} - T_{tank}\right)^4}{(n-1)(\frac{2}{\alpha_{MLI}} - 1)} \tag{18.15}$$

The heat radiated from the propellant tank influences the bus temperature. Iterations were used to find the values for heat dissipated for beta=0 and beta=90. For this propellant tank heat to be rejected, a Space Micro Pulse Tube Cooler [70] is used, tested upto a reject tempterature of 300K and upwards of 10 year operational lifetime. The results of this sizing and design are shown in Table 18.11.

[c]https://www.valispace.com/wp-content/uploads/2018/12/TCS-sizing-tutorial.pdf

Table 18.11: Propellant tank temperature control

Parameter	Symbol	Value		Unit
MLI layer absorptivity	α_{MLI}	0.0015		
Number of layers	n	5		
Propellant temperature	T_{tank}	209.2		K
Micro Pulse Tube Cooler		0.9		kg
Input Power		1		W
TIR		**beta=0**	**beta=90**	
Heat rejection temp. (max.)			276.87	K
Propellant tank area	A_{tank}	0.266		m^2
External temperature	T_{bus}	274.5	289.49	K
Q_{tank} heat to be radiated out	$Q_{radiated_{MLI}}$	0.01	0.01	W
MS		**beta=0**	**beta=90**	
Heat rejection temp. (max.)			269.74	K
Propellant tank area	A_{tank}	0.293		m^2
External temperature	T_{bus}	279.2	286.44	K
Q_{tank} heat to be radiated out	$Q_{radiated_{MLI}}$	0.00	0.02	W

Using a Space Micro Pulse Tube Cooler [70], this heat to be radiated out, can be rejected on the antisun surface of the spacecraft (surface 3 in Subsection 18.7.1. The external temperatures reported refer to the cold case (from the dynamic analysis) and the hot case bus temperatures in Subsection 18.7.1.

18.8. Component placement

The following decisions were taken with respect to component placement:

- The spacecraft tank is positioned as far away as possible from the battery and close to the Antisun surface as it is the one subjected to the lowest heat fluxes.
- The radiator dedicated to the instrument box is positioned on the Antisun surface (#3), as it is the one most often in shade.
- The compressor of the pulse tube is positioned in the spacecraft bus, with the cold finger reaching into the instrument box
- A thick layer of MLI is placed between the instrument box and the spacecraft bus to prevent heat transfer to the cooled area.

18.9. Verification and validation

For verification, both unit and system tests were performed. Examples of unit tests performed are shown for all code blocks below:

- TIR heat balance: set $\sigma = 0$ and, as expected, get errors of type ”cannot divide by zero” in temperature calculation.
- MS heat balance: increasing the orbital altitude by 100 km and observing a proportional decrease in view factor and in albedo and IR fluxes.
- Power dissipation by pulse tube: double specific power of pulse tube and observe doubled power dissipation.

A system test was performed on the instrument box radiator area estimation: by increasing the filter area, the radiator area increased and this in turn caused a proportional decrease in the equilibrium temperatures. Validation was done mainly for the passive thermal control results. The heat fluxes obtained were compared with the heat fluxes for FireSat II at beta=0 and beta=90 [17] and scaled for the difference in orbital altitude and surface area. The fluxes were of the same magnitude and the values were comparable (considering the difference in coatings).

18.10. Sustainability analysis

The most relevant aspects of sustainability for thermal control are sustainable production, resources and economic sustainability. In the design phase, economic sustainability is considered when a unique passive thermal control design is applied to all TIR and MS spacecraft in the constellation. Applying one type of coating to all spacecraft reduces the cost for series production. The overall attitude of reducing as much as possible the power consumption and looking for alternative, passive thermal control options (ie: baffle cooling design) favours the reduction of solar array area requested by thermal control and therefore of material and energy spending.

19 Structures and Mechanisms

Providing support and protection to all the subsystems and ensuring that parts are deployed or moved to the needed location or position are the responsibilities of the structures and mechanisms subsystem. This chapter starts with functional analysis where tasks of structures and mechanisms are listed (Section 19.1). Then, requirements for structures and mechanisms are shown (Section 19.2) and the assumptions used in this chapter are documented (Section 19.3). Then, attachment to the launcher and method for sizing it is discussed (Section 19.4). After that, the overall structures configuration (Section 19.5), structures and mechanisms mass estimation (Section 19.6) and a structures mass breakdown (Section 19.7) is shown. Furthermore, the mechanisms used and their deployment is discussed (Section 19.8). After that, sustainability aspects and risks related to structures and mechanisms are analysed (Section 19.10) and the overall mass budgets for the MIRA MS satellite and the MIRA TIR satellite are presented (Section 19.11).

19.1. Functional analysis

The Structures and Mechanisms subsystem should be designed with the goal to perform the functions specified in Figure 10.9:

- **6.9.1:** Provide structural support
- **6.9.2:** Provide environmental protection
- **6.9.3:** Provide structural integration
- **5.1.2:** Deploy solar arrays
- **6.7.1:** Point solar arrays
- **5.1.5:** Deploy communication subsystem
- **5.3.1:** Deploy telescope including the baffle

From the list of functions it is observed that many functions are dedicated to deployment. This is because many of the structures on the satellite are deployable.

19.2. Subsystem requirements

The requirements, their origin and a compliance with them for structures and mechanisms is outlined in Table 19.1.

Table 19.1: Structures and Mechanisms requirements

ID	Requirement	Origin	Analysis ref.	
MIRA-STRC-FUNC-1	The spacecraft structure shall be capable of supporting the subsystems for the duration of the entire mission.	BLR, MIRA-MIS-STRC-FUNC-9.5	FBS 6.9.1.3	✓
MIRA-STRC-FUNC-2	The spacecraft structure shall provide attachment points for the subsystems.	BLR, MIRA-MIS-STRC-FUNC-9.6	FBS 6.9.3.1	✓
MIRA-STRC-FUNC-3	The spacecraft structure shall be capable of withstanding launch loads.	BLR, MIRA-MIS-STRC-FUNC-3.2	FBS 6.9.1.1	✓
MIRA-STRC-FUNC-5	The spacecraft structure shall protect subsystems from debris.	BLR, MIRA-MISC-STRC-FUNC-3.3	FBS 6.9.2.2	✓
MIRA-STRC-FUNC-5.1	The spacecraft structure shall protect subsystems from solar and cosmic radiation flares	MIRA-SYS-FUNC-2	FBS 6.9.2.1	✓
MIRA-STRC-FUNC-6	The spacecraft shall be compliant with the integration requirements of the launcher.	BLR, MIRA-MISC-STRC-FUNC-3.4	FBS 6.9.3.2	✓
MIRA-STRC-FUNC-7	The satellite shall use metal materials for its surface area to protect itself from radiation and incoming projectiles.		Risk TR-E-01, TR-E-03	✓

Table 19.1: continued from previous page

ID	Requirement	Origin	Analysis ref.	
MIRA-STRC-FUNC-8	The satellite shall use at least 2 torsion springs, 2 dampers and a reliable thermal knife to prevent failure of deployment of the solar panel.		Risk TR-STRC-04	✓
MIRA-STRC-FUNC-9	The spacecraft structure shall be able to sustain loads from -2g to 6g in axial direction.		Falcon 9 load factors	✓
MIRA-STRC-FUNC-10	The spacecraft structure shall be able to sustain loads from -2g to 2g in lateral direction.		Falcon 9 load factors	✓
MIRA-STRC-FUNC-11	The baffle shall be deployed until at least the secondary mirror.		FBS 5.3.1.3	✓
MIRA-STRC-FUNC-12	The baffle shall be wide enough in deployed state to fit the deployed primary mirrors inside.		FBS 5.3.1.3	✓
MIRA-STRC-SUS-1	The number of ejected debris structure during separation from the launcher shall be 0.		Sustainability	✓
MIRA-STRC-PERF-1	The structures and mechanisms subsystem shall have a maximum weight of 105 kg for the TIR satellite.	BLR, MIRA-COST-STRC-PERF-2.9		✓
MIRA-STRC-PERF-2	The structures and mechanisms subsystem shall have a maximum weight of 105 kg for the MS satellite.	BLR, MIRA-COST-STRC-PERF-2.11		✓
MIRA-STRC-PERF-3	The structures and mechanisms subsystem shall use a maximum power of 5 W.	BLR, MIRA-COST-STRC-PERF-2.10		✓
MIRA-STRC-PERF-4	The satellite structure shall not contain tough steel and titanum.		Sustainability	✓

19.3. List of assumptions

The following assumptions were taken in this chapter:

- **A-STRC-01:** Mass fraction of structures and mechanisms subsystem compared to the total satellite mass for MIRA MS and MIRA TIR is the same.
- **A-STRC-02:** Similar satellites were exposed to loads and vibrations during launch similar to the loads and vibrations that MIRA satellites will be exposed to, therefore mass estimation based on similar satellites is assumed to be valid.

19.4. Launcher attachment

First, ways the satellites could be fitted and attached to the launcher were investigated. The deployment method was an important aspect. It was decided that the deployment method should be simple in order to increase reliability and it should minimise the risk of collision of satellites into each other during deployment as satellites have delicate mirrors around their exterior and the deployment method should satisfy requirement MIRA-STRC-SUS-1. Two feasible options were considered. The first option is to place satellites vertically in the launcher payload space and attach the bottoms of the satellites to the horizontal platform of the launcher. The second option is to have a big cylinder in the middle of the launcher payload space and then attach the side of each satellite to that cylinder. This way satellites would be placed vertically and they would be deployed horizontally. It was realised that the first option is not optimal for fitting as many satellites as possible in one launcher due to the width and footprint of the MIRA satellites. Therefore, the second option is chosen and is further analysed.

A method for sizing the cylinder in the middle of the launcher was developed. This cylinder will be used

with Falcon 9 and Atlas V rockets. The idea is to place as many satellites as possible in one level, therefore the cylinder with the attached satellites should be as wide as possible which means that satellites should be almost touching the interior part of the fairing. A MIRA MS satellite is slightly bigger than a MIRA TIR satellite. However, for the sizing of launcher attachment it is assumed that all MIRA satellites have the same dimensions as the MIRA MS satellite. An additional clearance of 5 cm is added to the sides of the satellites. Derivation of the diameter ($2r$) for launcher attachment cylinder is based on Figure 19.1 and is derived from Equation 19.1. $D = 2R$ is the available diameter of the payload space in the launcher, a is the width of the satellite, b is the length of the satellite. The number of satellites in one level (n) is given by Equation 19.2.

The height of the launcher attachment cylinder is limited by the available height of the launcher payload space. The mass of the launcher attachment cylinder scaled from attachments that have similar available launch configurations. Quad satellite launcher attachment for Galileo satellites shown in Figure 19.2 is used as a base for scaling. The attachment has a mass of 450 kg and carries a total mass of approximately 2900 kg [a]. This results in the ratio of approximately 0.16. Then this ratio is multiplied by the mass of a MIRA MS satellite, which is approximately 250 kg and the result is 40 kg. A factor of 1.25 is used to take into account that the attachment cylinder of MIRA satellites will have multiple levels. As a result, mass of launcher attachment cylinder is estimated to be 50 kg per satellite that is attached to it. The results obtained about the dimensions and mass of launcher attachment cylinders for different launchers are documented in Table 14.9. To attach satellites to launcher attachment cylinder, a separation system is used. The RUAG 381S 15 inch [b] is chosen and it would be attached to the front side of satellite shown in Figure 20.4. The part of separation system attached to the satellite has a mass of 1 kg, while the part attached to the launcher attachment cylinder has a mass of 3 kg. So the total mass of launcher attachment cylinder with separation system is 53 kg.

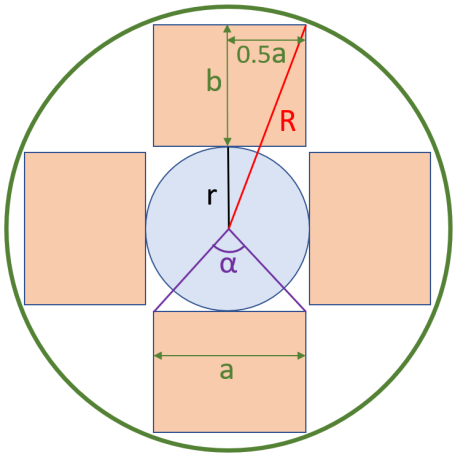

Figure 19.1: Sketch for derivation of the diameter for launcher attachment cylinder

Figure 19.2: Quad satellite launcher attachment for Galileo satellites[c]

$$D = 2 \cdot \sqrt{(b + r)^2 + (0.5 \cdot a)^2} \tag{19.1}$$

$$n = \frac{2 \cdot \pi}{2 \cdot \arctan\left(\frac{a}{2r}\right)} \tag{19.2}$$

For Vega rocket, the Vespa dual payload adaptor[d] could be used to accommodate 2 satellites in 1 launch. MIRA satellites have attachment place on the side so satellites could be placed horizontally or some kind of custom bracket is needed to place them vertically. Exact attachment mechanism or separation system needs further investigation.

19.5. Overall structures configuration

It was decided to use honeycomb structures as honeycomb panels are commonly used in structures of satellites. After looking at similar small satellites, it was observed that there are two possible options for the structure of the satellite using honeycomb panels. One option is to use several metal beams/bars that would create a frame, which carries most of the loads and then use honeycomb panels as sides, top, bottom and interior trays of the satellite. The other option is to have the structure of the satellite fully made out of honeycomb panels.

[a] https://www.gpsworld.com/galileo-ariane-5-dispenser-in-place/ [cited 19 June 2020]
[b] https://www.ruag.com/sites/default/files/2016-11/PAS_381S_Separation_System.indd_.pdf [cited 29 June 2020]
[c] https://www.esa.int/ESA_Multimedia/Images/2016/11/Quad_satellites_see_space [cited 19 June 2020]
[d] http://www.esa.int/Enabling_Support/Space_Transportation/Deploying_multiple_satellites_with_Sylda_and_Vespa [cited 30 June 2020]

The advantages of honeycomb panels is that they have high strength, good rigidity, vibration damping, heat insulation and they are lightweight, cost effective and provide good mounting capabilities for subsystems [e]. The disadvantages of honeycomb panels are some challenges with performance of the panels and challenges with connecting to other structural elements. This increases development time and cost [71]. Using knowledge about advantages and disadvantages of honeycomb panels, a trade-off is done between the first option (metal frame + honeycomb panels) and the second option (fully honeycomb). The first option is expected to be easier during assembly as it is expected that there is more access in terms of space due to frame structure. Also it is expected that bars cope better with load in longitudinal direction. In addition to that, the frame is not directly exposed to the environment. The second option is expected to be lighter and have less assembly components. However, a fully honeycomb structure is expected to be weak at the attachment points [71]. Also, because of the many holes in the panels due to thrusters and attachments of deployables, the stiffness and strength of the honeycomb panels would decrease. Therefore, thicker and heavier panels would have to be used. Based on the trade-off, the first option is preferred over the second one. Side views of both options are shown in Figure 19.3.

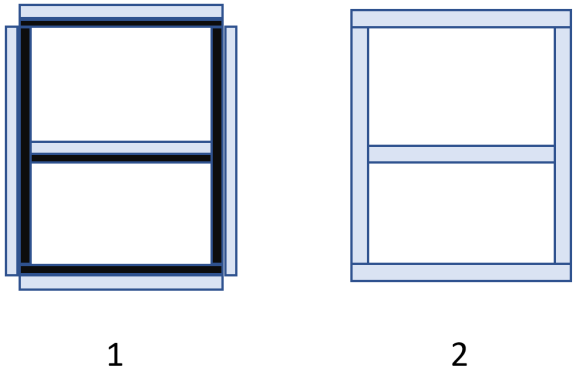

Figure 19.3: Option 1 and option 2 for the satellite. The metal frame is represented in a dark colour, honeycomb panels are represented in a light blue colour.

19.6. Mass estimations

The structure of a satellite is not very mission specific. There are different design options, such as different satellite shapes, configurations, materials and structures used, but the overall mass budget for the structures subsystem in percentage compared to the overall satellite mass is relatively similar for every mission. The mass of the structures subsystem usually occupies around 15 to 30 % [17] of the total satellite mass.

At this design stage, and taking into account the limited available time, it was decided to size the structures and mechanisms subsystem based on similar satellites. It is identified that at this design stage sizing based on physical principles would involve many assumptions that would significantly influence the outputs of the structural analysis, therefore sizing based on similar missions should be a more precise method.

From a list of satellites given in [17], satellites that had masses in the same order of magnitude as MIRA satellites were observed. Then satellites that have a too high altitude were removed and the satellites that do not carry any propellant were removed. The remaining satellites are documented in Table 19.2. Looking at those satellites, it is observed that the percentage of total mass of the structures part heavily depends on the payload percentage of the total mass. Therefore, payload percentages of total mass for MS and TIR satellites are calculated. The average of the payload percentages of four similar satellites is calculated and it is observed that the average value is between MIRA MS payload percentage and MIRA TIR payload percentage. Then the structures and mechanisms percentage of MIRA satellites is found by taking the average of the structures and mechanisms part of four similar satellites. An additional estimate of 3 % of the total mass is added to the structures and mechanisms subsystem as the satellites have many deployables, including the deployable baffle, and because the satellites have a non-uniform shape to deploy the telescope and to fit all the subsystems. Using the obtained structures and mechanisms percentage of 22 %, the structures and mechanisms mass of the MIRA MS and MIRA TIR satellites was found to be 54 kg and 47 kg respectively. Adding mass of the separation system part (1 kg) results in 55 kg and 48 kg. At this design stage it was decided to assign a 25 % contingency for structures and mechanisms mass estimations as configurations, altitudes and mission goals of

[e] https://www.arrow-dragon.com/10-things-you-need-to-know-about-aluminum-honeycomb-panel/ [cited 19 June 2020]

the satellites in Table 19.2 differ from MIRA satellites.

Table 19.2: Mass of structures and mechanisms estimated for similar satellites

Satellite	Total mass [kg]	Payload mass [kg]	Payload percentage [%]	STRC and MECH percentage [%]
Lewis	385	97	25	17
CALIPSO	577	283	49	10
EO-1	579	185	32	21
GRACE	471	70	15	29
MIRA MS	244	61	25	22
MIRA TIR	212	82	39	22

19.7. Structures breakdown

Aluminium sheets with an aluminium core are commonly used types of honeycomb panels for space applications, as aluminium honeycomb panels are lightweight, stiff and good for solar radiation protection. They are also capable of protection against space debris. Aluminium 2024 is used for skin and Aluminium 5056 is used for the core with adhesive Redux 312L connecting the skin to the core [f]. Also, aluminium is often used for the frame, so Aluminium 7075 is chosen [72]. It is estimated that out of 22 % of total satellite mass allocated for structures and mechanisms, 16 % should be dedicated to structures and 6 % to mechanisms. The structures mass breakdown for structural items is based on [73] and is documented in Table 19.3.

Table 19.3: Components of structure

Structural item	Ratio of structure mass [%]	Mass for MIRA MS [kg]	Mass for MIRA TIR [kg]
Beams/Frame	30	12	10
Honeycomb panels	35	13	12
Cleats	5	2	2
Brackets	10	4	3
Fasteners	20	8	7
Total structure	100	39	34

It is estimated that the thickness of the honeycomb panels used for the sides is 2 cm and the thickness of the honeycomb panels used for the shelves is estimated to be 3 cm.

19.8. Mechanisms

The satellites have many deployable structures, therefore a deployment sequence is developed to ensure that the satellites can safely transform from the launch mode, which has the most optimal packaging, to the fully operational mode. Firstly, solar panels are unfolded and then side solar panels is rotated 90 degrees. Secondly, the baffle is unfolded using a scissor mechanism. Thirdly, the primary mirrors are unfolded and struts with the secondary mirror are extended. Visual representation of the above-mentioned steps are shown in Figure 19.4.

Solar panels are unfolded using 2 torsion springs, 2 dampers and a thermal knife that cuts a Kevlar cable. Rotation of solar panels by 90 degrees using passive mechanisms will need to be further investigated. Otherwise electric motors will be used. The baffle consists of a scissor frame structure that is covered in thin foil. It deploys both radially and axially using a stepper motor. The telescope is deployed using foldable booms. The prototype for the deployable baffle is in the stage of development. The reaction wheels and magnetorquers are covered in detail in Chapter 15.

To deploy all the deployables, some power would be needed for a short amount of time. Once solar panels are passively unfolded it could start generating power and then all the other deployables can be unfolded. It

[f] https://www.apco-technologies.eu/apco-content/uploads/2018/04/Catalogue-PdV-LR.pdf [cited 29 June 2020]

is assumed that there is enough power for deployment of all deployables as they deploy in sequence and no power will be needed for the operation of the telescope, thermal control and ADCS during the stage of phase of deployment. Once satellites are in operational mode, no power should be supplied to the mechanisms except for the reaction wheels and magnetorquers.

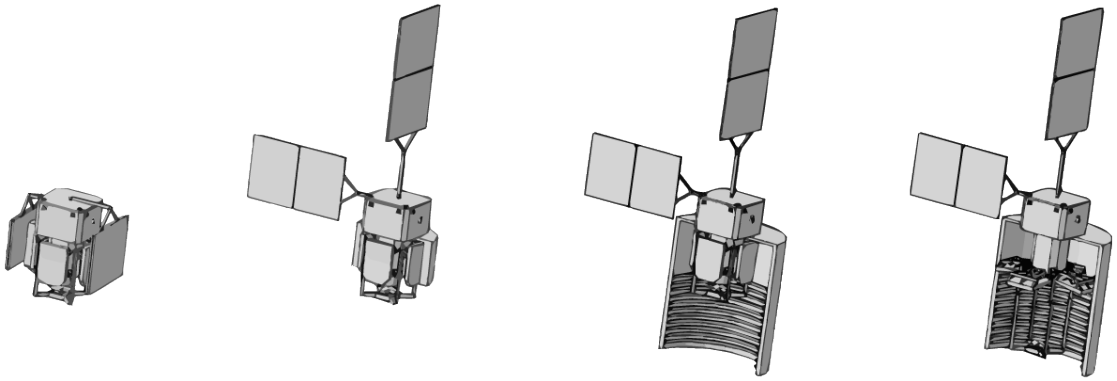

Figure 19.4: Deployment sequence from left to right: fully folded mode → solar panels deployed → baffle deploys → mirrors are unfolded

19.9. Verification and validation

In this chapter no extensive calculations, no coding and no special software was used. For all of the calculations excel was used. It is verified that the equations from Section 19.4 are entered correctly in excel by performing calculations by hand. For an input of $D = 4m$ and $a = 1.2m$, the values of the radius of the launcher attachment cylinder obtained by hand calculation and by using excel are approximately 0.708 m and 0.708 m respectively. For the same input the values of the number of satellites in one level obtained by hand calculations and by using excel are 4.47 and 4.47, respectively.

The method used for the mass estimation is verified by checking that the average payload percentage of total mass for similar satellites is in the same range as payload percentage of total mass for of MIRA MS and MIRA TIR satellites. The average payload percentage of the total mass for similar satellites is 30 % and payload percentage of total mass for of MIRA MS and MIRA TIR are 24 % and 36 % respectively.

Validation of the structures mass estimation is done by comparing the obtained values with the structure mass from some mission. The Supplemental Communications System (SCS) satellite is used as a reference. Structures and mechanisms mass of the SCS satellite is 55 kg and its total mass is 200 kg [17]. The structures and mechanisms mass of the MIRA MS satellite and MIRA TIR satellite is 55 kg and 48 kg respectively and their total mass is 235 kg and 203 kg respectively. It could be seen that the structures and mechanisms mass of the MIRA MS satellite and MIRA TIR satellite are relatively close to structures and mechanisms mass of the SCS satellite.

19.10. Sustainability analysis

By using a single launcher attachment structure, no space debris is generated during deployment of the satellites from the launcher. The frame structure provides enough space and simplicity during assembly allowing to reduce time for assembly. The satellite bus has a non-reflective coating on its exterior, therefore, the satellite bus should not contribute to light pollution. However, contribution of the baffle to light pollution will need to be further investigated.

To reduce risks, a simple separation from the launcher technique is used. Simple, passive and flight-proven mechanisms for deployment of solar panels are used. Protection of the satellites from radiation and small debris is performed by exterior panels.

19.11. Mass budget

The mass division of the MIRA TIR and MIRA MS satellites by subsystem is shown in Table 19.4. The budget is divided in three parts: *Common*, for the values that are the same for both platforms, *TIR sat*, for values specific to the TIR satellites, and *MS sat*, for values specific to the MS satellites. The contingencies displayed depend on the maturity of the design. Thermal control and structures show higher contingencies are their methods include more estimations and assumptions. The total dry mass does not include the propellant mass, but it is

included in the total wet mass. The different values are built in the same way as explained in Subsection 17.4.1.

The total values show that the actual value is below the target value in total and for each component, hence the mass budget is closed. Additionally, through the mass budget it becomes clear that the TIR satellites are lighter than the MS satellites, due to the difference in payload and structures mass. However, the propellant mass is higher for the TIR satellites as it is a smaller spacecraft and so requires more propellant to counteract drag. The active thermal control mass is zero for the MS satellite, because active control is not necessary.

Table 19.4: Mass budget (values in [kg])

		Actual value	**Target value**	**Contingency [-]**	**Current value**	**Specification value**
			Common			
ADCS	Actuators	4.73	15.00	0.15	5.43	17.25
	Sensors	2.71	15.00	0.15	3.12	17.25
C&DH	Storage Device	0.001	14.00	0.20	0.00	16.80
	OnBoard Computer	0.10	4.00	0.20	0.12	4.80
COMMS	Transceiver	0.22	16.00	0.10	0.24	17.60
	Patch antenna's	0.5	4.00	0.10	0.50	4.40
PROP	Tank	1.80	5.00	0.05	1.89	5.25
	Thrusters	3.00	5.00	0.05	3.15	5.25
	Lines, valves, fittings	2.50	6.00	0.05	2.63	6.30
	Power processing unit	4.00	5.00	0.05	4.20	5.25
	Digital control unit	0.83	1.00	0.05	0.88	1.05
GNC	Signal reciever	5.00	5.00	0.15	5.75	5.75
POWR	Solar array	15.76	40.00	0.15	18.12	46.00
	Batteries	2.55	5.00	0.15	2.94	5.75
	Power control unit	3.57	15.00	0.15	4.10	17.25
			TIR sat			
PAY	DDST TIR	60.52	64.00	0.10	66.57	70.40
PROP	Propellant	30.21	45.00	0.10	33.23	49.50
STRC + MECH		48.00	60.00	0.25	60.00	75.00
THRM	Passive	3.10	10.00	0.25	3.87	12.50
	Active	0.83	5.00	0.20	1.00	6.00
Total (dry mass)		**173.45**	**284.00**		**195.79**	**327.35**
Total (wet mass)		**203.66**	**329.00**		**229.02**	**376.85**
			MS sat			
PAY	DDST MS	81.76	95.00	0.10	89.94	104.50
PROP	Propellant	34.90	45.00	0.10	38.39	49.50
STRC+MECH		55.00	60.00	0.25	68.75	75.00
THRM	Passive	0.10	10.00	0.25	0.00	0.00
	Active	2.71	5.00	0.20	3.26	6.00
Total (dry mass)		**200.57**	**315.00**		**230.16**	**361.45**
Total (wet mass)		**235.47**	**360.00**		**268.55**	**410.95**

20

Configuration, Layout and Integration

After all the subsystems have been sized, the satellite as a whole can be configured. Integration is a key part of the design process, as all subsystems have to work together coherently for the spacecraft to meet its performance requirements. This chapter is split up into two parts. First, the layout (external) of the satellite is discussed. Afterwards, the configuration (internal) of the spacecraft bus is elaborated upon. Finally, a Manufacturing, Assembly and Integration (MAI) plan will be provided.

20.1. Series Production

Due to the number of satellites being quite large, it is important to take into account the extent to which series production can influence the cost of manufacturing and integration costs. When comparing the TIR and MS satellites, it can be noted that most of the subsystems show only small differences between the two. For example, the propellant needed for the MS satellite is only slightly larger than the propellant needed for the TIR satellite. Hence, instead of manufacturing different components, it has been decided to also use the subsystems, developed for the MS satellite, for the TIR satellite. This means that mainly the solar arrays and the propellant tank will be slightly overdesigned for the TIR satellite's needs. However, series production can now be taken advantage of for all of the satellites, which is a huge advantage in terms of cost. Furthermore, this complies with the initial user requirement that all of the satellites will use the same bus platform. Note, however, that for the MS satellite, no active cooling is required. The cryocooler can therefore simply be omitted for the MS satellite, without hindering the production chain.

20.2. Layout

In order to visualise and assess the layout, a complete custom CATIA model was constructed. The spacecraft layout in both stowed and deployed configuration can be seen in Figure 20.1. Before the satellite could be modelled as a whole, first the deployable space telescope had to be constructed. The model for the telescope was based on the official design as shown in the master thesis by Krikken [11]. This design however uses foldable booms, which are modeled in the official CAD model as rigid booms, which do not allow any articulation in the CATIA software. The model constructed for this DSE uses a scissor mechanism which is based on the folding principles as the official model but does allow articulation, shown in Figure 20.1 (a).

The centerpiece of the satellite is the deployable space telescope, which is always nadir pointing. In the thesis by Dolkens [9], it is given that the back part of the telescope is fully dedicated to the instrument box. This means that all subsystems have to be fitted into a separate bus. In order to protect the telescope from stray light, a deployable baffle is used. The actual design of the baffle is still in a early stage as it is actively being worked on by master students from the TU Delft, which have been consulted on multiple occasions throughout the construction of the model. As such, the design for this structure is kept at a high level. The baffle currently being designed is based on pantographic scissor mechanisms which stretch the MLI sheets making up the baffle walls. Due to little information on how it will look, the baffle is modelled as a cylinder with a flat cap on one side. This baffle will be attached onto the end of the instrument box and deployed both in longitudinal and radial direction to ultimately encase the whole telescope until just beyond the secondary mirror. The maximum achievable longitudinal and radial deployment ratios are 3 and 2 respectively. For both the stowed and deployed configuration, the diameter of the baffle is dictated by the mirrors while the height is dictated by the secondary mirror in its stowed or deployed state.

As described in Chapter 17, the solar arrays are to be in two different planes. One of the arrays will extend from the side of the bus while the other extends vertically from the top of the bus. As the baffle forms a large area extending downwards, the larger solar array was placed on top of the spacecraft such that the aerodynamic moments produced counter each other. The second solar array was placed in the direction of flight, such that the aerodynamic moment generated is as small as possible. In stowed configuration, the design was optimised to keep the volume of the satellite as small as possible such that more satellites could fit within the launcher. As such, the solar arrays were designed to fold down along the stowed baffle. The thruster is placed

opposite to the direction of flight such that continuous thrusting is allowed without needing to adjust the attitude of the spacecraft. Due to no direct nadir viewing area on the spacecraft bus, the phased array antenna was strategically placed on the secondary mirror support structure. Finally, all of the star trackers and sun sensors are in different planes, as required. A complete, detailed technical drawing with dimensions for both the MS and TIR satellites in stowed and deployed configuration can be seen in Figure 20.4. Note that the mirror elements in the baffle are not shown here as then the internal dimensions wouldn't be readable anymore.

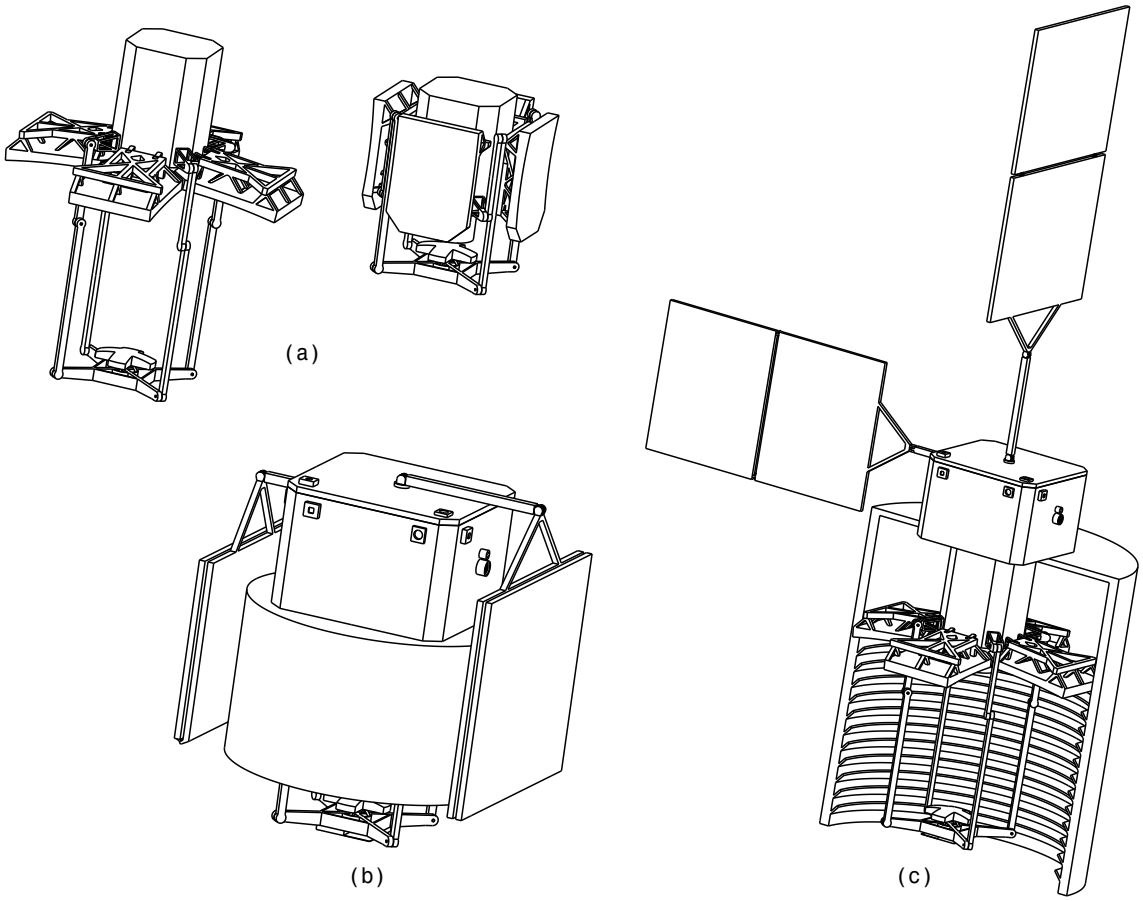

Figure 20.1: Layout of the Mira satellites. (a) Model of the deployable space telescope. (b) The stowed satellite layout. (c) The deployed satellite layout. The baffle is sectioned to show the deployed telescope.

20.3. Configuration

With the layout fixed, the internal configuration can be considered. For simplicity, the footprint of the bus is kept symmetric. The height is dominated by the magnetorquers while the width is kept such that the major components can be attached to the baseplate with additional clearances reserved for potential shelving and insulation.

A number of main considerations for the subsystems have been taken into account when putting together the configuration.

- The magnetorquers, gyroscopes and reaction wheels shall be placed in perpendicular planes.
- The propellant tank and the batteries shall be spaced as far apart as possible.
- The propellant tank shall be placed as close as possible to the wall on which the thruster is mounted.
- The compressor of the cryocooler shall be placed such that the cold tip can reach down into the instrument box to cool the TIR sensor.

The second constraint is due to the fact that the propellant tank will have to be cooled, while the batteries are the main source of internal heat generation. Given these constraints, the resulting spacecraft bus configuration with all the subsystems can be seen in Figure 20.2 and Figure 20.1 . It can be seen that the bus still contains some empty space which cannot be significantly reduced. Therefore, it is assumed that any fittings, valves, wiring, support structures and other small components can easily fit within the designed spacecraft bus. Furthermore, any shelving or insulation can be fitted, if necessary. thanks to the clearance provided between components.

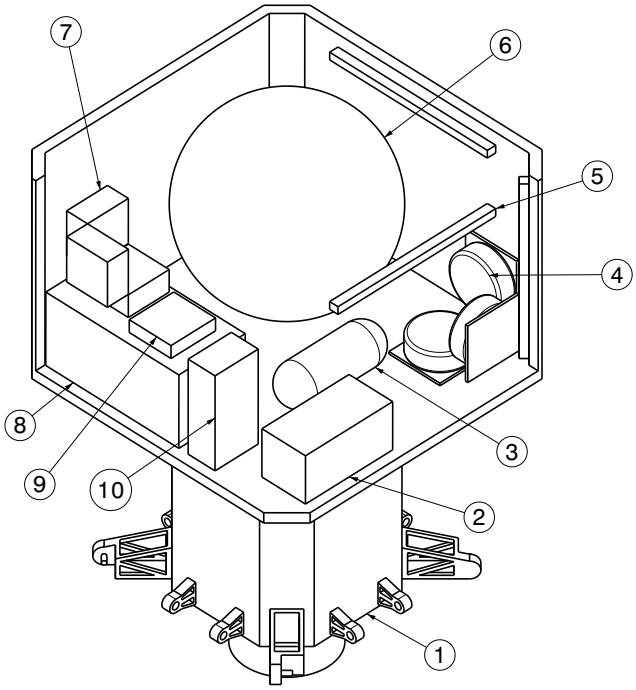

Figure 20.2: Isometric view of the bus configuration

Table 20.1: Bus components

Number	Component
1	Instrument box
2	Batteries
3	Cryocooler compressor
4	Reaction wheels
5	Magnetorquers
6	Propellant tank
7	Gyroscopes
8	PCDU
9	Data handling unit
10	Communications unit

20.4. Manufacturing, Assembly and Integration (MAI) Plan

The MAI plan is shown in Figure 20.3. It shows the flow from manufacturing to assembly and to integration. The manufacturing part is split in two: off-the-shelf and custom. The former denotes the components that are not mission specific and can be bought off the shelf. Custom components need to be manufactured for this mission specifically. The manufacturing or collection of these components happens in parallel. In assembly, most components come together to form the spacecraft bus, which is the same for both MS and TIR satellites. In integration the bus is combined with the specific payload as well as with the software, power connections and thermal insulation.

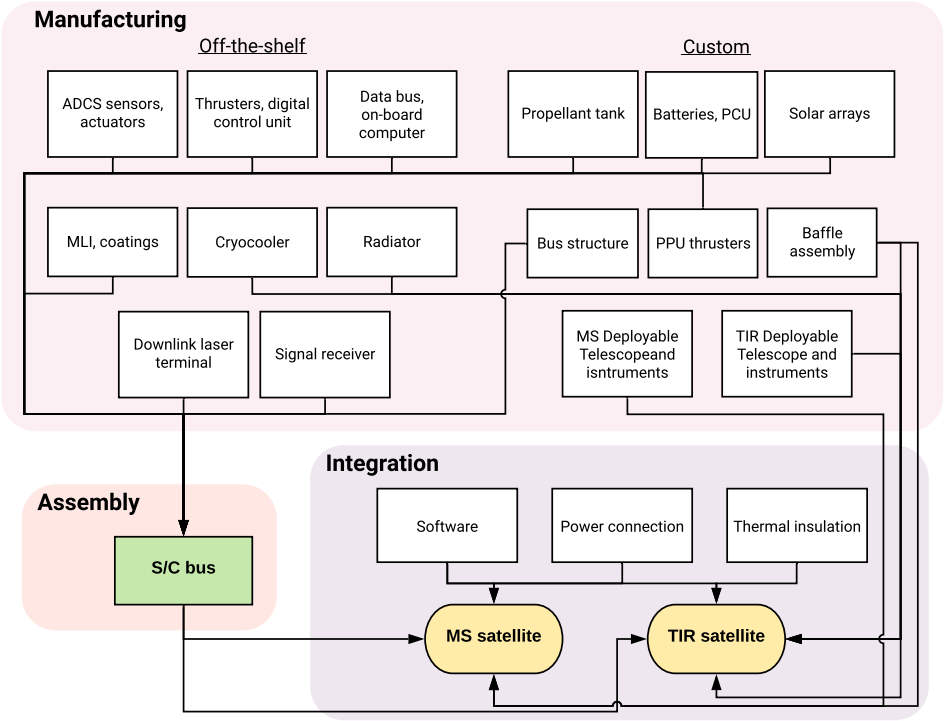

Figure 20.3: MAI plan

Components

1. Solar panel
2. Spacecraft bus
3. Deployable baffle
4. Delft Deployable Space Telescope
5. Phased array antenna
6. Thruster assembly
7. Louvres
8. Star tracker
9. Sun sensor

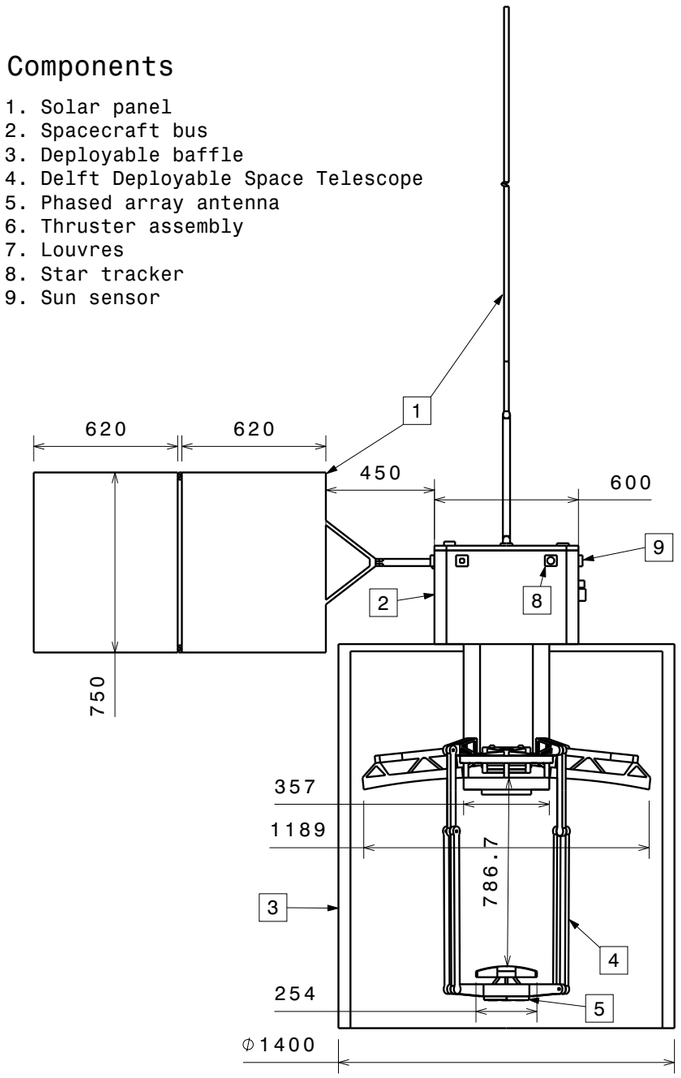

Front view - MS (Deployed)

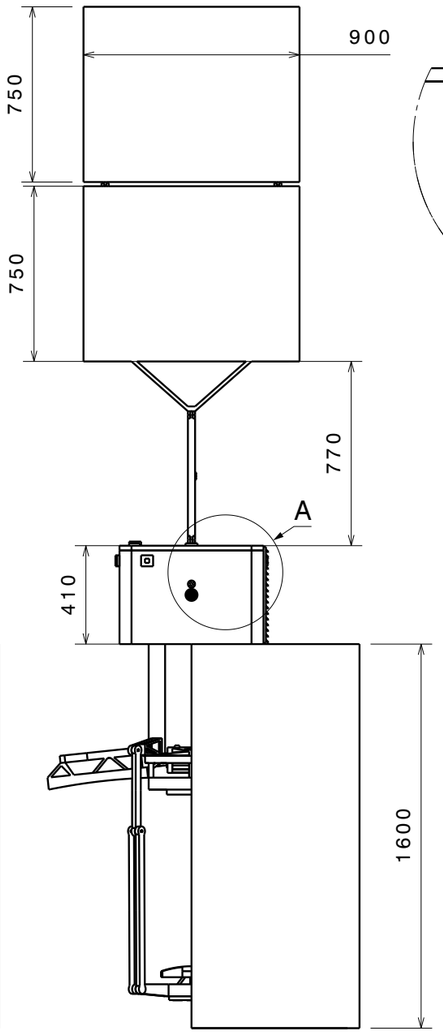

Right view - MS (Deployed)

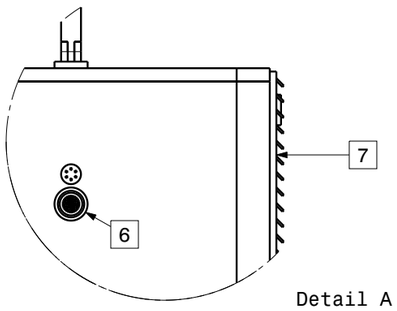

Detail A

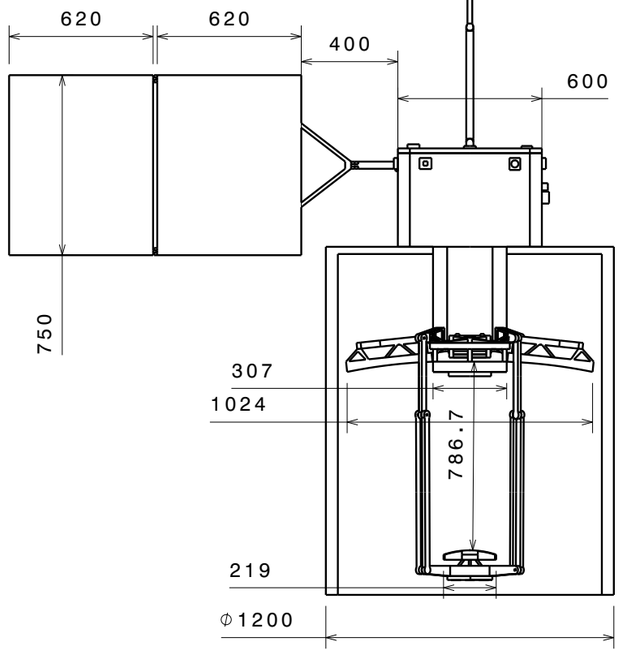

Front view - TIR (Deployed_

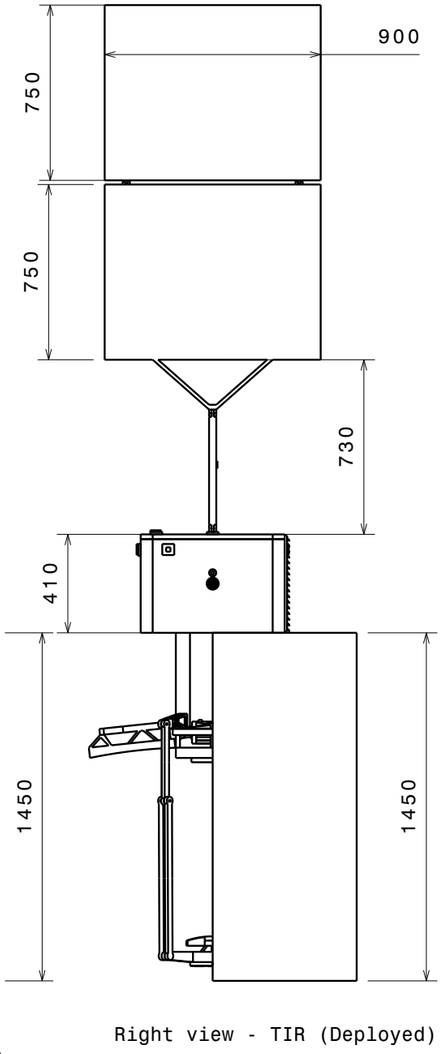

Right view - TIR (Deployed)

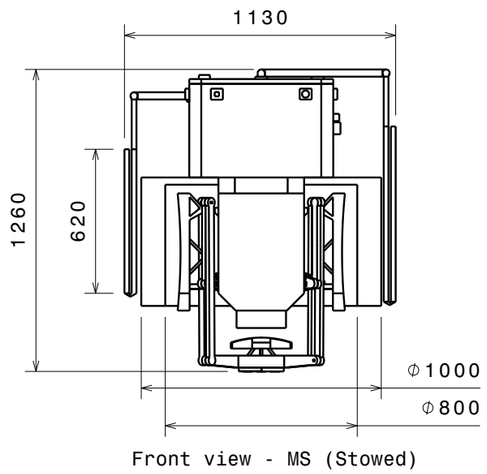

Front view - MS (Stowed)

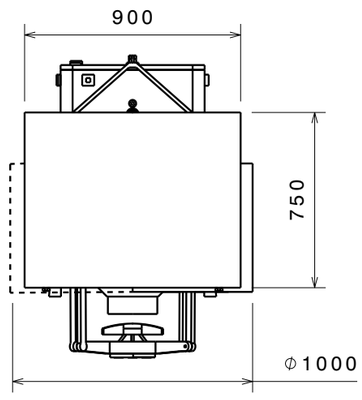

Right view - MS (Stowed)

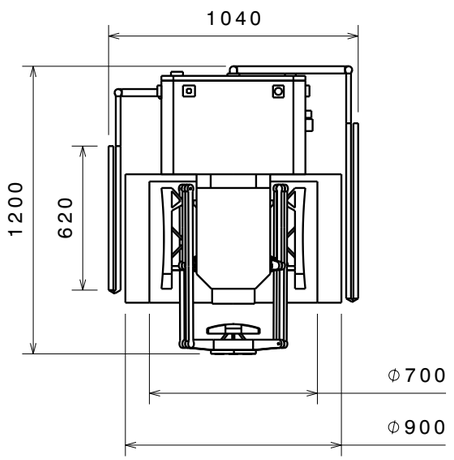

Front view - TIR (Stowed)

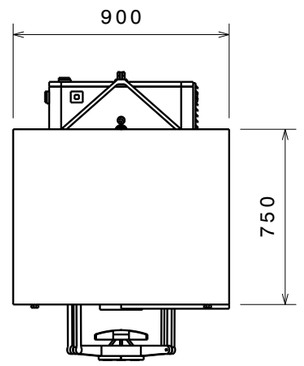

Right view - TIR (Stowed)

All dimensions in mm

Figure 20.4: Technical drawing of both the TIR and the MS MS and the TIR satellites. Note that the baffle is sectioned to show the telescope inside.

21 Final System Overview

This chapter presents the cost analysis for the whole system. Moreover, the system integration verification and validation is shown. Finally, the block diagrams illustrating the interaction of the subsystems are displayed.

21.1. Cost analysis

This section presents the cost requirements in Subsection 21.1.1, which are then fulfilled with the cost breakdown structure and cost budgets. The current cost budgets for the satellites and total constellation costs are presented in Subsection 21.1.2. Then, the CBS presents costs for activities post-DSE in Subsection 21.1.3.

21.1.1. Requirements

Table 21.1 shows the cost requirements for the design, their origin and whether or not they have been meet. Most of the requirements flow from the budget, or were derived from the customer. From the table it is clear that all requirements have been met and will be explained with help of the CBS or the cost budget.

Table 21.1: Cost requirements

ID	Requirement	Origin	
MIRA-USR-COST-1	The initial investment for an in-orbit qualification (demonstrating all aspects of the full spacecraft bus and including launch cost) shall be less than 200 M€.	PGB	✓
MIRA-USR-COST-2	The total investment cost shall be a maximum of 2000 M€ for the operation of the entire system (including ground segment and launch cost).	PGB	✓
MIRA-USR-COST-3	The operational cost shall be less than 100 M€ per year, including replenishment of dysfunctional and retired satellites (satellite plus launch cost).	PGB	✓
MIRA-SYS-MS-COST-1	The total cost of each multispectral satellite shall be a maximum of 12.5 M€ (FY2020).	MIRA-USR-COST-2 divided by # satellites	✓
MIRA-SYS-TIR-COST-1	The total cost of each thermal infrared satellite shall be a maximum of 12.5 M€ (FY2020).	MIRA-USR-COST-2 divided by # satellites	✓
MIRA-PAY-COST-1	The payload total cost for the MS satellite shall be 5 M€.	Target value in cost budget	✓
MIRA-PAY-COST-2	The payload total cost for the TIR satellite shall be 5 M€.	Target value in cost budget	✓
MIRA-PROP-COST-1	The total cost of the PROP and GNC subsystems shall be 0.5 M€ for the MS satellite.	Target value in cost budget	✓
MIRA-PROP-COST-2	The total cost of the PROP and GNC subsystems shall be 0.5 M€ for the TIR satellite.	Target value in cost budget	✓
MIRA-ADCS-COST-1	The total cost for the ADCS subsystem shall be 0.5 M€ (common for both platforms).	Target value in cost budget	✓
MIRA-C&DH-COST-1	The total cost for the C&DH subsystem shall be 1.5 M€ (common for both platforms).	Target value in cost budget	✓
MIRA-COMMS-COST-1	The total cost for the communication subsystem shall be 1.5 M€.	Target value in cost budget	✓

Table 21.1: continued from previous page

ID	Requirement	Origin	
MIRA-POWR-COST-1	The total cost for the power subsystem shall be 2 M€ (common for both platforms).	Target value in cost budget	✓
MIRA-THRM-COST-1	The total cost for the thermal subsystem shall be 0.5 M€ (common for both platforms).	Target value in cost budget	✓
MIRA-STRC-COST-1	The total cost for the structures subsystem of the TIR satellite shall be 1.5 M€.	Target value in cost budget	✓
MIRA-STRC-COST-2	The total cost for the structures subsystem of the MS satellite shall be 1.5 M€.	Target value in cost budget	✓

21.1.2. Cost budget

This section presents the cost budget for the average total and recurring cost, as well as the development costs. The launch and platform/step costs per step are also given.

The return-on investment is the relation between the number of products sold times their value and the total cost. However, as the aim of this program is to be a complete governmental program, most probably a cooperation between EU states the ROI is by definition zero.

As explained in Section 22.4 the constellation will be built up in steps. Step 0 accounts for the prototypes and in-orbit qualification. It is assumed that the prototypes will be tested on Earth and will take up 50% of the development costs as only the critical subsystems need to be present. Additionally, the production costs of the prototypes are assumed to be 50% of the average recurring costs presented in Table 21.2 as the prototypes can have some simplified subsystems. The remaining 50% of the development costs will be accounted for the in-orbit qualification costs. To complete Step 0 one MS satellite and one TIR satellite will be put in orbit with the Vega launcher. The total cost of the prototypes will be 122.25 M€ and the total cost for the in-orbit qualification will be 180.48 M€, where the launch will cost 32.56 M€. The individual step costs can be seen in Figure 21.1b.

Series production will be used to produce the units, so a learning curve is applied to each subsystem recurring cost. The units will follow the required satellites for the build-up steps, so Step 1 will have 13 MS units followed by 26 TIR units, Step 2 will have 26 MS units followed by 52 TIR units and so on. The in-orbit qualification satellites already count as the first unit. Equation 21.1 and 21.2 are used to introduce the learning potential [74]. The learning rate for the propulsion subsystem can be estimated by assuming 50% hand assembly and 50% machining[a], while for the other subsystems they were found in Fox et al. [74]. Based on the given development and total expected costs for the payload by the designers of the DDST, the recurring costs were derived.

Table 21.2: Spacecraft development and recurring costs (values in M€)

	S/C development (NR)		**Avg S/C recurring (R)**	
	MS	*TIR*	*MS*	*TIR*
ADCS	1.62	6.48	0.042	0.034
STRC	1.26	1.08	0.066	0.028
THRM	1.31	5.23	0.011	0.009
POWR	1.35	5.39	0.031	0.030
COMMS	1.06	4.23	0.038	0.033
C&DH	1.14	4.58	0.007	0.006
PROP	2.69	2.26	0.024	0.021
DDST	50-150	50-150	2.163	2.266
Total	**60.34-160.34**	**79.25-179.25**	**2.382**	**2.426**

[a] http://www.csgnetwork.com/learncurvecalc.html [Accessed June 16 2020]

$$C(N) = T_1 N^b \quad (21.1) \qquad b = \frac{\ln(slope)}{\ln(2)} \quad (21.2)$$

T_1 represents the recurring cost of the first unit. The first unit recurring and non-recurring costs are based on altered estimations [17, 75]. The estimations are altered in accordance with current Starlink costs. The assumed cost of 1 M€ for Starlink is only 0.067 of the value that Wertz et al. [17] gives so the cost estimations were corrected with this factor. The learning rate is represented by b in Equation 21.2. Table 21.2 shows the values for the non-recurring/development and the average recurring costs. Moreover, even if some components are said to be COTS in Section 20.4 their development costs are still included to ensure a valid comparison with Starlink which is entirely custom made. It is advised to perform a trade-off with regards to COTS and custom costs in future design phases.

The launch costs for the different build-up steps are shown in Table 21.3. The different use of launchers depends on the number of satellites that need to be launched.

Table 21.3: Launch costs for each buil-up step (values in M€)

	Launchers	**Launch costs**
In-orbit qualification	Vega	32.56
Step 1	1 Atlas V	96.8
Step 2	1 Atlas V	96.8
Step 3	2 Atlas V	193.6
Step 4	4 Falcon 9	176
Step 5	4 Atlas V / 4 Falcon 9	563.2
Step 6	4 Atlas V / 4 Falcon 9	563.2
Step 7	24 Falcon 9	1056
Step 8	48 Falcon 9	2112

Table 21.4 shows the average spacecraft total costs, which include the recurring costs and the development per satellite. The average platform costs per step are shown in Figure 21.1a. This value is merely to show the relation as the development costs are fully included in Step 0. The launch per constellation cost is found by adding steps 1-6. The in-orbit qualification cost includes its own launch costs. The maintenance costs includes the redundant satellites as well as the replacement ones including launch costs. The values shown for the everything row include the total costs from steps 0-6. The contingency for the payload cost is high due to several uncertain estimations. The contingencies and different values are built the same way as in Subsection 17.4.1.

Table 21.4: Cost budget (values in M€)

	Actual value	**Target value**	**Contingency [-]**	**Current value**	**Specification value**
Everything	3877.46	3600.00	0.10	4265.21	4000.00
Launch per constellation	1689.60	300.00	0.10	1858.56	330.00
In-orbit qualification	180.48	180.00	0.10	198.53	200.00
Maintenance cost	217.04	300.00	0.10	238.74	330.00
Average spacecraft total cost (NR + R)					
MS satellite					
ADCS	0.045	0.05	0.20	0.05	0.06
STRC	0.069	0.15	0.20	0.08	0.18
THRM	0.014	0.05	0.20	0.01	0.06
POWR	0.034	0.20	0.20	0.04	0.24
COMMS	0.040	0.15	0.20	0.05	0.18

Table 21.4: continued from previous page

	Actual value	Target value	Contingency [-]	Current value	Specification value
C&DH	0.009	0.15	0.20	0.01	0.18
PROP	0.030	0.05	0.20	0.03	0.06
PAY	2.376	2.50	0.50	3.24	3.75
BUS	**0.242**	**0.80**		**0.26**	**0.96**
Total MS sat	**2.618**	**3.30**		**3.51**	**4.71**
		TIR satellite			
ADCS	0.037	0.05	0.20	0.04	0.06
STRC	0.029	0.15	0.20	0.03	0.18
THRM	0.011	0.05	0.20	0.01	0.06
POWR	0.033	0.20	0.20	0.04	0.24
COMMS	0.035	0.15	0.20	0.04	0.18
C&DH	0.008	0.15	0.20	0.01	0.18
PROP	0.022	0.05	0.20	0.02	0.06
PAY	2.320	2.50	0.50	3.40	3.75
Bus	**0.175**	**0.80**		**0.17**	**0.90**
Total TIR sat	**2.495**	**3.30**		**3.59**	**4.71**

From Table 21.4 the costs are within the budget and the bus costs is compared to Starlink costs. The main cost contributor is payload and the values are still uncertain due to the novelty of the design, the values are actually expected to be lower. The high launch costs are due to the baffle that increases the volume of the spacecraft leading to a higher number of launches. The high constellation cost is due to the total number of spacecraft.

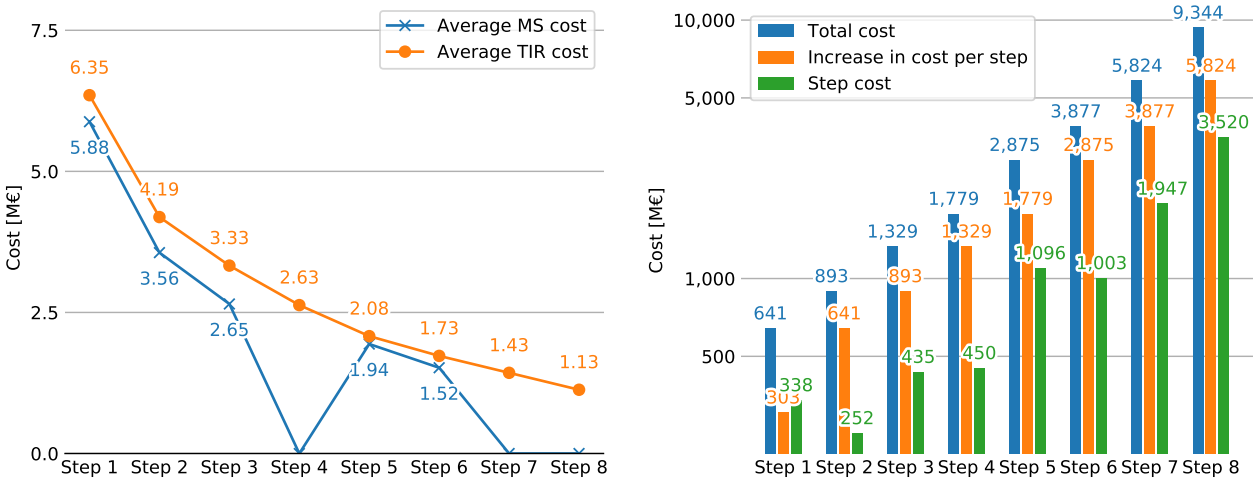

(a) Cost of platform

(b) Step and total costs

Figure 21.1: Cost relation per step

Figure 21.1a shows the average MS and TIR costs per step[b]. It can be clearly seen that the average costs decrease at each step due to series production. The curve shows an asymptotic behaviour as after a certain unit the minimum production cost is reached. The reason the MS cost is zero for step 4, 7 and 8 is because

[b] https://www.nextbigfuture.com/2019/12/spacex-starlink-satellites-cost-well-below-500000-each-and-falcon-9-launches-less-than-30-million.html[Accessed June 26 2020]

no additional MS satellites are added to the constellation. It is also noticeable that the MS satellite costs on average less than the TIR satellite.

Figure 21.1b shows the individual step costs, the total cost and the increase from one step to the next. The total cost of a step shows its individual cost plus all the step costs before that, so the value of 9344 M€ for Step 8 includes all the satellites and launch costs, the development costs and the prototypes. The vertical axis is a logarithmic scale and the increase in cost per step is the difference between the current total cost and the individual step cost.

21.1.3. Cost Breakdown Structure

The cost breakdown structure shown in Figure 21.2 is divided in 2 parts, one related to the initial investment costs and the other to the additional costs per satellite. It is an AND-tree that flows from the project life cycle and the total displayed on the top blocks is the sum of the bottom blocks. The duration of activities shown are explained in Chapter 23. The costs related to development are explained in Subsection 21.1.2, while the other values are obtained from various sources.

The cost estimates for project management and systems engineering relate to the sensor cost. The development and production costs are estimated with Equation 21.3 where values the mass for the sensor are estimated to be 1% of the payload mass [8].

$$C_{sensor} = 1.163 \cdot 0.01 m_{pay}^{0.328} P_{pay}^{0.537} DR_{pay}^{0.92} \tag{21.3}$$

The sensor mass, power and data rate are taken as a combination of the values for the MS and the TIR satellite: m_{pay} = 1.42 kg, P_{pay} = 10 W, DR_{pay} = 20,317.9 kB/s.

Moreover, Wertz et al. [17] presents a cost estimation for the software development, which is dependent on the source lines of code (SLOC). Following the example provided a total of 40545 SLOC is considered as necessary for a flight software. This source also gives an estimate to the cost of the headquarters building based on the typical size in m^2.

Equation 21.4 is used to estimate the costs of integration, assembly and testing where the category of spacecraft between 100-1000 kg is chosen in Brumbaugh [76].

$$C_{AIT} = 141.16 L_{design}^{0.302} m_{bus,dry}^{0.475} \tag{21.4}$$

Where the design life L_{design} is 7 years = 84 months, the $m_{bus,dry}$ = 155.12 kg. Additionally, this source is used to estimate the costs of manufacturing engineering, fabrication, ground station equipment and testing facilities.

The CBS shows values for the launch costs for the Falcon 9, listed in Section 14.4 and the propellant cost[c]. The flight and launch ground operation costs are found using Equation 21.6 and 21.5 respectively [77].

$$C_{GOC} = 8 M_0^{0.67} L^{-0.9} N_s^{0.7} \cdot 0.3 \cdot 0.5 \cdot 0.7 \cdot 1 \tag{21.5}$$

$$C_{FOC} = 20(\Sigma Q_N) L^{-0.65} \cdot 0.7 \cdot 1 \tag{21.6}$$

Where the launcher dry mass is M_0 = 27,900 kg, L is the launch rate of 12 launches per year for each generation start, the number of stages (N_s) for the Falcon 9 is 2 and the usual stage complexity factor Q_N is 0.3.

For costs related to research the facilities could not be estimated but it is assumed that research will be applied during 10 years with 10 employees [78]. Massey [79] gives values for infrastructure costs and maintenance, operations, communication and continuing engineering which was equally split into costs for maintenance, communication and continuing engineering. Finally, the values for insurance[d] and ground station procurement are given Section 16.7.

Note that the additional cost per spacecraft will vary along the mission in a non-linear way. The operational cost will increase but the 100th satellite is only expected to cost 10 times as much as the first one. The AIT cost will decrease with the introduction of the learning curve and so as the constellation is built-up the AIT cost per spacecraft will decrease.

[c] https://space.stackexchange.com/questions/32729/how-much-fuel-does-the-falcon-heavy-use-what-is-the-price-rp-1 [Accessed June 16 2020

[d] https://www.policyforum.net/tackling-stratospheric-costs-space-insurance/ [Accessed June 15 2020]

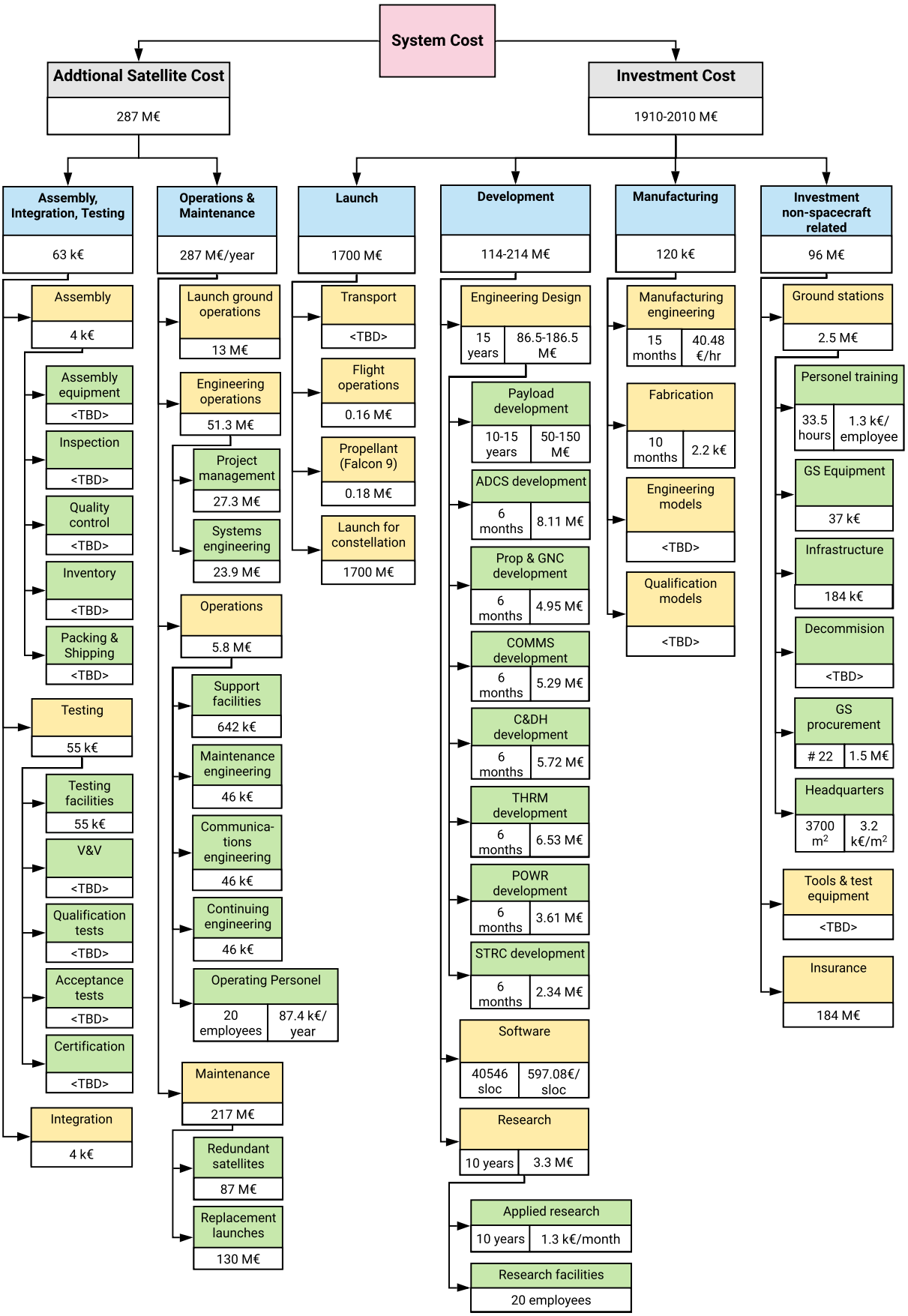

Figure 21.2: Cost breakdown structure for post-DSE activities

21.2. System integration verification and validation

Verification and validation of the whole system integration is important as it focuses on checking if the different subsystems design is combined correctly. The individual subsystems need parameter inputs from other subsystems and so when combining the design the model must be verified and validated on a system level. Figure 21.3 shows the structure that needs to be followed to verify and validate the whole system, starting with the customer needs.

After initial subsystem level unit tests, system level unit tests were conducted to verify that the parameters linking one subsystem and an other, were correctly interfaced. The different codes used for subsystem sizing were linked on a system level to observe the instantaneous changes induced. For example the electrical power system design requires several parameters from all the other subsystems; changing the power requirement for the thruster automatically changed the solar array size. By setting the frontal area to zero, the propellant mass decreases enormously, as well as the total momentum per orbit the reaction wheels need to counter. This verifies the fact that drag is limiting for both propulsion and ADCS design.

There are clear distinctions made between *definition-phase* requirements validation and *implementation-phase* system validation and verification. System robustness will be validated using techniques such as performance sensitivity analysis, system fault tree analysis, probabilistic risk analysis along with stress testing. Initial model validation is done to ensure simulations can be used safely to support requirements validation [80].

A Spacecraft Operational Simulator will be used to test all possible flight hardware and software against realistic mission conditions. The simulation will be modelled to the extent that to the flight control team, the telemetry generation is indistinguishable from the real spacecraft, as far as possible [81].

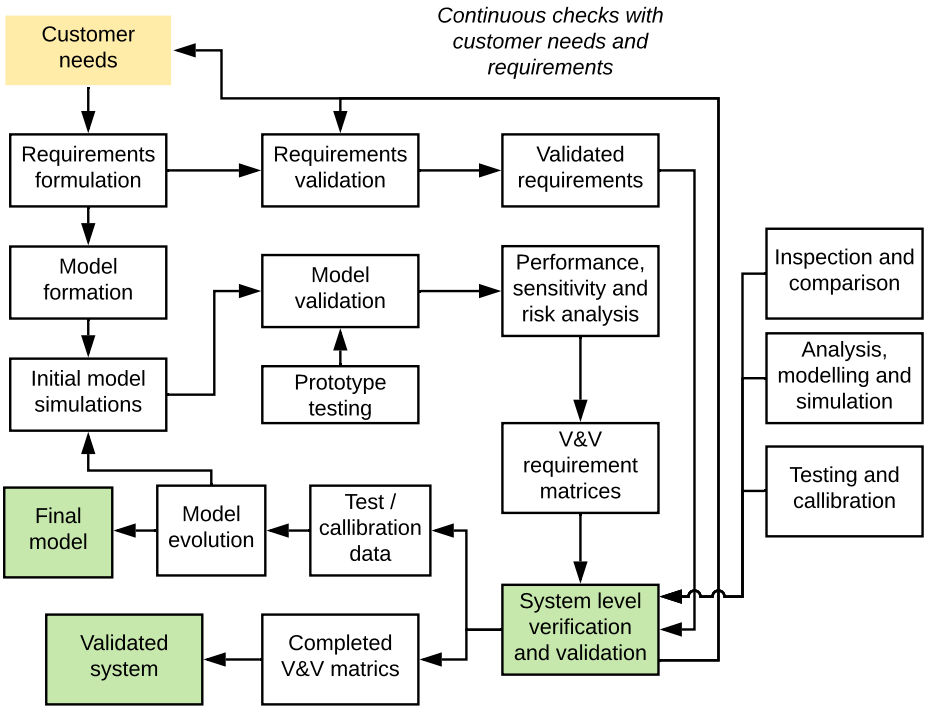

Figure 21.3: System integration verification and validation plan

21.3. Block diagrams

The hardware, data and electrical block diagram is shown in Figure 21.4. It shows power flow, command and data flow, along with the thermal control line for the payload. This thermal control line is highlighted in specific due to the importance with the mission and the spacecraft subsystem sizing parameters.

The software block diagram is shown in Figure 21.5 and highlights the command and data flow occurring in the spacecraft subsystem. The command and data centre are separated and pass on all messages through the central processing unit. The command centre provides instructions to all subsystem components and the data centre and collects all subsystem data parameters.

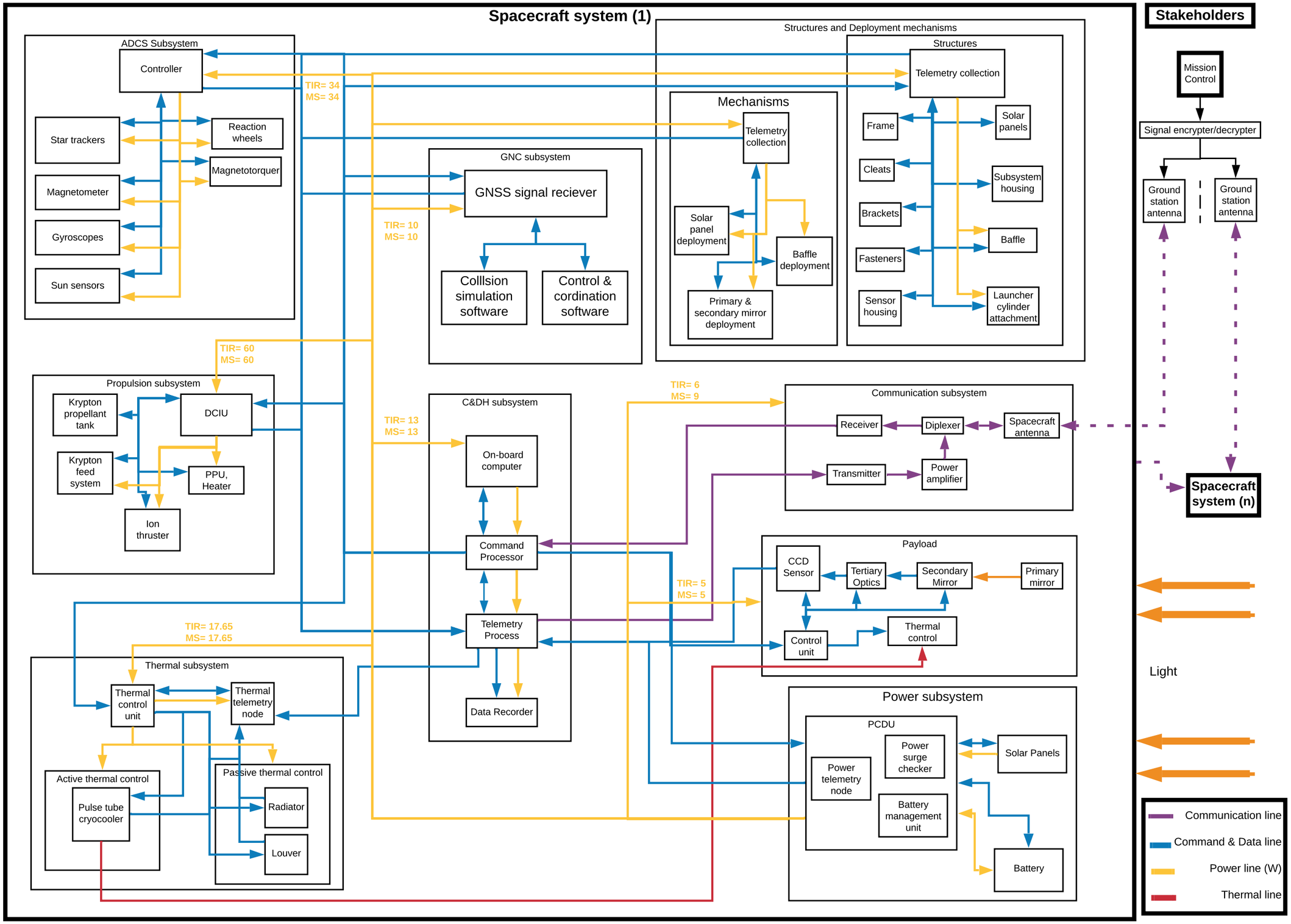

Figure 21.4: Hardware, data and electrical block diagram showing data and power flow throughout the system

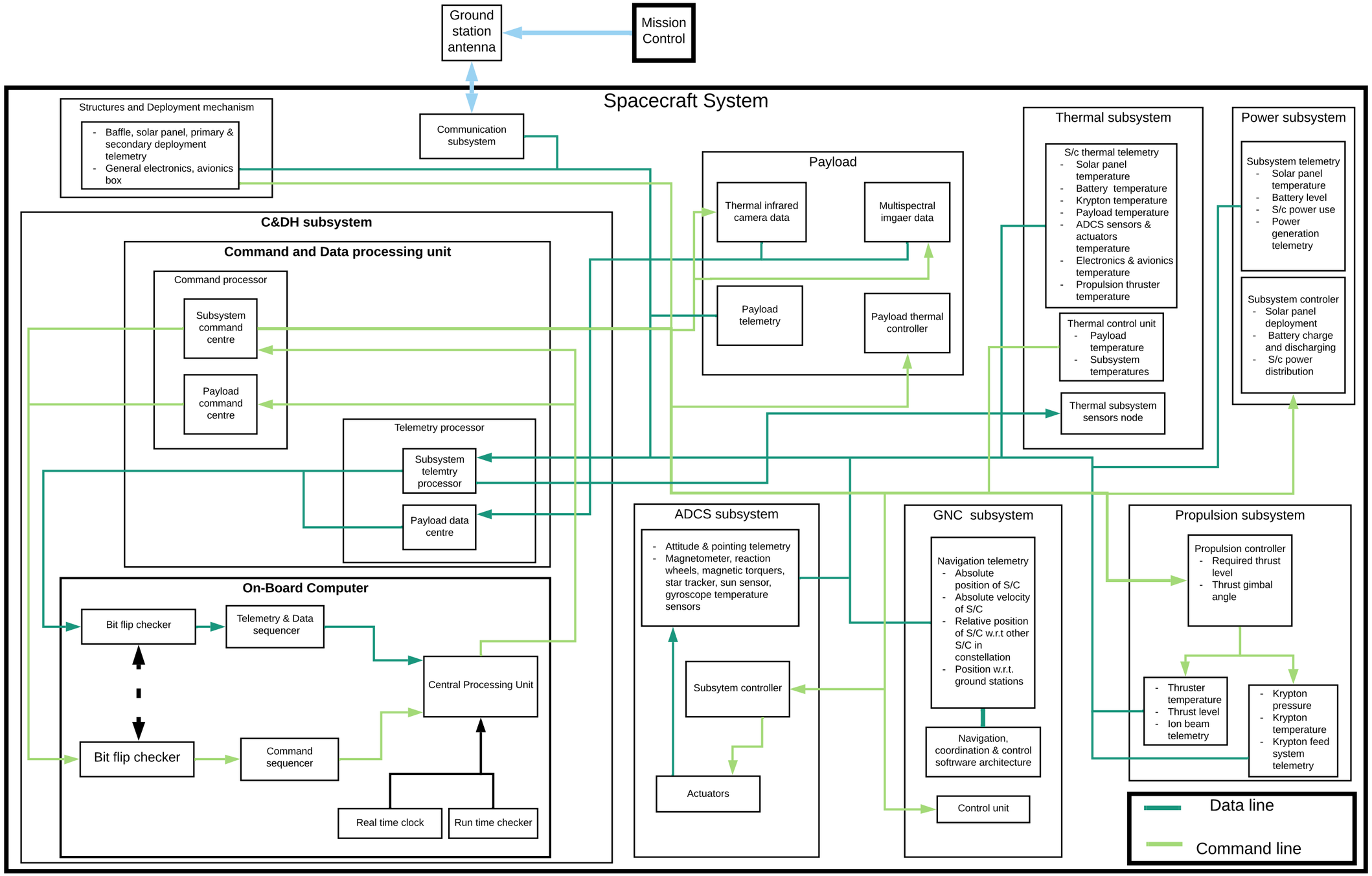

Figure 21.5: Software block diagram with command, telemetry and data flow throughout the system

22

Operations, Logistics and Scalability

In this chapter, the built-up of the constellation is described and shown in Section 22.2 with the different steps that will be taken. Furthermore, a launch schedule including dates is proposed. In Section 22.3, the logistics are shown and described. Finally, the relation between cost and temporal resolution is shown in Section 22.4.

22.1. Requirements on Operations, Logistics and Scalability

The requirements regarding operations, logistics and scalability and the compliance can be seen in Table 22.1.

Table 22.1: Operations, logistics and scalability requirements and compliance

ID	Origin	Link to analysis	
MIRA-USR-SR-5	Customer		✓
MIRA-SHED-PERF-1	BLR, MIRA-MIS-SHED-10.3	MIRA-USR-MIS-10	✓

22.2. Operations and Built-up of the Constellation

In accordance with MIRA-USR-SR-5, the constellation will be built-up in steps. The team identified 9 total steps which will be described below. But before the first step can be initiated, the satellites have to be manufactured and assembled. A prototype will be made of the TIR and MS satellite and thoroughly tested. Testing and transportation will be further addressed in the logistics. After that, adjustments and improvements will be made resulting in a final model for the TIR and MS satellite, which will be launched into space using a Vega launch vehicle for orbit qualification and further testing and monitoring for 6-12 months. They will be launched in an orbit with RAAN 0, this is Step 0. Since this is a dutch government space mission, operations will occur in the Netherlands, at the ESA ESTEC facility in Noordwijk.

After testing and ensuring everything works fine, the constellation can be built up. There are a total of 6 steps to be taken to end up at the reference design. During each step, it was tried to double the temporal resolution. This can be done for steps 2 and 3, and step 4 for only the TIR satellites, but not for step 5 and 6, due to the lay-out of the constellation, as can be seen in Figure 22.1. Here, the different colors represent the different steps taken in the launching sequence for step 1-6. The color, the RAAN of the orbits, temporal resolution of the TIR and MS satellites, the launch number and launch vehicle used for each step can be seen in Table 22.2. It can be noticed that there are two more steps added to Table 22.2, namely steps 7 and 8. These are extra options, which both double the temporal resolution of the TIR satellites, if that would be desired. This can be convenient during forest fires or wars for example.

Table 22.2: Built-up of the constellation

Step	Color	RAAN [°]	Temp. res. TIR [min]	Temp. res. MS [min]	Launch number	Launch vehicle
1	Red	0	720	720	1	Atlas V
2	Light green	90	360	360	2	Atlas V
3	Yellow	45 135	180	180	3-4	Atlas V
4	Purple	22.5 67.5 112.5 152.5	90	180	5-8	Falcon 9 FT

Table 22.2: continued from previous page

Step	Color	RAAN [°]		Temp. res. TIR [min]	Temp. res. MS [min]	Launch number	Launch vehicle
5	Light blue	7.5 52.5 97.5 142.5	30 75 120 165	60	120	9-16	Atlas V & Falcon 9 FT
6 (Ref. design)	Orange	15 60 105 150	37.5 82.5 127.5 172.5	30	60	17-24	Atlas V & Falcon 9 FT
7 (Extra)	-	3.75 18.75 ...	11.25 ... 176.25	15	60	25-48	Falcon 9 FT
8 (Extra)	-	1.875 9.375 ...	5.625 ... 178.125	7.5	60	49-96	Falcon 9 FT

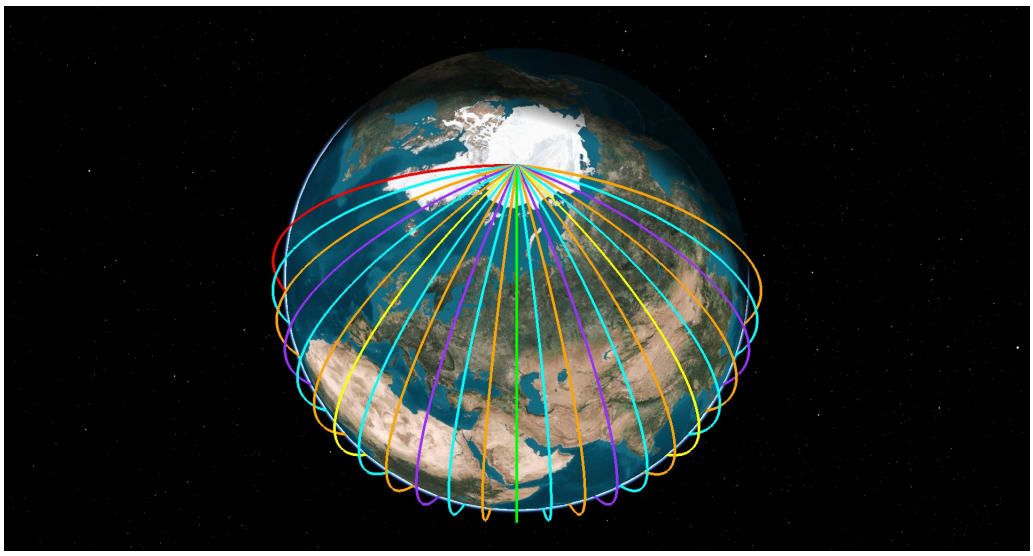

Figure 22.1: Top view of constellation showing the orbits to be filled during each step

22.2.1. Launch Schedule

Following the order of steps, a launch schedule is proposed in Figure 22.2. Step 0 is the launch of the final model, which will be used for final testing. This will be done half a year to a year prior to the scheduled first launch of the constellation. The colors in Figure 22.2 correspond to the same colored orbits shown in Figure 22.1. For each step, the satellites will be launched as fast as possible. There will be about a 3 day interval between each launch to ensure that each step can be finished quickly. Between the steps, periods of up to a month have been reserved. This was done, in case re-evaluation of the constellation or system is necessary or if more investments are required to proceed to the next phase. Note that this is a proposed schedule. If preferred, all launches could take place after one another, which means that the whole constellation would be up in space in around 70 days. This is up to the customer to decide. All satellites will be launched from the Vandenberg Air Force Base located in California in the USA.

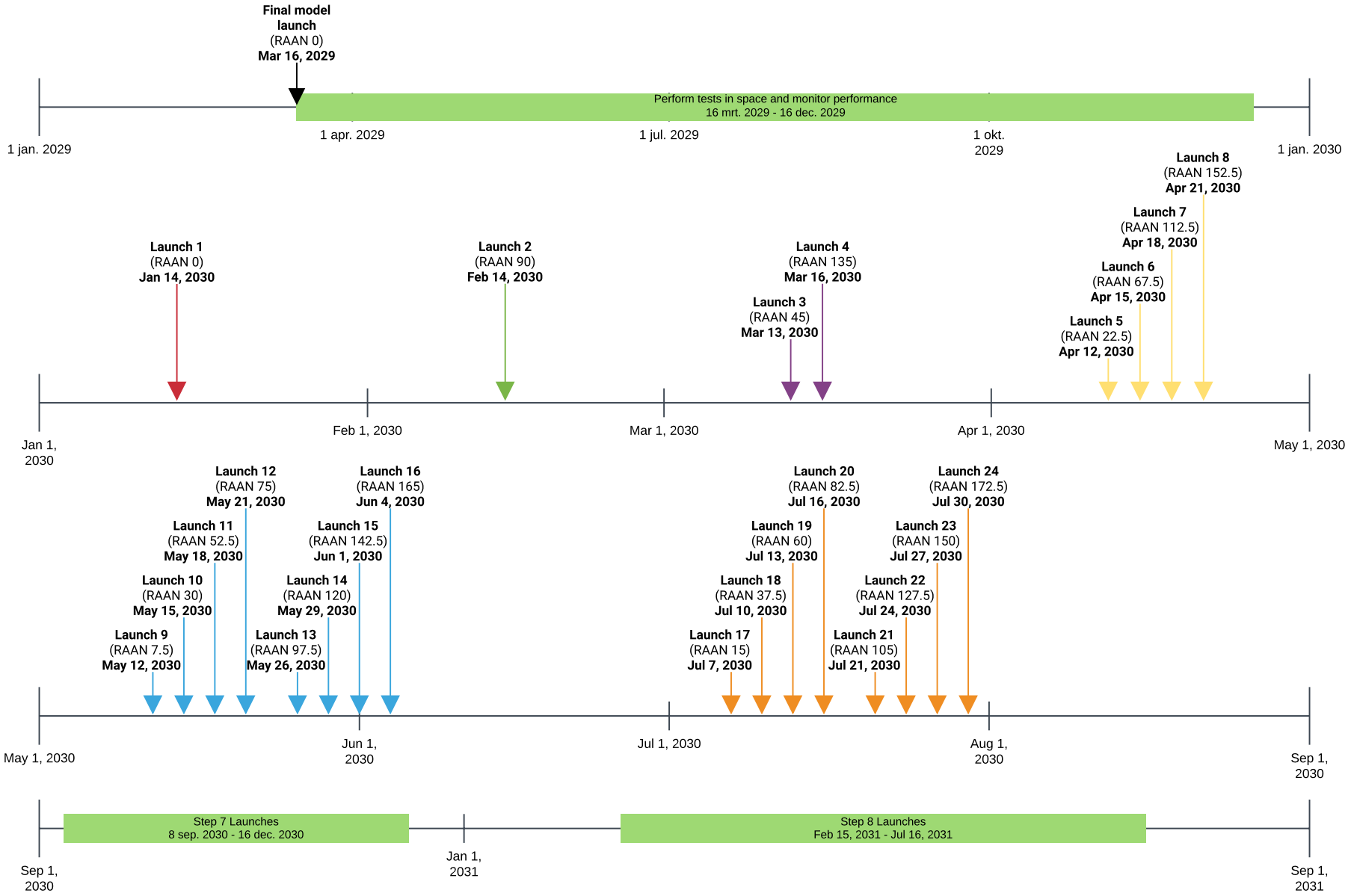

Figure 22.2: Launch Schedule

22.3. Logistics

A satellite consists of many subsystems, their parts have to be produced, which will be done by multiple manufacturers. In Table 22.3, a list is shown with different subsystems, potential manufacturers, and what their products. Notice that the payload does not have a manufacturer; since the deployable telescope is still in early development manufacturers can not be determined as of now.

Table 22.3: Subsystems and potential manufacturers

Subsystem	Manufacturer(s)	Production
Propulsion	Ariane group[a] or JAXA [26]	Ion thruster
ADCS	Blue Canyon[b], SpaceQuest[c], Andrews Space[d], KU Leuven[e], Honeywell[f], bradford[g]	Magnetometer, reaction wheels, gyros, sun sensors
Communications	Endurosat[h]	Phased arrays
Payload	<TBD>	Parts for the deployable space telescope
Thermal	Lockheed Martin, MLI Concepts Inc., NASA Goddard Space Flight Center and Thermacore Inc.[i]	Miniature Pulse Tube Cryocooler, MLI materials, thermal louvers and passive heat pipes
Power	Clyde Space, GomSpace, Blue Canyon Technologies[j]	Power systems, batteries, solar panels
Structures and Mechanisms	RUAG[kl], Airbus[m], APCO[n]	Honeycomb panels, thermal knife, separation system
Other	Tethers Unlimited[o]	De-orbiting devices and robotics

The next step is to assemble these subsystems at NASA facilities[p]. Afterwards, the satellites have to be tested, which can be done in the numeral locations owned by NASA, NTS[q] or corporations like Intelsat[r], all located in the USA. After testing, the satellites will be improved if necessary and a final model can be made. The final models will be transported to the launch site by either trucks or aircraft, where integration with the payload fairing will take place. The final models will then be launched and after 6-12 months, the mission can start by launching the first satellites. Three launch vehicles will be used throughout the whole mission: the Vega rocket, for in-orbit qualification and for satellite maintenance, the Atlas V launch vehicle, for orbits where both TIR and MS satellites are required, and the Falcon 9 FT, for orbits with only TIR satellites.

Vega is a rocket built by Avio for ESA. The rocket is build in Avio's manufacturing facility in Colleferro, Italy. Atlas V can be fabricated and assembled in a factory located in Harlingen, Texas or Decatur, Alabama, by the United Launch Alliance. Their headquarters is located in Centennial, Colorado, where they are responsible for program management, rocket engineering, testing, and launch support functions[s]. The Falcon 9 FT launch vehicle will be manufactured at SpaceX's headquarters, located in Los Angeles, California. Next to production

[a] https://space-propulsion.com/spacecraft-propulsion/propulsion-systems/electric-propulsion/index.html [cited 27 June 2020]
[b] https://www.bluecanyontech.com/static/datasheet/BCT_DataSheet_Components_ReactionWheels.pdf [cited 29 June 2020]
[c] https://satcatalog.com/datasheet/SpaceQuest%20-%20MAG-3.pdf [cited 29 June 2020]
[d] https://spaceflight.com/wp-content/uploads/2015/05/201501-Torque-Rods-Datasheet.pdf [cited 29 June 2020]
[e] http://www.cubesatpointing.com/DownloadFiles/Datasheets/KULSTDatasheet.pdf [cited 29 June 2020]
[f] https://aerospace.honeywell.com/content/dam/aero/en-us/documents/learn/products/sensors/brochures/GG1320ANDigitalLaserGyro-bro.pdf?download=true [cited 29 June 2020]
[g] https://www.bradford-space.com/assets/pdf/be_datasheet_mini_fss_2017jan.pdf [cited 29 June 2020]
[h] https://www.endurosat.com/cubesat-store/all-cubesat-modules/x-band-4x4-patch-array/ [cited 29 June 2020]
[i] https://www.nasa.gov/smallsat-institute/sst-soa/thermal-control [cited 27 June 2020]
[j] https://www.nasa.gov/smallsat-institute/sst-soa/power [cited 29 June 2020]
[k] https://www.ruag.com/sites/default/files/2016-11/PAS_381S_Separation_System.indd_.pdf [cited 29 June 2020]
[l] https://www.ruag.com/en/products-services/space/spacecraft/satellite-structures/honeycomb-panels-demand [cited 29 June 2020]
[m] https://www.airbusdefenceandspacenetherlands.nl/dsstuff/uploads/2016/02/HDRS.pdf [cited 29 June 2020]
[n] https://www.apco-technologies.eu/apco-content/uploads/2018/04/Catalogue-PdV-LR.pdf [cited 29 June 2020]
[o] https://www.tethers.com/products/ [cited 29 June 2020]
[p] https://www.nasa.gov/partnerships/center-capabilities.html [cited 29 June 2020]
[q] https://www.nts.com/industries/aerospace/space-satellites/ [cited 28 June 2020]
[r] https://www.intelsatgeneral.com/satellite-construction-oversight-launch-management/ [cited 29 June 2020]
[s] https://www.ulalaunch.com/about [cited June 27 2020]

and assembly, this location also acts as mission control[t]. Development and testing of the launch vehicle takes place at the SpaceX Rocket Development and Test Facility, in McGregor, Texas[u].

Since Vega is an European launcher, it has to be transported across the Atlantic ocean to be launched at the Vandenberg launch site in the USA. This can be done through the use of large cargo ships or aircraft. Aircraft are preferred, as they are much faster than ships. Transportation of the Atlas V rocket to the launch site will happen similarly to the Vega launcher[v]. The Falcon 9 FT rocket will be brought to the launch site by using multiple huge trucks[w].

In Figure 22.3 a operations and logistics diagram is shown. To start, the design of a prototype for the TIR and MS satellite is made. After that, production will start and after assembly of the subsystems, they will be tested individually followed by whole system testing in dedicated facilities. If needed, improvement and adjustments are made and then the final design is launched into space for more testing and in-orbit qualification. After completing testing, the first batch of satellites is launched.

When the satellites are operating correctly, they communicate with the ground stations. This will be done through the use of phased arrays. The ground stations have to be placed strategically such that real-time downlinking of data can occur. All of the data obtained by the ground station will be sent to mission control.

If any problem occurs during nominal operations, maintenance is not possible, hence the affected satellites will be de-orbited. Therefore, redundant satellites will be launched, such that they can fill in the gaps if satellite failure occurs, as explained in Chapter 6. If there are more gaps or the satellites are not able to fill the gaps, new satellite(s) will be launched, preferably, along with other missions planning to launch closely to a 350 km polar orbit. If there is no such opportunity, the new satellite(s) will be launched with a Vega launch vehicle, as they are cheaper than the Falcon 9 FT and Atlas V rockets and only an estimated one or a two satellites have to be launched each time failure of satellites occurs.

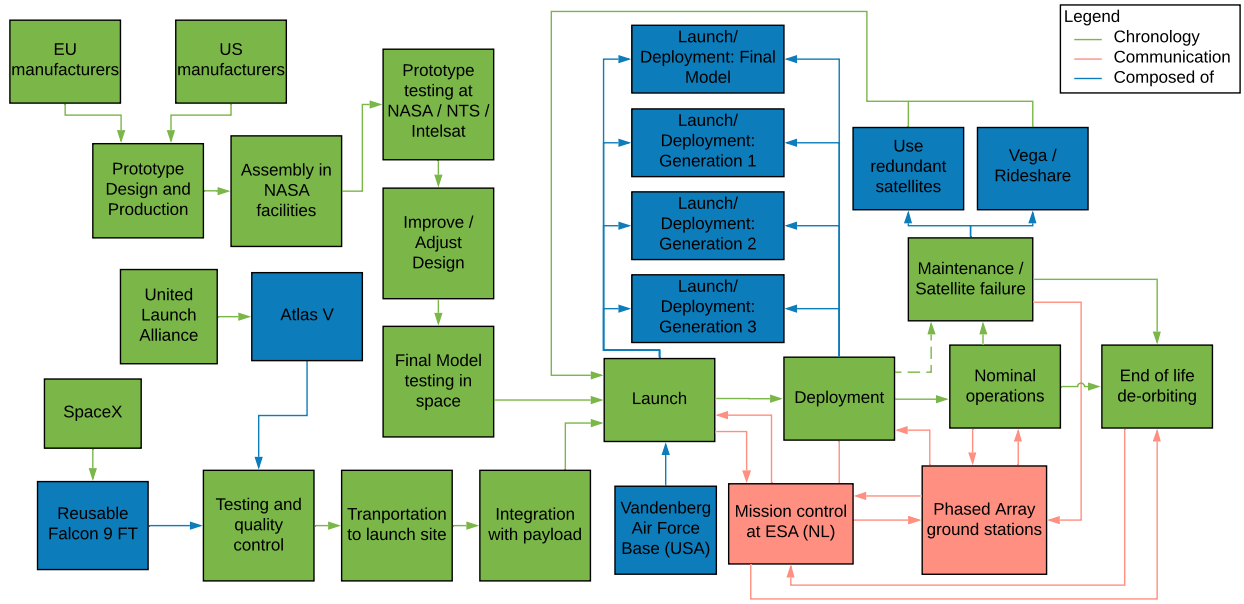

Figure 22.3: Operations and logistics diagram

22.4. Scalability

To investigate the relation between the temporal resolution and the cost during step 1 to 8, Figure 22.4 and Figure 22.5 were made to provide a quick overview. Furthermore, Table 22.4 shows how the temporal resolution changes for each step and the number of satellites required for both TIR and MS to obtain that temporal resolution. Note that for the number of satellites the extra ones for maintenance have not been taken into account. The total cost per step and the increase in total costs can be seen in Section 21.1. Also note that the Figure 22.4 and Figure 22.5 have a logarithmic scale on the y-axis.

[t]https://en.wikipedia.org/wiki/SpaceX [cited June 27 2020]
[u]https://en.wikipedia.org/wiki/SpaceX_launch_facilities [cited June 27 2020]
[v]https://www.af.mil/News/Article-Display/Article/631406/atlas-v-booster-lands-at-vandenberg/ [cited June 27 2020]
[w]https://www.aerotime.aero/aerotime.extra/23089-how-does-spacex-transport-the-falcon-9 [cited June 27 2020]

Table 22.4: Temporal resolution and cost for TIR and MS satellites for Step 1 to 8

Step	Temporal resolution TIR [min]	Temporal resolution MS [min]	TIR satellites needed	MS satellites needed
1	720	720	26	13
2	360	360	52	26
3	180	180	104	52
4	90	180	208	52
5	30	120	416	104
6	30	60	624	156
7	15	30	1248	156
8	7.5	30	2496	156

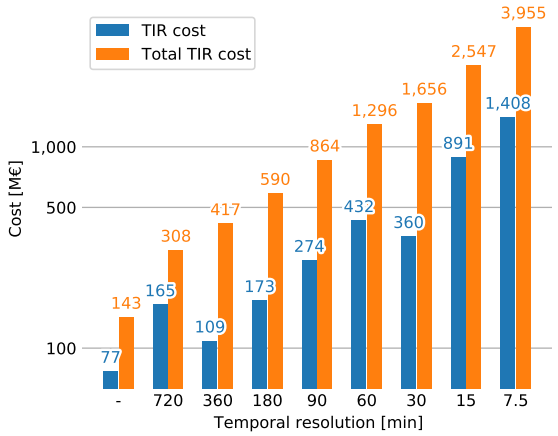

Figure 22.4: Cost against temporal resolution for TIR satellites

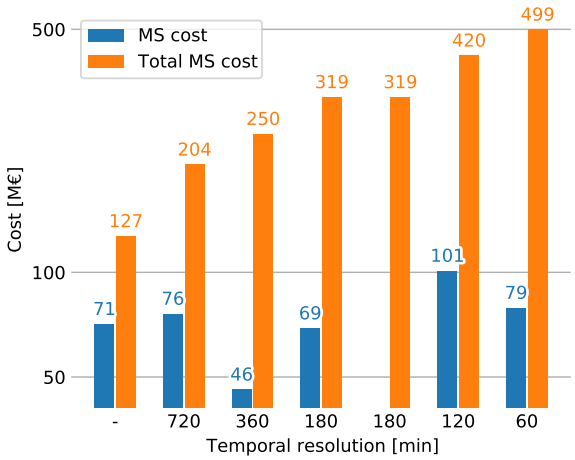

Figure 22.5: Cost against temporal resolution for MS satellites

23
Project Development

Project development covers the main steps and processes that are carried out during the life cycle of a mission. Figure 23.1 is created in order to visually represent the flow between the processes. The steps and processes are separated into 7 phases (Pre-Phase A, Phase A, Phase B, Phase C, Phase D, Phase E, Phase F) and each of these phases signifies a complete and significant part of the design. Pre-Phase A covers concept studies; Phase A covers concept and technology development; Phase B covers preliminary design and technology completion; Phase C covers final design and fabrication of test items; Phase D covers system assembly, integration, test and launch; Phase E covers operations and sustainment; Phase F covers de-orbit of satellites and decommission of the mission. On paper, DSE covers Pre-phase A, Phase A and Phase B, but it should be realised that in reality the result of the DSE will be seen as one of the concept studies, the end product of the Pre-phase A.

NASA's project life cycle process flow[a] was taken as a baseline and was adapted for the Mira mission. NASA's project life cycle works well for typical single satellite missions, therefore special attention was paid to adjusting it for a constellation mission. The main difference is that some of the processes are looped after first launches as second batch of satellites and the subsequent generations of satellites could have changes due to possible design flaws and due to technological development in the sphere of satellites. Figure 23.1 does not fully represent the project life cycle as iterations, design loops and few processes are not shown. These are elaborated in Section 23.1. The project timeline is described in Section 23.2. In addition to that, the whole mission lifecycle can be found in form of a Gantt chart in Figure 23.2 and 23.3.

23.1. Design iterations, testing, satellite generations and design reviews

It should be kept in mind that during the design phase (Pre-Phase A, Phase A, Phase B) some of the processes are reiterated several times in order to achieve the optimal design. Also, starting from the beginning up until launch and deployment step, there is technical planning and management process that runs in parallel.

During finalisation of the preliminary design some potential problems are identified. In order to ensure that quick design solutions are present in case design flaws are identified during testing or during checkout activities, Phase B is carried out for all the feasible concepts.

If there are design flaws related to a selected concept, the design team goes to Phase B and carries out all the design cycle from there. If there are design flaws related to a defective part or to a mistake during assembly, then the design team goes to the end of Phase C and carries out all the design cycle from there. If these flaws are identified during testing then the changes in the design cycle are implemented for the current satellite or batch. If the flaws are identified during checkout activities or during operation, then the changes in design cycle are implemented in the next satellites or batch.

In order to prevent design flaws and in order to detect assembly mistakes or faulty parts as early as possible, verification and validation should be done as early and as often as possible. This should minimise unforeseen expenses.

In order to minimise probability of design flaws in operational satellites, and in order to identify a possible problem as early as possible during Phase C, a few prototypes will be tested extensively. If necessary, improvements and adjustments will be made and the final models will be launched as a co-payload of satellites from different missions or, if that is not possible, with the Vega launch vehicle. This will be launched before the first batch of satellites to allow for testing new technology, such as the deployable telescope, and some aspects of overall design like de-orbiting. By doing so, any problems during operation can be identified and fixed before the first operational launch. If no test satellites are launched then there is a higher chance that there might be something wrong with a design of a whole batch of satellites, which could result in many satellites that are not functioning properly. Such a mistake could be quite costly, while launching a few prototypes does not cost much compared to the whole mission cost. Furthermore, successful prototypes could motivate customers or potential customers to invest in the mission.

[a] https://spacese.spacegrant.org/uploads/Project%20Life%20Cycle/PPF_WallChart_color.pdf [cited 11 May 2020]

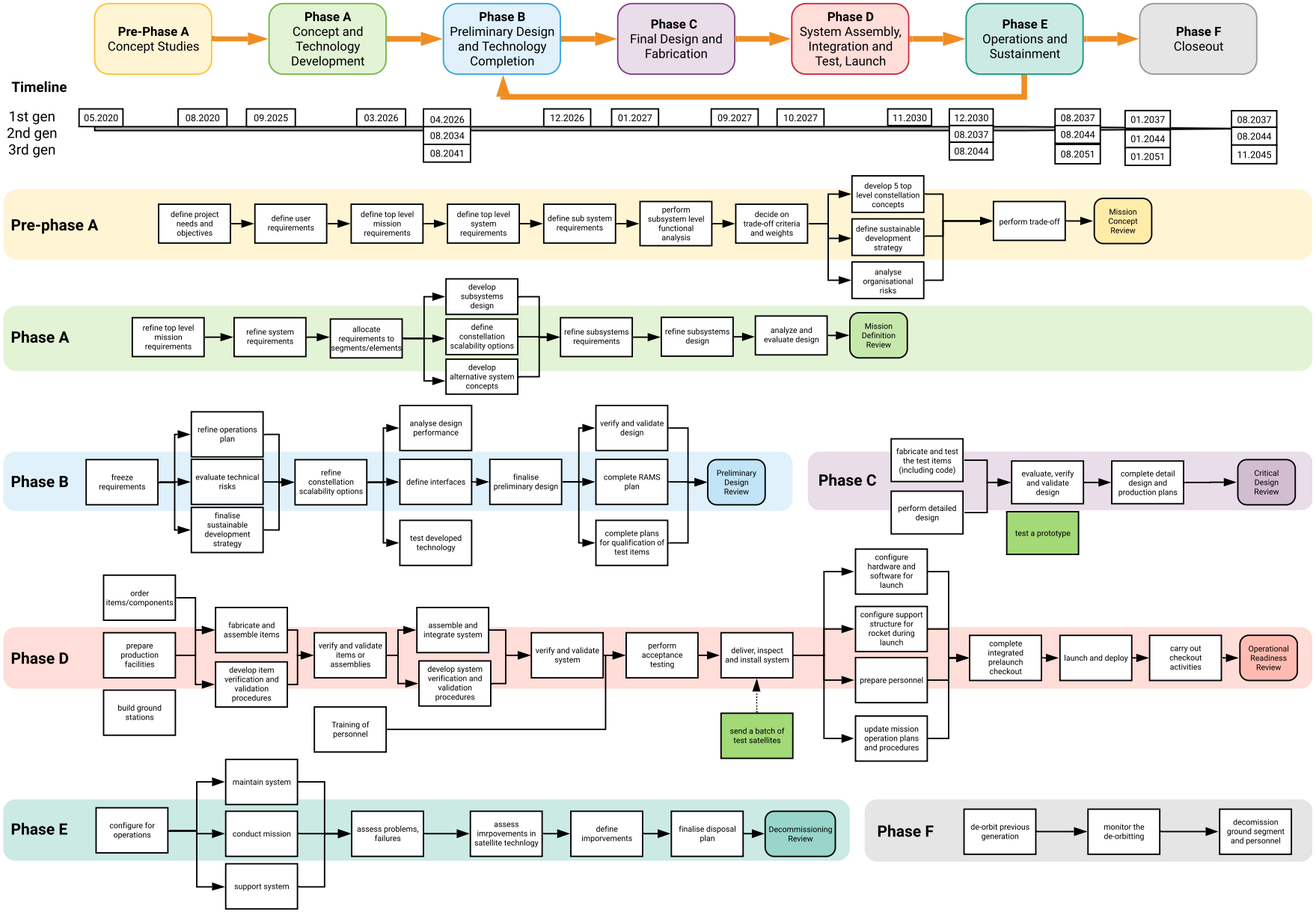

Figure 23.1: Project life cycle

It was decided to have three generations of satellites and it is estimated that one generation of satellites will last for seven years. New satellite technologies that could benefit the mission design might appear in this time period. If such technologies appear and they significantly influence the design for the new generation of satellites the team will go to the beginning of Phase A and carry out all the design cycles from there in order to ensure that requirements and other systems are adapted for this new technology. If new technologies do not significantly influence the design then for the design for the new generation of satellites, the team goes to the beginning of Phase B and carries out all of the design cycle from there. During mission operation of the first generation, problems, failures and improvements in satellite technology are assessed and the design for the second generation is updated by going at the beginning of Phase A or at the beginning of Phase B depending on the new technologies. The same is done during mission operation of the second generation for the design update of the third generation.

Each of the design phases, except for the decommissioning phase, is finalised with a review. Mission concept review mission is similar to midterm review. It assesses mission needs, mission requirements, mission feasibility in terms of market analysis, technical decisions, performance and estimated cost. Mission definition review is similar to intermediate final report review. It validates and fixes the requirements, and assesses performance of the mission. Preliminary design review is similar to the final report. It assesses completeness of the system design, whether the design satisfies the set requirements and is optimal in terms of verification and validation methods, production and operations. It also checks if the system design satisfies cost and schedule constraints imposed by the market. Critical design review assesses whether the detailed design meets requirements, whether system performance and operations are defined and assesses verification and acceptance testing plans. Operational readiness review assesses whether the deployed system is ready to perform the mission, whether it meets mission requirements, whether transition from developers to operators is possible and whether actual operations and performance are represented by plans and procedures. Decommissioning review assesses plans and procedures for disposal and assesses whether removal from service is acceptable. These reviews should be done also during design iterations, such as during detected design flaws and during update for the new generation.

23.2. Project timeline

Development time heavily depends on the technology readiness of the systems used. Most of the systems use technology that has been used before, however payload uses a new technology. The deployable telescope is a new technology that is still in the early phases of its development. Taking into account that the telescope development time is around 10 to 15 years it was estimated that the first launch of the mission could happen between 2030 and 2035. Once the deployable telescope technology is developed to a sufficient level, Phase A of the project life cycle could start. It is estimated that Phase A would take 6 months, Phase B would take 8 months, Phase C would take around 8 months and Phase D would take 30 months, resulting in approximately 4 to 5 years from phase A till the launch. This is a timeline for first few satellites. For the following satellites that have same design or have minor design changes it is expected that the timeline can be reduced. Significant time can be cut during integrating and testing, therefore time spent on Phase D can be significantly reduced for series production [82].

Once test satellites are launched and main aspects of operation are checked, the first operational batch of satellites could be launched. If no flaws are detected, then this period could take from half a year to a year. Detailed launching schedule is shown in Figure 22.2. After the launch of the first operational batch of satellites, the second batch of satellites could be launched in about one month. This time heavily depends on the production, integration and testing capabilities and on the availability of the launcher. If it is assumed that a new batch of satellites could be launched every week, then it should take about 7 months to build up the whole constellation (816 satellites).

It was estimated that the operation lifetime of a satellite is seven years, therefore after seven years from launch of first batch of operational satellites, first operational batch of second generation of satellites is launched and first operational batch of first generation is de-orbited. The same procedure is done for the rest of the batches and for the transition from second generation to third generation. After 20 years from the first operational launch, operational mission lifetime requirement (MIRA-USR-MIS-10) is satisfied and the first batch of third generation is almost at the end of its operational lifetime and one year later it is de-orbited.

ID	Task Name	Duration	Start	Finish
1	**Mira**	**8220 days**	**Fri 1-5-20**	**Wed 1-11-51**
2	**Prephase A**	**1391 days**	**Fri 1-5-20**	**Mon 1-9-25**
3	define project needs and objectives	22 days	Fri 1-5-20	Mon 1-6-20
4	define user requirements	22 days	Fri 1-5-20	Mon 1-6-20
5	define top level mission requirements	22 days	Fri 1-5-20	Mon 1-6-20
6	define top level system requirements	22 days	Fri 1-5-20	Mon 1-6-20
7	define sub system requirements	23 days	Mon 1-6-20	Wed 1-7-20
8	perform subsystem level functional analysis	23 days	Mon 1-6-20	Wed 1-7-20
9	decide on trade-off criteria and weights	23 days	Mon 1-6-20	Wed 1-7-20
10	develop 5 top level constellation concepts	24 days	Wed 1-7-20	Sat 1-8-20
11	define sustainable development strategy	24 days	Wed 1-7-20	Sat 1-8-20
12	analyse organisational risks	24 days	Wed 1-7-20	Sat 1-8-20
13	perform trade-off	24 days	Wed 1-7-20	Sat 1-8-20
14	Mission Concept Review	23 days	Sat 1-8-20	Tue 1-9-20
15	additional concept studies and technology development	1305 days	Tue 1-9-20	Mon 1-9-25
16	**Phase A**	**152 days**	**Mon 1-9-25**	**Wed 1-4-26**
17	refine top level mission requirements	23 days	Mon 1-9-25	Wed 1-10-25
18	refine system requirements	23 days	Mon 1-9-25	Wed 1-10-25
19	allocate requirements to segments/elements	23 days	Mon 1-9-25	Wed 1-10-25
20	develop subsystems design	67 days	Wed 1-10-25	Thu 1-1-26
21	define constellation scalability options	67 days	Thu 2-10-25	Fri 2-1-26
22	develop alternative system concepts	67 days	Fri 3-10-25	Sat 3-1-26
23	refine subsystems requirements	23 days	Thu 1-1-26	Sun 1-2-26
24	refine subsystems design	22 days	Fri 2-1-26	Mon 2-2-26
25	analyse and evaluate design	22 days	Sun 1-2-26	Sun 1-3-26
26	Mission Definition Review	24 days	Sun 1-3-26	Wed 1-4-26
27	**Phase B**	**197 days**	**Wed 1-4-26**	**Fri 1-1-27**
28	freeze requirements	23 days	Wed 1-4-26	Fri 1-5-26
29	refine operations plan	44 days	Wed 1-4-26	Mon 1-6-26
30	evaluate technical risks	44 days	Thu 2-4-26	Tue 2-6-26
31	finalise sustainable development strategy	44 days	Fri 3-4-26	Wed 3-6-26
32	refine constellation scalability options	23 days	Mon 1-6-26	Wed 1-7-26
33	analyse design performance	45 days	Wed 1-7-26	Tue 1-9-26
34	define interfaces	45 days	Thu 2-7-26	Wed 2-9-26
35	test developed technology	45 days	Fri 3-7-26	Thu 3-9-26
36	finalise preliminary design	23 days	Tue 1-9-26	Thu 1-10-26
37	verify and validate design	44 days	Thu 1-10-26	Tue 1-12-26
38	complete RAMS plan	44 days	Fri 2-10-26	Wed 2-12-26
39	complete plans for qualification of test items	45 days	Sat 3-10-26	Thu 3-12-26
40	Preliminary Design Review	24 days	Tue 1-12-26	Fri 1-1-27
41	**Phase C**	**195 days**	**Fri 1-1-27**	**Fri 1-10-27**
42	fabricate and test the test items (including code)	87 days	Fri 1-1-27	Sat 1-5-27
43	perform detailed design	87 days	Sat 2-1-27	Sun 2-5-27
44	evaluate, verify and validate design	45 days	Sat 1-5-27	Thu 1-7-27
45	test a prototype	23 days	Thu 1-7-27	Sun 1-8-27
46	complete detail design and production plans	45 days	Thu 1-7-27	Wed 1-9-27
47	Critical Design Review	23 days	Wed 1-9-27	Fri 1-10-27

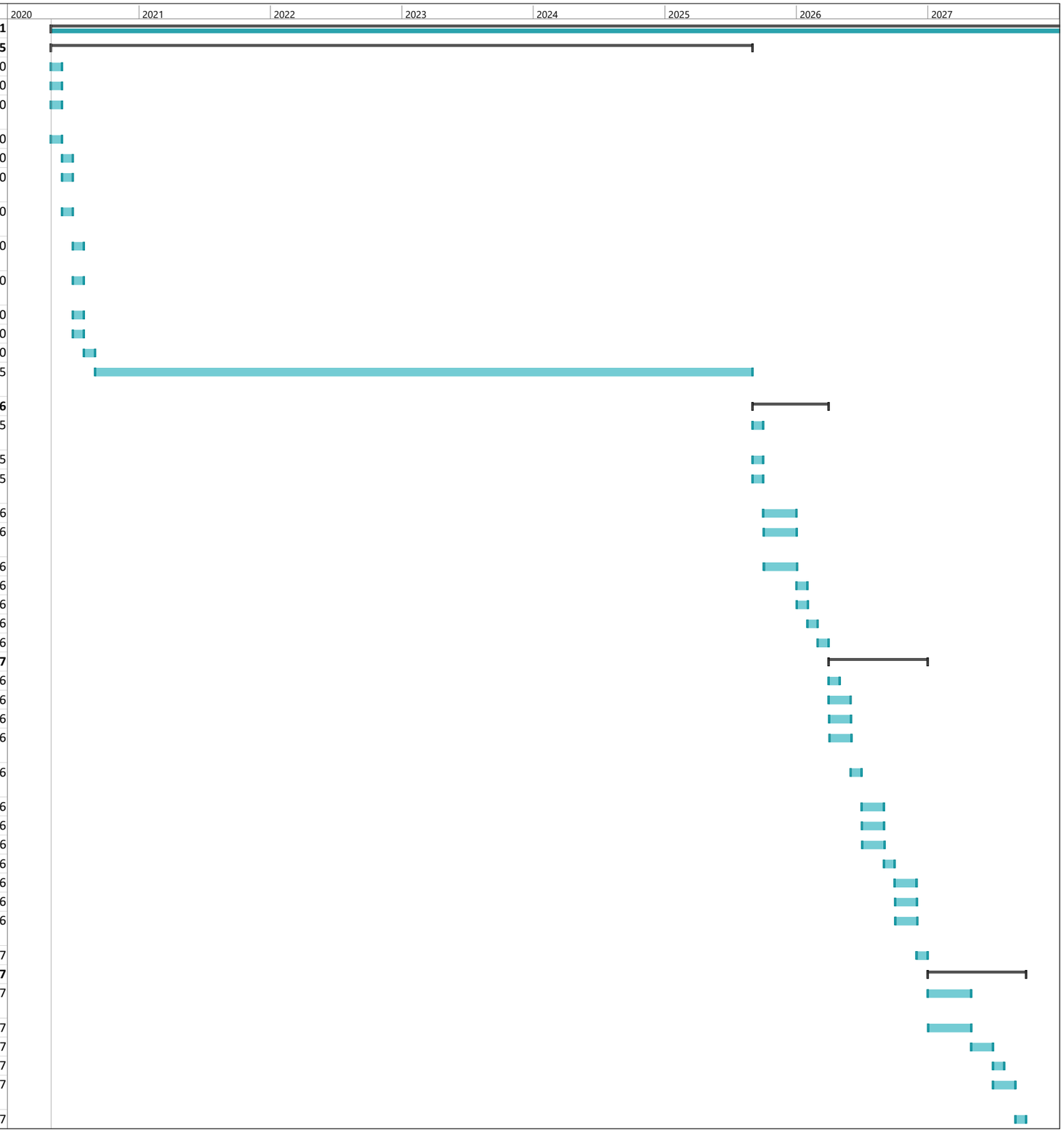

Figure 23.2: Gantt chart visualising the project planning throughout its lifetime

ID	Task Name	Duration	Start	Finish
48	**Phase D**	**915 days**	**Mon 31-5-27**	**Sun 1-12-30**
49	order items/components	22 days	Fri 1-10-27	Mon 1-11-27
50	prepare production facilities	1 day	Mon 31-5-27	Tue 1-6-27
51	build ground stations	88 days	Mon 1-11-27	Wed 1-3-28
52	fabricate and assemble items	132 days	Thu 1-6-28	Fri 1-12-28
53	develop item verification and validation procedures	1 day	Mon 31-5-27	Tue 1-6-27
54	verify and validate items or assemblies	1 day	Mon 31-1-28	Tue 1-2-28
55	training of personnel	23 days	Sat 1-1-28	Tue 1-2-28
56	assemble and integrate system	458 days	Tue 1-2-28	Thu 1-11-29
57	develop system verification and validation procedures	44 days	Wed 2-2-28	Sat 1-4-28
58	verify and validate system	1 day	Wed 31-1-29	Thu 1-2-29
59	perform acceptance testing	21 days	Thu 1-2-29	Thu 1-3-29
60	deliver, inspect and install system	23 days	Thu 1-3-29	Sun 1-4-29
61	send a batch of test satellites	87 days	Fri 1-6-29	Mon 1-10-29
62	configure hardware and software for launch	23 days	Sun 1-4-29	Tue 1-5-29
63	configure support structure for rocket during launch	110 days	Tue 1-5-29	Mon 1-10-29
64	prepare personnel	24 days	Tue 1-5-29	Fri 1-6-29
65	update mission operation plans and procedures	110 days	Mon 1-10-29	Fri 1-3-30
66	complete integrated prelaunch checkout	176 days	Fri 1-3-30	Fri 1-11-30
67	launch and deploy	177 days	Sat 2-3-30	Sat 2-11-30
68	carry out checkout activities	176 days	Sun 3-3-30	Fri 1-11-30
69	Operational Readiness Review	22 days	Fri 1-11-30	Sun 1-12-30
70	**Phase E**	**1762 days**	**Fri 1-11-30**	**Tue 4-8-37**
71	configure for operations	22 days	Fri 1-11-30	Sun 1-12-30
72	maintain system	1742 days	Sun 1-12-30	Sat 1-8-37
73	conduct mission	1741 days	Mon 2-12-30	Sun 2-8-37
74	support system	1740 days	Tue 3-12-30	Mon 3-8-37
75	assess problems, failures	1740 days	Wed 4-12-30	Tue 4-8-37
76	assess imrpovements in satellite technlogy	845 days	Thu 5-12-30	Wed 1-3-34
77	define imporvements	67 days	Wed 1-3-34	Thu 1-6-34
78	finalise disposal plan	23 days	Thu 1-6-34	Sat 1-7-34
79	Decommissioning Review	23 days	Sat 1-7-34	Tue 1-8-34
80	**Phase F**	**4435 days**	**Tue 1-8-34**	**Tue 1-8-51**
81	de-orbit previous generation	153 days	Thu 1-1-37	Sat 1-8-37
82	monitor the de-orbitting	239 days	Thu 1-1-37	Tue 1-12-37
83	**Second Generation**	**2609 days**	**Tue 1-8-34**	**Mon 1-8-44**
84	second generation development, production, assembly and testing	610 days	Tue 1-8-34	Mon 1-12-36
85	second generation launch	153 days	Thu 1-1-37	Sat 1-8-37
86	second generatin operation	1827 days	Sat 1-8-37	Mon 1-8-44
87	second generation de-orbiting	152 days	Fri 1-1-44	Mon 1-8-44
88	**Third generation**	**2608 days**	**Thu 1-8-41**	**Tue 1-8-51**
89	third generation development, production, assembly and testing	609 days	Thu 1-8-41	Tue 1-12-43
90	third generation launch	152 days	Fri 1-1-44	Mon 1-8-44
91	third generatin operation	1827 days	Mon 1-8-44	Tue 1-8-51
92	third generation de-orbiting	153 days	Sun 1-1-51	Tue 1-8-51
93	**Final**	**66 days**	**Tue 1-8-51**	**Wed 1-11-51**
94	decomission ground segment and personnel	67 days	Tue 1-8-51	Wed 1-11-51

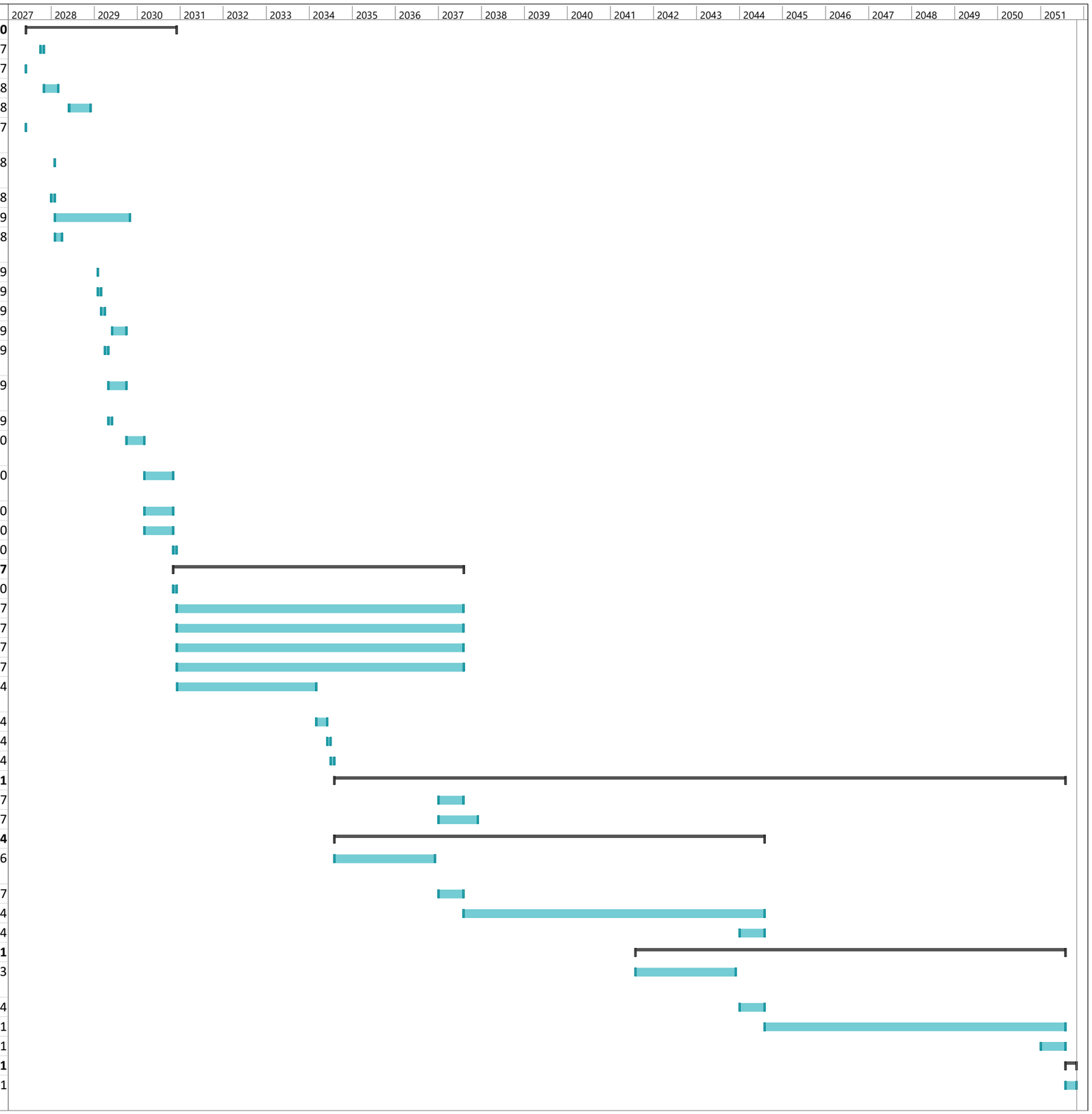

Figure 23.3: Gantt chart visualising the project planning throughout its lifetime (continued)

24 Performance Analysis

The performance analysis is key to define the overall performance of the spacecraft and the system. In Section 24.1 the technical performance measurements are listed which show key characteristics of the spacecraft. Then, in Section 24.2 the compliance of user and system requirements is analysed. Finally, a sensitivity analysis is performed in Section 24.3 to investigate the robustness of the design.

24.1. Technical performance measurements

The technical performance measurements are listed in Table 24.1. These parameters were defined in the Baseline Report and kept track of to see the evolution of the design. The contingencies vary with the level of maturity of the design and the values stem from subsystem calculations. The different values are set up in the same way as in Subsection 17.4.1.

Table 24.1: TPM budget

	Actual value	Target value	Contingency	Cur. value	Spec. value
		Common			
In-orbit qualification cost [M€]	180.48	180.00	0.10	198.53	200.00
Downlink time [min]	Constant	96.00	0.20	-	120.00
		TIR satellite			
On-board storage [GB]	600.38	700.00	0.15	690.43	805.00
Mass [kg]	203.66	329.00	0.15	234.21	378.35
Power [W]	160.43	185.00	0.20	192.51	222.00
ΔV [m/s]	2427.14	2850.00	0.10	2669.86	3135.00
Propellant mass [kg]	30.21	45.00	0.05	31.72	47.25
Volume [m^3]	1.12	1.25	0.30	1.46	1.63
Nominal data rate [MB/s]	198.75	200.00	0.10	218.63	220.00
		MS sat			
On-board storage [GB]	5407.50	6000.00	0.15	6218.63	6900.00
Mass [kg]	235.47	360.00	0.15	270.80	414.00
Power [W]	133.43	185.00	0.20	160.11	222.00
ΔV [m/s]	2445.08	2850.00	0.10	2689.58	3135.00
Propellant mass [kg]	34.90	45.00	0.05	36.64	47.25
Volume [m^3]	1.42	1.50	0.30	1.85	1.95
Nominal data rate [MB/s]	1950.00	2000.00	0.10	2145.00	2200.00

The values show common results for the in-orbit qualification cost (which includes sending one TIR satellite and one MS satellite) and the downlink time since that is done constantly for both platforms. The data recorder has a capacity of 600/5407 GB (TIR/MS), however on average a 20/119 GB capacity would be sufficient so this component is oversized as required by the risk mitigation plans Chapter 4. The MS satellite is heavier than the TIR satellite because the heavier payload leads to a heavier structure as well. The volume given is in stowed configuration. The MS satellite is also bigger than the TIR satellite which increases the total ΔV and the propellant mass. On the one hand a heavier satellite is easier to counteract for drag but on the other hand the increase in area is more detrimental for drag compensation hence why the MS satellite is heavier and requires more propellant mass. The power necessary for the TIR satellite is bigger because it requires more thermal control for the instrument box but both platforms will have the same solar panels. The big difference in data rate and storage capacity between the TIR and MS satellites is due to the difference of measured spectral bands

(18 for MS vs. 1 for TIR). More data is samples for MS so more data is stored during 2 hours and so more data has to be downlinked in the same amount of time for MS and TIR.

24.2. Compliance matrix

After defining the final performance of the system a requirement compliance matrix is used to check if all user, key, driving and system requirements are met. This determines if the design is approved by the customer and it explained in Table 24.2. Some requirements have not been met and need to be discussed with the customer. Other requirements cannot be verified right now and a plan needs to be formed.

Table 24.2: Requirement compliance table

Requirement	Explanation	
	User requirements	
MIRA-USR-MIS-2	In accordance with the customer it is considered acceptable to not meet this requirement as the data is constantly downlinked and so the information can be stored on the ground.	×
MIRA-USR-MIS-3	According the TIR temporal resolution and MS temporal resolutions, the whole Earth is monitored in 30 minutes by the TIR satellites and in 60 minutes by the MS satellites.	✓
MIRA-USR-MIS-4	As the spacecraft is constantly downlinking data because of the ground station configuration explained in Section 16.7 this requirement is automatically satisfied.	✓
MIRA-USR-MIS-6	Section 16.7 explains that the spacecraft are always in contact with the groundstations and continuously downlinking the information.	✓
MIRA-USR-MIS-7	Subsection 13.2.1 shows that the ground sampling distance for TIR satellite at 350 km km altitude is 5 m. Section 12.2 shows that the sensor for the TIR satellite is sized according to the 8-12 µm requirement.	✓
MIRA-USR-MIS-8	Subsection 13.2.1 shows that the ground sampling distance for MS satellite at 350 km km altitude is 10 m. As in explained in Section 11.2 the multispectral instrument chosen with a spectral range of 2.65-3.52 µm includes the absorption bands necessary to monitor the required emissions.	✓
MIRA-USR-MIS-9	All satellite components have a lifetime of 7 years and there is enough propellant to counter drag during 7 years (Section 14.3).	✓
MIRA-USR-MIS-10	Section 22.3 shows launch plans for 3 generations. 3 generations with a lifetime of 7 years means the mission will be operational during 21 years.	✓
MIRA-USR-MIS-11	The orbit altitude is 350 km as defined in Chapter 13.	✓
MIRA-USR-MIS-12	The number of MS satellites was determined using a temporal resolution of 60 minutes (Section 13.2).	✓
MIRA-USR-MIS-13	The number of TIR satellites was determined using a temporal resolution of 30 minutes (Section 13.2).	✓
MIRA-USR-SR-1	Binary Phase Shift Keying and Reed Solomon Viterbi are used.	✓
MIRA-USR-SR-2	Binary Phase Shift Keying and Reed Solomon Viterbi are used.	✓
MIRA-USR-SR-3	As explained in Subsection 14.7.3 collision avoidance during de-orbit has to be thoroughly investigated as there is a potential risk of collision with Starlink.	×
MIRA-USR-SR-4	As explained in Chapter 17 the solar panels will not be available during a solar eclipse but this is less than 1% of the orbital period. Other subsystems will always be available.	✓
MIRA-USR-SR-5	Section 22.2 shows that the constellation will be built up in steps.	✓

Table 24.2: continued from previous page

Requirement	Explanation	
MIRA-USR-SUS-1	The satellites are equipped with an on-board computer that continuously calculated the positions of the other satellites. If a collision risk is determined, the thruster will gimbal in a specific direction to avoid collision.	✓
MIRA-USR-SUS-2	The satellites will use the on-board computer that calculates whether a collision will occur and use the thruster to change position to avoid a crash.	✓
MIRA-USR-SUS-3	The TIR satellites will de-orbit in 117 days and the MS satellites will de-orbit in 116 days (Subsection 14.3.2).	✓
MIRA-USR-SUS-4	The satellites will be packed in such a way that as many satellites as possible can fit inside the launcher, resulting in less launches needed.	✓
MIRA-USR-SUS-5	The launchers are filled up to their volumetric capacity and only one launcher is needed per orbit.	✓
MIRA-USR-MISC-1	Section 20.1 shows that the same bus will be used for the two satellite platforms as this is beneficial for series production.	✓
MIRA-USR-MISC-2	In Chapter 12 the payload design is based on the DDST and this telescope is used in both satellite platforms.	✓
MIRA-USR-MISC-3	Three different launchers will be used to build-up the constellation: Falcon 9, Atlas V and Vega. For maintenance the Vega will be used. All of these are existing and flight proven.	✓
	Sustainability requirements	
MIRA-SUS-FUNC-1	Due to the low earth orbit the spacecraft de-orbits because of aerodynamic drag.	✓
MIRA-SUS-FUNC-2	The collision avoidance methods explained in Subsection 14.7.3 will ensure that no collision occurs and hence the spacecraft will not produce space debris.	✓
MIRA-SUS-FUNC-3	It was found that volume is limiting when fitting the spacecraft in the launcher and so smart-packing it applied with help of a column for attachment.	✓
MIRA-SUS-FUNC-4	In the mitigation plans presented in Chapter 4 it is considered necessary to include redundant ADCS and temperature sensors and redundant storage capacity. The ADCS and thermal control design include these sensors and the redundant storage is taken up by the high value of storage capacity when a way lower one would have been sufficient (Section 16.4).	✓
MIRA-SUS-PERF-1	During the design phase no paper is being used and no transportation as the work in being done from home. These factors limited the production of emissions. During the following design phases and testing limiting emissions needs to be kept in mind. For design a similar approach to the current one should be taken, while for testing care must be taken to choose emission limited options such as making sure to minimise transportation distances.	●
MIRA-SUS-PERF-2	During the life-cycle of the spacecraft emissions can be limited by minimising transportation distances, applying lean manufacturing and avoiding waste and reusing ground stations when possible.	●
	Scheduling requirements	
MIRA-SHED-PERF-1	The launch schedule in Section 22.2 shows that the in-orbit qualification will be launched in June 2029 and the following launches come afterwards with the last launch in August 2030.	✓
	Manufacturing requirements	
MIRA-MANU-PERF-1	Several subsystems limited the use of toxic materials (eg. not using nuclear power), nonetheless this was not checked for every subsystem (eg. use of coacting in thermal control) so this requirement requires more investigation.	●

Table 24.2: continued from previous page

Requirement	Explanation	
MIRA-MANU-PERF-2	This is explained in RAMS Chapter 6.	✓
MIRA-MANU-SUS-1	The use of series production is clearly shown in the cost analysis and the production plan (Subsection 21.1.2 and 20.1).	✓
	System requirements	
MIRA-SYS-TIR-PERF-1	As shown in Table 24.1 the total mass of the TIR satellites is 208.15 kg.	✓
MIRA-SYS-TIR-PERF-2	As shown in Table 24.1 the total power of the TIR satellites is 150.39 W.	✓
MIRA-SYS-MS-PERF-1	As shown in Table 24.1 the total mass of the MS satellites is 240.52 kg.	✓
MIRA-SYS-MS-PERF-2	As shown in Table 24.1 the power mass of the MS satellites is 133.43 W.	✓
MIRA-SYS-FUNC-1	Subsection 14.7.3 explains that no ΔV is necessary to avoid space debris. The small debris cannot be detected but are improbable and the thruster can be gimbaled to avoid larger debris.	✓
MIRA-SYS-FUNC-2	The spacecraft's structural panels protect from radiation and debris as explained in Chapter 19.	✓
MIRA-SYS-FUNC-3	Subsection 14.7.3 explains how satellites are equipped with an on-board computer that calculates whether collisions with other satellites in the constellation occurs.	✓
MIRA-SYS-FUNC-4	As mentioned in the subsystems chapter, a baffle to protect the payload is present and the deployment of the baffle is one of the functions of the structures subsystem.	✓
MIRA-SYS-PERF-1	The list of of redundant components is minimal: ADCS sensors and magnetometers, temperature sensors, GNSS signal receiver. The design could have more redundant components but it was decided to limit this as a philosophy.	✓

24.3. Sensitivity analysis

After finalising the design parameters and analysing the performance and requirement compliance a sensitivity analysis can be conducted. This is done to examine how changes affect the design. The aspects listed below are particularly interesting to analyse because of their impact on the whole system.

1. *Baffle deployment mechanism.* A more complex mechanism affects the total area and inner structure. It leads to an increase in cost and launch volume, which could lead to an increase in number of launches, which affects the way MIRA-USR-SUS-5 is dealt with. The deployment of the baffle has not been designed for but it is crucial so it is recommended that further investigation be conducted in this area. If the baffle deployment mechanism would increase due to the integration of the baffle passive cooling the launch volume would be affected. Checks were conducted for an increase in 5% and 10% of the stowed width and it was found that for 5% only 25 satellites fit in the Falcon 9 instead of the 30 before and only 50 fit in the Atlas V instead of the 59 before. However, there were no further changes for the 10% increase. This decrease in spacecraft per launch vehicle leads to two options: more launches with the same launcher or choosing different launchers; both mean an increase in launch costs and emissions.
2. *Baffle thermal control.* The design includes passive baffle cooling with reflective surfaces inside the baffle. They allow to lower the inner temperature and need to be at a certain angle to prevent the light to interfere with the secondary mirror. Their mass is considered negligible and so they affect the design only in terms of complexity as the number of moving parts increases since the mirrorlets need to be foldable and deployable. The deployment mechanism, the exact angles and the inner structure of the baffle also

require further investigation. However, another option would be to use active cooling which would require more power, a thicker baffle, and is more expensive. An increase in power required is detrimental for the design but a 20 W increase for thermal control can still be handled by increasing the solar panel without influencing the propulsion subsystem. The choice between types of thermal control affect requirements MIRA-SYS-TIR-PERF-2 and MIRA-SYS-MS-PERF-2, leading to a different power system design which could influence other aspects of the satellite as well.

3. *Solar array area.* The solar array area is directly affected by all the power requirements. An increase leads to more drag, so more propellant mass required, more thrust and in turn more power as well. Additionally, an increase in solar array area could affect the ADCS design and the launch volume. However, it was found that the ADCS design is mostly insensitive to the changes. Also the launch volume would not be affected as the solar panels are folded and the volume in stowed configuration is driven by the baffle. The solar array size would need to increase considerably for a third fold to be necessary. So the solar array area affects propulsion subsystem and the two are deeply linked.
4. *Propellant mass.* The propellant mass is affected by the frontal area; more area to generate drag means an increase in ΔV and with it the propellant mass. However, if the increase still results in a lower drag force than the thrust the propulsion system can give then the power consumption does not change and the propellant mass has little influence on the rest of the design. If the drag force turns out to be higher than the thrust the beam current needs to be increased (as explained in Chapter 14 increasing the voltage is more detrimental), which increases the power required. By doubling the current the power required is multiplied by a factor of 1.8 which increases the total power of the system by 35%. The baffle and bus have a frontal area of $1.84\,m^2$ and $2.34\,m^2$ for the TIR and MS, respectively. The maximum allowed increased size for the solar panel so that the power consumption of the propulsion subsystem does not change and is $1.48\,m^2$ for the TIR satellite and $1.45\,m^2$ for the MS satellite. Beyond these values, the power required changes which influences the solar array area considerably, which again influences the drag and this process continues until a certain convergence is found. These areas translate to a total of 180 W generated which equals a 25% increase from the actual values of the design. If the power value goes above the solar panel area, it has to be increased affecting the propulsion subsystem considerably. These changes affect power requirements, total mass of the system and launcher integration.
5. *Using current/target values for mass.* When using the current value a contingency is added to the actual values and the target value is the value that is aimed for as a maximum. Increasing the mass influences the cost as the estimations are relations dependent on mass, however as explained in Section 21.1 they are over estimations and so this check will not be performed. Besides the cost, the total mass also influences the launch mass and so the number of launches. If the target values are used as input the number of satellites per launcher is 30 for the Falcon 9 and 37 for the Atlas V. If the current values are used the number is 30 for the Falcon 9 and 52 for the Atlas V. As before, two options are available: more launches or bigger launcher, and both are costly unsustainable solutions. Changes in mass affect requirements MIRA-SYS-TIR-PERF-1 and MIRA-SYS-MS-PERF-1, as well as MIRA-USR-SUS-4. The values do not change for the Falcon 9 because the configuration of the launcher is volume limited.

25
Conclusion and Recommendations

This final work's findings are structured in three parts. The first presents the contexts and lays the basis for the design of the constellation. The second depicts the design of the system, specifically that of the space segment. Lastly, the third touches upon assembly, development, and cost analysis.

From the market analysis, it was found that the market share for Earth-observing optical mission is going to grow over the next ten years, with an increase of 9% per year. The main clients for this designed mission were found to be the EU and/or NATO countries. From technical risk analysis, sustainable development strategy, RAMS, and user requirements overview, sustainability and availability were identified as central factors throughout both the design and the production process.

The final report also explored every aspect of the constellation design: the satellite design, the ground segment design and the whole constellation design. Table 25.1 presents those findings.

Table 25.1: Conclusion table

High level	**MS**	**TIR**
Types of satellite	1 type monitoring gases	1 type monitoring sources of infrared
Aspects monitored	CO_2, CH_4, NO_2	humans, fires, vehicles
Minimum number of humans	-	minimum (2-11)
Resolution	10 by 10 m × m	5 by 5 m × m
Number of satellites	168	648
Whole Earth observation	60 minutes	30 minutes
Available during night?	No	Yes
Average cost per satellite	2.61 M€	2.49 M€
Launch area	Vandenberg Airforce base (US)	Vandenberg Airforce base (US)
Total satellite costs	371.6 M€	1,513 M€
Constellation cost	3.9 B€	
Mid level	**MS**	**TIR**
Monitored wavelengths	2.65-3.52 µm	8-12 µm
Data rate	1950 MB/s	199 MB/s
Area per picture	200 by 200 km × km	100 by 100 km × km
Launcher	Atlas V	Falcon 9 FT
Launcher for maintenance	Vega	Vega
Instrument type	Delft Deployable Telescope	Delft Deployable Telescope
Low level	**MS**	**TIR**
Satellite mass	235 kg	203 kg
Telescope mass	81	60
Number of solar arrays	2	2
Power usage	133 W	160 W
Items developed for the mission	ADCS and DDST	ADCS and DDST

The numbers of steps here shows the number of 'chapters' in a launch history, with each resulting in a specific

temporal resolution. These numbers of steps can be increased or decreased if another temporal resolution is desired. The temporal resolution options and their corresponding costs can be found in Table 25.2.

Table 25.2: Cost vs temporal resolution table

Step	Temporal resolution MS (min)	Temporal resolution TIR (min)	Total cost MS M€	Total cost TIR M€
1	720	720	204	308
2	360	360	250	417
3	180	180	319	590
4	180	90	319	864
5	120	60	420	1,296
6	60	30	499	1,656
7	60	15	499	2,547
8	60	7.5	499	3,955

Recommendations

A few recommendations can be made with regards to further analysis and steps to be taken towards finalising the preliminary design. Firstly, the temporal resolution gained (and lost in the not monitored parts) by slewing the satellites should be investigated, including all the implications slewing would have on the remaining design.

Thermal control turned out to be one of the most mission-specific system designs, and several recommendations thus flow from that analysis. The thermal control of the baffle with the potential use of an active cooling system for the baffle should be investigated. Better cooling might lead to a reduction of the risk of interference of the reflected light with the secondary mirror. The baffle's contribution to light pollution should also be minimised by choosing tailored outer coatings.

The spacecraft's heat capacity should be more accurately estimated, taking into account the heat capacity of the single internal components. Further mirrorlets deployment possibilities should be looked into, as the mirrorlets are mounted on a deployable surface (the baffle).

The baffle deployment mechanism should also be further designed to make sure it is the less space-taking and to ensure more straightforward launcher integration. A mechanism allowing passive rotation of the solar arrays (by 90 degrees after deployment) should also be looked into.

A dynamic analysis on the power generated by the solar arrays throughout the orbit of the satellite should be carried out to ensure the battery would be capable of powering the spacecraft in the time directly after leaving the eclipse when the solar arrays are generating smaller amounts of power then the average power estimated throughout the orbit.

The vibrations of internal components should be considered when sizing the bus structures, and mechanisms and mass and volume estimations for the payload should be refined. Furthermore, the telescope optics dimensioning needs to be iterated on to lead to a more precise instrument box and baffle sizing. The method used to attach the satellites to the Vega launcher should be designed with particular care, as the optical elements in the payload can only be subjected to a very limited amount of loads.

It would be recommendable to perform a cost-based trade-off for each component in terms of the cost of COTS versus custom-development. Furthermore, an overview of off-the-shelf versus self-developed component cost options should be laid out to facilitate a selection geared towards the minimisation of cost.

Bibliography

[1] Bouwmeester, J., *Project Guide Design Synthesis Exercise - Space Based Surveillance System*, Delft University of Technology, Delft, 2020.

[2] Hamann, R. J., and van Tooren, M. J. L., *Systems Engineering & Technical Management Techniques Part 1*, Delft University of Technology, Delft, 2006.

[3] Ayazyan, D., Capus, L., Faure, N., Gurumallappa, P., Heumassej, Y., Litjens, T., McSorley, K., Mottinelli, L., Riha, B., and van Voorbergen, T., "Baseline Report: Space Based Surveillance System for Safety, Justice & Environment," Delft University of Technology, May 2020 (unpublished).

[4] Ayazyan, D., Capus, L., Faure, N., Gurumallappa, P., Heumassej, Y., Litjens, T., McSorley, K., Mottinelli, L., Riha, B., and van Voorbergen, T., "Midterm Report: JASPIE," Delft University of Technology, May 2020 (unpublished).

[5] Castet, J.-F., and Saleh, J. H., "Satellite Reliability: Statistical Data Analysis and Modeling," *Journal of Spacecraft and Rockets*, Vol. 46, No. 5, 2009, pp. 1065–1076. doi: 10.2514/1.42243.

[6] Hirshorn, S. R., Voss, L. D., and Bromley, L. K., "NASA Systems Engineering Handbook," Tech. rep., NASA, 2017.

[7] Veefkind, J. P., Aben, I., McMullan, K., Förster, H., de Vries, J., Otter, G., Claas, J., Eskes, H. J., de Haan, J. F., Kleipool, Q., van Weele, M., Hasekamp, O., Hoogeveen, R., Landgraf, J., Snel, R., Tol, P., Ingmann, P., Voors, R., Kruizinga, B., Vink, R., Visser, H., and Levelt, P. F., "TROPOMI on the ESA Sentinel-5 Precursor: A GMES mission for global observations of the atmospheric composition for climate, air quality and ozone layer applications," *rse*, Vol. 120, 2012, pp. 70–83. doi: 10.1016/j.rse.2011.09.027.

[8] Wertz, J. R., and Larson, W. J., *Space Mission Analysis and Design*, Space Technology Library, Microcosm, 1999.

[9] Dolkens, D., "A Deployable Telescope for Sub-Meter Resolutions from MicroSatellite Platforms," Master's thesis, Faculty of Aerospace Engineering, TU Delft, Delft, 2015.

[10] Dolkens, D., Kuiper, H., and Corbacho, V. V., "The deployable telescope: a cutting-edge solution for high spatial and temporal resolved Earth observation," *Advanced Optical Technologies*, Vol. 7, No. 6, 2018, p. 365–376. doi: 10.1515/aot-2018-0043.

[11] Krikken, A., "Design of the Secondary Mirror Support Structure for the Deployable Space Telescope," Master's thesis, Faculty of Aerospace Engineering, TU Delft, Delft, 2018.

[12] Kuiper, J. M., "Chapter 32. Light: Reflection and Refraction," [Lecture], 2019.

[13] Veefkind, J., "TROPOMI on the ESA Sentinel-5 Precursor: A GMES mission for global observations of the atmospheric composition for climate, air quality and ozone layer applications," *Remote Sensing Environment*, Vol. 120, 2012, pp. 70–83. doi: 10.1016/j.rse.2011.09.027.

[14] Qian, S.-E., *Optical Payloads for Space Missions*, Space Technology Library, John Wiley & Sons, 2015.

[15] Rogalski, A., "Infrared Detectors at the Beginning of the Next Millennium," *Sensors and Material*, Vol. 12, No. 5, 2000.

[16] Meseguer, J., Pérez-Grande, I., and Sanz-Andrés, A., *Spacecraft thermal control*, Space Technology Library, Woodhead publishing, 2012.

[17] Wertz, J. R., Everett, D. F., and Puschell, J. J. (eds.), *Space Mission Engineering: The New SMAD*, Space Technology Library, Microcosm Press, Hawthorne, CA, 2011.

[18] Bouwmeester, J., Gill, E., Sundaramoorthy, P., and Kuiper, H., "Concept study of a LEO constellation of nanosatellites for near real time optical remote sensing," *62nd International Astronautical Congress 2011, IAC 2011*, Vol. 3, 2011, pp. 2534–2542.

[19] Analytical Graphics Inc., Systems Tool Kit (STK), Software Package, Version 12, Exton, PA, USA, 2020.

[20] Eshagh, M., and Alamdari, M., "Perturbations in orbital elements of a low earth orbiting satellite," *J. Earth Space Phys.*, Vol. 33, 2007, pp. 1–12.

[21] Fazio, N., Gabriel, S. B., Golosonoy, I. O., and Wollenhaupt, B., "Cost for Gridded Ion Engines using Alternative Propellants," *The 36th International Electric Propulsion Conference*, 2019, pp. IPEC–2019–831.

[22] Zaberchik, M., Lev, D. R., Edlerman, E., and Kaidar, A., "Fabrication and Testing of the Cold Gas Propulsion System Flight Unit for the Adelis-SAMSON Nano-Satellites," *Aerospace*, Vol. 6, No. 8, 2019, p. 91. doi: 10.3390/aerospace6080091.

[23] Dan M. Goebel, I. K., *Thruster Principles*, Jet Propulsion laboratory, California Institute of Technology, 2008, Chap. Thruster Principles, pp. 1 – 30.

[24] Patterson, M. J., and Grisnik, S. P., "Scaling of Ion Thrusters to Low Power," *International Electric Propulsion Confrence*, 1998, pp. 609 – 616. doi: IEPC-97-098.

[25] Oleson, S. R., and Sankovic, J. M., "Electric Propulsion for Low Earth Orbit Constellations," Tech. rep., NASA, 1998.

[26] Koizumi, H., Komurasaki, K., Aoyama, J., and Yamaguchi, K., "Engineering Model of the Miniature Ion Propulsion System for the Nano-satellite: HODOYOSHI-4," *Transactions of the Japan Society for Aeronautical and Space Sciences, Aerospace Technology Japan*, Vol. 12, No. ists29, 2014, pp. Tb_19–Tb_24. doi: 10.2322/tastj.12.tb_19.

[27] Brophy, J., Marcucci, M., Kakuda, R., Polk, J., Anderson, J., Brinza, D., Henry, M., Fujii, K., and Stocky, J., "Ion Propulsion System (NSTAR) DS1 Technology Validation Report," *Deep Space 1 Technology Validation Report*, Vol. 2014, 2014, pp. 1–11.

[28] Sandra Browne, S. R., "Ion Thruster Gimbal," Tech. rep., MOOG Space and Defense Group, Chatsworth, CA, 2019.

[29] Zandbergen, B. T. C., *Aerospace Design and System Engineering elements 1, Part: Spacecraft (bus) Design and Sizing*, Delft University of Technology, 2015.

[30] SpaceX, *FALCON USER'S GUIDE*, SpaceX, Hawthorne, CA, 2020.

[31] Stesina, F., "Validation of a test platform to qualify miniaturized Electric propulsion systems," 2019.

[32] Dion, A., Calmettes, V., Bousquet, M., and Boutillon, E., "Performances of a GNSS receiver for space-based applications," , 2010.

[33] Syderal Swiss, "Navileo GNSS Receiver," Tech. rep., Syderal Swiss, Switzerland, 2017.

[34] Alfriend, K., Vadali, S. R., Gurfil, P., How, J., and Breger, L., *Spacecraft Formation Flying: Dynamics, Control and Navigation*, Elsevier Astrodynamics Series, Elsevier Science, 2009.

[35] Bosch, P. R., *Improvements in Autonomous GPS Navigation of Low Earth Orbit Satellites*, Universitat Politecnica de Catalunya, Spain, 2008.

[36] Ramos-Bosch, P., "Improvements in Autonomous GPS navigation of Low Earth Orbit Satellites," Ph.D. thesis, Universitat Politecnica de Catalunya, Barcelona, Spain, 2008.

[37] European Space Agency (ESA), Debris Risk Assessment and Mitigation Analysis (DRAMA), Software Package, Version 3.0.3, Darmstadt, Germany, 2020.

[38] Yoshida, N., Takahara, O., and Kodeki, K., "Spacecraft with Very High Pointing Stability: Experiences and Lessons Learned," *IFAC Proceedings Volumes*, Vol. 46, No. 19, 2013, pp. 547–552. doi: 10.3182/20130902-5-de-2040.00144.

[39] Pong, C. M., "On-Orbit Performance & Operation of the Attitude & Pointing Control Subsystems on ASTERIA," *32nd Annual AIAA/USU Conference on Small Satellites*, 2018, pp. 1–20.

[40] Kuiper, H., Dolkens, D., Monna, B., Sweers, J., and Agocs, T., "A CUTTING EDGE 5U-6U CUBESAT SYSTEM SOLUTION FOR EARTH OBSERVATION WITH SUB-METER SPATIAL RESOLUTION AT 200-300 km ALTITUDE," *4S Symposium 2018 Proceedings*, The 4S Symposium 2018, 2018, p. 11.

[41] Ju, D., "Attitude Control Subsystem Design of the Stable and Highly Accurate Pointing Earth-imager," Master's thesis, Faculty of Aerospace Engineering, TU Delft, Delft, 2017.

[42] Sands, T. A., Kim, J. J., and Agrawal, B. N., "Nonredundant Single-Gimbaled Control Moment Gyroscopes," *Journal of Guidance, Control, and Dynamics*, Vol. 35, No. 2, 2012, pp. 578–587. doi: 10.2514/1.53538.

[43] Doupe, C., and Swenson, E. D., "Optimal Attitude Control of Agile Spacecraft Using Combined Reaction Wheel and Control Moment Gyroscope Arrays," *AIAA Modeling and Simulation Technologies Conference*, American Institute of Aeronautics and Astronautics, 2016, pp. 1–23. doi: 10.2514/6.2016-0675.

[44] Oland, E., and Schlanbusch, R., "Reaction wheel design for CubeSats," *2009 4th International Conference on Recent Advances in Space Technologies*, IEEE, 2009, pp. 778–783. doi: 10.1109/rast.2009.5158296.

[45] Cherukuri, S. D., "Integrating hardware data into simulation models for Attitude Control System design," Master's thesis, Faculty of Aerospace Engineering, TU Delft, Delft, 2019.

[46] Jonsson, L., "Simulations of Satellite Attitude Maneuvers - Detumbling and Pointing," Master's thesis, Luleå University of Technology, Luleå, SE, 2019.

[47] Early, D. A., Reth, A. D., and Rodriguez-Alvarez, O. I., "Spacecraft pointing stability constraints and instrument disturbance limits for optical remote sensing satellites," *Sensors, Systems, and Next-Generation Satellites VII*, Vol. 5234, International Society for Optics and Photonics, SPIE, 2004, pp. 560 – 571. doi: 10.1117/12.511166.

[48] Hasha, M. D., "High-Performance Reaction Wheel Optimization for Fine-Pointing Space Platforms: Minimizing Induced Vibration Effects on Jitter Performance plus Lessons Learned from Hubble Space Telescope for Current and Future Spacecraft Applications," *43rd Aerospace Mechanisms Symposium*, NASA, 2016, pp. 373–400.

[49] Carrara, V., and Kuga, H. K., "Current and Speed Control Operating Modes of a Reaction Wheel," *Applied Mechanics and Materials*, Vol. 706, 2014, pp. 170–180. doi: 10.4028/www.scientific.net/amm.706.170.

[50] Bayard, D. S., *High-Precision Three-Axis Pointing and Control*, Wiley-Blackwell, 2010, p. 13. doi: 10.1002/9780470686652.eae300.

[51] Baroni, L., and Kuga, H. K., "Analysis of Attitude Determination Methods Using GPS Carrier Phase Measurements," *Mathematical Problems in Engineering*, Vol. 2012, 2012, pp. 1–10. doi: 10.1155/2012/596396.

[52] Westgaard, M. F., "Software Design and Controller Evaluation for the ADCS on the NTNU Test Satellite," Master's thesis, Norwegian University of Science and Technology, Trondheim, NO, 2015.

[53] Fonod, R., and Gill, E., "Magnetic Detumbling of Fast-tumbling Picosatellites," *Proceedings of the International Astronautical Congress, IAC*, Vol. 2018-October, 2018.

[54] Hao, Z., "Detumbling and Aerostable Control for Cubesats," Master's thesis, Cranfield University, Cranfield, UK, 2013.

[55] Auret, J., "Design of an Aerodynamic Attitude Control System for a CubeSat," Master's thesis, Stellenbosch University, Matieland, SA, 2012.

[56] Fortescue, P. W., Stark, J., and Swinerd, G. (eds.), *Spacecraft Systems Engineering*, 4th ed., Wiley, Hoboken, N.J., 2011.

[57] Dang, K., "Phased Array Antenna Investigation for Cubesat Size Satellites," Master's thesis, Morehead State University, Morehead, April 2016.

[58] Reddy, M. H., Joany, R. M., Manikandan, G., and Nisha, A. S. A., "Design of microstrip patch antenna with multiple slots for satellite communication," *2017 International Conference on Communication and Signal Processing (ICCSP)*, IEEE, 2017. doi: 10.1109/iccsp.2017.8286482, URL https://doi.org/10.1109/iccsp.2017.8286482.

[59] Karpati, G., Hyde, T., Peabody, H., and Garrison, M., "Resource Management and Contingencies in Aerospace Concurrent Engineering," *AIAA SPACE 2012 Conference & Exposition*, American Institute of

Aeronautics and Astronautics, 2012, p. 1. doi: 10.2514/6.2012-5273.

[60] You, Z., *Space Microsystems and Micro/Nano Satellites*, Butterworth-Heinemann, 2017.

[61] Edries, M., Tanaka, A., and Cho, M., "Design and Testing of Electrical Power Subsystem of a Lean Satellite, HORYU-IV," *Transactions of the Japan Society for Aeronautical and Space Sciences, Aerospace Technology Japan*, Vol. 14, 2016, pp. Pf_7–Pf_16. doi: 10.2322/tastj.14.Pf_7.

[62] NASA, "Energy Storage Technologies for Future Planetary Science Missions," JPL D-101146 [Online], Dec. 2017.

[63] A, G., and YA, V., "Thermal Analysis of Satellite Libertad 2: a Guide to CubeSat Temperature Prediction," *J. Aerosp. Technol. Manag*, 2018. doi: 10.5028/jatm.v10.1011.

[64] Arink, J., "Thermal-Mechanical Design of a Baffle," Master's thesis, Delft University of Technology, Delft, 2019.

[65] Linlor, W. I., "Optical System with Reflective Baffles," US Patent 4,542,963, 1985.

[66] van de Pas, N., "Thermal Control Hardware," [Lecture Slides], 2018.

[67] Ross, Jr., R. G., and Bar-Cohen, Y., *Refrigeration Systems for Achieving Cryogenic Temperatures*, CRC Press, 2016, Chap. 6, pp. 109 – 181.

[68] Radebaugh, R., "Pulse Tube Cryocoolers for Cooling Infrared Sensors," *SPIE, The International Society for Optical Engineering, Infrared Technology and Applications*, Vol. 4130, 2000, pp. 363–379. doi: 10.1117/12.409878.

[69] Lee, J., Kim, D., Mun, J., and Kim, S., "Heat-Transfer Characteristics of a Cryogenic Loop Heat Pipe for Space Applications," *Energies*, Vol. 13, No. 7, 2020, p. 1616. doi: 10.3390/en13071616.

[70] T. Nguyen, M. m. J. R. E. T., M. Petach, "Space Micro Pulse Tube Cooler," Tech. rep., Northrop Grumman Aerospace Systems, Redondo Beach, CA, 2010.

[71] Bianchi, G., Aglietti, G. S., and Richardson, G., "Development of efficient and cost-effective spacecraft structures based on honeycomb panel assemblies," *2010 IEEE Aerospace Conference*, 2010, pp. 1–10.

[72] Ravanbakhsh, A., and Franchini, S., "Preliminary Structural Sizing of a Modular Microsatellite Based on System Engineering Considerations," Third International Conference on Multidisciplinary Design Optimization and Applications, 2010.

[73] Marjoniemi, K., Syvanen, L., Hoffren, M., and Langlois, S., "Modular structure for small satellite," *Proceedings of The 4S Symposium: Small Satellites, Systems and Services (ESA SP-571)*, 2004.

[74] Fox, B., Brancato, K., and Alkire, B., "Guidelines and Metrics for Assessing Space System Cost Estimates," Tech. rep., RAND Corporation, Santa Monica, CA, 2008.

[75] Broder, M., Mahr, E., Barkmeyer, D., Burgess, E., Alvarado, W., Toas, S., and Hogan, G., "Review of Three Small-Satellite Cost Models," *AIAA SPACE 2009 Conference & Exposition*, American Institute of Aeronautics and Astronautics, 2009, pp. 1–11. doi: 10.2514/6.2009-6689.

[76] Brumbaugh, K. M., "The Metrics of Spacecraft Design Reusability and Cost Analysis as Applied to CubeSats," Master's thesis, The University of Texas at Austin, Austin, 2012.

[77] Cás, P., Veras, C., Shynkarenko, O., and Leonardi, R., "A Brazilian Space Launch System for the Small Satellite Market," *Aerospace*, Vol. 6, 2019, p. 123. doi: 10.3390/aerospace6110123.

[78] Miller, D. W., Keesee, J., and Jilla, C., "Space Systems Cost Modelling," MIT Lecture Notes, 2003.

[79] Massey, D. E., "Satellite Ground Station Cost/Performance Appraisal," *International Telemetering Conference Proceedings*, International Foundation for Telemetering, 1997, p. 8.

[80] Duren, R. M., "Validation and Verification of Deep-space missions," 2002.

[81] Pantoquilho, M., "Testing and Validating Operational Spacecraft Simulators," 2010.

[82] NASA, "The Project Life Cycle Module," https://origins.sese.asu.edu/ses405 [Online], 2020.

A Appendix

A.1. Payload - Appendix

As said in the chapter for the payload design both the primary and secondary mirrors are parabolic. This means that they can be expressed by quadratic equations, Equation A.1. These in turn can be found to know the exact dimensions of the two mirrors. The point of origin of both mirrors is considered the center bottom of the primary mirror.

$$y = ax^2 + bx + c \tag{A.1}$$

Primary mirror For the primary, the elevation of the extremes is investigated to know the function of the quadratic describing the primary mirror.

As a benchmark, it was assumed that the actual length of the mirror could not be five percent larger than the actual aperture. This is because still enough effective surface area has to be directly exposed to incoming infrared waves. Higher lengths means that the mirror is more and more bent. Thus, using the equation to calculate the length of a parabolic arc, Equation A.2[a] the extreme's elevations of the primary mirror were found, e_I. A_1 being the aperture.

$$L = 0.5\sqrt{A_1^2 + 16e_I^2} + \frac{e_I^2}{8e_I^2}\ln\left(\frac{4e_I + \sqrt{A_1^2 + 16 \cdot y_I^2}}{A_1}\right) \tag{A.2}$$

Secondary mirror The second's mirror shape is found using the fact the relation between the reflected angle on the primary mirror and the fact that the secondary mirror's reflected ray has to pass through the secondary mirrors focal point, that is at the origin. Another point to take into account, is that the center of the secondary mirror is right above the center of the primary mirror at a distance equal to the intersection of the system focal length ray and the secondary mirror extremity (Figure A.1).

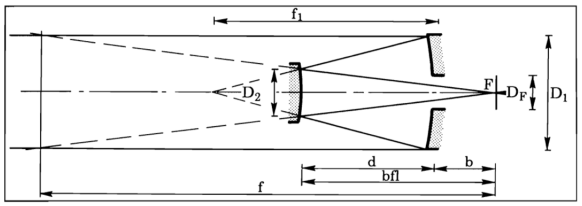

Figure A.1: Focal length demonstration. Here, D_2 is length of the secondary mirror, D_1 the aperture of the primary mirror, b is 0 and f is the system focal length[b].

Thus, the following dimensions can be computed from this.

- Primary mirror extremity elevation w.r.t origin (TIR/MS): 0.14339 m / 0.16643 m
- Secondary mirror extremity elevation w.r.t origin (TIR/MS): 0.89975 m / 0.920754 m

Furthermore, the equation's coefficients describing both the primary and secondary mirror for TIR and MS, with respect to the origin are as follows. Equation A.3 and Equation A.4 for the primary and secondary mirrors of the TIR telescope and, Equation A.5 and Equation A.6 for the primary and secondary mirror of the MS telescope.

$$y = 0.547x^2 \quad \text{(A.3)} \qquad y = 9.473x^2 + 0.7867 \quad \text{(A.4)} \qquad y = 0.471x^2 \quad \text{(A.5)} \qquad y = 8.332x^2 + 0.7867 \quad \text{(A.6)}$$

Width of primary and secondary mirror As mentioned in the chapter of payload design, the width of the primary and secondary mirror are approximated using the ratio between the reference and calculated aperture. Moreover, the width of the secondary mirror for the reference is not know. This can be approximated using the ratio between the primary and secondary mirror length and the width of the primary mirror.

[a] https://www.vcalc.com/wiki/vCalc/Parabola+-+arc+length [cited 3 Jun 2020]
[b] https://ccdsh.konkoly.hu/wiki/Cassegrain_Optics [cited 15 June 2020]